**Development and Mechanistic Implications of Nickel Pre-Catalysts for Organic Synthesis**

**by**

**Alex James Nett**

A dissertation submitted in partial fulfillment
of the requirements for the degree of
Doctor of Philosophy
(Chemistry)
in the University of Michigan
2018

Doctoral Committee:

Professor John Montgomery, co-chair
Professor Paul M. Zimmerman, co-chair
Professor Melanie Sanford
Associate Professor Nathaniel Szymczak
Professor Suljo Linic

Alex James Nett

alexnett@umich.edu

ORCID iD:  0000-0003-0209-0292

## Dedication

This dissertation is dedicated to my lovely wife and best friend, Alyssa. Without her I would have never embarked on this adventure. Her unconditional love, encouragement, and patience were crucial to me making it this far.

**Acknowledgements**

I would like to acknowledge both of my advisors, Professor John Montgomery and Professor Paul Zimmerman, for their mentorship and support during my time at the University of Michigan. They both gave me freedom to explore different avenues of my research. I believe independence is the most important aspect of developing the creativity necessary to be a successful scientist. Therefore, their willingness to allow me to explore new directions in my research was critical to my development as a scientist. I would also like to thank Professors Melanie Sanford, Nathaniel Szymczak, and Suljo Linic for serving on my committee and giving me feedback throughout my time in graduate school. Additionally, I would like to thank Professor Tim Cernak for serving on my committee during my defense and for useful discussions pertaining to my work. I would also like to extend a special thanks to the NSF Center for C-H Functionalization for their support and intellectual contributions to many of the projects I have worked on over the years.

Thank you to all of the members of both the Montgomery and Zimmerman labs. I especially would like to thank Dr. Wanxiang Zhao for his mentorship during my early years in the Montgomery group. I am also grateful for Ian Pendleton and Andrew Vitek for their support and guidance on the computational aspects of my work. I have been fortunate to have great collaborators in lab and I would like to acknowledge specifically, Michael Robo, Santiago Cañellas, Yuki Higuchi, Goki Hirata, Ellen Butler, Jeanne Kochkodan, and David Todd for their contributions to work related to the development and applications of stable Ni(0) pre-catalysts. Additionally, Takuya Yoshida for his efforts in exploring catalytic C-H activations related to the

work described in the Conclusions and Future Outlook. I would like to thank Dr. Kirk Shimkin, Alex Rand, and Wes Pein for editing my thesis in the early stages of writing.

I would also like to acknowledge Professor Michael Carney for giving me the opportunity to participate in undergraduate research during my time at University of Eau Claire. He taught me early on the value of hard work and independence, and for that I grateful.

A special thank you goes out to my family and friends without whom I would not have been able to accomplish the things I have. I am fortunate to have a family that has been very supportive and patient throughout my life, especially during my graduate school years, and I owe them a great deal. I hope that I can give them the kind of support provided to me.

Finally, I am thankful for my little family here in Ann Arbor, Alyssa, Chip, and Philly. Without my wife Alyssa none of this would have been possible. She is my biggest supporter and my best friend.

I am forever grateful for her.

## Table of Contents

## List of Tables



.

## List of Figures

**Abstract**

Nickel catalysis is a versatile tool for constructing complex molecules, but a variety of operational challenges limit the wide spread use of these methods outside academic labs. The use of experimental and computational tools for understanding and developing technical improvements related to pre-catalyst design are described herein. An off-cycle pathway stemming from pre-catalyst activation of $Ni(COD)_2$ for hydroarylation of alkynes via C-H functionalization has been identified. The use of computational methods has assisted in characterizing these complexes as potential off-cycle resting states and experimental support for this conclusion is described. Pre-catalyst adaptation by removing COD has allowed for rapid C-H functionalization at room temperature for a variety of structural manifolds. Additionally, a potential energy surface for nickel-catalyzed hydroarylation and a structure-activity relationship has been developed that uses computational data to predictive experimentally observed rates for nickel-catalyzed hydroarylations via C-H functionalization.

Furthermore, a new class of N-heterocyclic carbene (NHC)–supported Ni(0) pre-catalysts is described that display enhanced air-stability while retaining high reactivity. This is done through the employment of π-acidic ligands that stabilize electron-rich Ni(0). The use of this strategy is applied to several NHC ligands of varying steric profiles. Their stability and reactivity are evaluated for reductive couplings and amination cross–couplings. To this end, structure-activity relationships are developed that have led to the design of air-tolerant and catalytically active NHC–Ni(0) pre-catalysts.

# Chapter 1 Nickel Pre-Catalyst Activation Mechanisms

## Introduction

Scientists are confronted with the challenge of developing new technologies to meet the needs of society whether that be related to health, agriculture, or the development of materials. In chemistry these challenges often involve the conversion of raw materials found in nature into complex molecules to meet the needs of our global community. However specific the application, the role of transition metal catalysis as a tool for pushing the boundaries of chemical diversity is rooted in the modern synthetic strategy. Despite the advancements and evolutions of catalyst design, the practicality of employing any chemical method does not escape the laws of supply and demand. In that vein, there are many necessary catalytic processes that rely on unsustainable materials. Unfortunately, if there are not alternative, more sustainable methods available then we are left with no choice, but to accept the consequences associated with conducting such processes.

The demand for more sustainable catalysis has been met with significant efforts to create methods that utilize more earth-abundant metals, such as first-row transition metals. The sustainability of first-row transition metal catalysis should not overshadow the opportunity this class of metals offers for developing fundamentally unique and valuable chemical processes. It is important to recognize that the challenges presented here are not new ones, and many influential people have made contributions to what has become one of the most prominent and fruitful areas of chemical research.

Few transition metals have a history in catalysis as rich as that of nickel. An interesting, and often overlooked, aspect of sustainability is the technology with which metals are purified

from their raw source. One of the most significant advancements in the refinement of nickel was made by Ludwig Mond in 1889, when he and his colleagues accidentally discovered the extraction of nickel ore from nickel oxide (typical impurities include Fe and Co) could be done at elevated temperatures in the presence of carbon monoxide.[1,2] It was determined that these methods efficiently provided volatile nickel carbonyl ($Ni(CO)_4$) which could be plated out and isolated as pure nickel ore. Despite the acute toxicity of nickel carbonyl, this marked a monumental advancement in the efficient generation of nickel in its zero-oxidation state. Ni(0) is the most catalytically relevant form of nickel,[3] thus well understood and efficient processes for accessing this state from the raw nickel oxides preceded years of catalytic development.

Most notably, while exploring alternative methods for extracting of pure nickel using other gaseous compounds, Sabatier and Senderens observed that at high temperatures equal parts of hydrogen and ethylene produces ethane without any formation of by-product.[2] The hydrogenating power of nickel was subsequently applied to the reduction of acetylene to ethylene and it was noted that the nickel remained unchanged and could be recycled, marking this one of the earliest demonstrations of nickel catalysis. Sabatier was awarded the Nobel Prize in chemistry in 1912 for his impactful contribution to the field.[2] This initiated the beginning of an era for nickel catalysis, as stated so elegantly by Herman Emil Fischer during a tribute to the findings of Sabatier and Senderens:

*"This chapter on catalysis is unlimited and it is here that a systematic investigation promises to bring a rich reward."* -Emil Fischer , 1912[2]

One of the underlying themes of the work of Mond and Sabatier is the unique chemical environment necessary to both generate and stabilize nickel in its catalytically active form. Typically, Ni(II) is the most naturally abundant oxidation state, but examples of catalytically active

Ni(II) are rare. Ni(0) and Ni(I) are much more catalytically relevant oxidations states for homogenous catalysis, but their general instability in the presence of oxygen limits access to stable pre-catalysts of this form.

Chemist have engineered a variety of ways to make Ni(II) compounds relevant for homogenous catalysis. Early work by Kumada demonstrated that Ni(II)-dihalide complexes can be used for cross-coupling organo-halides and Grignard reagents.[4] Under these reaction conditions pre-catalyst activation is straightforward and presumably proceeds via iterative transmetalations by a strong nucleophile followed by reductive elimination, generating Ni(0) prior to catalysis.[5] However, reactions that lack strongly reducing reagents provide a more complicated scenario. This chapter is designed to highlight unique routes for which the "active" form of nickel is generated for several classes of reactions. Because an exhaustive and comprehensive discussion on pre-catalyst activation for nickel catalysis is beyond the scope of this chapter, an emphasis will be place on reactions that do not require strong nucleophiles or super-stoichiometric metal reductants, as plausible activation mechanisms are often straightforward for these classes of reactions. Discussion of these types of methods will mostly be by means of comparison to more recent developments in pre-catalyst activations. In doing so, this chapter should inform the reader of reaction features that are necessary for pre-catalyst activation of a given class of pre-catalyst. Special attention will be given to the use of well-defined nickel pre-catalysts and reactions that contain weak nucleophiles, as these present unique challenges in catalyst activation. Examples where simple ligand substitution from $Ni(COD)_2$ efficiently leads to the active form of the catalyst will be minimally discussed, unless it is evident that COD plays a crucial role in regulating catalysis. Finally, pre-catalyst activations that promote undesired reactivity or when a specific pre-catalyst ancillary ligand is necessary for catalysis will be addressed.

## C-N Bond Forming Cross-Couplings

The first demonstration of nickel-catalyzed C-N bond formation, via cross-coupling of an amine and an aryl halide, was reported by Wolfe and Buchwald in 1997.[6] In their seminal report, they employed $Ni(COD)_2$ as the pre-catalyst which led to good catalytic activity (entries 1 and 5, Table 1-1). An air-tolerant protocol was also adapted for this reaction where the authors demonstrated that sub-stoichiometric quantities of methyl magnesium bromide could be used to generate Ni(0) from $L_2NiCl_2$, which is necessary for catalytic activity. For cases where *in situ* reduction was used, higher catalyst loadings were required and it was substrate specific (entries 2 and 6, Table 1-1). Notably, the use of activated Zn(0) to reduce $L_2NiCl_2$ was unsuccessful.[6]

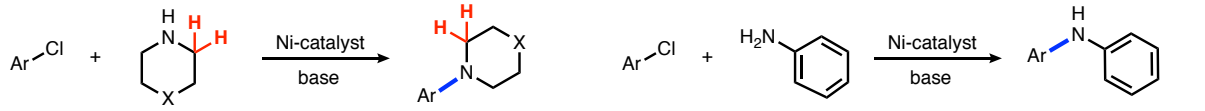


| Entry | Ni-catalyst | Conditions | Yield [%] | Entry | Ni-catalyst | Conditions | Yield [%] |
|---|---|---|---|---|---|---|---|
| 1 | $Ni(COD)_2$/dppf | NaOtBu, toluene (100 °C) | 81-96 | 5 | $Ni(COD)_2$/dppf | NaOtBu, toluene (100 °C) | 88-96 |
| 2 | (dppf)$NiCl_2$/MeMgBr | NaOtBu, toluene (100 °C) | 54 | 6 | (dppf)$NiCl_2$/MeMgBr | NaOtBu, toluene (100 °C) | 0-83 |
| 3 | $Ni(acac)_2$/SIPr/NaH | NaH/t-BuOH, THF (65 °C) | 53-99 | 7 | $Ni(acac)_2$/SIPr/NaH | NaH/t-BuOH, THF (65 °C) | 55-99 |
| 4 | $Ni(acac)_2$/phen/PMHS | NaOtBu, toluene (130 °C) | 62-96 | 8 | $Ni(acac)_2$/phen/PMHS | NaOtBu, toluene (130 °C) | N.R. |

**Table 1-1.** *In situ* generation of nickel catalysts for amination aryl chlorides.

Fort and co-workers also reported that Ni(0) could be accessed for coupling secondary amines and aryl chlorides using excess NaH as both a reductant during pre-catalyst activation and a base for the amination reaction.[7] In this case, it was noted that the presence of amine was necessary to generate Ni(0). This could arise from a β-hydride elimination event being crucial for catalyst activation, but conclusive data was not reported. Later Fort and co-workers adapted the catalyst for SIPr ligands, which proved to be much more reactive for amination, and the amount of NaH could be reduced to sub-stoichiometric amounts. Once reduced to Ni(0) alkoxide bases were sufficient for promoting catalysis (entries 3 and 7, Table 1-1).[8]

To avoid the involvement of a strong reductant, Knochel and co-workers demonstrated that an active Ni(0) catalyst could be generated from $Ni(acac)_2$ using super-stoichiometric amounts of silane (entries 4 and 8, Table 1-1).[9] It was proposed that silane could also stabilize catalytic intermediates throughout the course of the reaction.[10] Although this method is attractive due to the use of mild reductants, coupling amines that lack β-hydrogens could not be done indicating that the amine is potentially influencing catalyst reduction (entry 8, Table 1-1).[9]

One of the early demonstrations of a reductant-free amination from a Ni(II) precatalyst was conducted by Nolan and co-workers in 2005, where they synthesized a variety of (NHC)Ni(II)CpCl complexes (**1-1**, Figure 1-1). In that report the (NHC)Ni(II)CpCl complexes displayed moderate activity for the cross-coupling of aryl chlorides and amines without exogenous reductant, but temperatures of 105 °C were required.[11] Though the exact activation mechanism for this class of pre-catalyst was not discussed in that report, it was later proposed by Nicasio and co-workers that the moderate activity of these catalysts could be attributed to highly deactivating Cp moieties during pre-catalyst activation/reduction.[12] Nicasio's solution to this challenge was to employ π-allyl ligands in place of Cp to reduce the hapticity and increase the liability of this group during catalyst activation.[12] In that report, Nicasio successfully demonstrated improved yields with (IPr)Ni(II)(π-allyl)Cl (**1-3**, Figure 1-1) compared to the Cp analogs of these complexes. Later, Nolan and co-workers supported another hypothesis that increasing the ligand size could also increase the rate of Cp dissociation, as a similar trend has been demonstrated for other metal types. By using IPr*OMe, a highly sterically hindered NHC, (IPr*OMe)Ni(II)CpCl (**1-2**, Figure 1-1) resulted in enhanced catalytic activity.[13]

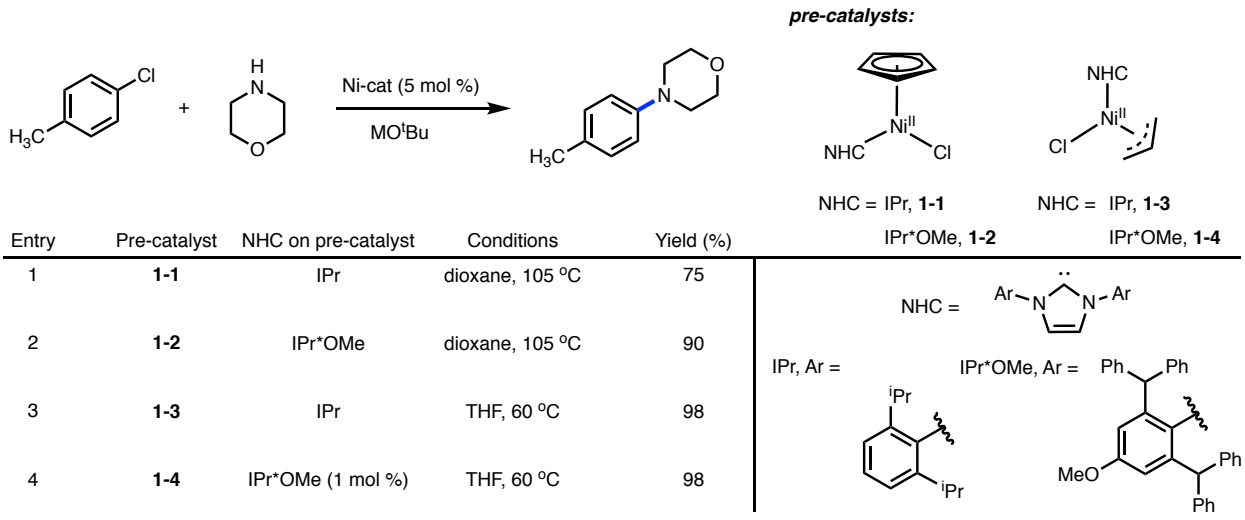


| Entry | Pre-catalyst | NHC on pre-catalyst | Conditions | Yield (%) |
|---|---|---|---|---|
| 1 | **1-1** | IPr | dioxane, 105 °C | 75 |
| 2 | **1-2** | IPr*OMe | dioxane, 105 °C | 90 |
| 3 | **1-3** | IPr | THF, 60 °C | 98 |
| 4 | **1-4** | IPr*OMe (1 mol %) | THF, 60 °C | 98 |

**Figure 1-1.** Cp and π-allyl stabilized pre-catalysts performance for N-arylation of aryl chlorides.

It was unclear if steric effects by the NHC ligand are responsible for the increased activity compared to IPr, but later Nolan and co-workers reported that (IPr*OMe)Ni(II)(π-allyl)Cl (**1-4**, Figure 1-1) was even more active than the Cp analog of this complex supporting both the fact that π-allyl ligands initiate faster than Cp ligands and that more sterically hindered NHC perform better for amination cross-coupling.[14] Although removing the X-type ligands from Ni(II) solves the issue of opening coordination sites, the reduction of these catalysts appears to be dependent on amines that have β-hydrogens, which could participate in elimination as a means of generating Ni(0). Though higher temperatures are required, this catalyst system can also couple anilines, presumably because there is a higher barrier for initiation. However, the mechanism for initiation of aniline couplings is not clear. One mechanism for initiation that has not been discussed in the literature is the potential for transmetalation between two nickel centers generating (NHC)Ni(II)(π-allyl)$_2$ and (NHC)Ni(II)Cl$_2$ and the former undergoes reductive elimination to form 1,5-hexadiene, a process which has precedent[15] (Figure 1-2).

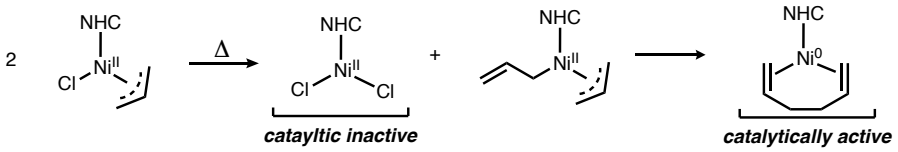


**Figure 1-2.** Potential activation mechanism of π-allyl pre-catalysts.

Another promising class of Ni(II) pre-catalyst that has been used for C-N bond formation, via cross-coupling, are *trans*-$(PR_3)_2$Ni(II)(σ-aryl)X complexes (Figure 1-3).[16–18] Although these complexes were first synthesized by Chatt in 1960,[19] they haven't received a significant amount of attention by the synthetic community until recently. Yang and co-workers demonstrated that *trans*-$(PPh_3)$Ni(II)(σ-aryl)X complexes could be activated coupling amines and aryl chloride by the addition of NHC ligands, like IPr.[16] Stoichiometric experiments probing catalyst activation were performed, which led to the observation that complexes with bromide ligands activated faster than chlorides, and σ-napthyl activates faster than σ-o-tolyl. There was no further discussion for the origin of these differences (Figure 1-3). Yang and co-workers took a similar approach to aminating triarylphosphates.[18]

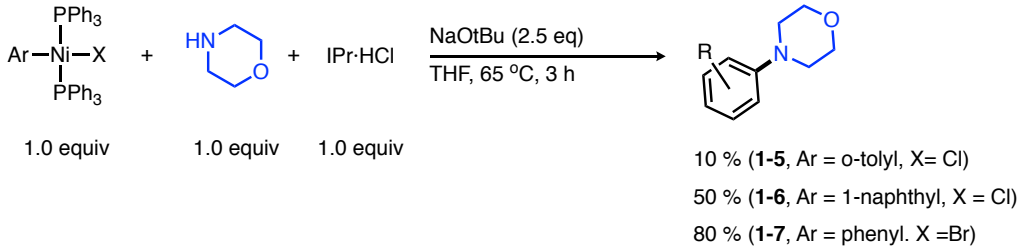


**Figure 1-3.** The first demonstration of *trans*-$(PR_3)_2$Ni(II)(σ-aryl)X complexes as pre-catalyst for amination.

Following the work by Yang, several other groups have demonstrated how σ-aryl complexes of nickel can be used for amination reactions.[20–25] However, in most of the recent examples, the σ-aryl and the halide ligands are in the *cis*-orientation. Figure 1-4 shows other examples of *cis*-σ-aryl complexes that have been used for nickel-catalyzed amination reactions of aryl chlorides (Figure 1-4).

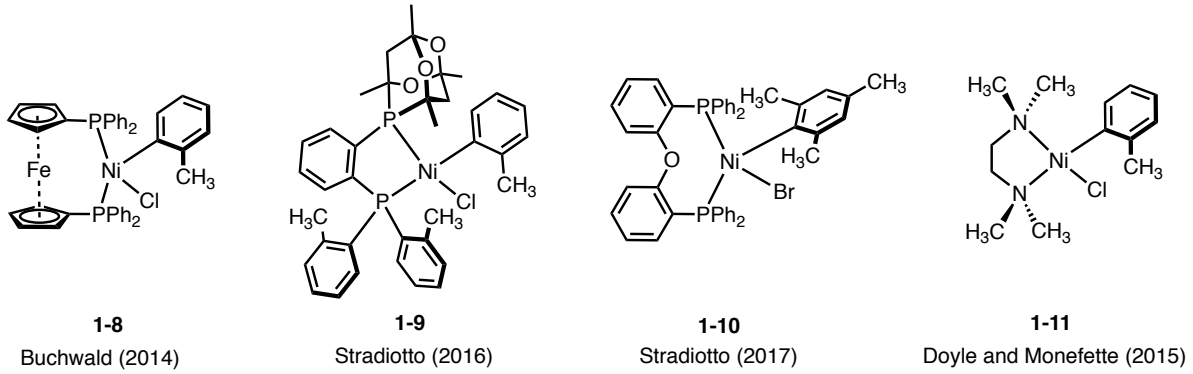


**1-8**
Buchwald (2014)

**1-9**
Stradiotto (2016)

**1-10**
Stradiotto (2017)

**1-11**
Doyle and Monefette (2015)

**Figure 1-4.** Examples of *cis*-σ-aryl complexes that have been used for amination.

In Buchwald's report, it was shown that pre-catalyst **1-8** promoted a variety N-arylations of both aryl chlorides and mesylates.[21] Insights into the activation mechanism were provided when coupling morpholine and 1-butyl-3-chlorobenzene a trace amount of the aminated o-tolyl product was observed, although it wasn't observed in all of the reactions (Figure 1-5). Therefore, a plausible activation mechanism could be base-mediated metalation of an amine followed by reductive elimination. Advancements on this pre-catalyst structural motif were made by Stradiotto (**1-9** and **1-10**, Figure 1-4) using various phosphines that showed improved activity compared to pre-catalyst **1-8**.[25] In their work, it was observed that adding sub-stoichiometric amounts of phenyl boronic acid produced a much more active catalyst, presumably via transmetalation of the boronic acid followed by reductive elimination (Figure 1-5).[23] Doyle[20] and Monfette[22] independently reported (TMEDA)Ni(II)(o-tolyl)Cl (**1-11**) which is a highly modular pre-catalyst due to lability of TMEDA toward ligand substitution which can be replaced with a variety of ligands to promote desired reactivity. Although ligand substitution does occur with TMEDA, it has been documented that pre-catalyst **1-11** routinely requires higher temperatures to generate the active catalyst. The success of **1-11** pre-catalyst is also ligand dependent as it has been reported by Stradiotto that **1-11** is unreactive for aminations in the presence of some phosphines.[23]

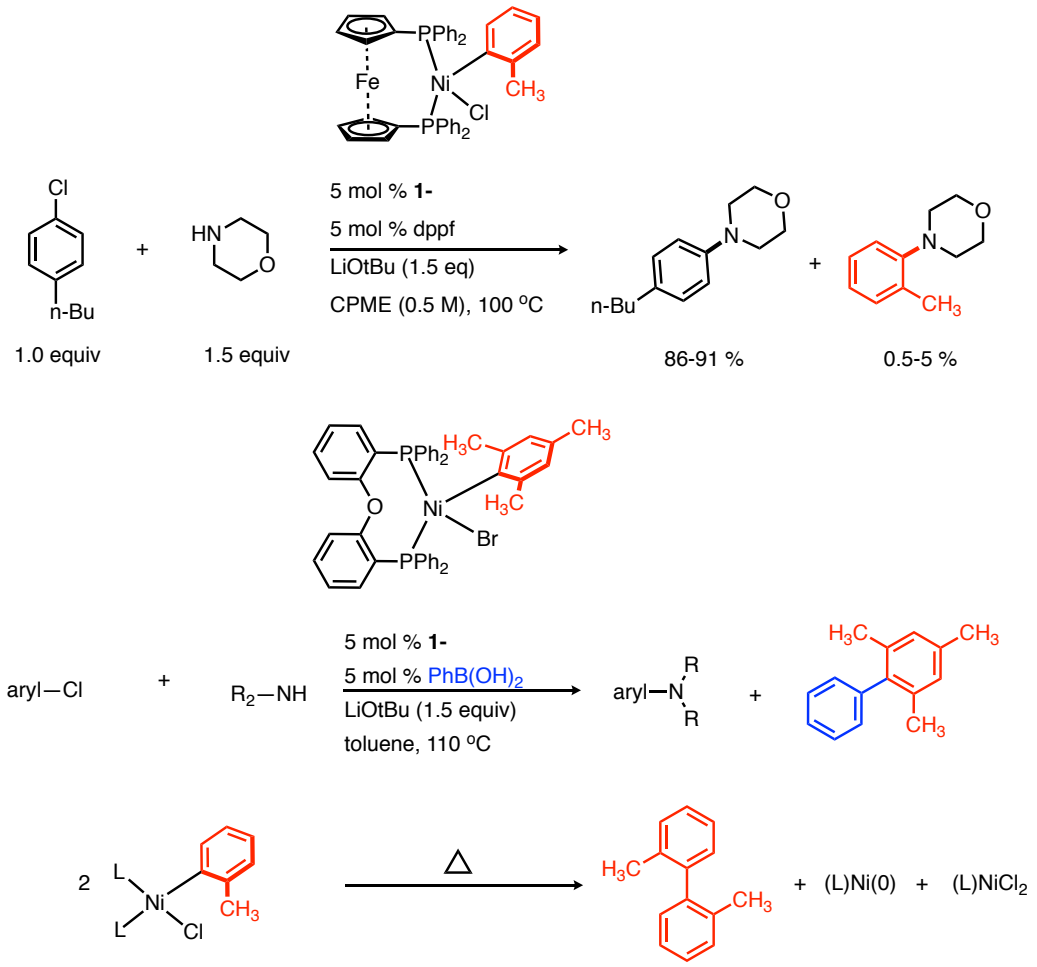


**Figure 1-5.** Potential activations mechanism for *cis*-σ-aryl complexes for amination.

A final mode of activation for these types of pre-catalysts is a non-substrate mediated pathway that proceeds via nickel-nickel transmetalation of the o-tolyl ligands. Subsequent reductive elimination produces 2,2'-dimethyl-1,1'-biphenyl, $(L)_nNi(0)$, and $(L)_nNiCl_2$. Since Ni(II) dihalides are typically unreactive without strong reductants, it is a mild yet sacrificial means of catalyst generation (Figure 1-5).[20] It should also be noted that this the above process would be second-order in nickel resulting in higher catalyst loadings being necessary. Although the modes of activation for **1-11** are shown here to be sensitive to reaction conditions, it should not overshadow the achievement of this technology to access many useful cross-couplings while avoiding strict air-free protocols.

Photocatalytic reductions are a more recent method for generating Ni(0) from Ni(II). Although the proposed chemistry is supported by favorable redox match-ups, an example from MacMillan, Buchwald, and co-workers demonstrated that even in the presence of a photocatalyst, the reduction of the Ni(II) salt precursors for N-arylation was only operative in the presence of amines with β-hydrogens. In order to efficiently couple nucleophiles such as anilines using this method, sub-stoichiometric amounts of pyrrolidine to activate the catalyst.[26]

A beautiful demonstration of the role nickel pre-catalysts can play during catalytic couplings of amines and aryl halides was reported by Hartwig and co-workers in a method development and mechanistic study.[27] In that report, Hartwig and co-workers employed a BINAP-Ni(0) pre-catalyst stabilized by a benzonitrile ligand, BINAP-Ni(0)($\eta^2$-NC-Ph) (**1-12**, Figure 1-6). This pre-catalyst was used in order to eliminate any issues with reduction prior to productive catalysis. Furthermore, kinetic analysis revealed that the reaction was overall first-order in aryl chloride and catalyst and inverse first-order in benzonitrile. In this case, pre-catalyst activation is not necessary since the pre-catalyst, itself, serves as a catalytic resting state for amination. It is proposed that benzonitrile reversibly binds prior to oxidative addition of the aryl chloride and following product forming reductive elimination. Similar conclusions could be drawn from the analogous reaction with aryl bromides, but in that case, the reaction is zero-order in benzonitrile, thus indicating that it is also involved in the oxidative addition of the aryl bromide.[27]

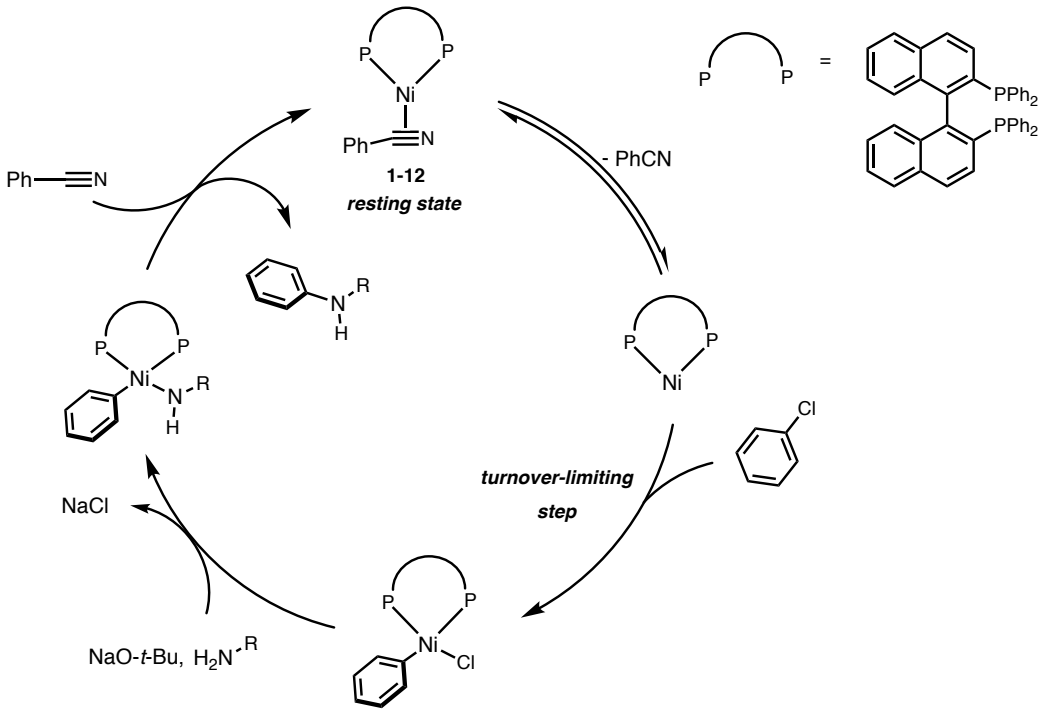


**Figure 1-6.** General mechanism for nickel-catalyzed amination of aryl chlorides as proposed by Hartwig and co-workers.

In summary, there are a variety of routes that access an active nickel catalysts for C-N bond forming cross-couplings.[28] Since Ni(0) is the most common oxidation state necessary for catalysis, general and facile ways of generating Ni(0) are crucial to the development of robust methods for constructing C–N bonds. Outlined here, are several advancements in the field that allow for the rapid generation of Ni(0) from air-stable Ni(II) precursors, many of which do not require exogenous reductants, but come with their respective limitations. It should be noted, that based upon the summary above there are limited strategies that employ air-stable Ni(0) pre-catalysts, a topic that will be discussed in chapter 3.

**Nickel Hydride Catalyzed Transformations and Other Hydrofunctionalizations**

Although coordinatively unsaturated nickel hydride complexes have been reported,[29] the high energy nature of these species typically leads to dimerization via bridged hydrides or renders them non-isolable. As a result, many methods have been developed to generated reactive nickel

hydride equivalents *in situ*, which can be stored in units of unsaturation (i.e. alkenes) and later generated when needed via β-hydride elimination. A hallmark example of this strategy is used in the Shell Higher Olefin Process (SHOP) which is one of the most widely used nickel hydride catalyzed reactions (Figure 1-7).[29,30] Reaction classes and respective nickel hydride generation routes that will be discussed in this section include: nickel-catalyzed hydrovinylations, hydrosilylations, and hydroarylations. A more comprehensive review on the synthesis and reactivity of nickel hydrides can be found in a recent review by Guan and co-workers.[29]

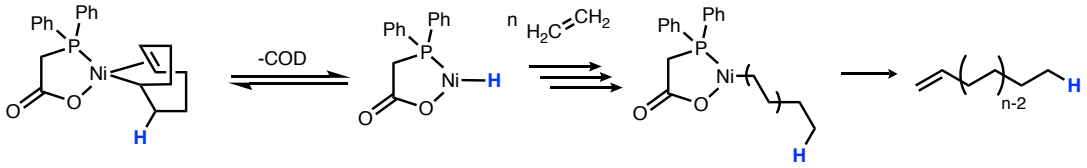


**Figure 1-7.** Shell Higher Olefin Process (SHOP).

## Hydrovinylations

Although many methods for olefin dimerization catalyzed by cationic nickel hydrides has have been reported,[2] there have been several advancements in the methods used to generate cationic nickel hydrides which have made this process amenable to milder conditions. One of the early routes used to generate *in situ* nickel hydrides for hydrovinylation was reported by Wilke.[2] In that report, a dimeric allyl nickel halide in the presence of a strong Lewis Acid like $EtAlCl_2$ and an olefin produced a cationic nickel hydride, a sequence which is highlighted in Figure 1-8a. Initial extraction of a chloride ligand with $EtAlCl_2$ opens a coordination site for an olefin to bind, thereby generating a cationic nickel center with an $[EtAlCl_3]^-$ counter ion. Migratory insertion of the olefin into the allyl–Ni bond followed by β-hydride elimination generates a reactive cationic nickel hydride (Figure 1-8a). The use of a strong Lewis acids to generate catalytically relevant species limited the widespread use of this methodology in synthetic organic chemistry. RajanBabu and co-workers were able to replace the strong Lewis acids, needed during activation, with halide

scavengers with weakly coordinating anions like triflates and borates (Figure 1-8b).[31–33] These milder conditions allowed for asymmetric catalysis using chiral phosphine ligands to mediate the coupling vinyl arenes and ethylene.[33] Detailed mechanistic data provided by RajanBabu and Jemmis show that the rate of activation, via ethylene insertion of the allyl–Ni bond, is greatly enhanced by using hemi-labile ligands.[31]

Another route to accessing cationic nickel hydride complexes was provided by Jamison and co-workers. An analogous NHC-supported cationic nickel hydride was generated as an intermediate during alkene-aldehyde couplings that are mediated by a silyl triflate (Figure 1-8c).[34] Under those reaction conditions it was shown that oxidative cyclization of an alkene and an aldehyde followed by σ-bond metathesis with a silyl triflate led to a $[(NHC)Ni(II)(alkyl)]^{+}OTf^{-}$. Subsequent β-hydride elimination leads to the formation of the desired product and a cationic nickel hydride. Ho and co-workers employed this catalytic intermediate for hydrovinylation catalysis.[35] The advantage of this route to accessing cationic nickel hydride is that it avoids the synthesis of organometallic precursors and ionic sources of triflate, which can cause undesired reactivity. Ho and co-workers have also recently demonstrated that NHC-Ni(II)(π-allyl)Cl complexes are also competent pre-catalyst for cationic nickel hydride formation in the presence of halide abstractors like $NaBAr^{F}_{4}$ (Figure 1-8b).[36]

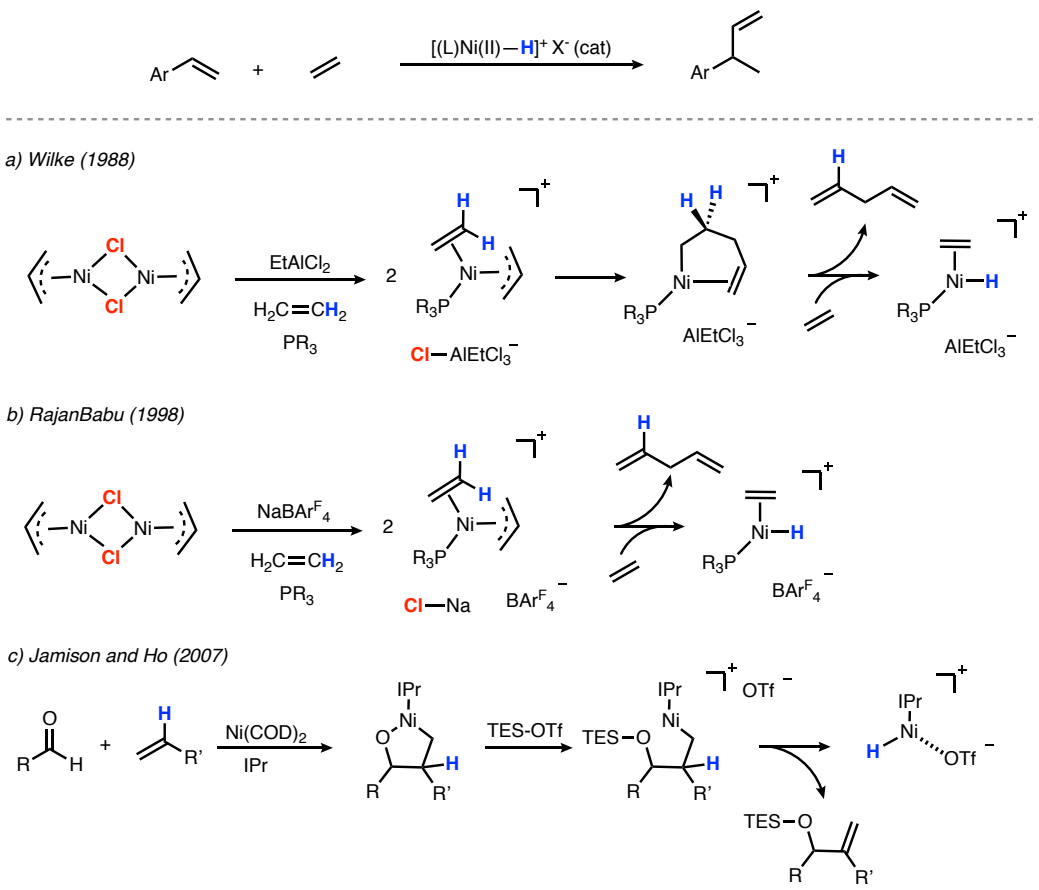


**Figure 1-8.** Generating cationic nickel hydrides from allyl nickel halide.

## Hydrosilylation

Additionally, nickel hydrides and pseudo-hydrides have been used to carry out hydrosilylation of alkynes,[37–40] alkenes,[41,42] allenes,[43,44] aldehydes,[45–47] and ketones.[47,48] Nickel-catalyzed hydrosilylations have been done with pre-catalysts in the 0, I, and II oxidation state, which can all be associated with different modes of pre-catalyst activation. Typically, when a Ni(I) or Ni(II) pre-catalyst is employed the reaction can be initiated either via discrete nickel hydride precursors or a nickel hydride can be generated via σ-bond metathesis. In the case of Ni(0) pre-catalysts, two possible mechanisms can occur. The first being oxidative addition of a Si-H bond, which is extremely rare,[49,50] or a Si-H bond can be added across a π-acceptor in a concerted fashion.[51] Subsequent reductive elimination forms product and regenerates active Ni(0).

Early work of Kumada[4] and Orenski,[41] studying phosphine-supported nickel catalysts for alkyne and alkene hydrosilylation, proposed a low-valent nickel must form prior to a formal oxidative addition of a silane in forming an active Ni(II)-hydride. Although this is possible, there is little mechanistic evidence for this type of pathway with monodentate phosphines. To the best of my knowledge, the only nickel complex that has been demonstrated to undergo Si-H oxidative additions of trialkyl or dialkyl silanes, which are most common for hydrosilylations, is a bis-(NHC)Ni(0)(COD) complex reported by Radius and co-workers.[29,52] In that report, the data suggests that there is possibly a dative Si···H interaction resulting from $\eta^2$-Si-H binding mode.[52]

Montgomery and co-workers have reported on hydrosilylation of alkynes, allenes, and ketones using NHC/$Ni(COD)_2$, and they were able to demonstrate in an unrelated study that IR spectroscopy suggests that Ni(0)/$PCy_3$ doesn't consume silane on its own.[53] In fact, computational analysis by Xie and Xiong on allene hydrosilylation supports a concerted transfer of the hydride of a silane to an allene (Figure 1-9).[51] Mechanisms like this are common in C-H functionalization since it avoids high energy Ni-hydride intermediates. Concerted transfer of Si-H to a π-acceptor proceeds via an oxidative processes and requires a Ni(0) catalyst to do so. When $Ni(COD)_2$ is the pre-catalyst redox activation is unnecessary and likely proceeds via straightforward ligand substitution.

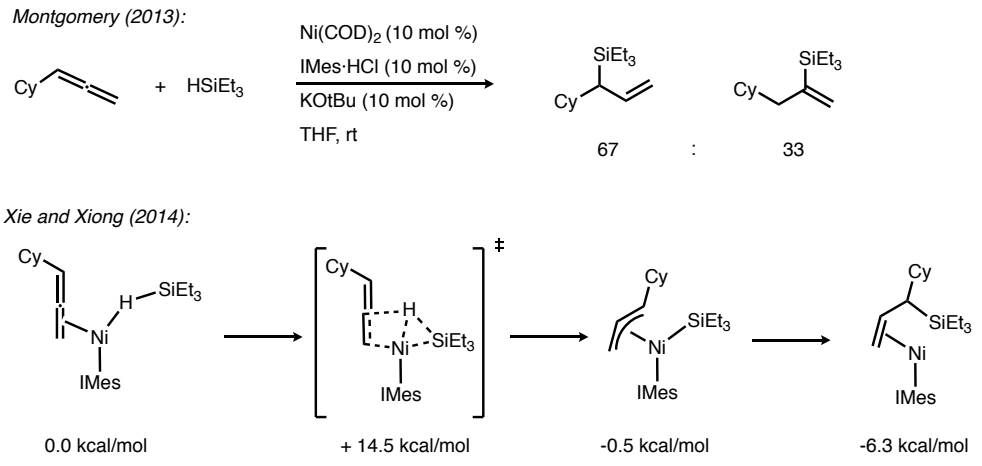

**Figure 1-9.** Hydrosilylation of allenes and associated mechanistic analysis (B3LYP/6-31g(d)/LANL2DZ).

The use of discrete nickel pre-catalysts has allowed for the synthesis of stable nickel hydride complexes for hydrosilylation. Mindiola and co-workers used a dimeric nickel pre-catalyst with bridging halides (**1-13**) for hydrosilylation of aldehydes.[45] In their report, it was noted that the catalyst was completely inert in the absence of KOtBu base, which is used to activate the pre-catalyst (**1-14**, Figure 1-10). This is consistent with a previous report that demonstrated Ni(II) halides were not competent pre-catalysts for hydrosilylation without adding a reductant.[41] Activations of this type are likely driven by the thermodynamic stability of Si-O bonds formed during σ-bond metathesis. Other groups have used this strategy for activating Ni(II)-halide complexes for hydrosilylation catalysis. Guan and co-workers were able to more conclusively assign σ-bond metathesis of a silane and a Ni(II)-alkoxy as the terminal step in nickel-catalyzed hydrosilylation of aldehydes using tridentate pincer complexes.[29] In Guan's report, a discrete monomeric Ni(II)-hydride complexes was isolated and reacted with an aldehyde yielding the insertion product. Subsequent exposure to silane formed a silyl-protected alcohol and a Ni(II)-hydride complex.

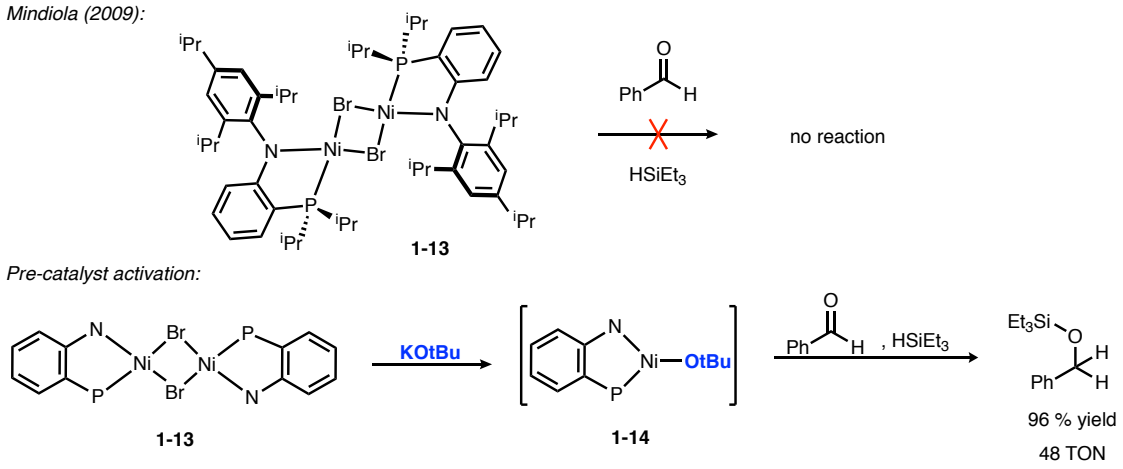


**Figure 1-10.** Hydrosilylation using **1-13** as a catalyst initiated by KOtBu.

The use of Ni(II)-alkoxy precursors for alkene hydrosilylation was recently applied by Hu and co-workers. They isolated stable a (*N,N,N*)-Ni(II)OMe pincer complex, which rapidly undergoes metathesis with $Ph_2SiH_2$ to yield a nickel-hydride. This complex was demonstrated to be a competent pre-catalyst for selective alkene hydrosilylation yielding the anti-Markovnikov product.[54]

Ritleng, Sortais and co-workers reported IMesNi(II)(Cp)Cl as a competent pre-catalyst for hydrosilylation of aldehydes using dialkylsilanes.[47] Although the chloride complex on its own does not promote the coupling of a silane and an aldehyde, activating the catalyst with substoichiometric amounts of $NaHBEt_3$ resulted in nearly quantitative conversion after 15 minutes at 25 °C. This result further supports the difficulty of generating active catalysts for hydrosilylation from Ni(II)-halide complexes. Another report by Royo and co-workers showed (NHC-Cp)Ni(II)OtBu (**1-15**, Figure 1-11) was a highly active pre-catalyst for aldehyde hydrosilylation.[46] In that report, they were able to successfully synthesis both a Ni(II)-alkoxy (**1-15**) and an analogous Ni(II)-hydride (**1-16**) complex for aldehyde hydrosilylation (Figure 1-11). The robustness of pre-catalyst **1-15** was demonstrated on several substrates and in most case high yields were observed after 5 minutes. More importantly, in the Royo's report it was shown via stoichiometric labeling studies experiments between $D_2SiPh_2$, PhCOH, and **1-16** that PhCHDO–SiPhD was formed and the hydride in **1-16** was completely retained ruling out a conventional hydride mechanism. This result brings into question whether or not the formation of a discrete nickel-hydride is necessarily forming during pre-catalyst activation. It should be noted, that $D_2SiPh_2$ does not undergo H/D exchange with **1-16** under the reaction conditions.[46]

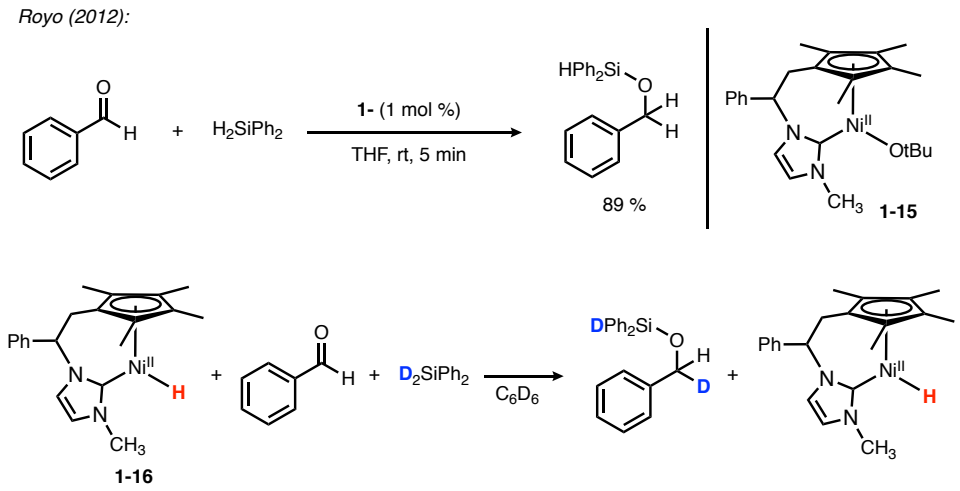


**Figure 1-11.** Hydrosilylation of aldehydes using CpNi(II) pre-catalysts.

Finally, Chirik and co-workers have reported the use of discrete Ni(I) hydride complexes for anti-Markovnikov hydrosilylation of alkenes using trialkylsilanes, which was not demonstrated previously in the literature.[42] A redox non-innocent diimine ligand was used to stabilize a Ni(I) dimer with bridging hydride ligands (**1-17**). The catalytically active nickel-hydride complex, **1-17**, can be synthesized and isolated via σ-bond metathesis of triethyoxysilane with Ni(II)–carboxylate in the presence of ligand. Alternatively, it can be generated *in situ* following the same protocol and used that way. Pre-catalyst **1-17** was shown to hydrosilylate 1-octene and the rate law shows a 1/2-order in **1-17**, suggesting that the active catalyst is a monomeric nickel-hydride that forms via dissociation of **1-17**.

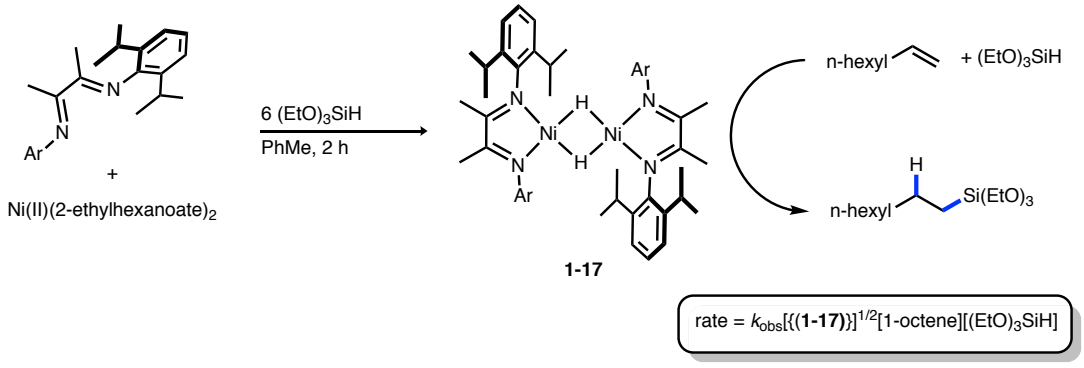


**Figure 1-12.** Chirik's report of using stable Ni(I) pre-catalyst for hydrosilylation.

In summary, there are a variety nickel pre-catalysts of different forms that can be used to generate active catalysts for hydrosilylation chemistry. Previous work suggests that oxidative addition of Si–H of dialkyl- and trialkylsilane by relevant nickel hydrosilylation complexes is rare. Rather hydrosilylations from Ni(0) pre-catalyst are likely to proceed through a concerted transfer mechanism that avoids the formation of nickel-hydrides during catalysis. Generally, Ni(II) and Ni(I) pre-catalysts for hydrosilylation can proceed through discrete nickel-hydride complexes and the fastest initiating pre-catalysts are those that contain a Ni–$O^{alkoxy}$ group, which undergoes rapid σ-bond metathesis, producing a reactive nickel-hydride.

**Pseudo Nickel Hydrides for C-H Functionalization**

The use of nickel catalysis for the functionalization of C-H bonds has emerged as valuable synthetic tool.[55–57] Although many distinct transformations have been demonstrated, hydroarylation of alkenes and alkynes via arene C-H bond activation have been especially robust.[56,58] Analogies can be drawn to the previously discussed hydrosilylations in the sense that unique mechanistic features have been observed to avoid the formation of coordinatively unsaturated nickel-hydride intermediates. The generally accepted mechanisms for catalysis by low-valent nickel catalysts have been shown to proceed via a concerted oxidative addition/migratory insertion pathway termed ligand-to-ligand hydrogen transfer (LLHT).[59] Pre-catalysts in this area are most commonly simple Ni(0) pre-cursors such as $Ni(COD)_2$, but observations of COD-mediated LLHT has led to use of COD-free pre-catalysts. Regardless of the choice of stabilizing ligand for the pre-catalyst, it is proposed that ligand substitution pathways with alkyne or alkene substrate is the main pathway to generate the active catalyst. In this section, select pre-catalysts for this transformation will be illustrated.

Seminal work from Nakao and Hiyama revealed the lability of acidic C-H bond in the presence of nickel and a π-acceptor, such as an alkyne.[60] In these cases, rapid production of vinyl arenes resulted at elevated temperatures.[56] In their early works, $Ni(COD)_2$ was the choice of nickel precursor, but reports by Johnson and co-workers demonstrated LLHT of acidic C-H bonds to COD leading to the formation of π-allyl complexes.[61] In that same report, Johnson and co-workers reported an anthracene stabilized Ni(0) complex (**1-18**, Figure 1-13) for mechanistic studies of the alkenylation of fluoroarenes. Later Hartwig and co-workers observed COD-derived products in olefin hydroarylation via C-H functionalization which led to the use of noraboranene based catalysts (**1-19**), as well as, $Ni(0)(IPr)_2$ (**1-20**), which does not participate in undesired reactivity.[62] When Hartwig's observations were first reported, our group was concurrently troubleshooting COD-mediated activity where we observed thermodynamically limiting intermediates that greatly impede catalysis. This observation led to the use of 1,5-hexadiene stabilized IMes-Ni(0) complexes which diminish off-cycle activity and promote catalysis at room temperature (**1-21**, Figure 1-13).[63] Furthermore, an even more substitutionally labile pre-catalyst was reported for hydroarylation of alkenes when Hartwig and Nakao employed $\eta^6$-arene stabilized pre-catalysts,[64] which require the use of large NHC ligands (**1-22**, Figure 1-13).[58]

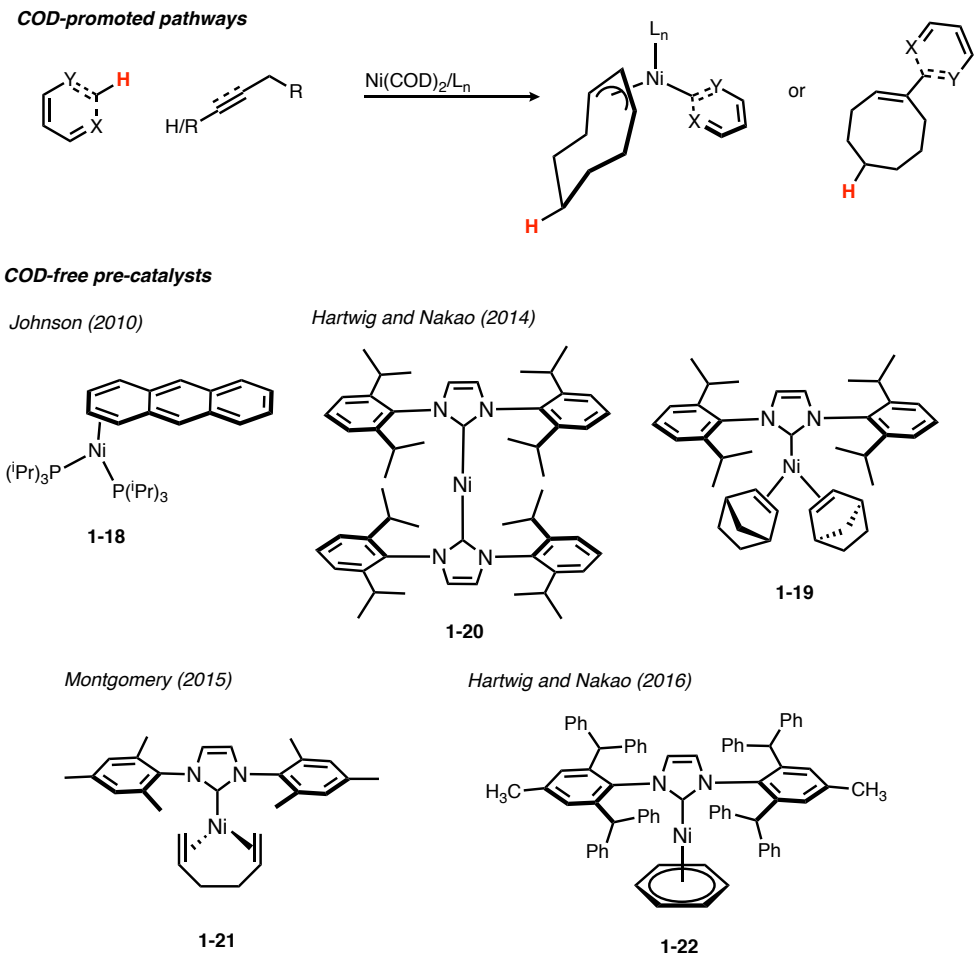


**Figure 1-13.** Ni(0) pre-catalysts for C-H functionalization. Synthesis of **1-21** was first reported Hazari.[15]

In summary, simple ligand substitution pathways are proposed for pre-catalyst activation. Most notably, COD-derived activity has led to the design of new pre-catalyst for this class of reaction and off-cycle pathways promoted by COD will be discussed in great detail in chapter 2.

### π-π Couplings and Other Alkene Couplings

The ability of nickel catalysts to promote the coupling of multiple π-components dates back to the early work of Reppe and co-workers in 1948.[2] Reppe and co-workers demonstrated that nickel could promote the tetramerization of acetylene to yield cyclooctatetraene.[2] This field has evolved into many robust classes of reactions that can couple a wide variety of π-components from cycloadditions to polar π-components. This reactivity is an artifact of Ni(0) being electron-rich,

thus contributing to its high philicity for olefins via strong back-bonding interactions. The mild nature of these types of ligands makes the use of Ni(II) pre-catalysts, particularly challenging without adding strong reductants. As a result, π-π couplings typically require Ni(0) pre-catalysts, like $Ni(COD)_2$.[3]

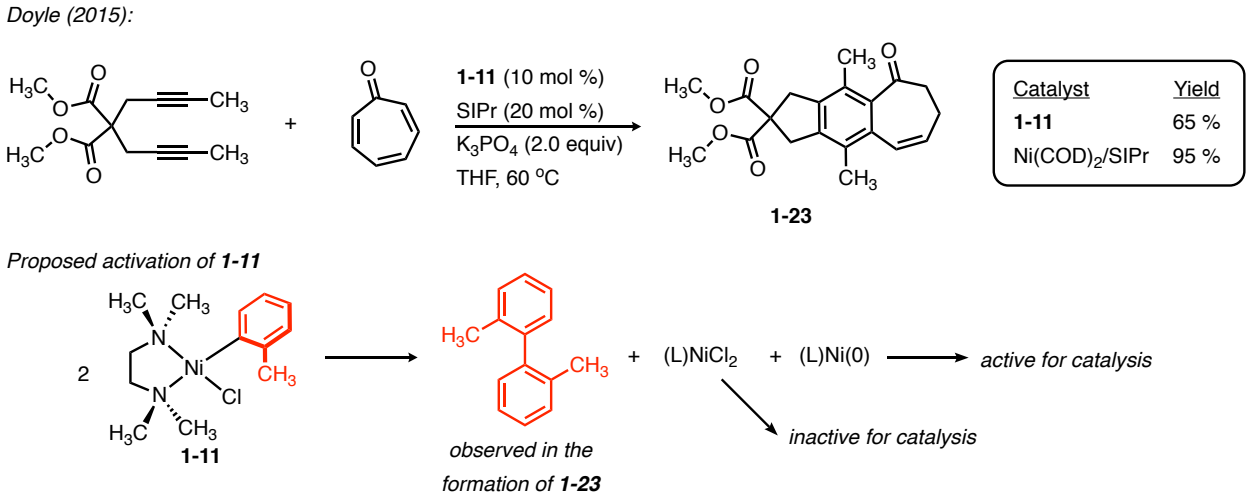


**Figure 1-14.** Proposed pre-catalyst activation for **1-11**-catalyzed [2+2+2] reactions.

Recent advancements in the development of stable Ni(II) pre-catalyst that can activate without adding reductant, such as (TMEDA)Ni(II)(o-tolyl)Cl (**1-11**, Figure 1-14), have been demonstrated to perform [4+2] and [2+2+2] reactions (Figure 1-14).[20] Doyle and co-workers successfully employed **1-11** and SIPr as a pre-catalyst for coupling diynes and tropones, as previously reported by Louie and co-workers using $Ni(COD)_2$/SIPr.[65] Although appreciable yields were observed when using **1-11**, significantly lower yields were observed compared to the $Ni(COD)_2$ protocol (Figure 1-14). In these cases, nickel-nickel transmetalation leads to the formation of biphenyls, catalytically active Ni(0) and Ni(II) dihalide, which is inactive under the reaction conditions. While this method avoids the addition of reducing agents, it does require sacrificing half of the nickel catalysts in the system. Despite this drawback, this self-activating mode should not deter from the advancement of modular complexes, like **1-11**, which enable

bench-top reaction protocols which are valuable to increasing the widespread use of nickel-catalyzed reactions.

Reduction protocols that utilize mild reductants like silanes have also been developed to generate active Ni(0). Wen, Li, and co-workers have shown that Ni(0) can be efficiently accessed from $Ni(acac)_2$ for [2+2+1] cycloadditions between isocyanates, isonitiriles, and alkynes.[66] The efficiency of this method is made evident by their observation of high yields even at 0.3 mol % catalyst loadings. The exact mechanism for catalyst reduction was not discussed in this study. Unpublished results from our group have also observed mild reduction of $Ni(acac)_2 \bullet H_2O$ with sub-stoichiometric amounts of potassium tert-butoxide and excess trialkylsilane for silane-mediated reductive couplings (Figure 1-15).[67] This method proved to be quite robust tolerating a similar substrate scope and reaction conditions to protocols that employed $Ni(COD)_2$. This is proposed to proceed through ligand substitution of acac with tert-butoxide which undergoes σ-bond metathesis with a silane generating a Ni(II)–hydride. Reductive elimination gives Ni(0) and pentane-2,4-dione.

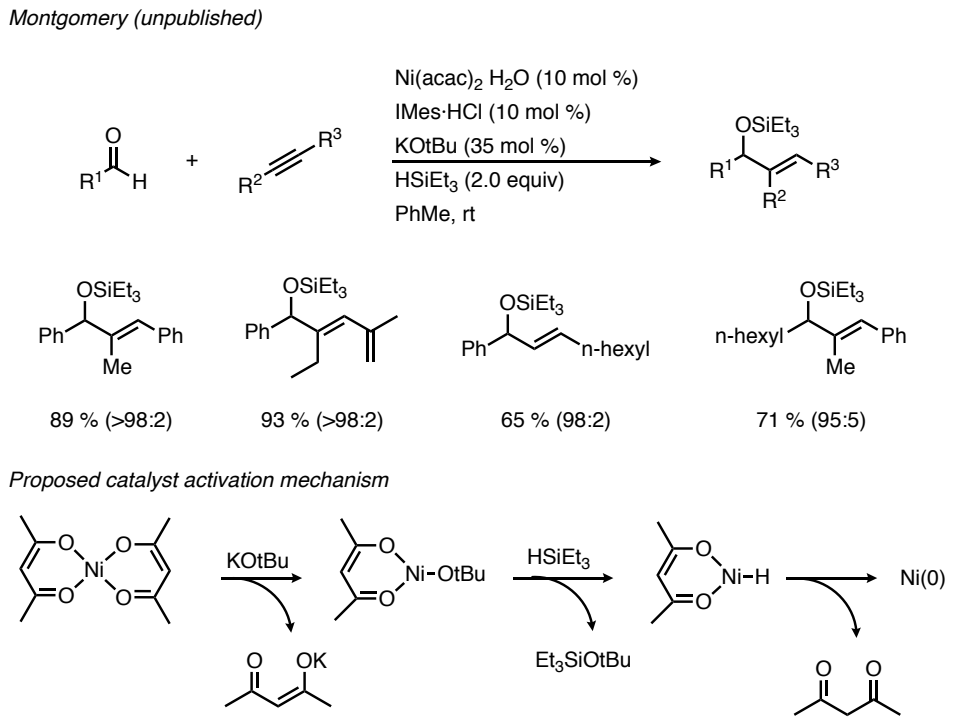


**Figure 1-15.** *In situ* reduction protocol of $Ni(acac)_2$ for reductive couplings.

A similar challenge exists for activating catalysts for couplings alkene electrophiles or alkene insertion reactions. It is common for $Ni(COD)_2$ to be employed in these transformations to observe high yields, but recently mild *in situ* reduction protocols have been developed for air-stable Ni(II) salts, similar to the work from our group. Ranu and co-workers have reported in multiple studies that the combination of $Ni(acac)_2$ and $Cs_2CO_3$ readily produces Ni(0).[68–70] Mechanisitic insights were provided by Ranu and co-workers while applying this reduction methods for copper-assisted nickel-catalyzed coupling of vinyl halides and phenols (Figure 1-16).[69] While exploring different pre-catalysts for this transformation it was noted that although $Ni(acac)_2$ was a competent catalyst in the presence of $Cs_2CO_3$, $NiCl_2$ required the addition of Zn powder to observe appreciable yields. UV spectroscopy was used to characterize the formation of Ni(0) upon addition of $Cs_2CO_3$. Shown in Figure 1-16, the spectra of $Ni(acac)_2$ is shown where an absorbance band is observed at 298 nm, and after the addition of $Cs_2CO_3$ a red shifted band appears

at 376 nm indicating the formation of Ni(0) (Figure 1-16).[69] This method for catalyst activation has also been applied for other vinyl halide couplings.

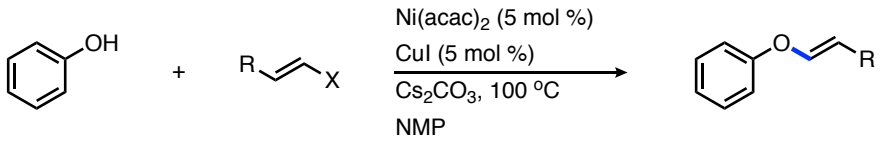


*Evidence for Ni(0) formation upon addition of $Cs_2CO_3$*

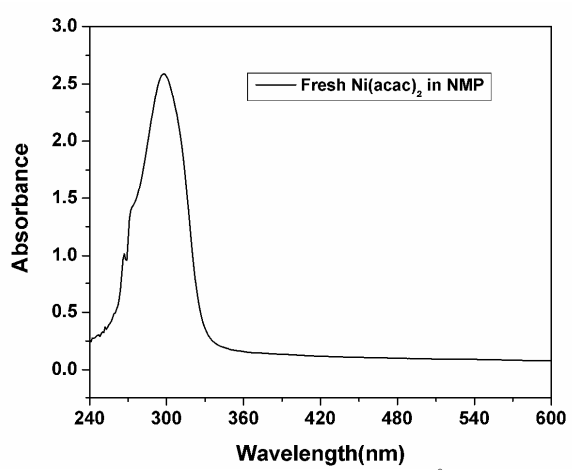


UV-spectra of fresh $Ni(acac)_2$ in NMP at 100 $^0$C

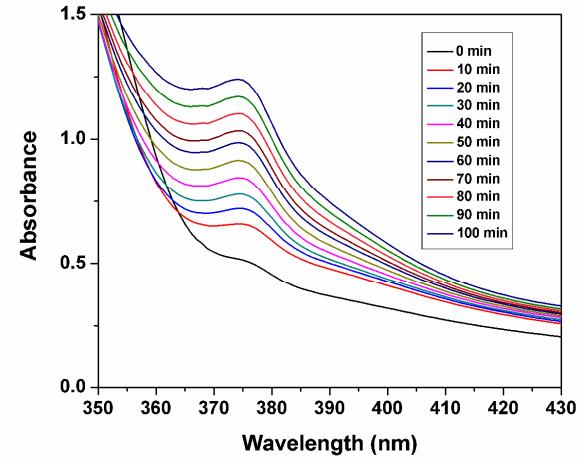


UV-spectra of $Ni(acac)_2$-NMP solution after addition of $Cs_2CO_3$ at 100 $^o$C

**Figure 1-16.** *In situ* reduction of $Ni(acac)_2$ with $Cs_2CO_3$. UV spectra provide evidence for the formation of a Ni(0) species upon addition of $Cs_2CO_3$. UV spectra are reproduced from the Supporting Information from DOI: 10.1021/ol500134p. Copyright, 2014 ACS.

Jamison and co-workers were able to utilize *trans*-$(PCy_2Ph)_2Ni(II)(o\text{-}tolyl)Cl$ (**1-24**, Figure 1-17), a general structural motif originally reported by Chatt and co-workers,[19] for coupling terminal alkenes and benzyl chlorides.[71] In this scenario, a nickel-nickel transmetalation is proposed as the route to generating Ni(0), which inherently forms catalytically inactive $(PCy_2Ph)_2Ni(II)(OTf)Cl$ (Figure 1-17). The inability of $(PCy_2Ph)_2Ni(II)(OTf)Cl$ to promote the reaction was noted in their report.

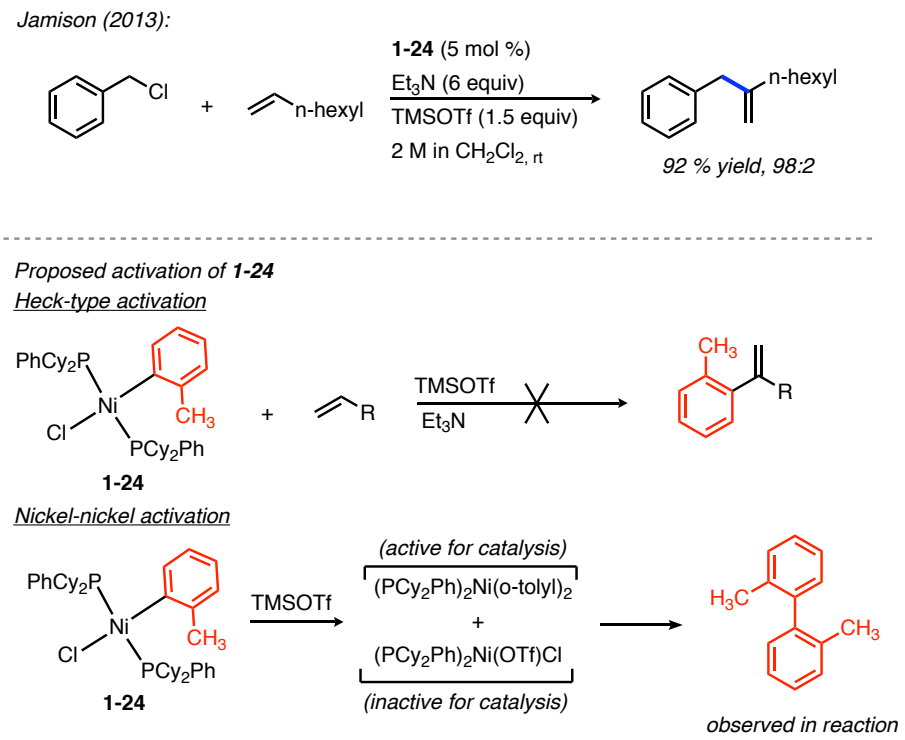


**Figure 1-17.** σ-Aryl Ni(II) complexes for coupling alkyl halides and terminal olefins.

There have been minimal developments in stable Ni(0) pre-catalysts for π-π couplings and other alkene couplings. Ogoshi and co-workers were able to make use of arene stabilized (SIPr)Ni(0)($\eta^6$-toluene) (IPr*OMe variant shown in Figure 1-13) for silane-mediated intramolecular coupling of aldehydes and alkenes.[72] Although this proved to be a valuable method for selectively obtaining aliphatic benzyl alcohols or silyl-protect allylic alcohols, COD and excess SIPr was found to serve a beneficial role and thus outperformed the arene stabilized discrete complex.

To recap, nickel-catalyzed couplings of π-components presents a considerable challenge for pre-catalyst design. This is impart due to the mild reaction conditions that are typically not amenable to Ni(II) reduction. The development of self-activating pre-catalysts, as described by Jamison and Doyle, have provided a means of air-stable reaction protocols, but high catalyst loadings are required due to poor efficiency of pre-catalyst activation.[20,71] Furthermore, progress

by our group, as well as others, have demonstrated that $Ni(acac)_2$ is uniquely suited to be reduced under relatively mild conditions.[67] The development, and employment thereof, for discrete Ni(0) pre-catalysts for this class of reaction are rare. The use of $\eta^6$-arene analogs of Ni(0) offer a promising class of pre-catalyst that should be more broadly examined in catalysis. Chapter 3 will provide a detailed discussion of our progress and contributions to this area.

**Nickel(I) Catalyzed Reactions**

Although Ni(I) complexes for catalysis have received significantly less attention compared to Ni(0) and Ni(II). Recently there has been a surge in the observation of, and direct employment of, Ni(I) complexes for a variety of transformations.[73,74] Organometallic Ni(I) complexes were first reported in 1914 by Belluci and Corelli when they synthesized $K_4[Ni_2(CN)_6]$.[74] In that vein, many interesting transformations have been reported for the synthesis and reactivity of Ni(I) organometallic complexes. These fundamental studies provide insight into whether or not it is plausible for Ni(I) complexes to form during catalysis and how we might harness its unique reactivity for the development of novel transformations. A hallmark study on the role of Ni(I) in catalysis was reported by Kochi and co-workers in studying the mechanism for Kumada couplings.[75] Ni(I) is commonly proposed in alkyl-alkyl couplings because nickel is more likely to facilitate alkyl radical mediated single-electron transformations than its palladium counterpart. Furthermore, key studies by groups like the Hillhouse group have provided a glimpse of how catalytically relevant ligands behave in the Ni(I)-alkyl complexes.[76] In this section, cases where Ni(I) has been observed in some capacity as the propagating species for catalysis will be explored, but a more comprehensive discussion on synthesis of Ni(I) complexes can be found in a recent review by Powers and Lin.[74] Several reports have stemmed from these studies to justify off-cycle formation of unreactive Ni(I) complexes which will be discussed at the end of this section.

There are four general strategies for accessing Ni(I), these include 1) single-electron reduction of Ni(II) 2) oxidation of Ni(0) 3) comproportionation of Ni(II) and Ni(0) 4) leveraging multidentate ligands or sterically hindered coordination spheres that favor Ni(I) as a result of the instability of corresponding Ni(II) complex. Several examples where Ni(I) is either the propagating species in a catalytic reaction or where Ni(I) is formed as an off-cycle by-product that inhibits catalysis will be highlighted in this chapter. It should be noted, that there are many examples where Ni(I) is proposed as an intermediate in catalysis, but this chapter is focused on highlighting strategies where discrete Ni(I) pre-catalysts are used or where Ni(II) and Ni(0) pre-catalyst are activated to Ni(I) in order to facilitate the early steps in a catalytic cycle.

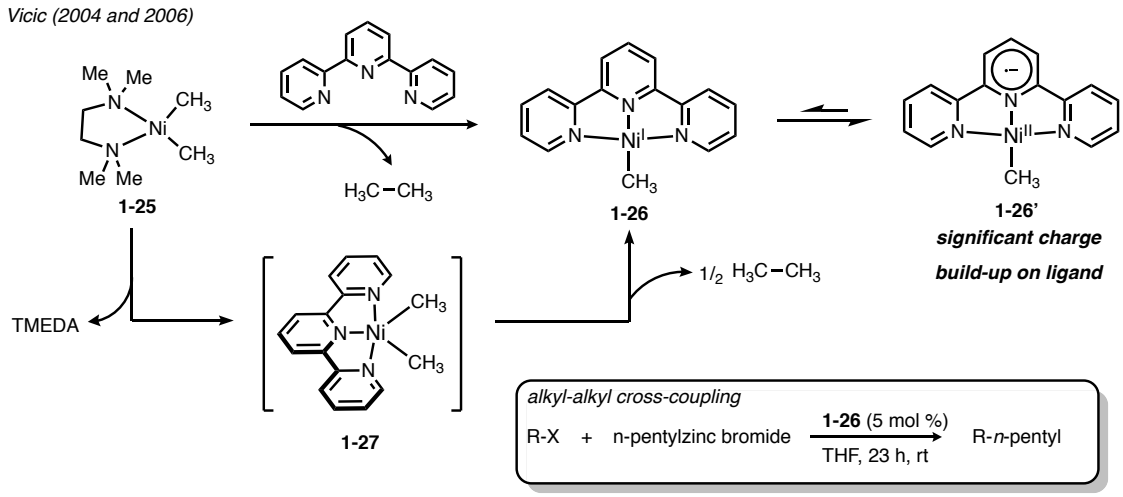


**Figure 1-18.** Instability of **1-27** leads to (terpy)Ni(I)$CH_3$ (**1-26**) which is more accurately described as **1-26'** in the Ni(II) state.

Vicic and co-workers made an interesting observation when (TMEDA)Ni(II)$(CH_3)_2$ (**1-25**) was mixed with terpyridine resulting in a square planar (terpy)Ni(I)$CH_3$ (**1-26**) and an equilavent of ethane (Figure 1-18).[77] The implications of complexes such as **1-26** interesting since nickel is a prolific catalyst for aliphatic cross-couplings where complexes analogous to **1-26** have been proposed. Although 1-26 was initially assigned as Ni(I), later work by Vicic and co-workers assigned **1-26** as having significant charge build-up on the central ring of the terpyridine ligand,

making the nickel center better described as Ni(II) with an anionic, reduced, terpyridine ligand (**1-26'**, Figure 1-18).[78] Additionally, a labeling experiment provided insight into the generation of ethane during the formation of **1-26**. Using (TMEDA)Ni(II)$(CH_3)_2$ (**1-25**, Figure 1-18) and the deutero-version of this complex (TMEDA)Ni(II)$(CD_3)$ (**1-25**-*d*) addition of terpy ligand formed $H_3C–CH_3$ and $D_3C–CD_3$ exclusively indicating that ligand substitution with terpy promotes reductive elimination. It is proposed that as concentration of (terpy)Ni(0) builds up, a comproportionation event leads to the formation of **1-26**.[78] Investigation of the specific mechanism for ethane formation was motivated by earlier asymmetric alkyl-alkyl couplings which will be discussed in this section.

Prior to the disclosure of **1-26** by Vicic, Fu and co-workers had demonstrated that tridentate pybox ligands could be used to facilitate Negishi couplings using alkyl halides and alkyl-zinc reagents.[79] When Fu and co-workers developed an asymmetric variant of this reaction[80] it brought into question the fundamental role that Ni(I) intermediates, analogous to **1-26**, were playing during catalysis, since alkyl-alkyl couplings are likely to proceed via stereo-undefined radical intermediates. To this end, Cárdenas and co-workers reported on the electronic structure of (pybox)Ni(I)$CH_3$ (**1-28**, Figure 1-19a). In this report **1-28** assigned as a pseudo-Ni(I) with a significant amount of negative charge on the ligand, thereby making it better represented as Ni(II) (**1-28'**).[81] Similar to what was proposed by Vicic, the formation of active Ni(I)-alkyl complexes (**1-26**), in this case, are proposed to form the sequence: transmetalation of Ni(II)$X_2$ with organo-zinc, reductive elimination, and comproportionation (Figure 1-18).

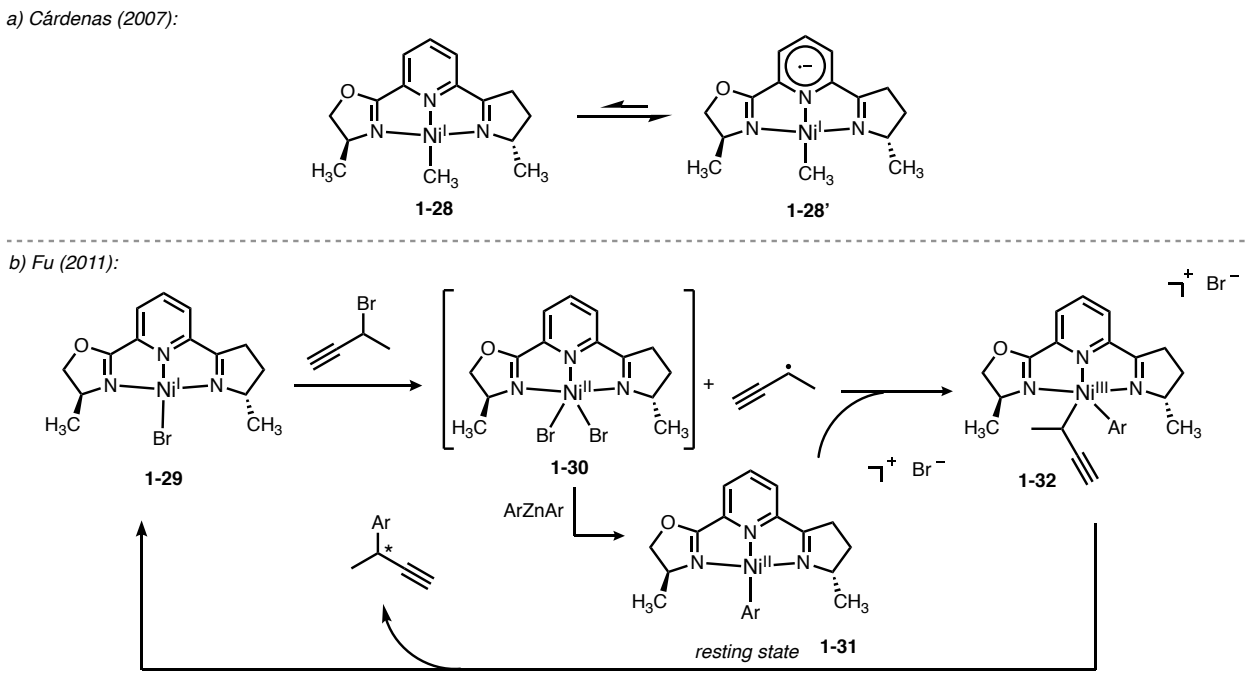


**Figure 1-19.** Routes to accessing Ni(I) for asymmetric coupling of alkyl-halides and organozincs.

In a detailed mechanistic study by Fu and co-workers, it was revealed that the active (terpy)Ni(I)Br (**1-29**) complex was not the resting state for catalysis, but the promotor for the homolytic X-alkyl bond cleavage that forms an alkyl radical and (terpy)Ni(II)$Br_2$ (**1-30**).[82] **1-30** is proposed to rapidly transmetalate with diarylzinc to form [(terpy)Ni(II)Ar]Br (**1-31**), which was determined the resting state of catalysis. Radical addition to **1-31** and reductive elimination from Ni(III) (**1-32**) forms product and regenerates Ni(I) complex, **1-29** (Figure 1-19).

Ni(I) pincer complexes have also been used as pre-catalysts to mediated asymmetric hydrodehalogenation reactions. As reported by Gade and co-workers, starting from a different tridentate pincer ligand, which has a formal negative charge, a stable (*N,N,N*)Ni(II)Cl complex can be synthesized (**1-33**, Figure 1-20).[83] Consequentially, reacting **1-33** with $LiEt_3BH$ results in a Ni(II)-hydride complex **1-34**. **1-34** undergoes reversible $H_2$ extrusion leading to the formation of T-shaped three-coordinate Ni(I) complex **1-35** (Figure 1-20). Both **1-34** and **1-35** were characterizing my X-ray diffraction. In Gade's report on hydrodehalogenation it is proposed that

**1-35** reacts with a gem-dihaloalkane to form an organic radical and Ni(II)X complex analogous to **1-33**. Ligand substitution with $LiEt_3BH$ forms **1-34** which resolves the dehalogenated product via a similar mechanism for $H_2$ elimination during the formation of **1-35** (Figure 1-20).[83]

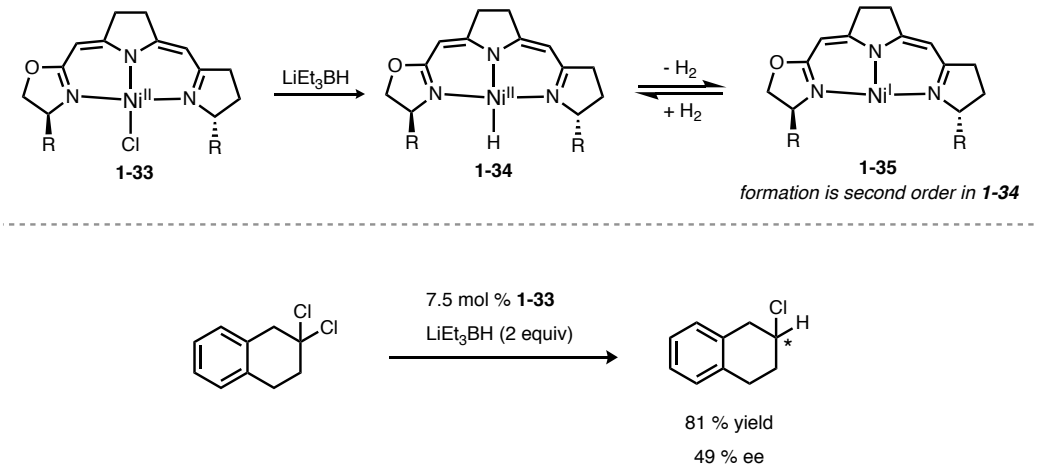


**Figure 1-20.** Elimination of $H_2$ from Ni(II) to form catalytically active Ni(I).

NHC–Ni(I) complexes have also received a considerable amount of attention from the synthetic community. While studying aerobic oxidation of Ni(I), Sigman and co-workers reported the synthesis of planar bis-μ-chloronickel(I) dimers substituted with NHC ligands (**1-36**, Figure 1-21).[84] The synthesis of **1-36** could be achieved by comproportionation of Ni(0) and Ni(II) in the presence of IPr ligand to afford **1-36** in high yield. In light of this discovery, complex **1-36** is commonly referred to as "Sigman's dimer." Matsubara and co-workers later studied the role of exogenous ligand, like $PPh_3$, in decomposing dimeric **1-36** into its monomeric form (**1-37**, Figure 1-21).[85,86] Although it was demonstrated that **1-36** was a competent pre-catalyst for N-arylation of aryl chlorides, a significant rate boost was observed when sub-stoichiometric amounts of $PPh_3$ was added (Figure 1-21).[85] A related study by Nakamura and co-workers investigated other ligands that promoted formation of monomeric Ni(I) species from **1-37**.[86] Another demonstration showcasing the catalytic activity of **1-36** was reported by Hillhouse and co-workers for the conversion of aryl azides and isonitriles to carbodiimides.[64] Although these are just two examples

of **1-36** being used as pre-catalyst, a more comprehensive discussion of applications of **1-36** can be found in a recent review by Matsubara and co-workers.[73]

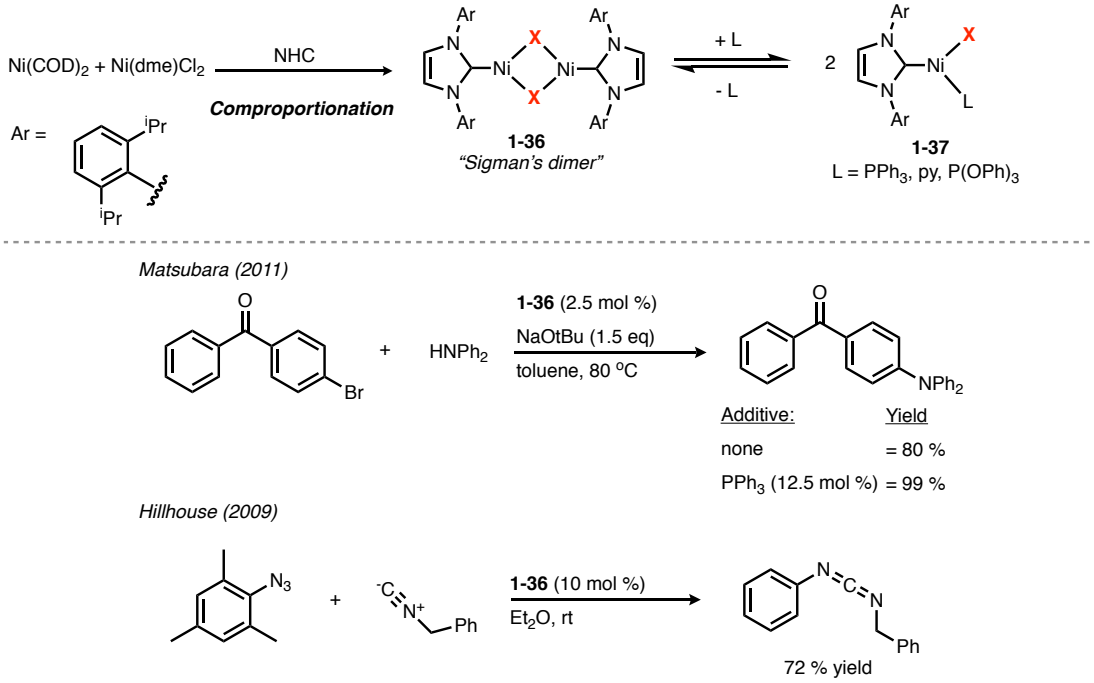


**Figure 1-21.** Sigman's dimer and select catalytic applications.

Matsubara and co-workers were also able to access monomeric (NHC)Ni(I) complexes via reacting $(IPr)_2Ni(0)$ with chloroarenes.[85] Oxidation of $(IPr)_2Ni(0)$ by aryl chloride rapidly leads to the formation of a T-shaped $(IPr)_2Ni(I)Cl$ complex (**1-38**, Figure 1-22). Computational analysis of **1-38** revealed that in contrast to previous work on pincer complexes for alkyl-alkyl couplings, the unpaired electron resided solely on the nickel center. In this same report, Matsubara demonstrated that **1-38** was a highly active pre-catalyst for Kumada couplings. A detailed follow-up on this class of Ni(I) pre-catalyst was reported by Louie and co-workers. In that report Louie was able to demonstrate that the production of three-coordinate Ni(I) complexes (**1-39**, Figure 1-22) via oxidation by aryl halide which is likely due to steric implications since it was shown that with small NHC ligands the expected four-coordinate (NHC)Ni(II)(aryl)X oxidative addition complexes resulted (**1-40**, Figure 1-22).[87] The synthesis of **1-40** was accompanied by the formation

of benzene, which is formed presumably via H-atom abstraction of THF which is the solvent. Furthermore, as part of the investigation by Louie it was shown that **1-39** does not react with aryl electrophiles, but readily transmetalates with phenyl boronic acid. It was concluded that **1-39** is formed in the first step of the Suzuki-Miyuara and Kumada couplings via radical halide abstraction yielding aryl radical. Transmetalation yields $(NHC)_2Ni(I)(aryl)$ which oxidatively adds into an aryl halide generating a Ni(III) complex prior to product forming reductive elimination.

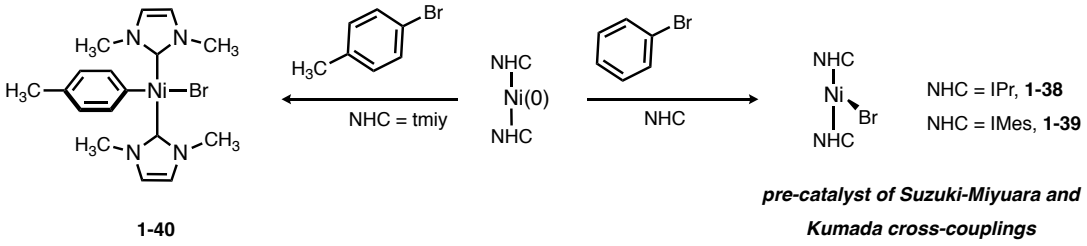


**Figure 1-22.** Ligand sterics govern the formation of Ni(I) versus Ni(II) as oxidative addition products.

Although most of the examples discussed thus far demonstrated how ligand sterics and chelation influences can promote the formation of stable Ni(I) complexes, Martin and co-workers demonstrated that Ni(I) intermediates of monodentate phosphines were crucial for silane-mediated reduction of aryl methylethers (Figure 1-23).[88] Using both computation and experimental techniques, it was concluded that the formation of Ni(I)-silyl species (**1-41**, Figure 1-23) were formed during an induction period where silane is consumed prior to the formation of product. The mechanism for the formation of **1-41** is proposed to proceed through oxidative addition of $HSiEt_3$, forming $(PCy_3)_2Ni(II)(SiEt_3)H$ (**1-42**) followed by comproportionation with $(PCy_3)_2Ni(0)$, thus creating an inactive bis-(μ-hydride)nickel(I) dimer, **1-43** and the catalytically active $(PCy_3)_2Ni(I)(SiEt_3)$ (**1-41**, Figure 1-23). Insertion of **1-41** into 2-methyoxynapthylene and elimination of $Et_3SiOMe$ forms $(PCy_3)_2Ni(I)$(napthyl) (**1-44**), which is proposed as resting state for catalysis. The assignment of a Ni(I) resting state was based on observed EPR signals for Ni(I) that formed during the induction period and persisted throughout the reaction (Figure 1-23).

Although bis-(μ-hydride)nickel(I) dimer **1-43** was not a catalytically relevant intermediate and is likely converted into a more active form. The lack of reactivity is in contrast to Chirik's bis-(μ-hydride)nickel(I) dimer **1-17**[42] which was discussed in the previous section, is highly active for alkene hydrosilylation under mild conditions.

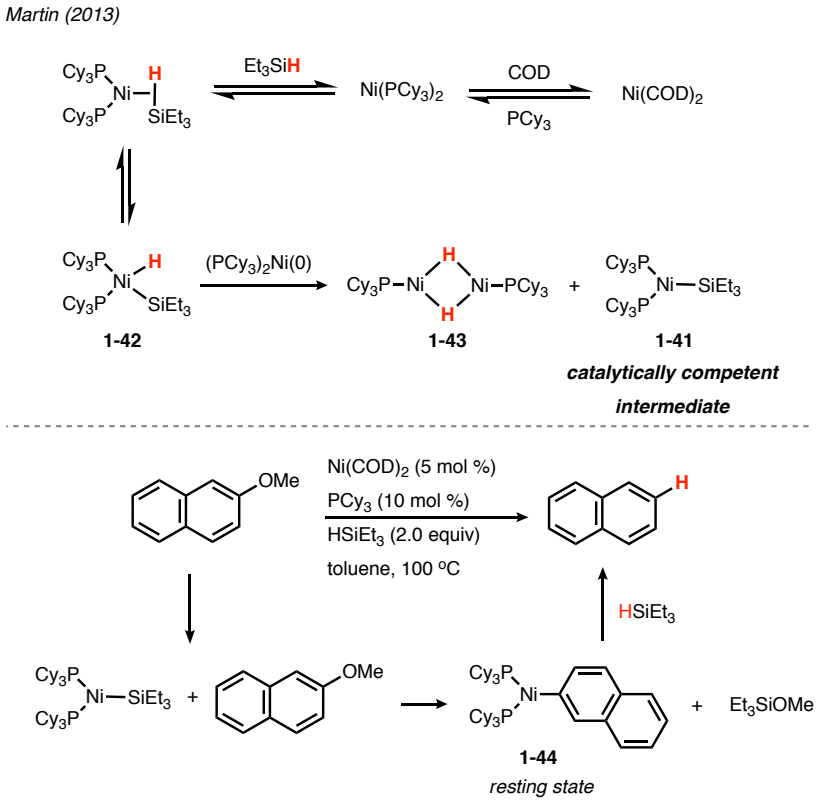


**Figure 1-23.** Ni(I)-silyl complex **1-41** generated during initiation period prior to catalysis. Top figure adapted from DOI: 10.1021/ja311940s.

Finally, active Ni(I) complexes can be accessed via metal-metal reduction by adding a super-stoichiometric amount of metal reductant. Although the use of super-stoichiometric metal reductants is not emphasized in this chapter, the use of this method for reducing Ni(II) to Ni(I) appears to be rather selective this reduction. Moreto and co-workers reported that iron powder reacted with $Ni(acac)_2$ formed catalytically relevant Ni(I) intermediates as assigned by EPR. In their study, it was proposed that Ni(I) facilitated oxidative addition required for the

cyclocarbonylation of allyl halides and alkynes. It was reported that iron powder plays dual roles during the reaction, which also turned over the catalyst in the final step of the reaction.[89]

Ni(I) complexes have been reported as off-cycle species in a variety of transformations, but in most cases they're not studied under catalytic conditions or isolated and shown to be catalytically inactive. Recently, the Hazari group has reported on the role of Ni(I) complexes that can form under catalytic conditions and have characterized organic products indicative of the formation of Ni(I), as well as, organometallic Ni(I) complexes formed along the way.[90–92] Nevertheless, when three-coordinated Ni(I) complexes with halide or sulfamate ligands are involved Ni(I) intermediates are reported as detrimental to catalytic activity

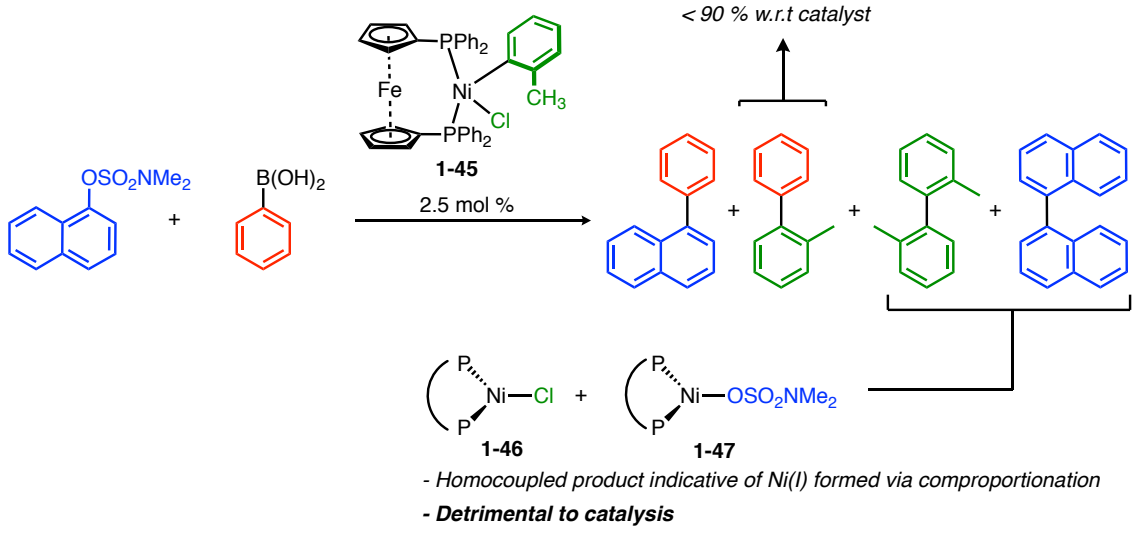


**Figure 1-24.** Pre-catalyst activation products indicate formation of Ni(I) complexes via comproportionation which are detrimental to catalysis.

In a recent report from 2017,[90] Hazari and co-workers tested (dppf)Ni(II)(σ-aryl)Cl complexes (**1-45**), previously reported by Buchwald,[21] for Suzuki-Miyaura couplings of naphthyl sulfamates and aryl boronic acids. The presumed activation of **1-45** for Suzuki-Miyaura couplings is initiated by transmetalation of phenyl boronic acid followed by reductive elimination of 2-methyl-1,1'-biphenyl (Figure 1-24). By tracking the formation of 2-methyl-1,1'-biphenyl, the

percentage of remaining un-activated catalyst can be evaluated. It was typically observed that although there was no remaining pre-catalyst in the early stages of the reaction, there was always significantly less than 90 % 2-methyl-1,1'-biphenyl as would be expected for complete consumption of **1-45**. Instead, homocoupling of the *o*-tolyl ligands and homocouplings of naphthyl sulfamates was observed in appreciable amounts. It was determined that these products indicate the formation of undesired Ni(I) complexes, such as **1-46,** which would result from comproportionation of (dppf)Ni(II)(Ar)X and (dppf)Ni(0) via mechanisms previously discussed. Decreased catalytic activity resulted in the cases where Ni(I) complexes were formed with chloride or sulfamate ligands **1-46** and **1-47**, respectively (Figure 1-24).

In summary, Ni(I) complexes proposed as propagating species in catalysis for a variety of reactions. Characterization of Ni(I) in catalytic reactions is much less common, unfortunately. A variety of demonstrations of stoichiometric reactivity of Ni(I) has been performed, but this level of investigation is not often reflected in catalytic applications. Highlighted herein are select reactions that have provided insights into the crucial role that Ni(I) intermediates play in initiating and propagating catalysis. The use of this class of pre-catalyst will especially impact $sp^3$-$sp^3$ couplings, which are particularly difficult using alternative palladium-based methods.

**Conclusion and Outlook**

Nickel pre-catalysts that can be activated under mild conditions to necessary oxidation state have benefited the widespread use of nickel catalysis for organic synthesis. There is still a growing need to develop mild pre-catalyst activations that are free of troublesome by-products that can tolerate highly sensitive environments. Herein, this chapter has highlighted several challenging scenarios for pre-catalyst activation and in many cases, the development of air-tolerant methods has enabled access to valuable nickel-catalyzed transformations. Although there are mild methods

for *in situ* generation of Ni(0) for the construction of difficult C-N bonds, highly active discrete Ni(II) and Ni(I) pre-catalysts have emerged as a promising alternative to existing methods as they offer lower catalyst loadings. The use of Ni-hydrides for catalysis have been demonstrated since the infancy of nickel-catalysis, but the way in which we synthesize Ni-hydrides has changed substantially over the years. The mild nature of methods for accessing Ni-hydride and psuedo hydrides has led to a number of examples of highly regioselective or asymmetric methods for hydrofunctionalization. The emergence of Ni(I) as a catalytically viable state and the potential to serve as an off-cycle species has impacted the way catalytic mechanisms are proposed. The work described in this chapter highlights a few examples of Ni(I) being generated and used for catalysis

Finally, the evolution of nickel-based pre-catalysts has yielded many catalyst systems that are available in different oxidation states and that host a variety of ligand environments. Many Ni(II) pre-catalysts have been developed that feature facile activations as additives are not required to mediate nickel reduction. The advent of nickel pre-catalysts designed to catalyze reactions that lack strong nucleophiles, such as π-π couplings, is an unsolved challenge. Although the development of novel nickel-catalyzed transformations does not always hinge on carefully designed pre-catalysts, the widespread use of these methods would be positively impacted by stable pre-catalyst that undergo expedient activation. Given the growing interest in applying nickel-catalysis in a variety of manifolds, it is likely that this field will continue to see rapid advancements in pre-catalyst activation technologies.

## Chapter 2 : Entrances, Traps, and Rate-Controlling Factors in Nickel-Catalyzed C-H Functionalization

*The following content is associated with these publications:*

- Nett, A.J.; Zhao, W.; Zimmerman, P. M.; Montgomery, J. Highly Active Nickel Catalysts for C-H functionalization Identified through Analysis of Off-Cycle Intermediates. *J. Am. Chem. Soc.*, **2015**, *137,* 7636-7639,

- Nett, A. J.; Montgomery, J.; Zimmerman, P. M. Entrances, Traps, and Rate-Controlling Factors for Nickel-Catalyzed C-H Functionalization. *ACS Catal.,* **2017**, *7*, 7352-7362.

### Introduction

Carbon-hydrogen bond functionalization has emerged as an atom-economical route to many interesting chemical scaffolds.[57,93,94] Although the bulk of these methods utilize second and third row transition metals, recent developments have enabled many unique and promising transformations that employ base metal catalysis.[37,57,95] Nickel catalysis is a widely recognized sustainable method for conducting a broad range of catalytic methods for C-H bond functionalization. Although nickel has been demonstrated to stoichiometrically insert into C-H bonds as early as the 1960's, bond forming catalytic turnovers of this sort were not achieved until 1990 when Saegusa and co-workers reported a method for nickel-catalyzed hydroacylation of alkynes using aliphatic aldehydes (Figure 2-1).[96] As proposed by Saegusa in 1990, there are several potential mechanisms that can be considered for this transformation. One is a route initiated by nickel-mediated C-H bond activation of the acyl C-H bond of an aldehyde followed by migratory insertion of an alkyne into the nickel-hydride bond. This mechanism was speculative due to limited

mechanistic data. Subsequent reductive elimination leads to the formation of an α,β-unsaturated ketone (Figure 2-1). Following the work of Saegusa and co-workers, the area of nickel-mediated hydrofunctionalization of alkenes or alkynes via C-H bond activation or conclusive mechanistic evidence thereof remained relatively unexplored until in the mid-2000's.

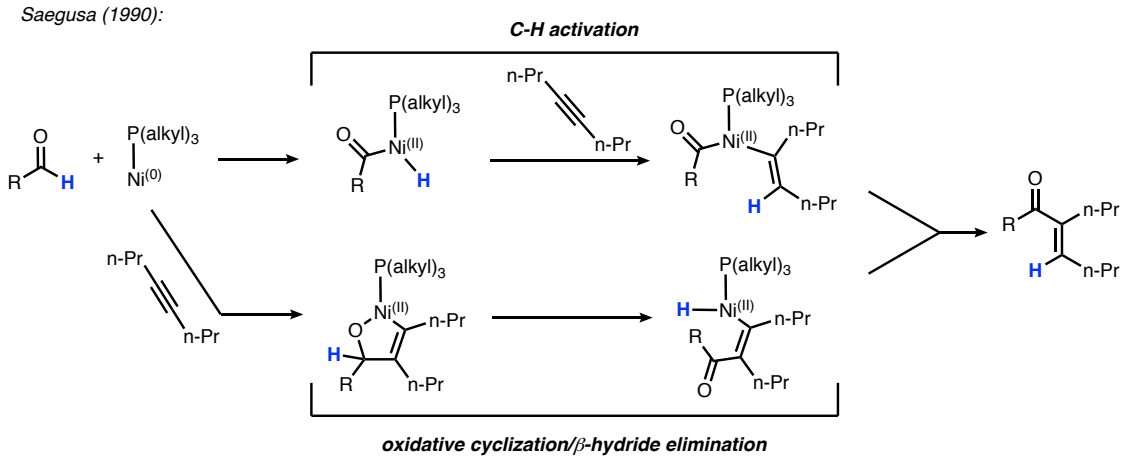


**Figure 2-1.** Proposed mechanisms for hydroacylation report by Saegusa and co-workers.

Seminal contributions to this field were made when Nakao, Hiyama and co-workers discovered unexpectedly that phosphine-supported low-valent nickel catalysts are effective for adding simple alkynes to the C-2 C-H bond of substituted indoles resulting in a net alkyne hydroarylation.[60] The robustness of this transformation shows that it tolerates a variety of five-membered heterocyclic C-H bond coupling partners. Elaboration of this work showed that nickel can efficiently activate many different acidic arene C-H bonds including perfluoroarenes, and a variety of nitrogen-, oxygen- and sulfur-containing heterocycles.[56] Although there were select examples from this initial work of C-H alkylation via alkene couplings, significant advances in this area were realized later using NHC ligands, as reported by Nakao and Hartwig.[58] It should be noted that in all of these synthetic advancements the nickel catalyst is highly selective for the most acidic C-H bond on the molecule leaving the remaining C-H bonds untouched.

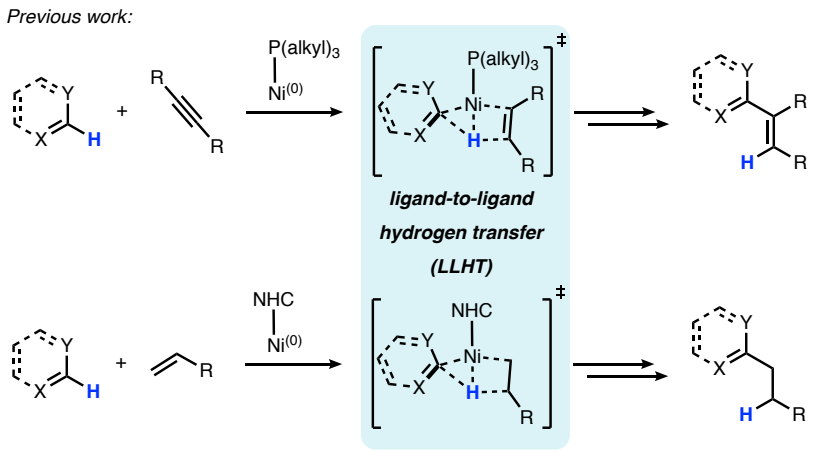


**Figure 2-2.** Ligand-to-ligand hydrogen transfer during nickel catalyzed C-H functionalization.

The area of nickel-catalyzed C-H functionalization has been supplemented with several in-depth experimental and computational mechanistic investigations which have provided many valuable details regarding the intricacies of nickel-mediated C-H bond cleavage.[59,97] Although the proposed mode of activation varies based upon reaction class, the way in which nickel activates C-H bonds during hydroarylations is unique in the sense that it avoids the formation of stable nickel-hydride intermediates. Unlike traditional C-H oxidative addition, which is operative for other transition metal catalysts, nickel-mediated C-H activation during hydroarylation processes proceeds through a concerted oxidative addition of an arene C-H bond and migratory insertion to an unsaturated coupling partner directly forming a vinyl- or alkyl-nickel specie.[59]

The use of DFT methods for describing this process was reported by Perutz, Eisenstein, and co-workers where they used density functional theory to assess the likelihood of forming a formal nickel-hydride or proceeding through a concerted transfer of the hydrogen via a transient nickel-hydride and direct transfer to the unsaturated ligand.[59] Is this seminal paper their data supported a concerted transfer mechanism, termed ligand-to-ligand transfer (LLHT), as the preferred pathway for C-H bond cleavage. Furthermore, in this report the complete mechanism for nickel/phosphine catalyzed alkyne hydroarylation was described.

Since the initial report of the LLHT mechanism it has been generally accepted as the mode of C-H bond cleavage in hydrofunctionalizations of alkynes and alkenes via C-H functionalization. The generality of LLHT in nickel-mediated C-H bond cleavage was also highlighted in a more recent discovery of nickel-catalyzed hydroacylation of alkynes via aldehyde C-H bond activation. Reported by Xu and Zhou, it was shown that nickel/phosphine catalyst systems can efficiently couple a variety of alkyl aldehydes with functionalized styrenes (Figure 2-3).[98] Given the precedent for nickel to mediate oxidative cyclization of polar π-components and simple alkynes and alkenes Xu and Zhou used DFT to investigate a mechanism where a nickellacycle is formed in the first step. Net hydroacylation would then proceed through a β-hydride elimination and reductive elimination of the product from the nickel-hydride intermediate (Figure 2-3). This pathway was deemed unlikely since the geometric constraints of 5-membered nickellacycle do not allow to proper orbital overlap necessary for facile β-hydride elimination. It was instead concluded that, similar to the hydroarylation described above, a concerted LLHT process is likely operative in these systems. This was supported by rapid scrambling of a deuterium labelled aldehyde under the reaction conditions suggesting the C-H bond cleavage event is highly reversible, but unlike alkenylation reactions, bond rotation of the nickel-$C_{alkyl}$ followed by β-hydride elimination would result in protio-aldehyde (Figure 2-3). The disclosure of the study from Xu and Zhou raises the question of whether Saegusa's initial nickel-catalyzed alkyne hydroacylation mechanism proceeds through a very similar mode of activation making Saegusa's finding the first example of nickel-mediated LLHT.[96]

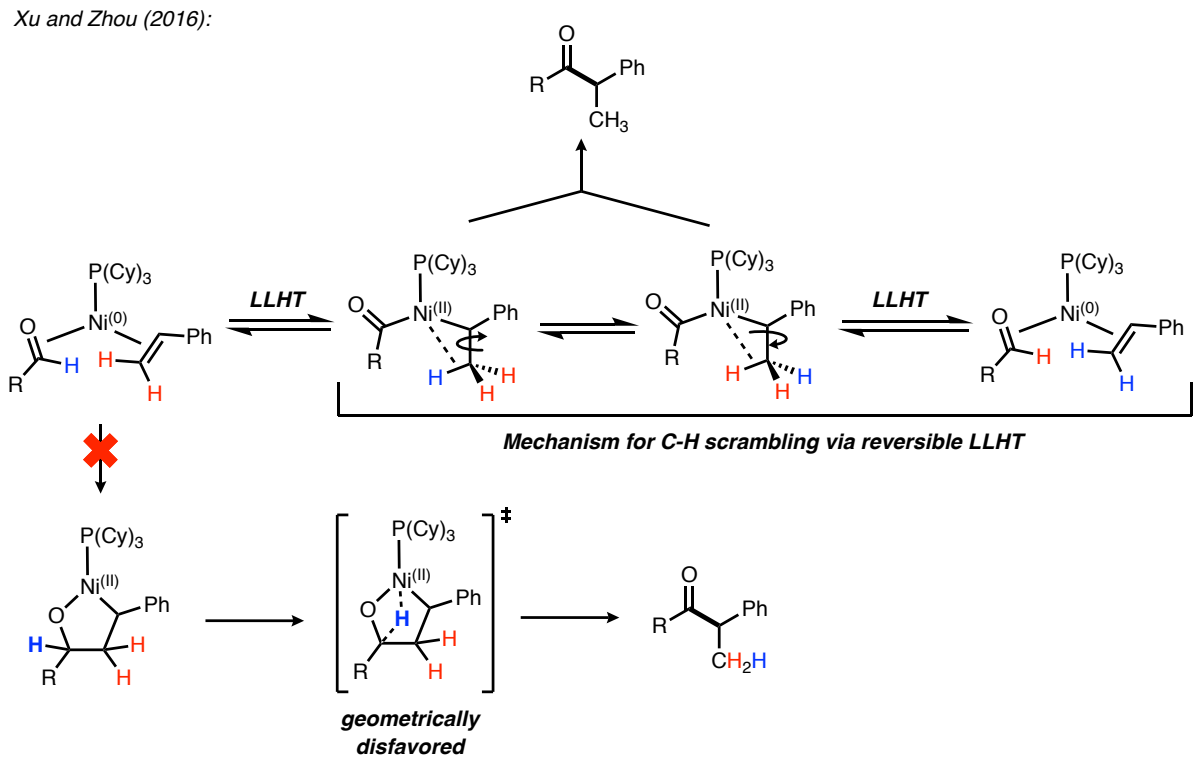


**Figure 2-3.** Hydroacylation of olefins via LLHT from aldehyde C-H bonds to vinyl arenes.

While unique reactivity, cost, and availability of nickel make it an attractive tool for promoting catalysis, nickel-catalyzed methods can often be plagued by high catalyst loadings.[3] Furthermore, limitations in substrate[71,99,100] scope and elevated reaction temperatures have hindered the widespread use of nickel-catalyzed methods for C-H functionalization.

Although many valuable transformations have been developed and mechanistic insights have been gained, little attention has been placed on the role of ancillary ligands on the nickel pre-catalyst and the potential for off-cycle intermediates that could impede efficient catalysis. In the vast majority of Ni(0)-catalyzed processes, $Ni(COD)_2$ is employed as the pre-catalyst. While a few reports have noted synthetic implications of the presence of cyclooctadiene (COD) in altering catalyst performance,[71,100] little understanding of the basis for these effects has been elucidated.

Our specific interests are in the unique capabilities and mechanistic features of nickel-based C-H functionalization catalysis, as well as the role COD-based pre-catalysts play in

promoting off-cycle activity. Furthermore, the work discussed in this Chapter will focus on elucidating mechanistic details of alkyne hydroarylation, identification of rationally designed catalysts that demonstrate improved scope and activity and development of predictive models for nickel-mediated C-H bond activation (Figure 2-4).

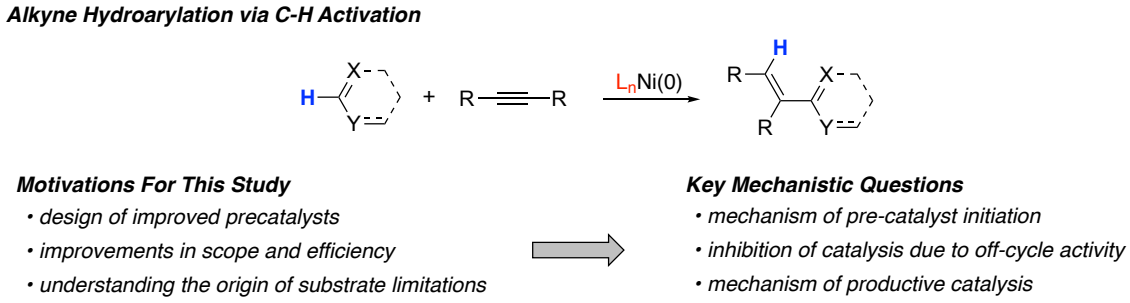


**Figure 2-4. Motivation for investigating nickel-catalyzed hydroarylation.**

## Unexpected COD-Mediated C-H Insertion

Initial insights into the role of COD in C-H functionalization processes were provided by an unexpected result while exploring the use of pentafluorobenzene-derived precursors to access Ni(0) *N*-heterocyclic carbene (NHC) complexes. Following the procedure described by Waymouth and Hedrick,[101] precursor **2-1** was treated with $Ni(COD)_2$, anticipating extrusion of pentafluorobenzene ($C_6F_5H$) and formation of the Ni(0) adduct of SIMes. To our surprise, stable Ni(II) π-allyl complex **2** was instead obtained (Figure 2-5). It is likely that formation of the expected Ni(0)-SIMes complex along with an equivalent of $C_6F_5H$ occurs, then addition of the SIMes-Ni(0) complex to $C_6F_5H$ proceeds via C-H activation. Hydride migration to bound COD followed by sequential chain walking steps ultimately forms π-allyl complex **2-2**. Whereas an analogous π-allyl complex had previously been prepared from a Ni(0) complex of P(*i*-Pr)$_3$,[61] the direct capture of the fluoroarene extruded from an NHC precursor such as **2-1** was to our knowledge unprecedented.

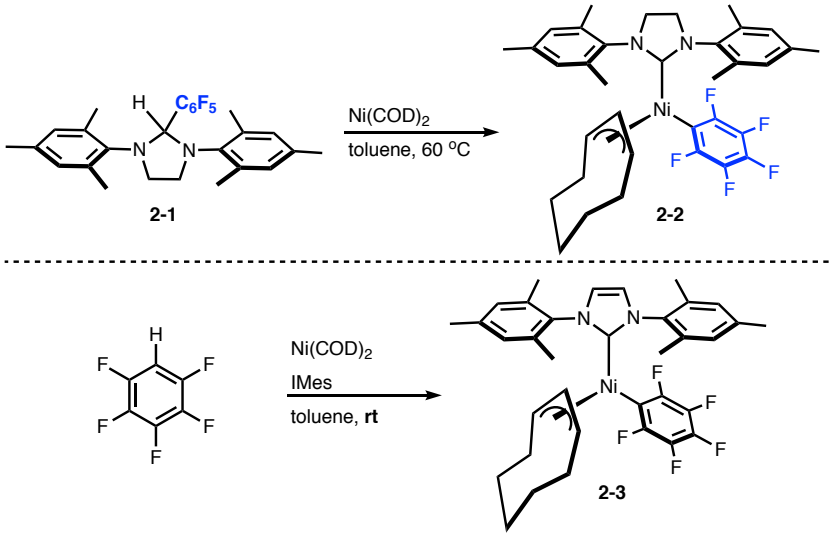


**Figure 2-5. Two routes to π-allyl formation.**

π-Allyl complex **2-3** (Figure 2-5) can be generated in a similar fashion by stirring $C_6F_5H$, IMes and $Ni(COD)_2$, in support of the mechanism postulated above. Although **2-2** was not characterized by x-ray diffraction, the structure of **2-3** was confirmed by x-ray analysis (Figure 2-6). The rapid and efficient capture of low concentrations of $C_6F_5H$ formed during generation of NHC-Ni(0) complexes raised the question of the impact of this process in arene C-H functionalizations. Given the widespread employment of $Ni(COD)_2$ as a pre-catalyst, these observations suggest that complexes analogous to **2-2** and **2-3** could be potentially playing a role during nickel-catalyzed arene C-H bond functionalization.

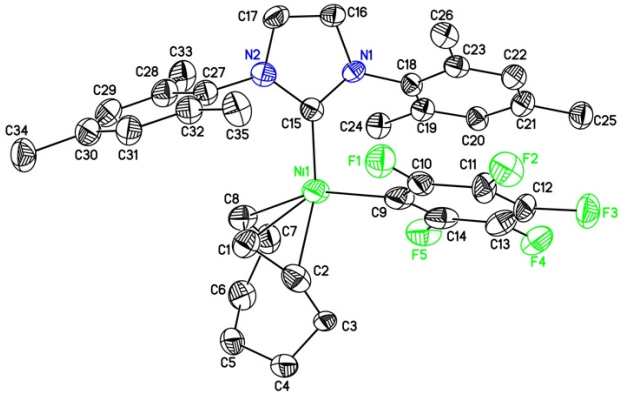

**Figure 2-6.** ORTEP diagram of **2-3** showing 50 % probability thermal ellipsoids. Hydrogen atoms have been omitted for clarity. Structure solved by Dr. Jeff Kampf.

To elucidate the mechanism for the formation of **2-3**, reaction discovery methods developed in our laboratory were employed. These methods hypothesize and evaluate plausible elementary reaction steps,[102,103] providing detailed descriptions of thermodynamics and kinetics at a rapid pace.[103–105] Although the use of transition metal-mediated chain walking, specifically with nickel, has shown great synthetic value,[42,106–108] there are limited examples of β-agostic interactions in neutral nickel complexes.[109–113] Therefore, the pathways to **2-3** from **2-4** were investigated in detail.

Although at the time of this finding computational details regarding C-H activation for couplings alkynes was known, reaction discover tools developed in the Zimmerman group were employed to probe various pathways for C-H bond cleavage. The method used in this case was Zstruct[102,103,114] which uses a graph-based approach to propose intermediates that may arise in a single elementary step from a given starting structure. This method in combination with the growing string method (GSM)[103–105] for identifying transition states allowed us to realize mechanistic details that would have otherwise been overlooked by intuition-guided mechanistic inquiries. This double-ended approach greatly reduced the degrees of freedom for a specific transformation which expedites reaction path calculations. Advancements in both the Zstruct and growing string methods have evolved by integrating intermediate finding and transition state searching which allows a path to be calculated starting from a single structure and a set of driving coordinates. The driving coordinates in this case are user input that describes the desired structural features of the product. These typically contain key information about bond making and breaking steps but can also include information regarding torsions and angles.[105]

The resulting mechanism predicted via this method starts from complex **2-4**, and cleavage of the C-H bond in pentafluorobenzene proceeds through LLHT to COD (Figure 2-7). This process has a relatively low barrier of 5.5 kcal/mol (**TS-2-4-5**) and is exergonic by -11.5 kcal/mol (**2-5**). Intermediate **2-5** has a strong β-agostic interaction with the newly formed C-H bond and consequentially is slightly elongated (Figure 2-7). While this activation opens the possibility for β-hydrogen elimination and reinsertion to walk around the ring, we also found a second mechanism could be operative. The second case involves reversing the LLHT C-H activation at a unique COD hydrogen, permuting the ring's attachment point to nickel.

These two possible mechanisms were studied, the first involving traditional chain walking, and the second involving nontraditional H-transfer directly to the C-H activated ligand. Both mechanisms begin at agostic complex **2-5**, where rotation of the Ni-$C_{COD}$ bond (via **TS-2-5-6**) transfers the agostic interaction towards a productive alignment for π-allyl formation (**2-6**, Figure 2-7). At this point (**2-6**) the two mechanisms for π-allyl formation diverge, where traditional chain walking through β-hydride elimination results in a nickel-hydride complex (**2-7a**), or alternatively LLHT reforms the C-H bond in pentafluorobenzene (**2-7b**, Figure 2-8).

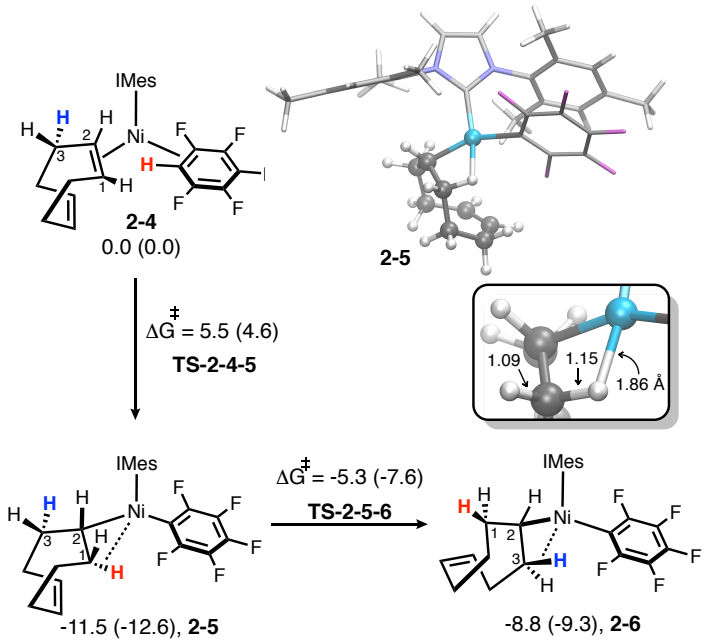


**Figure 2-7.** Agostic transfer from Ni-H-C1 to Ni-H-C3. All free energies (/ ω B97X-D/cc-pVTZ/SMD) in kcal/mol, with enthalpies in parenthesis.

For traditional chain walking, β-hydride elimination forms an unstable and short-lived square planar nickel hydride complex **2-7a**, where the hydride is *trans* to the carbene. The endergonic nature of **2-7a** is consistent with β-agostic C-H bonds to nickel generally being stronger than the analogous Ni-H bonds.[112,113] Through a nearly barrierless transformation (**TS-2-7a-8**), the newly formed olefin in **2-7a** inserts into the nickel-hydride to give agostic complex **2-8,** where the ring is one carbon closer to the second olefin. In analogous steps to the **2-5, 2-6, 2-7a, 2-8** sequence, the pathway through **2-8, 2-9, 2-10a, 2-11** walks the ring to position the C-Ni bond proximal to the olefin. From **2-11**, transfer of the σ-allyl-Ni interaction to π-allyl coordination results in complex **2-3**, which is exergonic by 31.4 kcal/mol from **2-4** (Figure 2-8).

Alternatively, hydrogen transfer (LLHT) to the pentafluorobenzene ligand in **2-6** allows chain walking without the formation of any discreet nickel hydride intermediates. The 5.8 kcal/mol barrier for LLHT from $C3^{COD}$ to pentafluorobenzene (**TS-2-6-7b**, Figure 2-8) is consistent with

the reverse of the C-H activation LLHT step forming **2-4** from **2-5** (Figure 2-7). By placing the H on pentafluorobenzene, rather than on nickel, the barrier for a single chain-walking step is similar to traditional chain walking, but the resulting intermediate (**2-7b**) is much more stable, at 4.8 kcal/mol below **2-7a**. LLHT from pentafluorobenzene back to 1,4-cyclooctadiene results in complex **2-8**, which marks the completion of a single chain walking step. Repeating the LLHT swapping process ultimately leads to the formation of **2-3**, as shown in Figure 2-8.

The early steps to the formation of **2-3** show that chain-walking via transient nickel-hydrides or iterative LLHT are energetically similar. Later in the pathway, there is an energetic preference to proceed through reversible LLHT as a means of olefin migration. Nevertheless, both pathways are kinetically feasible at room temperature and likely compete to reach formation of **2-3**. The exergonic nature of the formation of **2-3** (Figure 2-8) suggests that complexes analogous to **2-3** may be associated with an off-cycle resting state that diminishes productive catalysis.

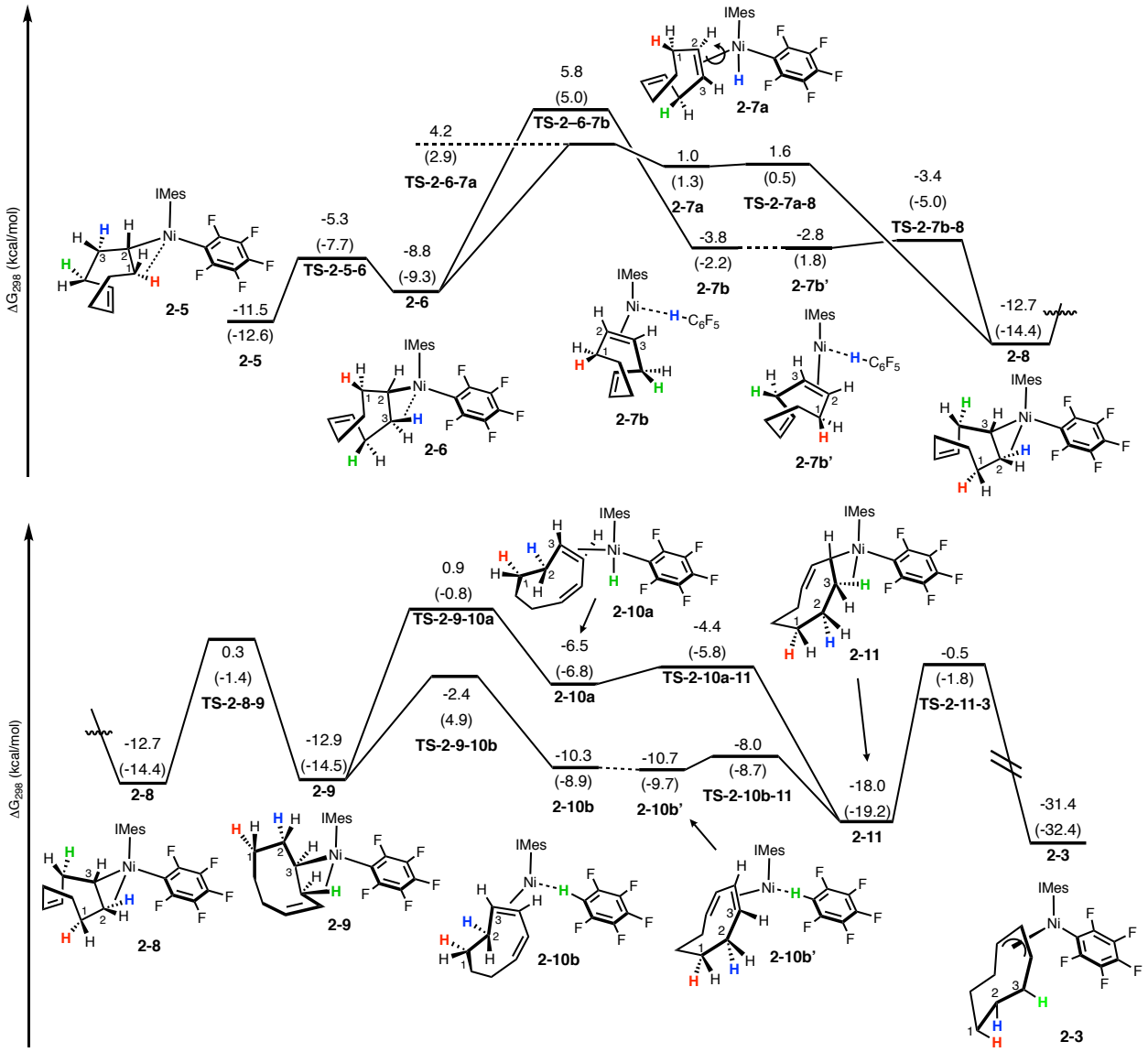


**Figure 2-8.** Complete mechanism for chain walking via iterative nickel-hydride formation and LLHT. All free energies ( $\omega$ B97X-D/cc-pVTZ/SMD) in kcal/mol, with enthalpies in parenthesis.

## Implications of COD-Based Off-Cycle Activity on Catalysis

Following the seminal precedent from Nakao and Hiyama,[56] the coupling of 4-octyne with $C_6F_5H$ to generate product **2-12** was used as a test case, monitoring reactions using $^{19}F$ NMR (Figure 2-9). When a catalyst derived from 10 mol% $Ni(COD)_2$ and free IMes was used, the reaction was very slow at room temperature, resulting in a 2% yield after 1 h. Notably,

characteristic $^{19}F$ peaks associated with **2-3** were observed in low concentrations throughout the reaction. At 80 °C, product formation was observed, and a yield of 60% was obtained after 1 h (Figure 2-9a). π-Allyl complexes **2-2** and **2-3** as pre-catalysts for the coupling of 4-octyne and $C_6F_5H$ were unreactive at room temperature but afforded an 80 and 83% yield, respectively, upon stirring at 80 °C for 3 h. We thus considered that forming **2-3** in reactions using $Ni(COD)_2$-derived catalysts might inhibit catalysis throughout the reaction; alternatively, it may slowly release a more active form of the catalyst following an induction period.

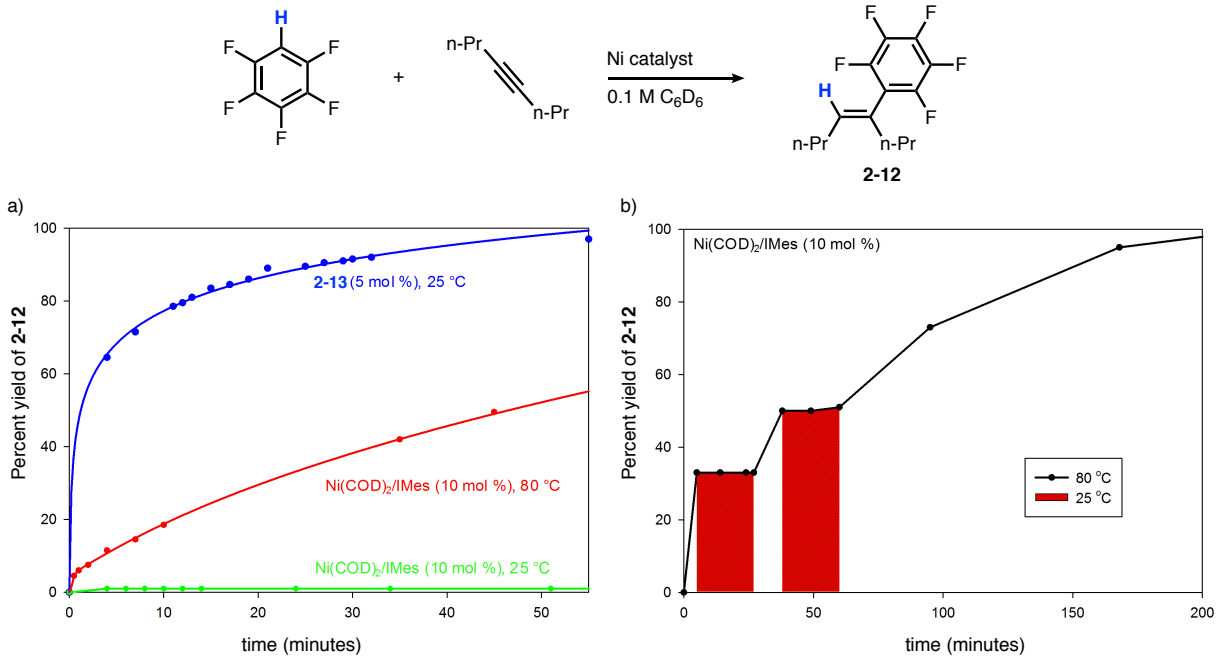


**Figure 2-9.** (a) Reaction progression plots showing the formation of **2-12** over time. (b) Reaction progression plot using $Ni(COD)_2$/IMes with temperature cycles between 80 and 25 °C. In the cases where $Ni(COD)_2$/IMes was used the two were pre-stirred in $C_6D_6$ for 15 minutes.

To address this question, the reaction using $Ni(COD)_2$/IMes was heated to 80 °C for 5 min to initiate catalysis. The $^{19}F$ NMR spectrum illustrated a 33% yield, and after 20 min at room temperature, the yield remained unchanged (Figure 2-9b). This procedure was repeated for another heating/ cooling period, and similar results were observed. Notably, under these reaction conditions no allyl-$C_6F_5H$ is observed that would result from reductive elimination of **2-3**. Given

the high barrier for the reversion of **2-3** to **2-4**, the conversion of **2-3** to an active catalyst likely proceeds through a ligand substitution of the alkyne with an alternative intermediate. This outcome suggests that **2-3** is formed as an off- cycle resting state that persists throughout the entire reaction and that replacement of COD with an alternative ancillary ligand might increase overall reaction rates.

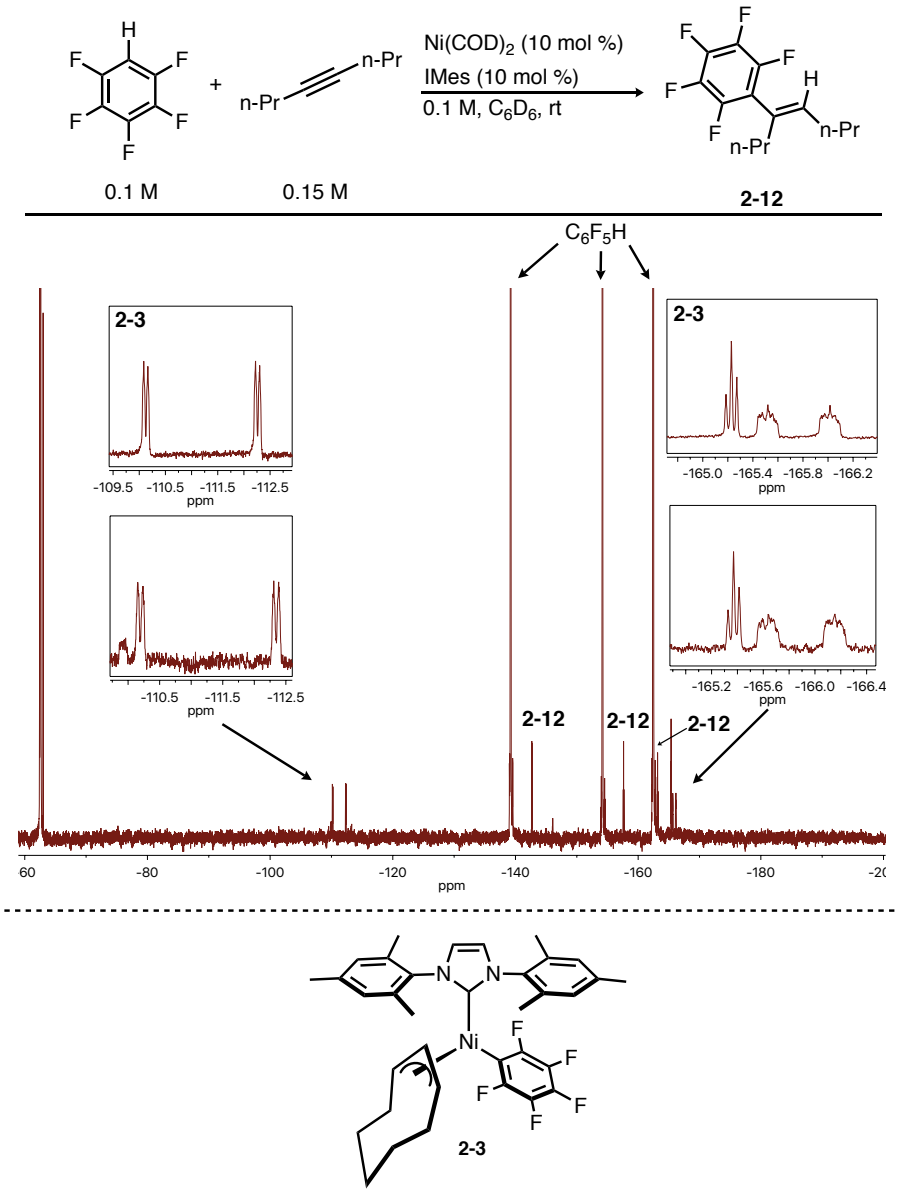

**Figure 2-10.** Reaction monitored by $^{19}F$ NMR which shows the presence of **2-3** in a productive reaction. The full spectrum and lower inlays are of the catalytic reaction. The upper inlays are of independently synthesized complex **2-3**.

Other than $Ni(COD)_2$, there is an absence of commercially available Ni(0) compounds that lack either strong donors, which lead to coordinatively saturated NHC complexes, or π- acidic ligands, which typically lead to considerably lower reactivity.[99] *In situ* reduction of Ni(II) sources is commonly employed in nickel catalysis, but the limited solubility of nickel halides restricts solvent choice. The reactivity of the $(iBu)_2Al(acac)$ byproduct can also complicate catalytic reactions that utilize DIBAL-H reduction of $Ni(acac)_2$.[115] Furthermore, *in situ* reduction of Ni(II) and coordination of an NHC ligand result in poorly defined catalysts that are difficult to generate in a controllable fashion. For these reasons, identifying a well-defined NHC-Ni(0) pre-catalyst that can be generated in the absence of COD, strong donor ligands, or strong π-acids is highly desirable for C−H activation processes. With these criteria in mind, the 1,5-hexadiene-supported NHC-Ni(0) complexes developed by Hazari are an especially attractive catalyst class to consider (Figure 2-11).[15]

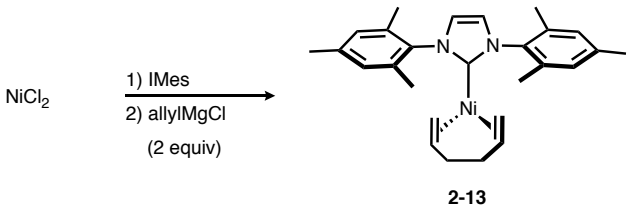


**2-13**

**Figure 2-11.** Synthesis of 1,5-hexadiene supported nickel-complexes from stable Ni(II) precursors.

## 1,5-Hexadiene Support IMes-Ni(0) Pre-Catalyst Diminishes Off-Cycle Activity

These complexes may be prepared by adding allylmagnesium chloride to a solution of ligand (i.e., NHC or phosphine) and $NiCl_2$, which generates the 1,5-hexadiene Ni(0) complex by reductive elimination of the Ni(II) bis-allyl intermediate. The 1,5-hexadiene complexes span a

range of NHCs, providing access to well-defined NHC-Ni(0) complexes. The IMes variant **2-13** was isolated and tested for catalytic activity. Interestingly, when **2-13** was used as a catalyst (5 mol%) for the coupling of $C_6F_5H$ and 4-octyne, high yields at room temperature after 1 h were observed (Figure 2-9). This significant increase in efficiency suggested that off-cycle activity involving the ancillary ligand was greatly diminished.

To test the role of diene ligands on catalysis COD and 1,5-hexadiene were used as additives to either promote on- or off-cycle activity. As shown in Table 2-1 the overall efficiency of $Ni(COD)_2$/IMes catalyzed reactions was positively impacted by the addition of 1,5-hexadiene. Dosing in 10 and 20 mol % 1,5-hexadiene prior to catalysis boosted the overall yield of desired product to 27 and 30 % respectively, compared to 8 % with no 1,5-hexadiene (Table 2-1). It should be noted that although the reaction benefited from the addition of 1,5-hexadiene, doubling the amount from 10 to 20 mol % only resulted in a 3 % increase in overall product yield. This demonstrates that the inhibitory role of COD will still impact reaction efficiency even in low concentrations. Likewise, the addition COD to reactions that are catalyzed by **2-13** were drastically inhibited due to the promotion of off-cycle formation of products analogous to **2-3** (Table 2-1).

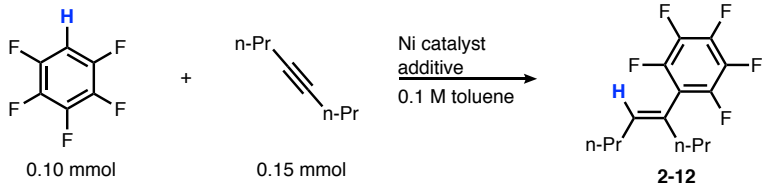


| entry | pre-catalyst | additive | amount | % yield |
|---|---|---|---|---|
| 1 | $Ni(COD)_2$/IMes | none | -- | 8 |
| 2 | $Ni(COD)_2$/IMes | 1,5-hexadiene | 10 mol % | 27 |
| 3 | $Ni(COD)_2$/IMes | 1,5-hexadiene | 20 mol % | 30 |
| 4 | **2-13** | none | -- | 93 |
| 5 | **2-13** | COD | 20 mol % | 50 |
| 6 | **2-13** | COD | 40 mol % | 30 |

**Table 2-1.** Effects of diene additives on reaction efficiency. Reactions using $Ni(COD)_2$/IMes were conducted with 10 mol % catalyst loading. Reactions using **2-13** as a catalyst were conducted with 5 mol % catalyst loading.

In principle, a π-allyl complex analogous to **2-3** could form as a result of direct insertion of 1,5-hexadiene (**2-14**, Figure 2-1). In an effort to determine the accessibility of **2-14**, the mechanism and feasibility of its formation were computationally examined. Following a similar path as described for COD, the LLHT reaction has a net barrier of 26.3 kcal/mol (**TS-2-13-15**), suggesting that the formation of **2-14** is not kinetically feasible at room temperature (Figure 2-12). The increased barrier is hypothesized to be a result of the inherent stability of **2-13**. It is plausible that the increased barrier for the formation of **2-14** stems in part from the terminal alkene being less electron-rich than an internal alkene. This could also be an artifact of the inherent stability of **2-13** versus analogous COD-based structures which will be discussed later in this Chapter. Either of these factors will result in more difficult LLHT. Treatment of $C_6F_5H$ with **2-13** returned only starting material at room temperature, and no evidence for the formation of **2-14** was obtained by $^{19}F$ NMR analysis of the reaction mixture. Therefore, both computation and experiment suggested that **2-13** does not activate $C_6F_5H$ at rt. Upon heating to 60 °C, NMR analysis suggests the formation of various isomers of **2-14**.

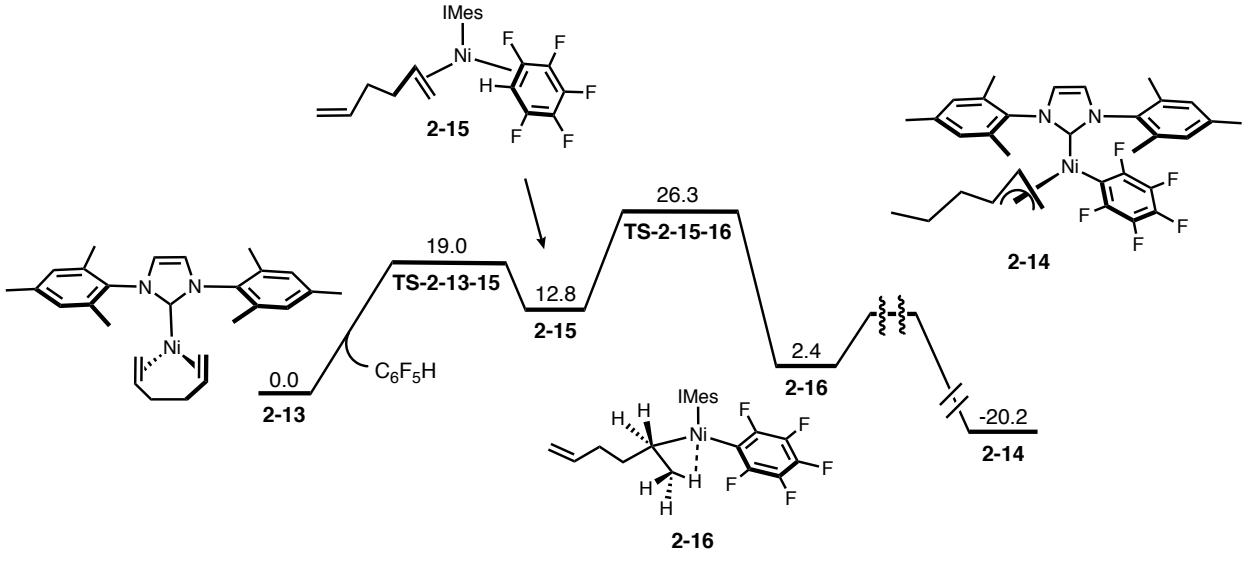


**Figure 2-12.** Mechanism for entry to off-cycle π-allyl formation stemming from **2-13.**

Comparing the two reaction pathways for off-cycle activity of COD and 1,5-hexadiene based systems (Figure 2-7 and Figure 2-12) it becomes clear that the barrier for C-H LLHT with COD (5.5 kcal/mol) is kinetically feasible at room temperature, whereas 1,5-hexadiene (26.3 kcal/mol) is not. Therefore, in the presence of COD, off-cycle activity forming complexes analogous to **2-3** becomes operative leading to a significant decrease in reaction efficiency. As a result, elevated reaction temperatures are necessary for productive catalysis with COD-based catalyst systems.

With highly active pre-catalyst **2-13** in hand, the inhibitory role of COD on hydroarylation via LLHT C-H activation could be tested on a variety of substrates (Figure 2-13). Efficient coupling of 4-octyne with fluoroarenes and fluoropyridine was observed at room temperature when using **2-13** as a pre-catalyst, whereas $Ni(COD)_2$/IMes based systems were inefficient under the same reaction conditions (**2-12** and **2-17**, Figure 2-13). Significant increase is catalytic activity for **2-13** versus COD-based systems was observed for benzoxazole resulting in nearly quantitative yields when using **2-13**. For less activated substrates like benzofuran and benzothiophene the differences between the two catalyst systems were less pronounced, but **2-13** outperformed $Ni(COD)_2$/IMes (**2-19** and **2-20**, Figure 2-13). The benefits of removing COD from the reaction mixture is also evident for substrates that require exogenous Lewis acid activation like 1,3-dimethyluracil (**2-21**).

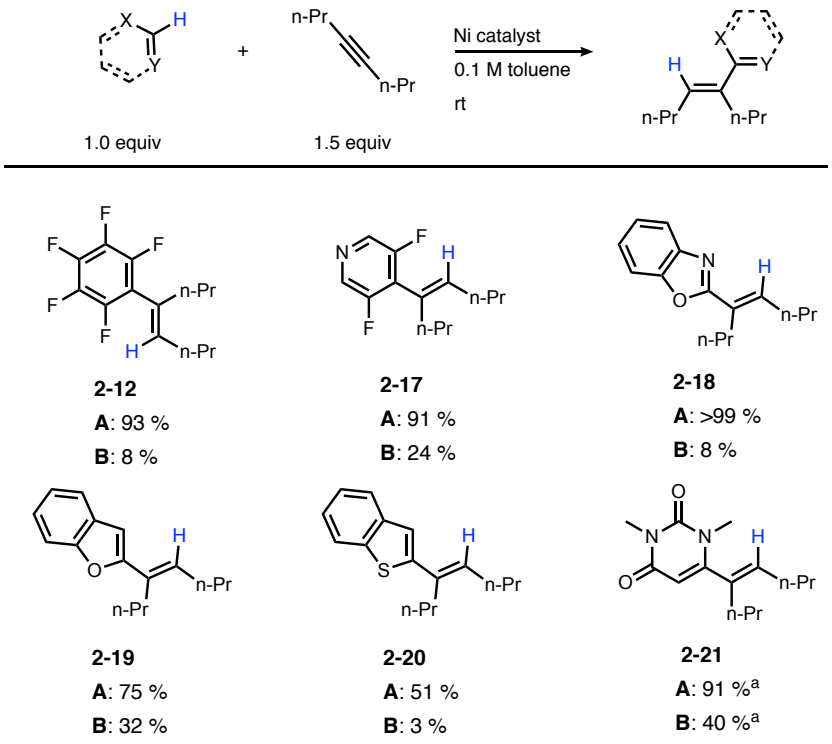


**Figure 2-13.** Pre-catalyst comparison. Yields shown are of isolated product. Procedure **A**: 5 mol % **2-13**. Procedure **B**: 10 mol % $Ni(COD)_2$/IMes pre-stirred for 15 minutes prior to the addition of substrates. [a]20 mol % $AlMe_3$ used as a co-catalyst.

Despite COD being widely used as a stabilizing ligand for Ni(0) precursors, it can have significant inhibitory effects on C-H functionalization catalysis. This is a result of low barrier pathways that promote COD-mediated C-H bond cleavage via a LLHT ultimately forming π-allyl complexes which thermodynamically limit productive catalysis. Adapting to a COD-free catalyst, like **2-13**, can diminish off-cycle activity resulting in highly active nickel-catalyzed C-H functionalization at room temperature.

## Mechanism for Hydroarylation of Alkynes via C-H Functionalization

### Pre-Catalyst Initiation

To fully understand the relationship between choice of pre-catalyst and entry into either productive catalysis or off-cycle $\pi$-allyl formation, we began assessing hydroarylation pathways

starting from either IMes-Ni-COD, **2-22**, or the analogous 1,5-hexadiene stabilized pre-catalyst, **2-13**. The model system was chosen to be the coupling of 4-octyne and $C_6F_5H$, and various intermediates that form via ligand substitution en route to the active catalyst were investigated (Figure 2-14). The binding energy of 1,5-hexadiene to the Ni center in **2-13** is 15.6 kcal/mol more stable than **2-2**, which explains why **2-13** is isolable, but **2-22** must be made *in situ*. The origin of this difference in binding energy can be explained based on the relative geometry of the olefins bound to nickel. A detailed investigation of this concept for $Ni(C_2H_4)_4$ was done by Hoffman and co-workers which describes that the difference in binding energy of co-planar olefins (i.e. 1,5-hexadiene) versus orthogonally bound olefins (i.e COD). Since the σ-donor geometry is independent of olefin binding geometry, it is proposed to result from the π*-orbitals of the co-planar olefins stabilize orbitals xy and $x^2$-$y^2$, whereas the π*-orbitals of the orthogonally bound olefins stabilizing xz and yz based orbitals.[116] From these two precatalysts, Figure 2-14 shows the thermodynamic landscape leading to the most plausible intermediates of active catalysis.

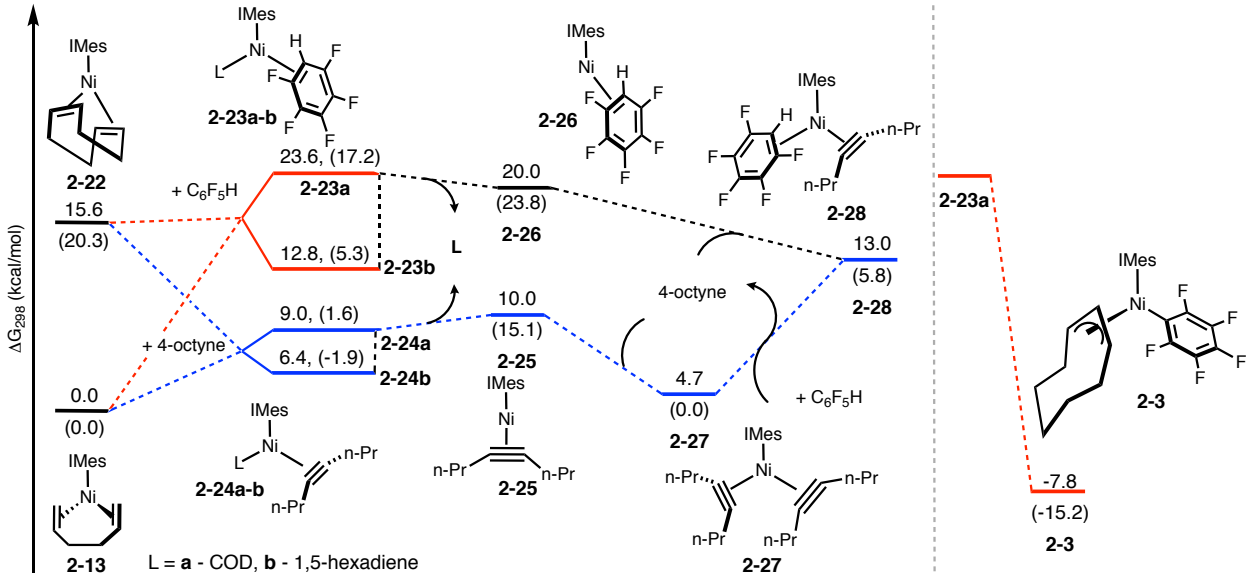


**Figure 2-14.** Thermodynamic map of intermediates preceding catalysis. All free energies (ωB97X-D/cc-pVTZ/SMD) in kcal/mol. Enthalpies are shown in parentheses in kcal/mol. Red: leads to off-cycle pathways. Blue: leads to product forming catalysis.

From **2-22**, pentafluorobenzene addition to form complex **2-23a** is endergonic by 8.0 kcal/mol, whereas the coordination of 4-octyne is exergonic by 6.6 kcal/mol (**2-24a**). In each case, one of the Ni-$\pi$ bonds is displaced to produce 3-coordinate Ni-complexes. The preference for octyne over pentafluorobenzene is likely due to increased back-bonding by alkynyl ligands compared to $\eta^2$-arene $\pi$-coordination. From precatalyst **2-13**, coordination of either substrate is endergonic due to the stability of the 1,5-hexadiene complex. This endergonicity holds for full dissociation of the diene ligand from **2-23** or **2-24** to yield 2-coordinate complexes with 4-octyne (**2-25**) or pentafluorobenzene (**2-26**). Coordination of an additional 4-octyne to **2-25** forms three-coordinate complex **2-27**, which is exergonic by 5.3 kcal/mol from **2-25**. Likewise, coordination of 4-octyne to **2-26** leads to complex **2-28**, which is the first species taking part in productive catalysis. Although complex **2-28** with an arene and an alkyne is needed for catalysis, the bis-alkyne intermediate **2-27** is 8.3 kcal/mol more stable (Figure 2-14).

Overall, the computational analysis suggests that regardless of pre-catalyst choice, the most thermodynamically favorable ligand substitution proceeds with 4-octyne, through intermediate **2-25**. Attachment of another 4-octyne is thermodynamically favorable and leads to complex **2-26** where the nickel center is coordinated to two alkyne ligands (blue, Figure 2-14). Precatalyst initiation via ligand substitution thus requires alkyne as the first substrate.

**Potential Energy Surface for Catalysis**

Having established the mechanistic aspects of off-cycle activity, the mechanism for product-forming catalysis was investigated. Using **2-13** as an energetic reference, catalysis conceptually begins with intermediate **2-28**, where the NHC-Ni(0) is ligated by 4-octyne and pentafluorobenzene (LLHT to 1,5-hexadiene was previously shown to be implausible due to its high activation barrier). From **2-28**, C-H activation proceeds through LLHT from

pentafluorobenzene to 4-octyne (**TS-2-28-29**, Figure 2-15) with a barrier of 8.9 kcal/mol. This pathway is relatively low barrier because it leads directly to stable β-agostic complex **2-29**, which is 9.3 kcal/mol downhill from **2-28** (Figure 2-15) and avoids high energy Ni-hydride intermediates. C-H activation was previously demonstrated to be reversible for related systems[58,98,117] and this is consistent with the reverse reaction (**2-29** to **2-28**, with a 16.8 kcal/mol barrier) being kinetically feasible. To achieve C-C bond forming reductive elimination from **2-29**, cleavage of the β-agostic interaction and rotation of the nickel-$C^{vinylic}$ bond is required. Rotation of the vinyl-nickel bond to form complex **2-30** has a 13.8 kcal/mol barrier through **TS-2-29-30**. From **2-30**, reductive elimination via **TS-2-30-31** has a barrier of 16.8 kcal/mol to form **2-31**, which has bidentate coordination of the product to the nickel center and is exergonic by 7.9 kcal/mol from **2-30**. Alternatively, reductive elimination could be assisted by coordination of an additional equivalent of 4-octyne to form four-coordinate complex **2-32**. Although complex **2-32** is higher in energy than **2-30** by 12.7 kcal/mol, reductive elimination from **2-32** proceeds through **TS-2-32-33a** and requires 18.9 kcal/mol which is only 2.5 kcal/mol above **TS-2-30-31** (Figure 2-15). Reductive elimination from **2-32** results in the formation of three-coordinate complex **2-33a**, 16.6 kcal/mol downhill from **2-32**. The free energy for reductive elimination from **2-32** is in part due to negative entropy of association, where the enthalpic requirement for **TS-2-32-33a** is 7.2 kcal/mol lower than **TS-2-30-31**. With an excess of 4-octyne in the reaction mixture, **2-32** will be further populated, and **TS-2-32-33a** will likely be more prevalent.

To complete the catalytic cycle, **2-31** or **2-33a** returns to an active catalytic species via substitution of the newly formed styrenyl product with 4-octyne. This mechanism proceeds via **2-31** by addition of 4-octyne, giving **2-33b**, 1.3 kcal/mol downhill from **2-31** (Figure 2-15). Next,

complete dissociation of the styrenyl product from **2-33** by coordination of an additional equivalent of 4-octyne reforms **2-27**.

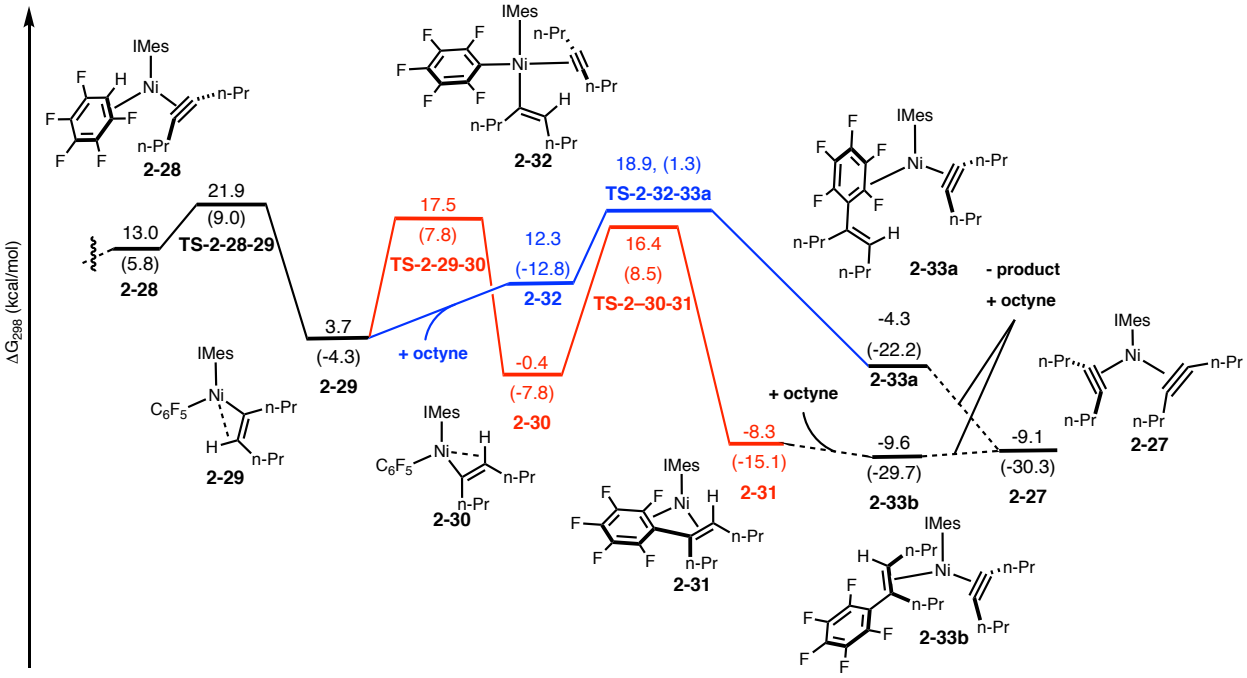


**Figure 2-15.** Mechanism for Ni-IMes catalyzed hydroarylation of alkynes, referenced to **2-13**, **Figure 2-14**. All free energies ( $\omega$ B97X-D/cc-pVTZ/SMD) in kcal/mol, with enthalpies in parenthesis. Red - three-coordinate reductive elimination pathway. Blue - four-coordinate reductive elimination pathway.

The data shown in Figure 2-15 suggest that either reductive elimination from a three-coordinate (**TS-2-30-31**) or a four-coordinate (**TS-2-32-33a**) intermediate is rate limiting. The net-change in free energy for the transformation is -13.8 kcal/mol (Figure 2-14 and Figure 2-15). The assignment of rate-limiting reductive elimination contrasts a related study using phosphines, where rotation of the vinyl-nickel bond prior to reductive elimination was proposed to be rate-limiting.[59]

## Experimental Kinetics

Since the two pathways for reductive elimination (Figure 2-15) are similar in energy, we next investigated the reaction profile using experimental kinetic analysis to provide further insights into the complete mechanism. Specifically, NMR was used to continuously monitor the progress

of the reaction, generating profiles shown in Figure 2-16a-c. Although the computations described above (Figure 2-15) used pentafluorobenzene as the arene substrate, the rapid rate of reaction with this substrate made it challenging to obtain reliable rate data. Therefore, the coupling of 3,5-difluoropyridine, a less activated arene, and 4-octyne was used to study the kinetics of these processes (Figure 2-16).

Protocols from Reaction Progress Kinetic Analysis (RPKA), including "different-excess" and "same-excess," were also used to identify the concentration dependencies on the rate of the reaction and catalyst stability, respectively.[118,119] In these experiments, "different excess" refers to varying the difference in initial concentration of alkyne and arene. "Same excess" experiments adjust the initial concentrations of substrates while maintaining the same absolute difference in initial concentration of alkyne and arene. The significance of "same excess" is that these conditions represent the same reaction started from different points. The initial conditions are calculated such that the initial substrate concentrations for one reaction equals those of a second same excess reaction when it reaches a chosen conversion level, e.g., 25-50%. From that conversion onward, these two reactions should exhibit identical rates since they exhibit identical substrate concentration. "Overlay" between the two kinetic profiles indicates that the catalyst is robust, while a difference in rates between the two reactions implicates either catalyst deactivation or product inhibition.

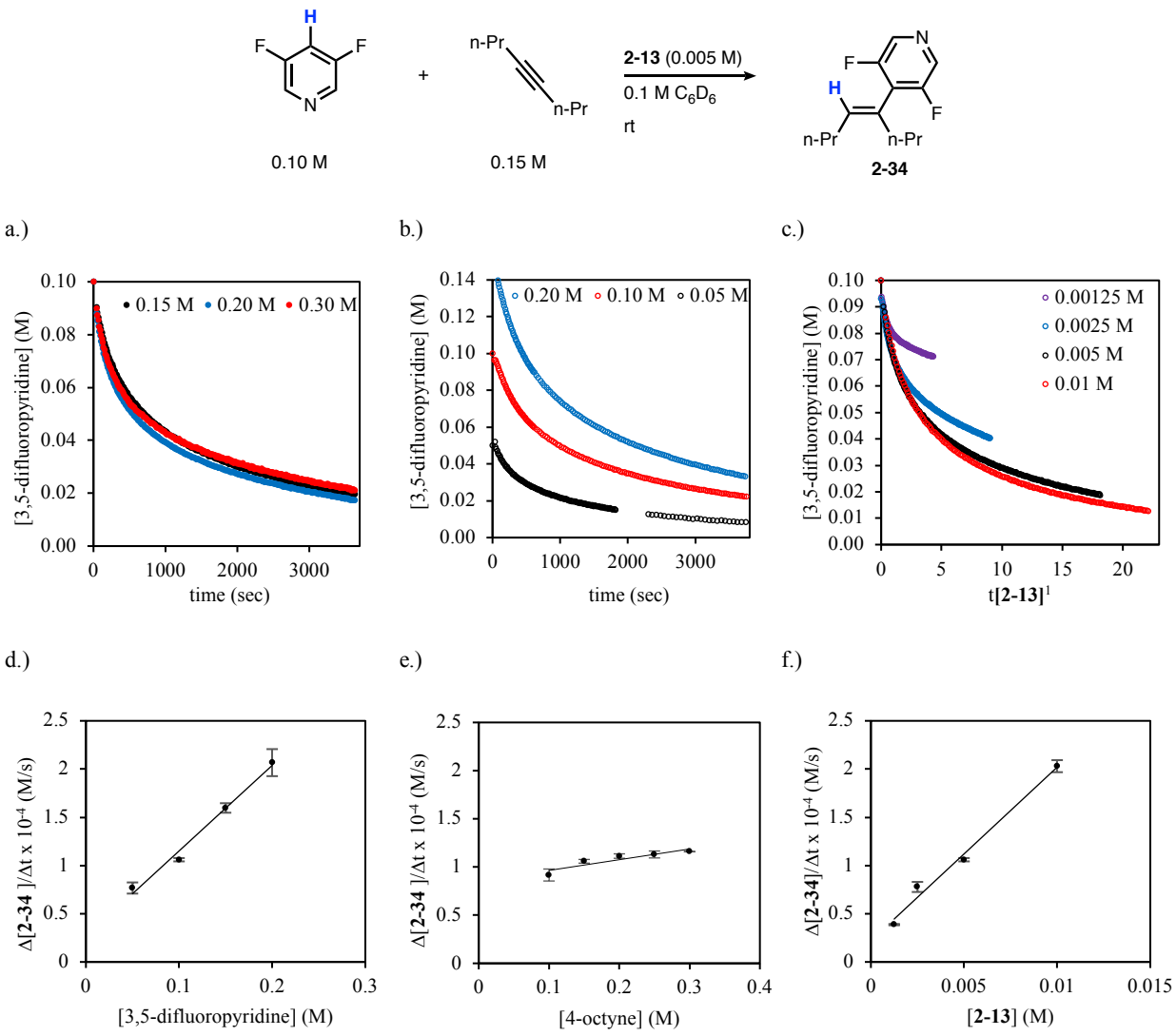


**Figure 2-16.** Plots of the initial rate of consumption of starting material. a.) Different excess experiment varying the concentration of 4-octyne. b). Different excess varying the concentration of 3,5-difluoropyridine. c.) Different excess varying the concentration of catalyst. Initial rate points are an average of three runs as a function of 3,5-difluorpyridine (d), 4-octyne (e), and **2-13** (f).

The standard reaction initial concentrations (black lines in Figure 2-16a-c) are as follows: 3,5-difluoropyridine (0.10 M), 4-octyne (0.15 M) and precatalyst **2-13** (0.005 M). Varying the concentration of 3,5-difluoropyridine shows a first-order rate dependence in arene substrate, suggesting that the arene is involved in the rate-limiting step of the reaction (Figure 2-16a and d) Varying the initial concentration of 4-octyne shows zero-order kinetics in alkyne (Figure 2-16b and e). The initial rate data shows there is a slight positive-order rate dependence at low

concentrations, but as the concentration increases, the slope of the rate as a function of alkyne concentration approaches zero. Implications of the zero-order dependence in alkyne are discussed below.

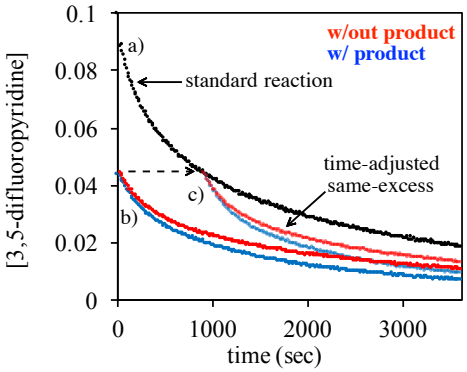


**Figure 2-17.** Concentration of 3,5-difluoropyridine as a function of time. (a) - standard reaction plot. (b) "same-excess" experiment. (c) - time adjusted "same-excess" experiment. Experiments were monitored by $^{19}$F NMR, details and raw data can be found in the Supporting Information.

Varying the initial concentration of **2-13** showed a first-order rate dependence in catalyst. Furthermore, we analyzed the full reaction profiles using a normalized time scale method. This method, reported by Burés, compares substrate concentration on a normalized time scale t[catalyst]$^n$, where n equals reaction order in catalyst.[120,121] Varying n until all reaction profiles at different concentrations overlay reveals the catalyst order. For all plots to overlay, the catalyst concentration must be constant over the course of the reaction. At low catalyst loadings (0.0025 and 0.00125 M, Figure 8c) the reaction plots do not overlay, however, suggesting that the catalyst concentration is not constant over time.[122]

To further examine catalyst stability, "same excess" protocols were used to probe the degree of deactivation at later stages of the reaction (Figure 2-17). The initial concentrations of arene and alkyne for the "same excess" experiment 2-17(b) are the same as the standard reaction 2-17(a) at the time-point indicated. The resulting time-adjusted reaction 2-17(c) is much faster

than 2-17(a), which suggests that the concentration of active catalyst in 2-17(a) is lower than in 2-17(c). This observation corroborates the result from the catalyst-order analysis (Figure 2-16c) that the catalyst is deactivating over time. The "same excess" experiment with added product illustrates that catalyst deactivation is not occurring due to product inhibition (Figure 2-17). Although there appears to be a slight rate enhancement of adding product at the beginning of the reaction, the difference is minor and could arise from styrenyl-product displacing 1,5-hexadiene on the pre-catalyst to form complexes analogous to **2-33b** (Figure 2-15). We speculate that trace impurities in the reaction mixture could be deactivating the catalyst. The high sensitivity of the active nickel-catalyst at low concentrations has been observed,[122] which is likely why relatively high catalyst loadings are needed for many nickel-catalyzed organic transformations.[3]

The results from the computational analysis and kinetics experiments corroborate several aspects of the reaction: (1) an alkyne-ligated intermediate, i.e. **2-27** (Figure 2-15), is proposed as the resting state for catalysis, (2) there is a first-order rate dependence for catalyst and arene substrate, and (3) product inhibition is not occurring. Finally, computations predict that the rate-limiting step is reductive elimination from either a three- (**TS-2-30-31**) or four-coordinate complex (**TS-2-32-33a**). Since the proposed resting state for catalysis contains two alkyne ligands (**2-27**, Figure 2-15), ligand substitution with arene to form **2-28** would result in inverse first-order dependence in alkyne (Figure 2-14). Therefore, if the reaction is overall zero-order in alkyne, incorporation of alkyne in the rate-limiting step is likely. The kinetic data presented herein suggest that rate-limiting reductive elimination occurs from four-coordinate complex, **2-32**, which requires a second alkyne (TS-2-32-33a, Figure 2-15). Due to the typically high concentration of alkyne in the reaction, this assignment is plausible.

**Kinetic versus Thermodynamic Control**

A common limitation in nickel-catalyzed C-H functionalization reactions is the restriction of substrates to those bearing relatively acidic C-H bonds. Since the success of employing both computation and experiment for determining the underlying principles that govern reactivity has been previously demonstrated,[59] we evaluated the relationship between free energies for nickel-mediated C-H bond cleavage and initial rates for the coupling of a variety of C-H bond substrates with 4-octyne.

Previous examples of this type of energetic analysis for C-H bond activation have focused on quantifying M-C bond dissociation energies (BDE), which are difficult to obtain, and identifying correlations with well-known C-H BDEs.[123–126] Few studies, however have evaluated correlations between the initial rate of C-H functionalization versus computed barriers and thermodynamic driving forces for C-H bond cleavage.

Here, we consider the correlation between experimentally determined initial rates with reaction barriers ($\Delta G^{\ddagger}$) and thermodynamics ($\Delta G$) of C-H bond cleavage and nickel-$C_{aryl}$ bond formation (Table 2-2). Initial rates for **2-13**-catalyzed coupling of 4-octyne with each of the substrates in Table 2-2 were obtained using $^{1}H$ and $^{19}F$ NMR in $C_6D_6$. Due to limitations in the experimental setup, pentafluorobenzene was the fastest substrate where a reliable initial rate could be obtained, with an initial rate of $7.30 \times 10^{-4}$ M $s^{-1}$ (entry 2, Table 2-2). Conversely the slowest substrate tested was benzothiophene with an initial rate of $1.71 \times 10^{-7}$ M $s^{-1}$ (entry 9, Table 2-2)

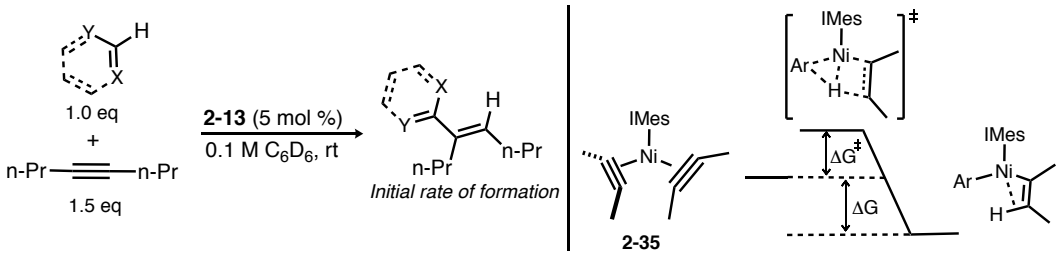


| entry | substrate | initial rate (M/s) | ΔG (kcal/mol)[a] | ΔG‡ (kcal/mol)[a] |
|---|---|---|---|---|
| 1 | benzoxazole | --[d] | -7.8 | 12.7 |
| 2[c] | pentafluorobenzene | $7.30 \times 10^{-4}$ | -6.8 | 12.5 |
| 3[c] | 1,2,4,5-tetrafluorobenzene | $3.62 \times 10^{-4}$ | -6.6 | 8.8 |
| 4[c] | 3,5-difluoropyridine | $1.10 \times 10^{-4}$ | -4.7 | 14.6 |
| 5[b] | 1,3-dimethyluracil | $4.89 \times 10^{-5}$ | -3.2 | 22.5 |
| 6[b] | 4,5-dimethylthiazole | $2.54 \times 10^{-5}$ | -3.1 | 11.0 |
| 7[b] | benzofuran | $2.60 \times 10^{-5}$ | -2.7 | 12.4 |
| 8[c] | 1,2,3,4-tetrafluorobenzene | $3.70 \times 10^{-6}$ | -0.7 | 12.3 |
| 9[b] | benzothiophene | $1.71 \times 10^{-7}$ | 0.8 | 11.9 |
| 10 | fluorobenzene | -- | 5.6 | 20.8 |

**Table 2-2.** Initial rate and energetic parameters for LLHT. [a]All free energies ( $\omega$ B97X-D/cc-pVTZ/SMD) in kcal/mol. [b,c]Initial rates were obtained from either $^{1}H$[b] or $^{19}F$[c] NMR. [d]Reaction rate too high for analysis.

The free energies for C-H activation ($\Delta G^{\ddagger}$) and Ni-C bond formation ($\Delta G$) were obtained using density functional theory, with barriers being calculated using the growing string method[105] (Table 2-2, see Supporting Information for full details). Although the initial rates were obtained using 4-octyne, the LLHT step was calculated for each arene using 2-butyne as a model system. Energies for the transition state for C-H bond cleavage and the resulting nickel-aryl complex were referenced to a bis(butyne)-ligated nickel complex (Table 2-2).

The fastest C-H activation substrate, pentafluorobenzene, has a barrier of 12.5 kcal/mol (entry 2, Table 2-2), whereas the lowest barrier LLHT is with 1,2,4,5-tetrafluorobenzene (8.8 kcal/mol, entry 3, Table 2-2). 1,3-Dimethyluracil has the highest barrier for C-H activation, 22.5 kcal/mol (entry 5, Table 2-2), but it is not the slowest reaction. Unsurprisingly, all the barriers calculated for C-H bond cleavage are surmountable at room temperature. The C-H bond insertion thermodynamics ranged from benzoxazole (entry 1, Table 2-2) being the most favorable, and fluorobenzene being the least favorable and endergonic (entry 11, Table 2-2).

When ΔG and ΔG‡ for each of the substrates in Table 1 are plotted versus initial rate, ΔG correlates well, and ΔG‡ does not (Figure 2-18). In Figure 2-18a, significant scatter exists between ΔG‡ and the initial rate, indicating that C-H activation is not rate-controlling, consistent with our studies shown above. For example, benzofuran (entry 8, Table 2-2) and benzothiophene (entry 9, Table 2-2) have virtually the same barrier for C-H bond cleavage, yet the initial rate for benzofuran is two-orders of magnitude faster than benzothiophene.

On the other hand, comparing ΔG for benzofuran to benzothiophene shows that C-H activation is approximately 3 kcal/mol more thermodynamically favorable for benzofuran (entry 8, Table 2-2) than benzothiophene (entry 9, Table 2-2). The same sensitivity to ΔG is observed throughout the remaining substrates, and a linear free-energy relationship is observed with a correlation factor ($R^2$) of 0.95 (Figure 2-18b) for ΔG compared to ln(rate). To validate the hypothesis that thermodynamics of C-H activation correlates to reactivity, the energetics for fluorobenzene (entry 10, Table 2-2), a substrate that does not form product under the reaction conditions, show that the barrier for C-H activation was calculated to be 20.8 kcal/mol, but more importantly the C-H bond cleavage event is endergonic by 5.6 kcal/mol. According to the proposed thermodynamic control in this reaction, product formation is unfavorable, consistent with experiment.

Interestingly, this means that thermodynamically favored C-H activations are favored across several classes of substrates, which fully accounts for the chemoselectivity for nickel-catalyzed C-H functionalization. This is plausible considering that computations support reductive elimination (**TS-2-32-33a**, Figure 2-15) as the rate-limiting step of the reaction. Given this rate-limiting step, populating the C-H inserted intermediate prior to it controls the rate. It can be speculated that if the transition state energies for reductive elimination of all of substrates in Table

2-2 were calculated they should have a linear free energy relationship to the initial rate of the reaction. Identifying ligand scaffolds that do not follow this trend or ligands that promote thermodynamically favorable C-H bond activations for less activated C-H bonds, for example benzothiophene, could lead to either unique C-H bond selectivity or significant increases in reactivity.

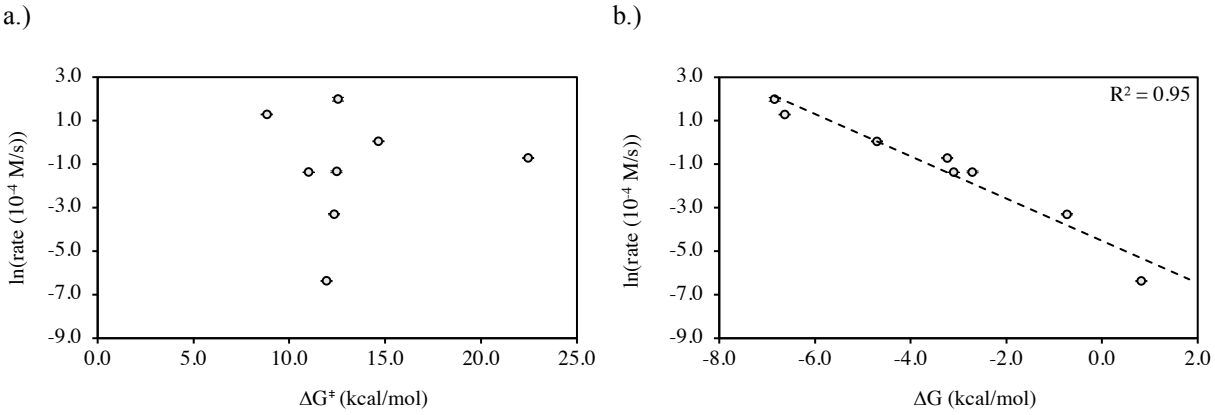


**Figure 2-18.** (a) Initial rate versus transition state energy for C-H bond cleavage. (b) initial rate versus thermodynamics for C-H bond cleavage.

## Conclusion

Ligand substitution during pre-catalyst initiation and potential off-cycle inhibitory activity lead to considerable complexities in nickel-catalyzed C-H functionalizations. In support of this, there is potential for competing reactivity involving COD whenever $Ni(COD)_2$ is the pre-catalyst. As discussed in this chapter, COD-mediated pathways ultimately result in the formation of π-allyl complexes (**2-3**, Figure 2-5), which significantly inhibit catalysis. The current report shows that the formation of **2-3** (Figure 2-8) can proceed through either traditional chain walking via nickel-hydrides or through reversible LLHT events. Complementary to these studies, experiments show π-allyl complexes form during hydroarylation catalysis regardless of order of substrate addition. To avoid off-cycle π-allyl forming activity it is necessary to adapt the catalytic system to remove

COD. Our efforts have focused on employing **2-13** which utilizes 1,5-hexadiene as a stabilizing ligand on the nickel pre-catalyst which does not promote off-cycle LLHT at room temperature.

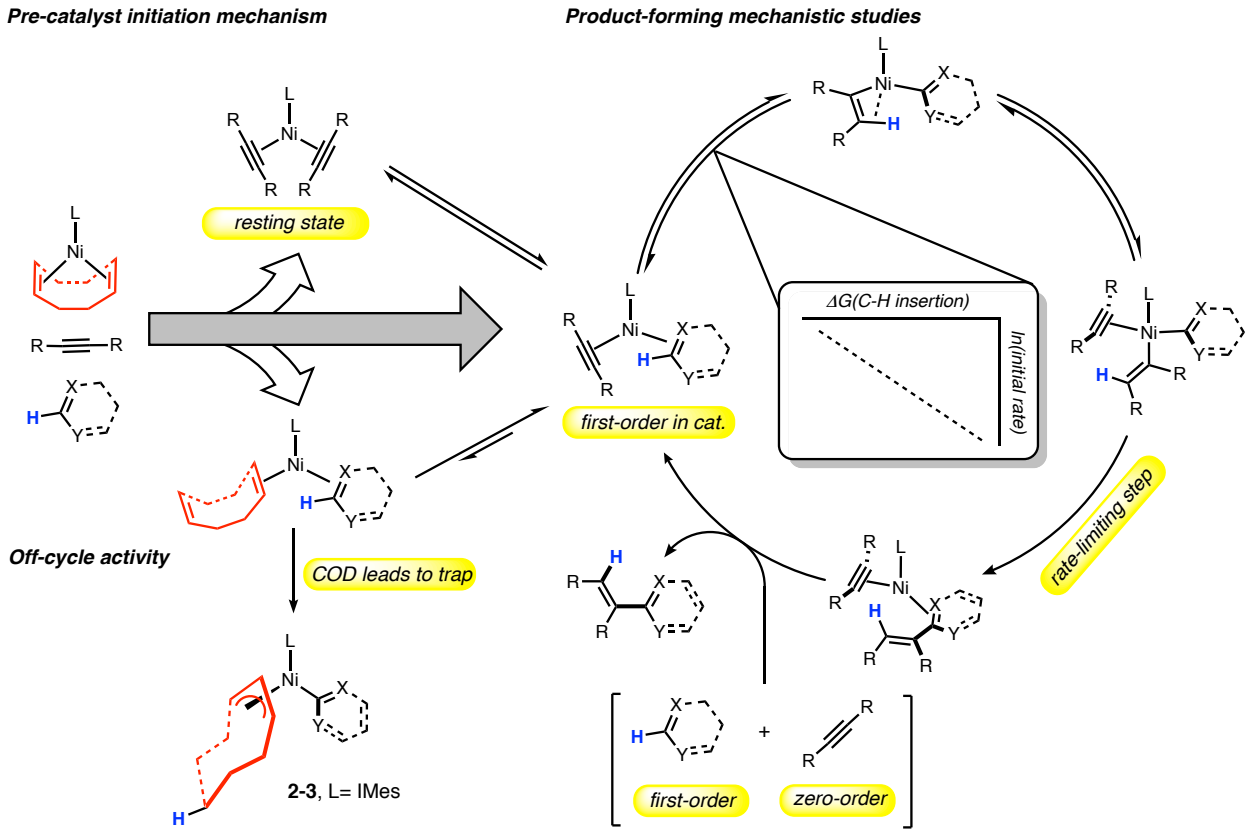


**Figure 2-19.** Overall map of catalyst deactivation, activation, and productive catalysis.

Kinetic and computational analysis of nickel-catalyzed hydroarylations via C-H functionalization reveals that the reaction is overall second-order, being first-order in arene and catalyst. Zero-order kinetics in alkyne agree with the simulation results that suggest the resting state for catalysis is a bis-alkyne ligated nickel species (**2-27**, Figure 2-15). Computation and kinetic data also suggests that the rate limiting step is reductive elimination (**TS-2-32-33a**, Figure 2-15). These results are corroborated by correlations between experimentally measured initial rates and computed energetic parameters. Specifically, the results of this study support the reaction being under thermodynamic control, where a linear free-energy relationship was identified

between initial rate and the thermodynamics of the LLHT C-H bond cleavage event (Figure 2-18). This is consistent with the strength of the Ni-C bond strongly influencing reactivity and previous computational investigations that have shown that the Ni-$C_{aryl}$ bond is formed early in the transition state.[59] The identification of thermodynamic control in these systems will potentially expedite catalyst design efforts that aim to increase the activity of nickel-mediated C-H bond activation.

The overall complexity of nickel-catalyzed hydroarylation via C-H functionalization reactions, including multiple competing reaction pathways, and the energetic parameters influencing reactivity and selectivity elucidated by this investigation are highlighted in Figure 2-19. The details elucidated by this investigation will help assist in the development and widespread use of nickel-catalysis for the functionalization of C-H bonds. Since the off-cycle activity described by in this chapter stems from ancillary ligands on the nickel pre-catalyst, this work will help guide the development of future protocols for the general application of nickel-catalysis for organic synthesis.

## Chapter 3 : Well-Defined N-Heterocyclic Carbene Supported Nickel Pre-Catalysts

### Introduction

Employment of nickel for catalytic bond forming processes has a rich history that spans many applications from the synthesis of bulk chemicals to highly complex molecules. Due to cost advantages of using earth-abundant metals for catalysis, there has been a surge in the development of nickel-catalyzed methods in a number of areas of chemistry. Although many valuable advancements have been made in this area there are still operational challenges that have yet to addressed. First and foremost, the bulk of these methods require the generation of Ni(0) as the active form of the catalyst, which is inherently sensitive to air.[3] The most direct route to accessing catalytically relevant zero-valent nickel catalysts would be to directly ligate a commercially available Ni(0) catalysts, of which there are few available (Figure 3-1), under stringent air-free techniques.

Available through the Strem Chemicals Catalog (*accessed March, 2018*)

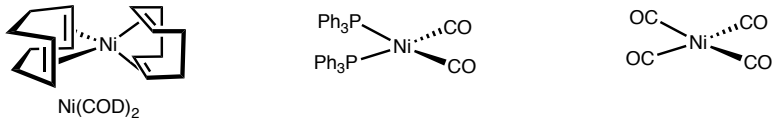


**Figure 3-1.** Commercially available Ni(0) complexes through the Strem Catalog (*accessed March, 2018).*

As discussed in Chapter 1, traditionally, the most common way of circumventing challenges regarding air stability and the user friendliness of this chemistry is to generate the active oxidation state of catalyst *in situ* typically starting from common air-stable Ni(II) sources, such

$Ni(acac)_2$ or $NiCl_2$. These techniques typically require a super-stoichiometric amount of reductant to generate Ni(0) prior to initiating catalysis.[3]

The use of NHC ligands for catalysis presents another complication for *in situ* generated catalyst in that NHC ligands are usually generated *in situ* due to their general instability in the free form.[127] Similar to challenges discussed earlier for reductive processes during catalyst activation, the efficiency of NHC deprotonation and subsequent coordination of the free carbene to the metal center is not always straightforward. Although stable well-defined pre-catalyst of NHC-Ni complexes would be particularly useful, they have not received the attention or widespread use that phosphine and amine analogs have.

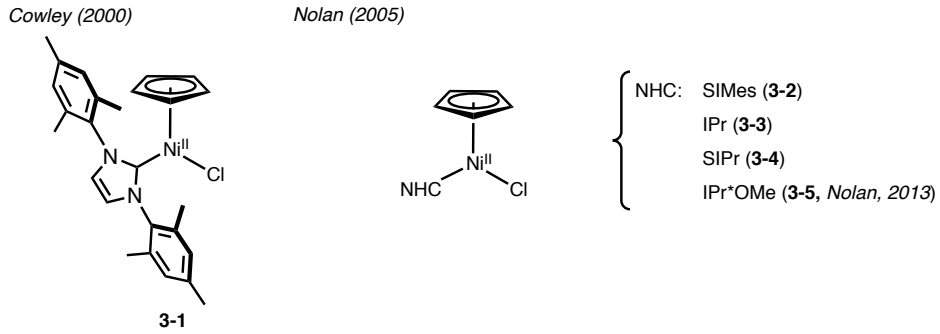


**Figure 3-2.** Cyclopentadienyl Cp-NHC-Ni(II) complexes.

Although progress has been made in this area, attention has been mainly focused on the development of NHC-Ni(II) pre-catalysts, while comparatively few Ni(0) complexes have been developed. The two main classes of NHC-Ni(II) complexes that are commonly used as pre-catalyst have either a Cp or π-allyl ligand in addition to σ-bound X-type ligand (i.e. Cl, Br, I...).[13,14,28,128]

First, Cp(IMes)NiCl was reported by Cowley and co-workers in 2000, but widespread use of these types of complexes as pre-catalyst for organic reactions did not come until years later.[129] In a report from Nolan and co-workers they demonstrated that this class of metal complexes could be expanded to include a variety of NHC ligands including SIMes (**3-2**), IPr (**3-3**), and SIPr (**3-4**).[11] In that same report the IPr-based pre-catalysts (**3-3**) had modest activity in Buchwald-Hartwig

couplings of aryl bromides and chlorides (Figure 3-3). It was later hypothesized by Nicasio that moderate activity of Ni(II)-Cp complexes **3-2**, **3-3**, and **3-4** was potentially due to challenging to reduction and dissociation of Cp to generate the active Ni(0) state, thus impeding catalysis.[130] Nolan and co-workers later demonstrated that Ni(II)-Cp complexes of much larger NHC ligands, like IPr*OMe (**3-5**, Figure 3-2), formed more catalytically active complexes for Buchwald-Hartwig couplings.[13] Based on the data from Nolan's report it is unclear whether the larger NHC promotes faster initiation or if a larger NHC is required to promote more challenging bond forming reductive eliminations such as those in N-arylation mechanisms.

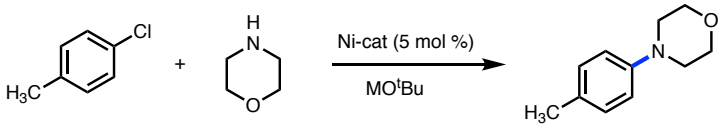


| entry | pre-catalyst | NHC on pre-catalyst | conditions | yield (%) |
|---|---|---|---|---|
| 1 | **3-3** | IPr | dioxane, 105 °C | 75 |
| 2 | **3-5** | IPr*OMe | dioxane, 105 °C | 90 |
| 3 | **3-6** | IPr | THF, 60 °C | 98 |
| 4 | **3-7** | IPr*OMe (1 mol %) | THF, 60 °C | 98 |

***pre-catalysts:***

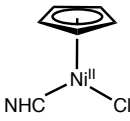


NHC = IPr, **3-3**
IPr*OMe, **3-5**

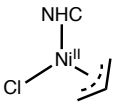


NHC = IPr, **3-6**
IPr*OMe, **3-7**

**Figure 3-3.** Comparison of pre-catalysts for reported examples of coupling p-chlorotoluene and morpholine.

Although there are many synthetic demonstrations using Cp(NHC)NiX complexes as pre-catalysts for organic synthesis, challenges in activation have led to the development of superior NHC-Ni(II) pre-catalysts. Most notably, the hypothesis by Nicasio that by replacing the Cp ligand with a more labile π-allyl ligand, complexes originally reported by Sigman,[131] could facilitate a more rapid generation of Ni(0), had a profound impact in the development of this Ni(0)-NHC pre-catalysts. Indeed, Nicasio and co-workers synthesized a subset of (π-allyl)(NHC)NiCl complexes (**3-6** and **3-7**) under similar conditions to Nolan's previous report the π-allyl-based pre-catalyst were much more active for Buchwald-Hartwig couplings (Figure 3-3).[130] For the amination

reaction shown in (Figure 3-3), Cp complexes of IPr form 75 % yield of the desired product when conducting the experiment in refluxing dioxane (entry 1, Figure 3-3). Whereas, π-allyl complexes of IPr performed the N-arylation with in 98 % yield under much milder conditions (entry 2, Figure 3-3). The same trend is true for IPr*OMe-based pre-catalyst although the enhanced reactivity when switching out Cp or π-allyl is much less pronounced. Ultimately, the comparison of Cp- versus π-allyl-based pre-catalysts demonstrates the complications that can arise in generating catalytically active Ni(0).

A logical route to averting issues with nickel reduction prior to catalysis is to engineer nickel pre-catalysts that are already in the zero oxidation-state, but this does not come without its own set of unique challenges. This strategy presents several operational barriers in that the majority of well-defined complexes of this type are extremely air and moisture sensitive.[12,64,15,132] In most cases, the presence of a strong electron-donors, such as NHC ligands, exacerbate oxidative instability compared to common Ni(0) precursors such as $Ni(COD)_2$. Nevertheless, under air-free conditions a variety of highly active pre-catalysts have emerged in recent years.

The general approach to stabilizing NHC-Ni(0) complexes and rendering them isolable is to exploit the back-bonding interactions between electron-rich Ni(0) and the π*-orbitals of olefins or conjugated π-systems. As a result, a low lying LUMO π*-orbital of an olefin will contribute a strong back-bonding interaction with the Ni(0)-center, thus producing a more stable complex. There is also a significant stabilization associated with olefin binding geometry, as discussed in Chapter 2, where co-planar binding between the olefins should also result in a more stable interaction. Although several notable advances in synthesis and catalytic application of well-defined olefin-stabilized NHC-Ni(0) complexes have been made, select examples are highlighted here (Figure 3-4). First, Cavell and co-workers showcased the ability for strong π-acceptors to

greatly stabilize NHC-Ni(0) complexes when they synthesized air-stable Ni(0)IMes (dimethyl fumarate)$_2$ (**3-8**) and Ni(0)IPr(dimethyl fumarate)$_2$.[133] These complexes could be accessed from Ni(COD)$_2$ in the presence of a NHC free carbene, and represented some of the few air-stable NHC-Ni(0) complexes. Unfortunately, the strength of the fumarate-Ni(0) interaction hinders catalytic utility of these complexes. To overcome this challenge, much weaker π-acceptor ligands must be used to produce a more active catalysts (Figure 3-4). With these goals in mind, Nicasio and co-workers demonstrated that (IPr)Ni(0)(stryene)$_2$ (**3-10**) complexes could be readily synthesized from Ni(COD)$_2$, IPr and excess styrene in good yields.[12] Furthermore, Hazari and co-workers developed a clever synthesis of 1,5-hexadiene stabilized NHC-Ni(0) complexes (**3-9**) that started from simple, air-stable nickel(II) salts. In that case, transmetalation of allyl magnesium chloride with $NiCl_2$ yielded a bis(π-allyl)Ni(II) and subsequent reductive elimination formed 1,5-hexadiene *in situ*, which could be directly captured as the stabilizing ligand for a variety of NHC ligands.[15]

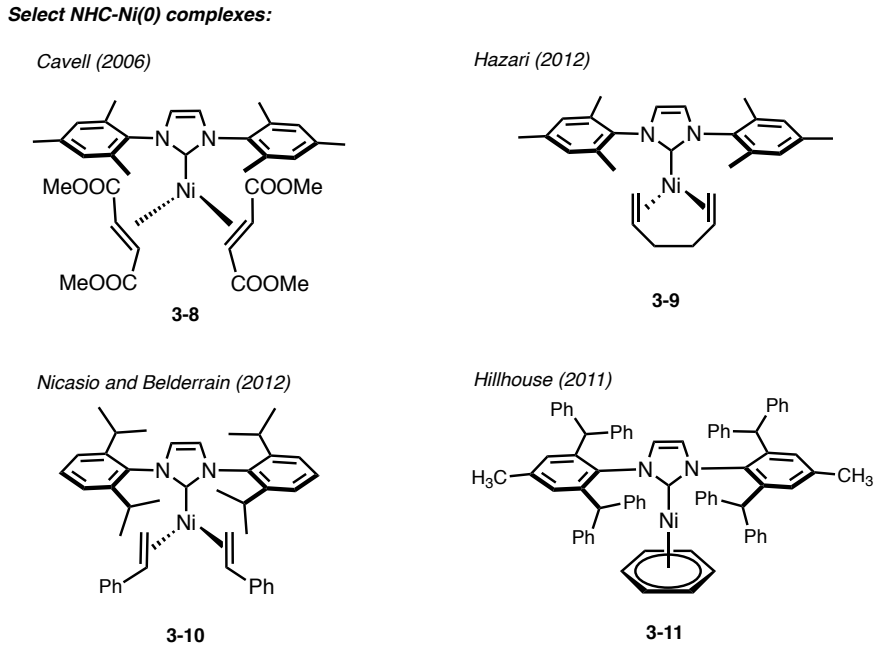


**Figure 3-4.** NHC-Ni(0) pre-catalysts.

In addition to stabilization by $\eta^2$-olefins, Hillhouse and Cundari reported the synthesis of ($\eta^6$-arene )Ni(0)(NHC) (ANCs) complexes (where NHC = IPr*, **3-11**, Figure 3-4).[64] An improved synthetic approach to ANCs was provided by Ogoshi and co-workers where they demonstrated that they could be readily generated from $Ni(COD)_2$ via hydrogenation of COD in the presence of NHC ligands using toluene or benzene as a solvent.[132] These reactions led to clean conversion to ($\eta^6$-arene)Ni(0)(NHC) complexes. This technology tolerates large NHC ligands such as IPr* and IPr, but stable analogs of IMes or smaller NHC ligands are not stable.

There are several examples of highly active NHC-Ni(0) complexes that can be used for organic synthesis. Unfortunately, the stability and structural limitations of many of these impeded their widespread use as pre-catalysts by the greater synthetic community. We envisioned that tuning the electronic and steric properties of $\alpha,\beta$-unsaturated esters would provide access to an interesting class of reactive, yet stable, NHC-Ni(0) pre-catalysts. Toward this goal we have synthesized a variety of NHC-Ni(0) complexes that bear NHCs of varying size using stabilizing acrylate and fumarate ligands. Herein is a detailed discussion of the structural and stability aspects, as well as selected synthetic applications including aldehyde-alkyne reductive couplings and Buchwald-Hartwig cross-couplings.

## IMes-Ni(0) Pre-Catalyst for Silane-Mediated Aldehyde-Alkyne Reductive Couplings

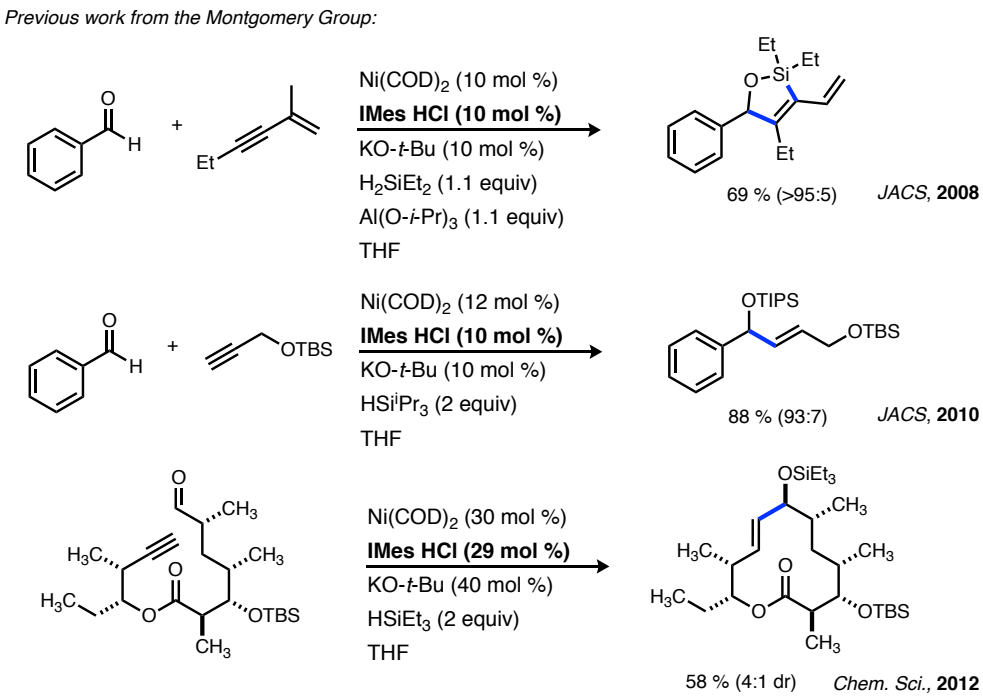


**Figure 3-5.** Select examples from the Montgomery group where IMes was used as a ligand for nickel-catalyzed reductive couplings.

Previous work in the Montgomery lab has showcased the utility of IMes as a promotor for a variety of nickel-catalyzed reductive couplings (Figure 3-5).[134–136] The advantage of using NHCs ligands versus phosphines, which are also known to promote reductive couplings, is that NHCs are much stronger σ-donors resulting in a more nucleophilic and reactive nickel catalyst. Furthermore, many of the reductive couplings that are of interest to our group utilize alkynes as the nucleophilic coupling partner, which can be problematic as alkynes are well documented to undergo rapid alkyne trimerization in the presence of nickel-phosphine complexes. These undesired processes are still operative when using NHC ligands, but the large steric profile of imidazolium NHCs versus phosphines retards alkyne trimerization. There are a few things that can be taken away from the examples shown in Figure 3-5 regarding generation of the active catalyst, which is presumably IMes-Ni(0) The typical method for catalyst formation proceeds via

deprotonation of IMes•HCl with a *tert*-butoxide base generating free IMes which undergoes ligand substitution with $Ni(COD)_2$. Although this does require the use of a glove box, IMes is a relatively well-behaved NHC ligand and this process is generally consistent and reliable, employing *in situ* catalyst synthesis typically requires high catalyst loadings (≥ 10 mol %). We envisioned that the development of well-defined stable IMes-Ni(0) pre-catalysts would allow for low catalyst loadings and make this chemistry more broadly accessible by removing the need for a glove box.

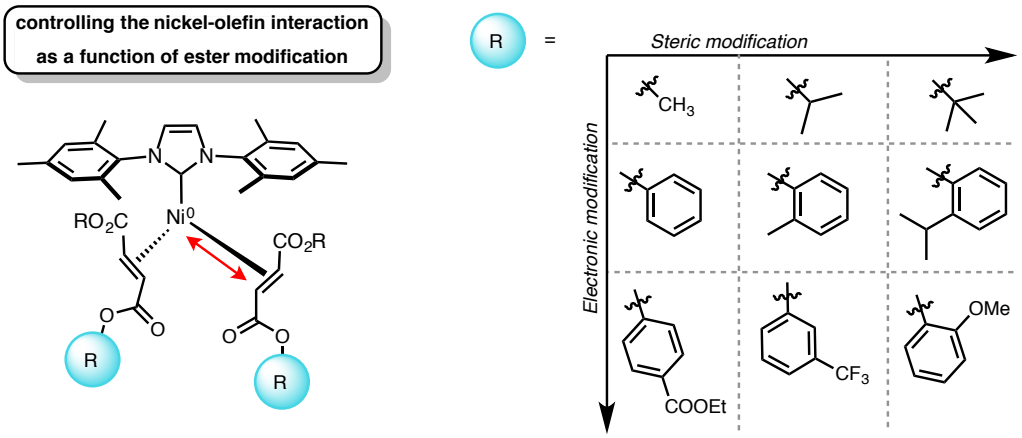


**Figure 3-6.** General strategy for tuning activity and stability of IMes-Ni(0) pre-catalysts.

**Synthesis and Structure of IMes-Ni(0) Fumarate Stabilized Pre-Catalysts**

Influenced by the seminal work from Cavell and co-workers,[133] a series of fumarates of varying steric and electronic profiles were synthesized and tested as ligands to assess how structure modifications affect stability and reactivity of the resulting nickel pre-catalyst (Figure 3-6). Since the fumarate structure is highly modular, access to a broad scope of ester moieties can be achieved via simple coupling of fumaryl chloride with the respective alcohol. Using this method, a small library of fumarate ligands could be generated (Figure 3-7).

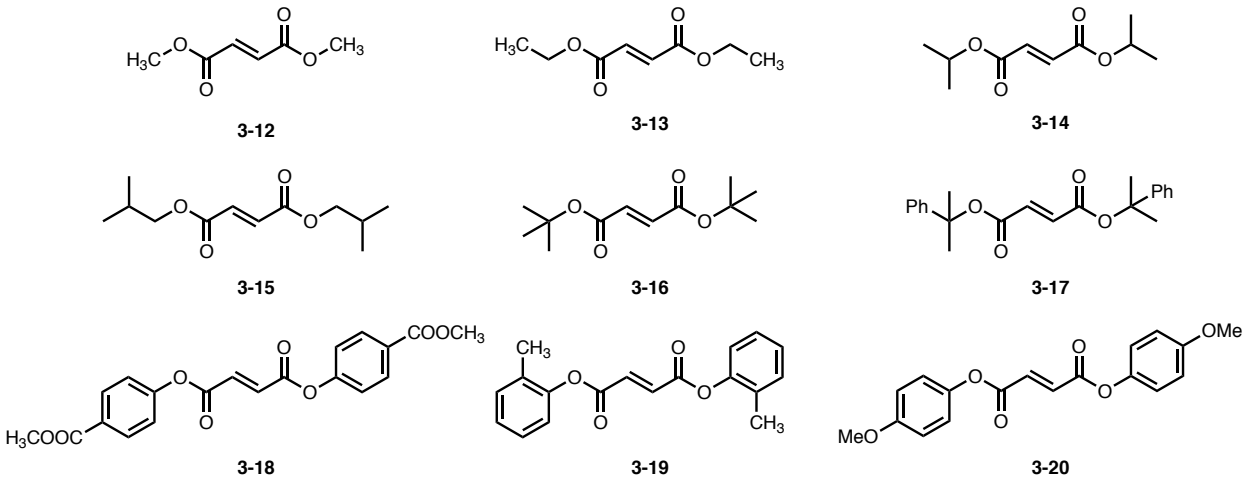


**Figure 3-7.** Fumarate ligands tested for Ni(0) complexes.

A broad range of fumarates structures were targeted, forming both an aliphatic and aromatic series (Figure 3-7). The sterics of fumarate ester moiety could be systematically increased from DMFU (**3-12**) to *tert*-butyl fumarate (**3-16**). In that series is also *iso*-butyl (**3-15**) because it could be envisioned that this fumarate provides steric interactions near the metal similar to an ethyl group but possesses a greater steric shielding in the outer-sphere due to β-branching. The largest ester moiety tested was 2-phenyl-2propanol (**3-17**). In addition to the aliphatic series, a variety of phenol derivatives were also tested (**3-18** to **3-20**, Figure 3-7). Since it is important to gain an understanding for the influences electronic modifications of the fumarate had on catalyst activity, a 4-ethyl benzoate fumarate (**3-18**) analog was synthesized to address this need.

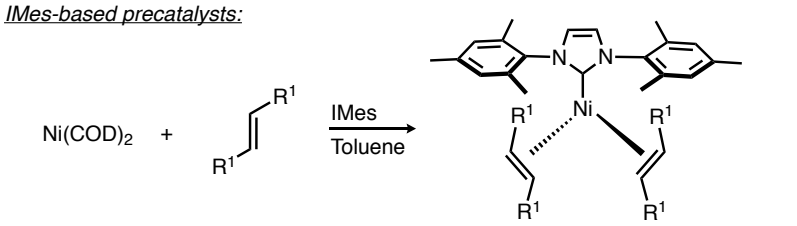


**3-21**: $R^1$ = -$CO_2$Me
**3-22**: $R^1$ = -H, $R^2$, $R^3$ = -$CO_2$Et
**3-23**: $R^1$ = -H, $R^2$, $R^3$ = -$CO_2$*i*Pr
**3-24**: $R^1$ = -H, $R^2$, $R^3$ = -$CO_2$*i*-Bu
**3-25**: $R^1$ = -H, $R^2$, $R^3$ = -$CO_2$*t*-Bu
**3-26**: $R^1$ = -$CO_2$(2-phenylpropan-2-yl)
**3-27**: $R^1$ = -$CO_2$(o-tolyl)
**3-28**: $R^1$ = -$CO_2$(4-OMe-Ph)
**3-29**: $R^1$ = -$CO_2$(4-COOEt-Ph)

**Figure 3-8.** Synthesis of fumarate stabilized IMes-Ni(0) pre-catalysts

We were pleased to see that all of the fumarates describe in Figure 3-7 could be complexed to nickel via simple and rapid ligand displacement of $Ni(COD)_2$ (**3-21** - **3-29**, Figure 3-8). Regardless of the range of steric profiles for the aliphatic fumarates (**3-21** - **3-26**), they all behaved similarly and formed deep red highly crystalline products. By visual analysis, the reaction seems to proceed faster in THF, but by using toluene as the solvent a simple filtration of the crude reaction through a celite plug removes any metal decomposition products which commonly form in small amounts. Once filtered, the complexes were concentrated and typically recrystallized from pure pentane at -20 °C or dissolved in a small amount of THF and crystallized by vapor diffusion with pentane (for details regarding the isolation of each of the complexes shown in Figure 3-8 please refer to Chapter 5). It should be noted that for the synthesis of **3-26** product was formed in low yields (24 %) and precipitated out of the reaction crude and be isolated as an orange solid via filtration. The filtrate was purple and NMR analysis of the toluene soluble portion suggested potential dimer formation, but the it was not conclusive. This could result from high steric hindrance of **3-17** favoring dimer formation. Complexes of the aromatic fumarates (**3-18** - **3-20**) were made in the same way, but isolation of these complexes typically require recrystallization from more polar solvents like THF, but in the case of **3-27** crystalline product precipitated out of the reaction crude upon the addition of pentane at room temperature. Additionally, X-ray quality crystals could be grown via vapor diffusion in THF/pentane and the ORTEP for this complex is shown in Figure 3-9.

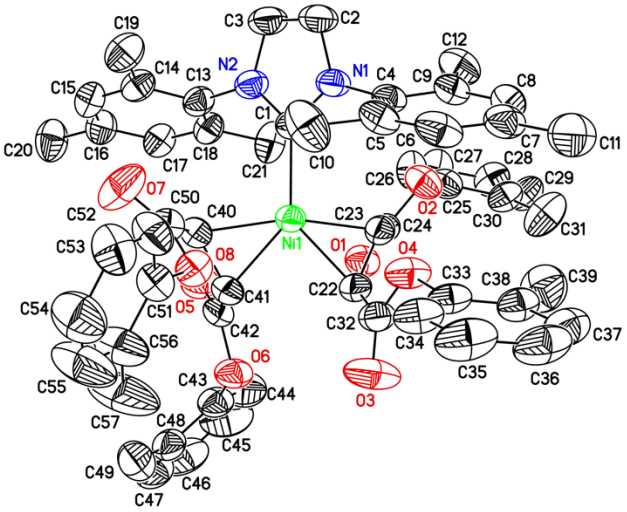


**Figure 3-9.** ORTEP of (IMes)Ni(0)(D(o-tolyl)FU)$_2$ (**3-27**) with thermal ellipsoids at 50 % probability. Hydrogens have been omitted for clarity.

Silane-mediated reductive coupling of aldehydes and alkynes was used as a model reaction to determine how differing the nature of the π-accepting ligands impacted catalytic activity and stability for a subset of the complexes **3-21 - 3-25**, **3-27**, and **3-29**. The mild nature of these reaction conditions represents a challenging environment for pre-catalyst activation compared to examples that use strong nucleophiles or transmetalating agents, which are often necessary for the activation of other stable nickel(II) pre-catalysts.

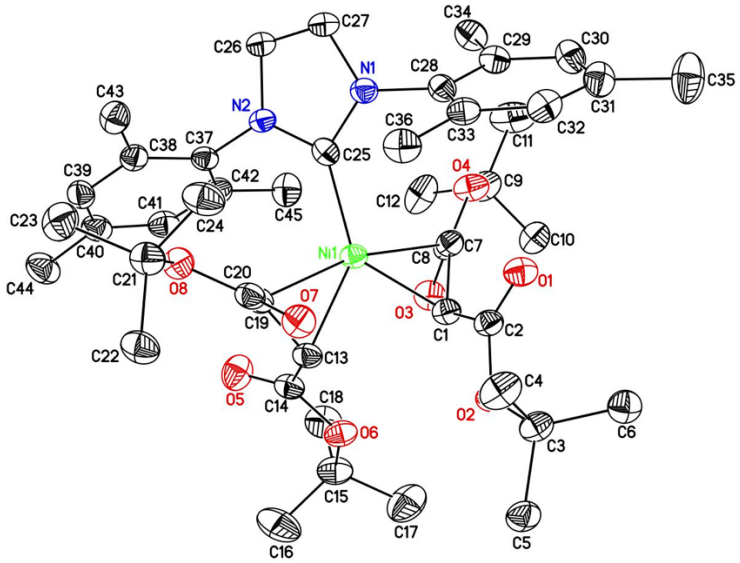

**Figure 3-10.** ORTEP of (IMes)Ni(0)(di-*tert*-butyl)FU$_2$ (**3-25**) with thermal ellipsoids at 50 % probability. Hydrogens have been omitted for clarity.

## Reactivity of IMes–Ni(0) Fumarate Pre-Catalysts

The coupling of 4-fluorobenzaldehyde, 1-phenyl-1-propyne, and triethylsilane was conducted because formation of product **3-30** could be easily evaluated by $^{19}$F NMR (Figure 3-11). Real time monitoring of the reaction provides several metrics for catalyst activity, including initiation rates. Notably, the aliphatic fumarate complexes, **3-21** - **3-25**, were all competent pre-catalysts for this transformation (Figure 3-11a). However complex **3-21**, with DMFU ligands, only formed trace amounts of product after 60 minutes. This is likely due to the high stability[133] of this complex, which compromises catalytic activity. Based on the trends in Figure 3-11a, there appears to be a direct relationship between the rate of product formation and steric profile for the fumarate series (**3-21** - **3-25**, Figure 3-11a). This becomes evident in complex **3-25**, with di-*t*-butyl fumarate ligands, which performed the best. In the case of **3-25** product formation seized at 74 % after 45 minutes. This is likely due to alkyne trimerization consuming starting material since nearly all of the mass balance is accounted for in the $^{19}$F NMR. Interestingly, **3-23** and **3-24** had similar reactivity and it should be noted that after 2 hours these reactions also approached approximately 80 % conversion. Complex **3-22**, with di-ethyl fumarate ligands, was also a sluggish pre-catalyst, but significantly more reactive that the DMFU variant, **3-21**, which is consistent with the trend in steric hindrance of the fumarates governing catalytic activity.

Testing aromatic fumarate stabilized complexes **3-25** and **3-29** revealed that di-*o*-tolyl fumarate formed a relatively active pre-catalyst, but the electron-withdrawing nature of **3-29** rendered it inert under the reaction conditions (Figure 3-11b).

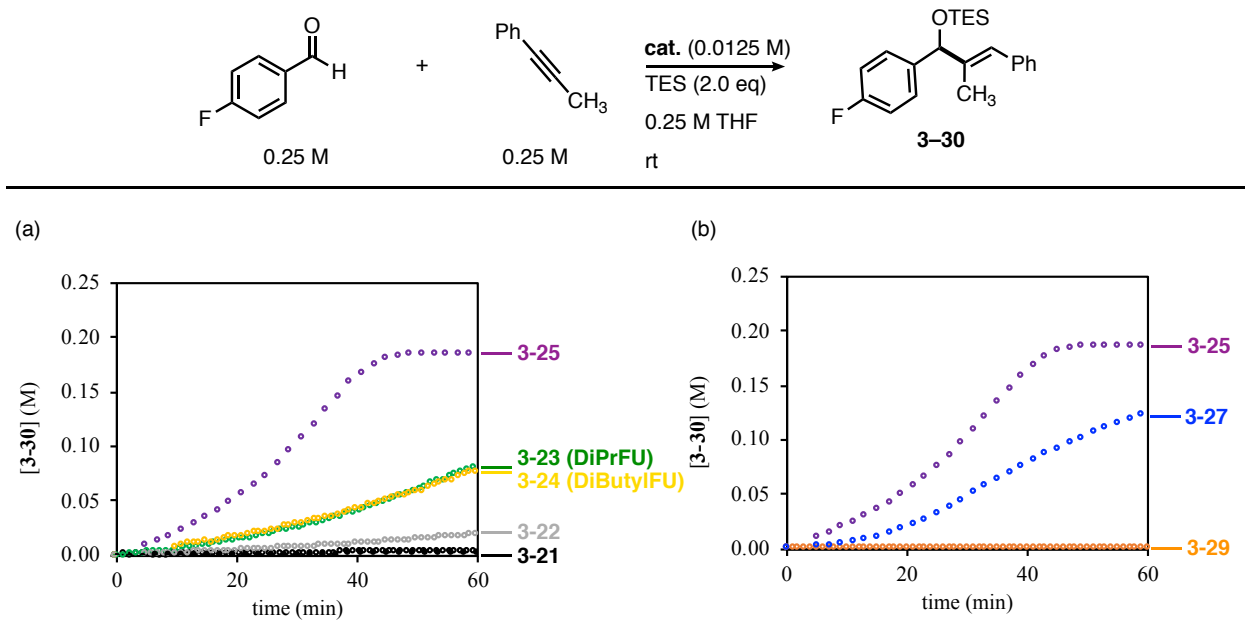


**Figure 3-11.** Reaction progression plots for the reductive coupling shown at the top of figure. Reaction monitored by $^{19}F$ NMR using α, α, α-trifluorotoluene as an internal standard. (a) Alkyl fumarate complexes. (b) Select aryl fumarates tests, including **3-25** as a reference.

## Synthesis and Structure of IMes-Ni(0) Acrylate Stabilized Pre-Catalysts

In addition to synthesizing a broad range of fumarate ligands and well-defined pre-catalysts, acrylates were also tested as stabilizing ligands for NHC-Ni(0) complexes (Figure 3-12). Since acrylates are much weaker π-acids, it was envisioned that dissociation of acrylate ligands would be more facile than fumarates, allowing for greater catalyst activity. The acrylates tested include methyl acrylate, methyl methacrylate, phenyl acrylate, and phenyl methacrylate (Figure 3-12). Following the same general synthetic protocol as the fumarate complexes, rapid ligand displacement from $Ni(COD)_2$, complexes **3-31** - **3-34** were accessed in good yields as yellow or orange crystalline solids (Figure 3-12).

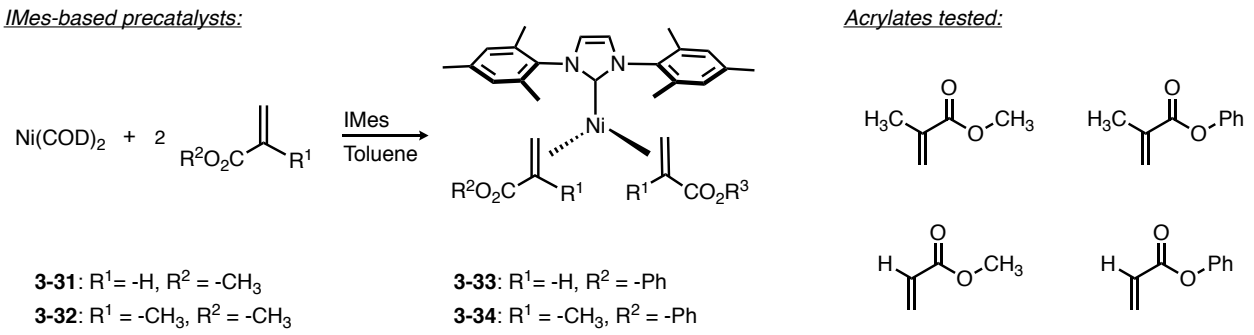


**Figure 3-12.** Synthesis of acrylate stabilized IMes-Ni(0) pre-catalysts

## Reactivity of IMes–Ni(0) Acrylate Pre-Catalysts

The standard reductive coupling described previously was also used to evaluate a structure-activity relationship of the acrylate-based complexes. Using the reaction profile for **3-25** as reference (Figure 3-11), the acrylate complexes displayed a wide range of activities (Figure 3-13). Interestingly, methyl methacrylate complex **3-31** was highly active for this reaction reaching completion at around 80 % conversion after only 10 minutes. Additionally, the reaction profile shape is significantly different than the fumarates. The rate of product formation for the fumarate-based pre-catalyst increased over time and near 50 % conversion the rate slowed, leading to a sigmoidal-like curve. In the case of methyl methacrylate supported pre-catalyst **3-31**, the shape is more reminiscent of a hyperbolic curve, which would be expected for a normal 1$^{st}$-order reaction. Alternatively, methyl and phenyl acrylate-based complexes, **3-32** and **3-33**, respectively, displayed sigmoidal reaction profiles similar to the fumarate pre-catalysts. The exact origin of this effect is not known, but the sterics implications of having a $\alpha$-methyl to the carbonyl of the methyl acrylate could weaken the Ni-acrylate interaction potentially leading to a more active pre-catalyst. Additionally, placing a methyl group on the olefin binding to Ni(0) makes the olefin inherently more electron-rich and thus a weaker $\pi$-acceptor.

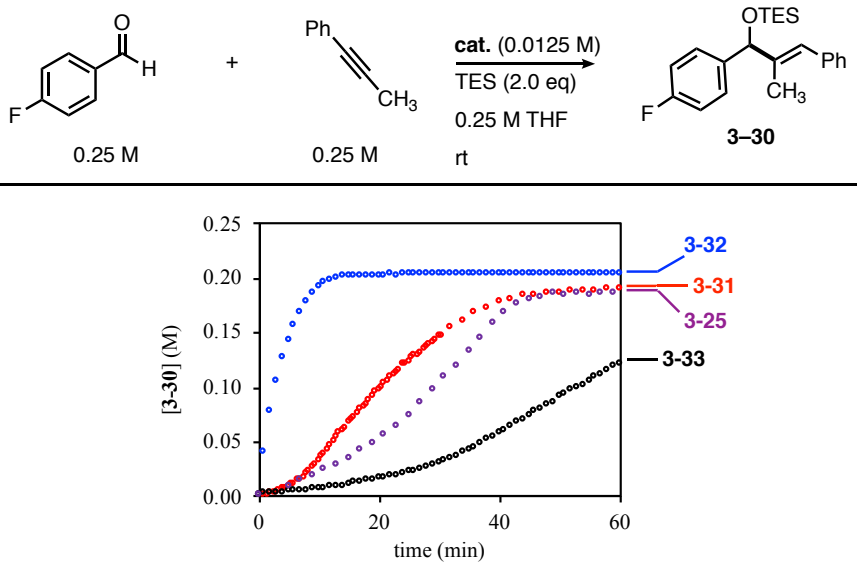


**Figure 3-13.** Reaction progression plots for the reductive coupling shown at the top of figure. Reaction monitored by $^{19}$F NMR using α, α, α-trifluorotoluene as an internal standard. **3-25** is shown as a reference.

Although the long-term air-stability of **1** has been well documented, as shown in Figure 3-11 the stability comes at the cost of catalytic activity. Multiple factors can influence the bench stability of a compound including, but not limited to, particle size, moisture, and airflow, making it difficult to quantitatively assess air-stability. Encouraged by the broad range of catalytic activities shown by all of pre-catalysts, the relationship between activity and air-stability was next investigated. To obtain a qualitative sense for the stability of each of the complexes in Figure 3-11 and Figure 3-13, the complexes were weighed into their respective vials and left on the bench with the *cap off* for 24 hours. The catalysts were then brought back into a glove box and the test reaction was setup following normal procedures. Again, each of the reactions could be monitored by $^{19}$F NMR (Figure 3-14b).

### Air-Stability of IMes–Ni(0) Pre-Catalysts

Interestingly, the fumarates appeared to maintain their activity and in most cases the plots overlay with their air-free reactions (Figure 3-14a). The exception to this was pre-catalyst **3-23**, which completely decomposed after 24 hours on the bench (color change from red to light brown).

This result was confirmed via duplication with a different lot of **3-23**. Since the *tert*-butyl fumarate stabilized pre-catalyst **3-25** retained its activity it suggests that the *t*-butyl groups on the fumarate potentially provide a shielding effect on the Ni-center that the *i*-propyl groups do not. Nevertheless, the catalytic competency of the acrylate complexes was completely compromised, likely as a result of oxidative decomposition (**3-31**, Figure 3-14b). Interestingly, **3-32**, the most active pre-catalyst of the series, retained a small amount of activity and a quick burst of product formation was observed, but the reaction stopped producing product after 10 minutes (Figure 3-14a).

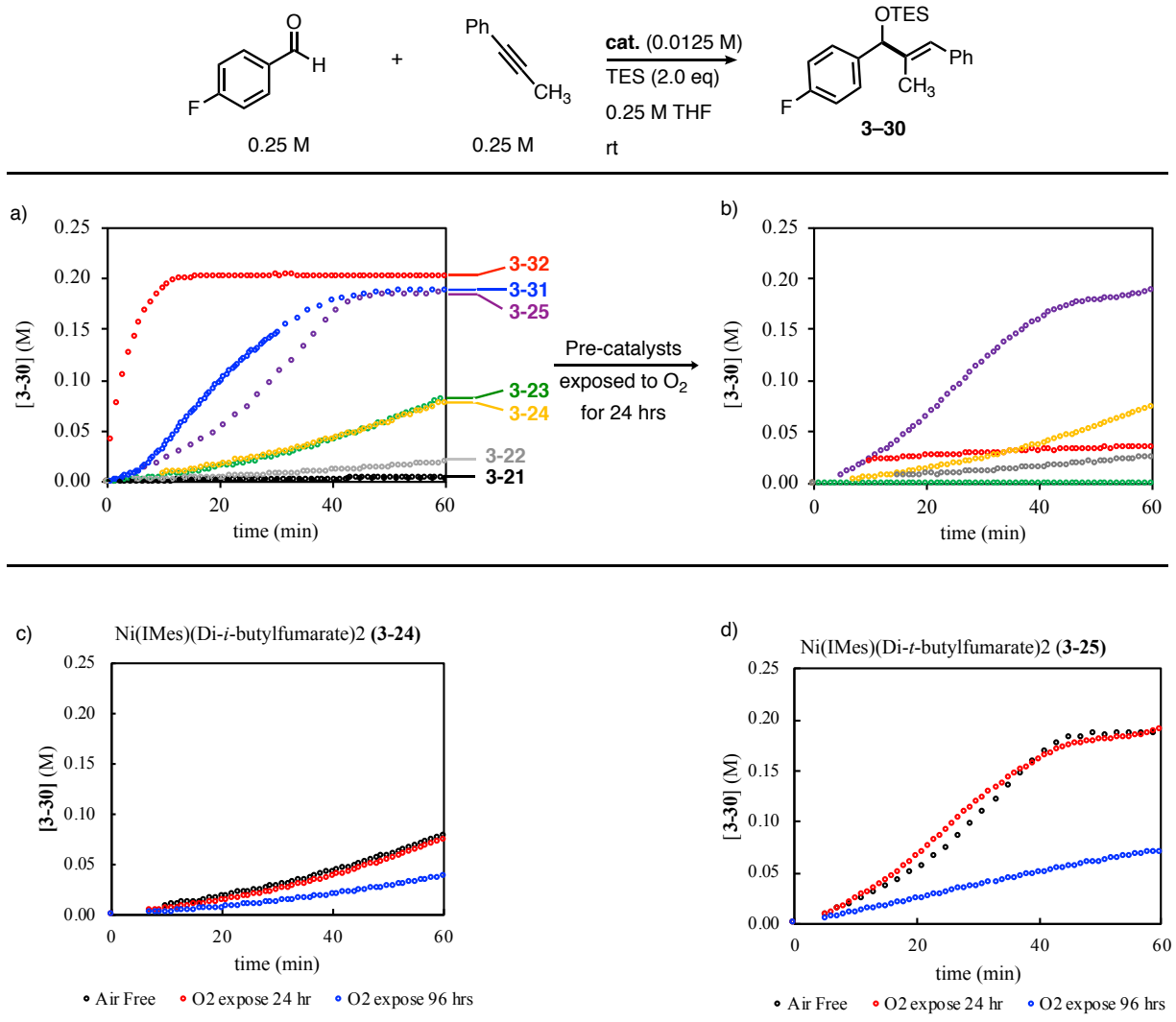


**Figure 3-14.** Oxidative stability studies. Reaction monitored by $^{19}F$ NMR using α, α, α-trifluorotoluene as an internal standard.

Long-term oxygen stability was tested for **3-25** and **3-24** since they were the most active of the fumarate series that completely retained catalytic activity after 24 hours of air exposure. Following a similar protocol as mentioned before, the two pre-catalysts were weighed into their respective vials and placed on the bench with the cap off for 96 hours. The result from these experiments are shown in Figure 3-14c and 3-13d. Both of the pre-catalyst catalytic activities dropped off, but there was still a significant amount of active catalyst that remained. Since these two complexes (**3-25** and **3-24**) show promising activities as air-tolerant pre-catalyst it is recommended that they be stored under a blanket of nitrogen in a desiccator, but during normal use air-free conditions are not necessary.

**Synthesis and Reactivity of [IMes–Ni(0)(mesaconate)]$_2$**

Intrigued by the high activity of methyl methacrylate supported IMes-Ni(0) pre-catalyst (**3-32**), it was envisioned that by substituting the fumarate scaffold with an α-methyl (using a mesaconate) that a balance of the activity of the methacrylate and stability of a fumarate could be achieved. When dimethyl mesaconate was evaluated as a ligand the desired product which has an empirical formula NHC:Ni:mesaconate of 1:1:2 was not observed. Instead a dark purple dimeric NHC-Ni(0) complex resulted (**3-35**, Figure 3-15). The structure of **3-35** was supported by the $^1$H NMR spectra, which definitively showed a single mesaconate for each IMes-Ni unit, and the dimeric nature of this complex was also supported by the crude X-ray structure. Interestingly, in the $^1$H NMR the vinylic proton was shift significantly up field (3.10 ppm) indicating a strong degree of back-bonding, which is expected if there is a single π-acceptor ligand versus two which is seen for the previously described fumarate complexes (Figure 3-8). From this result, it is likely that the steric profile of IMes cannot tolerate two mesaconate ligands resulting in the formation of

a bridged dimer as the most stable complex. In the dimer each nickel has one mesaconate bound as a π-acid and another bound in a σ-donor orientation.

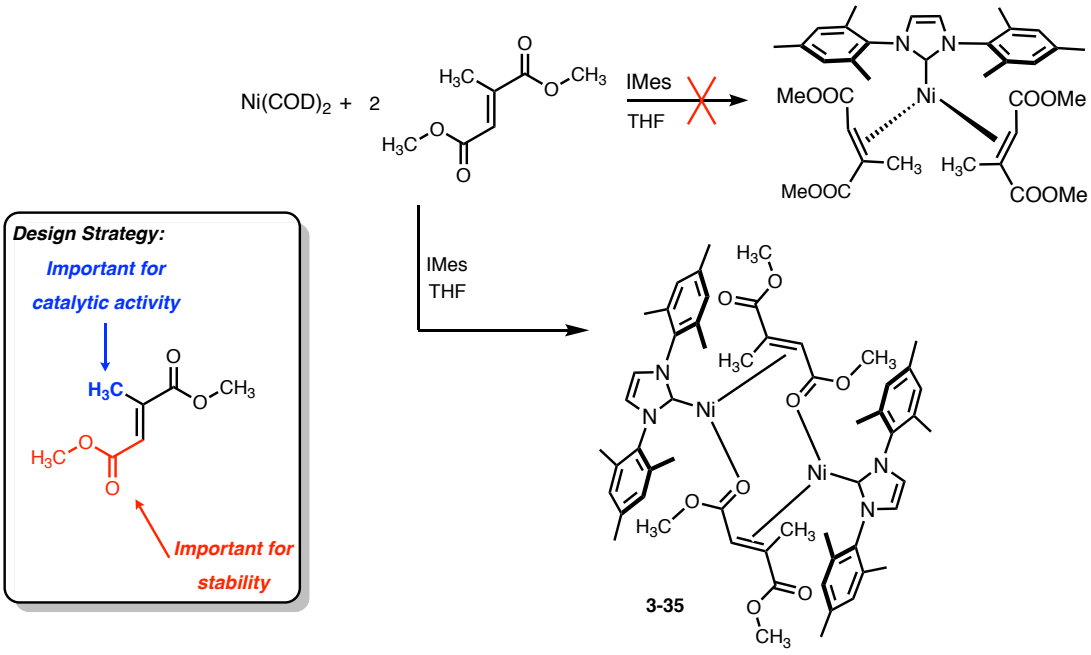


**Figure 3-15.** Synthesis of a dimeric nickel complex with mesaconate ligands.

Although **3-35** does not match ligand ratios of the other fumarate/acrylate complexes described above, its reactivity as a pre-catalyst for reductive couplings was investigated. We were pleased to see that **3-35** was a highly active pre-catalyst for this transformation (Figure 3-16). The rate of reaction and the overall profile looked similar to **3-32**, which has methyl methacrylate ligands. Although **3-35** showed promising activity, rapid discoloration of the complex when exposed to air was indicative of the air-sensitivity of **3-35** and the mesaconate ligand scaffold was not investigated further for IMes-Ni(0) complexes. This did however does provide a boundary for the steric limitations of this class of pre-catalyst.

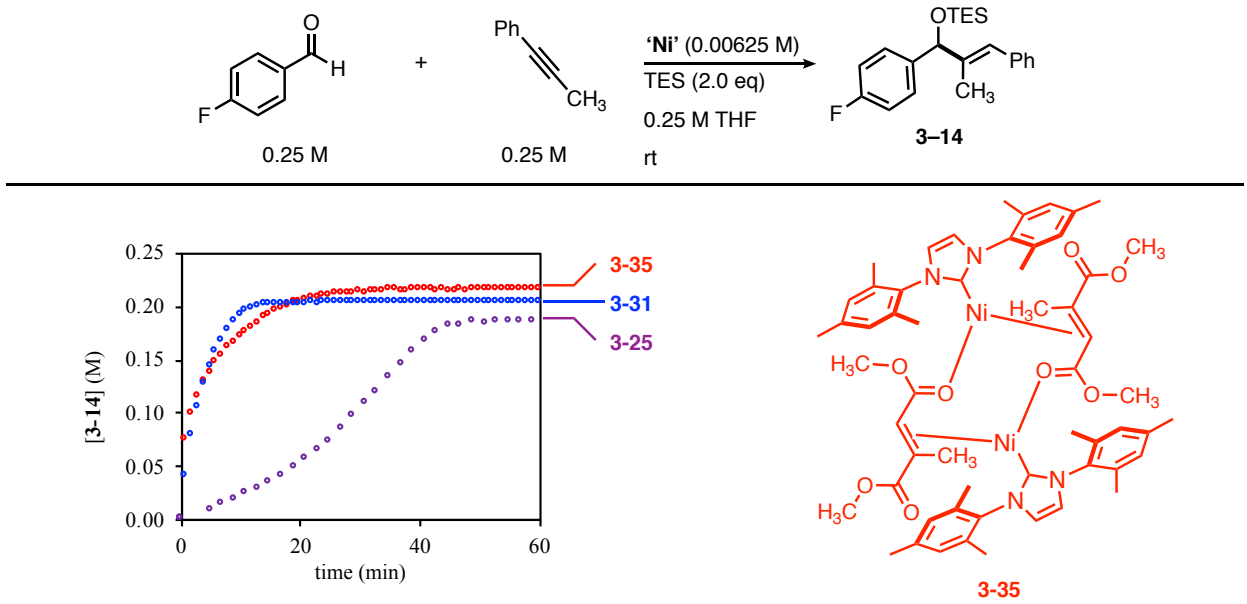


**Figure 3-16.** Catalytic activity of mesaconate dimer **3-35**. Reaction progression plots for the reductive coupling shown at the top of figure. Reaction monitored by $^{19}F$ NMR using α, α, α-trifluorotoluene as an internal standard. Note*- [**3-35**] = 0.00625 M to account for dimer.

## Substrates Scope for Reductive Couplings

Taking stability, reactivity and crystallization into consideration, it was determined that di-tert-butyl fumarate ligands are optimal for IMes-Ni(0) (**3-25**). To showcase the versatility of this **3-25** as a pre-catalyst a brief investigation of its scope and limitations in more complex reductive couplings were performed (Figure 3-17). Notably, catalyst loading could be lowered to 2 mol% which is exceptionally low for nickel-catalyzed reactions. In addition to electron-deficient aromatic aldehydes as described during the reactivity studies (Figure 3-11), aliphatic aldehydes work well as shown in **3-36**, in addition to other challenging substrates including Boc-protected amines. Additionally, both triethylsilane and di-tert-butylsilane can be used as terminal reductant for this transformation providing good yields of silyl-protected allylic alcohols (**3-37** and **3-38**). Compounds **3-37** and **3-38** also demonstrate that propargyl ethers and acetals are tolerated under the reaction conditions. One of the more interesting classes of substrates that are tolerated in this reaction are those containing aryl chlorides. Aryl chlorides are well precedented to undergo activation by Ni(0). As shown by **3-39** and **3-40**, 4-chlorobenzaldehyde readily couples with

enynes. In the case of **3-40** the silyl protected allylic alcohol couples dehydrogenatively with the diene that forms upon the reductive coupling, resulting in the formation of a silacycle. Transformations similar to this have been reported by our group.[134]

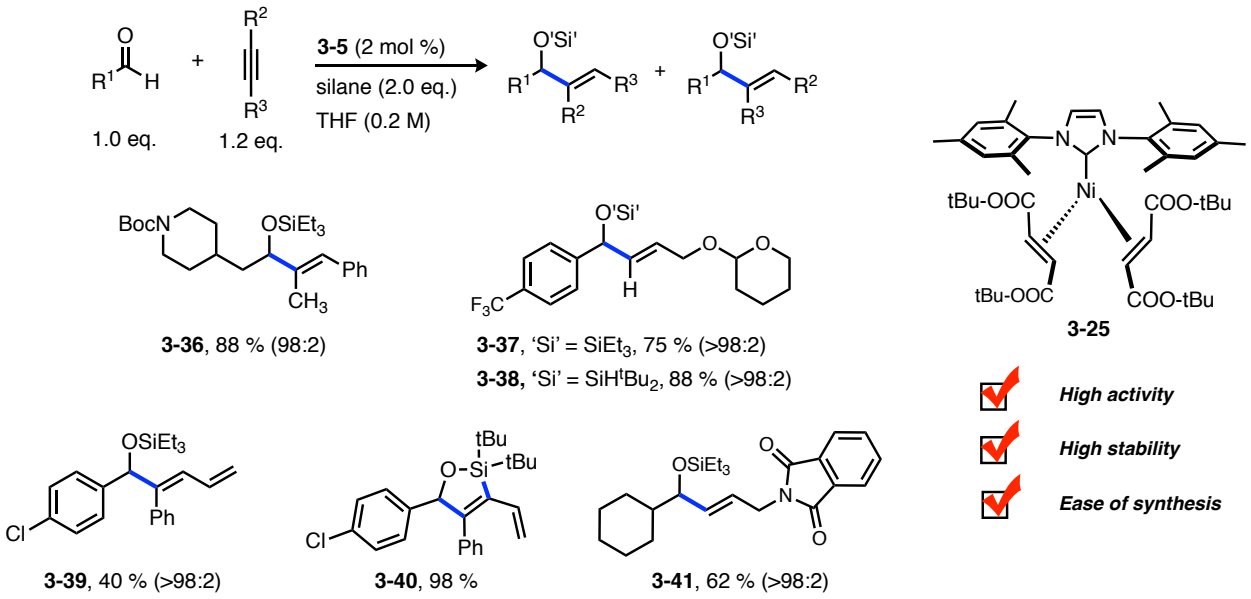


**Figure 3-17.** Substrate scope for reductive couplings.

## IPr*OMe-, IPr- and SIPr–Ni(0) Pre-Catalysts for Buchwald-Hartwig Couplings

### NHC–Ni Catalyzed C–N Bond Forming Cross-Couplings

Although the majority of cross-couplings carried out in synthetic chemistry employ palladium catalysis, nickel-catalyzed C–C and C–heteroatom bond forming reactions have a rich history and have played a crucial role in the development of this Nobel Prize winning field. Early work in the infancy of the field of cross-coupling, Kumada and Corriu demonstrated nickel-catalyzed couplings of Grignard reagents and $sp^2$ organic halides.[4] Later work by Negishi showed similar types of reactivity with organozinc reagents,[137] where it was also demonstrated that palladium-based catalysts were capable of performing this reaction with improved selectivity and minimized byproduct formation. For these reasons, in addition to the overall robustness of

palladium catalysis, the scientific community has developed an overwhelming preference for palladium when construct $sp^2$-$sp^2$ bonds. Although there are many advantages to employing palladium for cross-couplings, there are several drawbacks such as limited electrophile scope and low natural abundance that have led to a significant effort to develop novel and/or analogous methods that utilize nickel.

One of the hallmarks of nickel-catalyzed cross-coupling procedures is the unique ability for nickel to readily activate traditionally unreactive electrophiles. Most notably, nickel is a prolific catalyst for activating electrophiles like aryl chlorides and a variety of protected phenols. Shown in Figure 3-18 are several examples highlighting the unique reactivity of NHC-Ni catalysts in cross-coupling reactions. Nickel is known to participate in Suzuki-Miyaura cross-couplings between aryl boronic acids and complex imidazolium electrophiles to construct a C–C bonds (Figure 3-18). Although pseudo-halides such as aryl triflates work well with palladium-catalyzed protocols, triflates are expensive to make and are highly sensitive making them non-ideal for multi-step synthesis.[3] Our group, as well as several others, have demonstrated that typically inert C–O bonds like silyl and carbamate protected phenols have entered the lexicon of useful aryl electrophiles when employing nickel catalysis for cross-couplings (Figure 3-18).[14,138,139] Finally, the development of Buchwald-Hartwig coupling that has completely changed the way C–N bond are constructed traditionally uses palladium-catalysis with complex designer phosphine ligands. Recently there has been several examples demonstrating the utility of nickel for coupling aryl-chlorides in this chemistry which is traditionally difficult for palladium catalysts.[3]

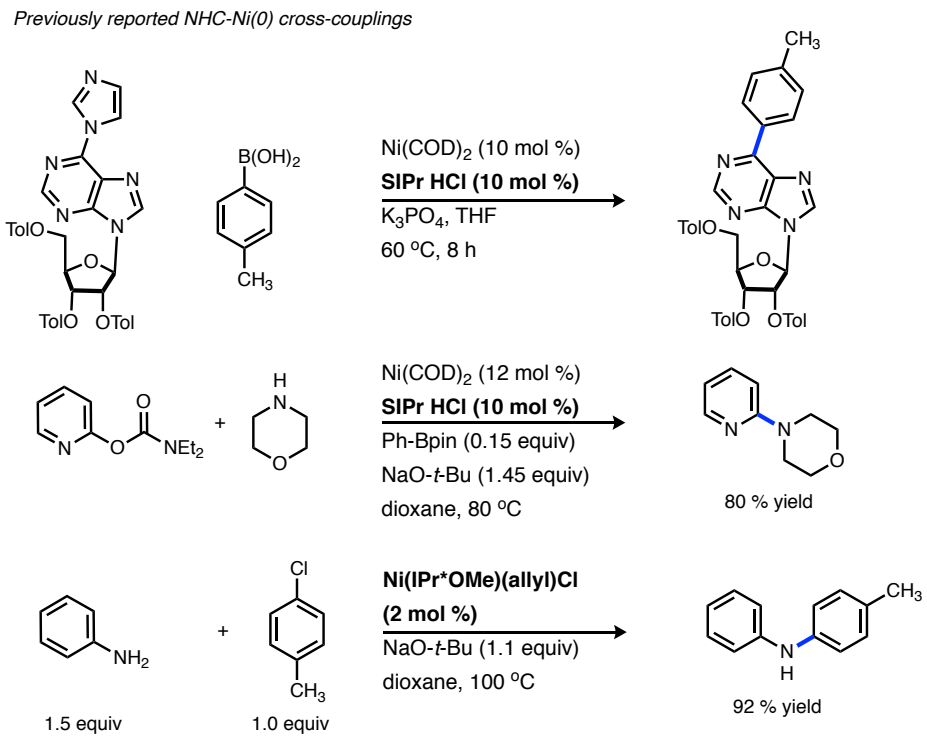


**Figure 3-18.** Select examples of nickel-catalyzed cross-couplings reported in the literature.

It should be noted that in the examples highlighted in Figure 3-18 the NHC ligands employed have large sterically hindered N-aryl groups. This strategy is relatively common for NHC-Ni catalyzed cross-couplings methods regardless of the electrophile used. Since nickel is more nucleophilic than palladium the barrier for oxidative addition should be lower when using nickel versus palladium. A consequence of this inherent electronic bias is that reductive elimination to form challenging bonds is likely more difficult for nickel-catalysts, hence the need for larger ligands. As it is well known, increasing sterics at the metal center facilitates a more rapid reductive elimination (Figure 3-19).

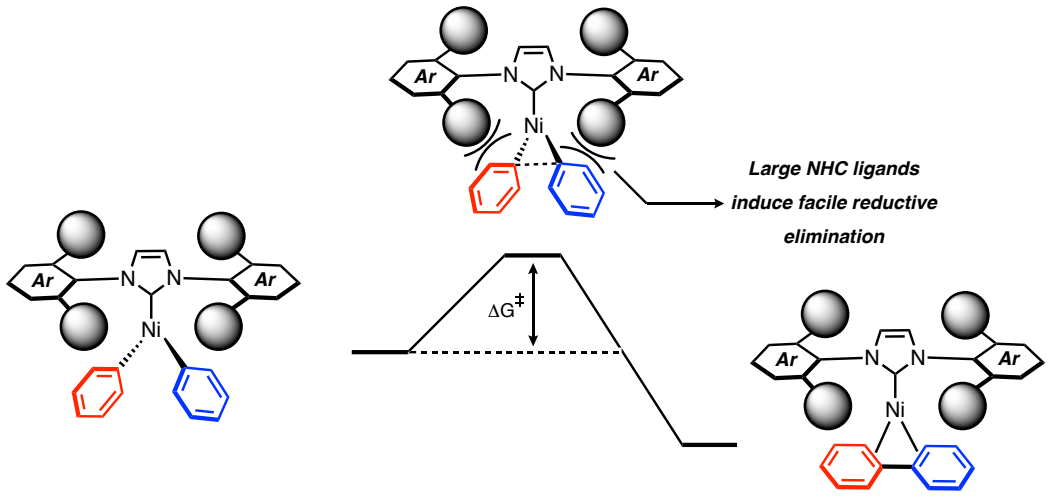


**Figure 3-19.** Larger NHC ligands facilitate reductive elimination.

To further aid the development of well-defined NHC-Ni(0) pre-catalysts for organic transformations, we envisioned building a suite of NHC-Ni(0) complexes that are stabilized by π-acidic ligands that could be used for cross-couplings. The NHC ligands that were chosen for this study were IPr, SIPr, and IPr*OMe as they have all been shown to form highly active nickel-catalysts for cross-couplings (Figure 3-20). IPr and SIPr are broadly used NHC ligands that have been employed for various transition metals-mediated reactions. Our group specifically has used these NHC ligands to control regioselective outcomes in reductive couplings and tune chemoselectivity in a variety of reactions. For these reasons, we envisioned the development of stable pre-catalyst bearing NHC ligands would be broadly useful to the scientific community. A more recent advancement in novel NHC structures is the development of IPr*OMe which has a very large steric profile and has gained traction as a ligand for C–N bond forming reactions using nickel. We also realized early on in the development of this subset of NHC-Ni(0) pre-catalysts that the need for larger NHC ligands presented new challenges in the acrylate and fumarate ligands that are tolerated.

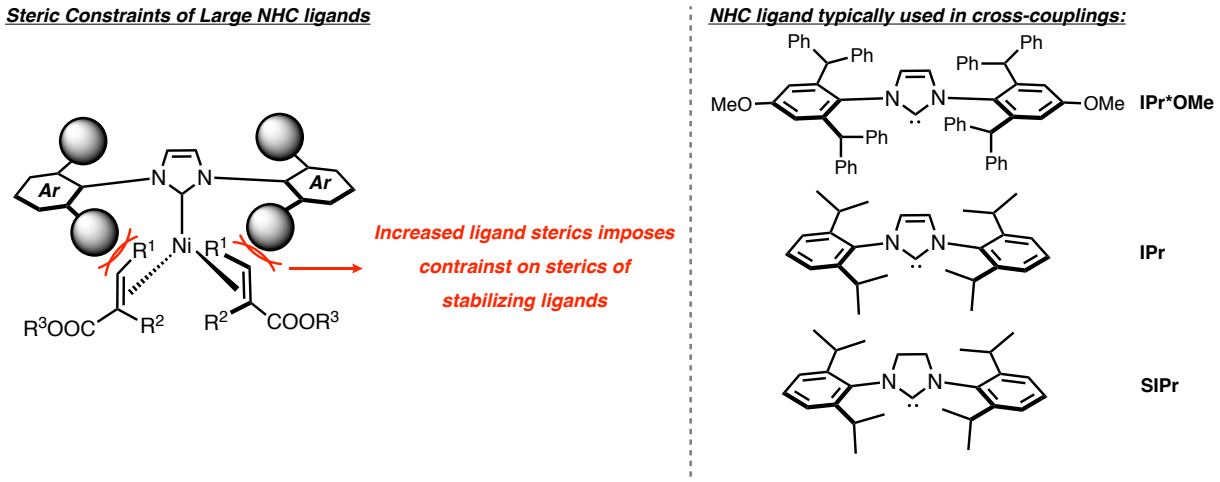


**Figure 3-20.** Consequences of NHCs typically used in cross-couplings on designing well-defined and stable NHC-Ni(0) complexes.

Complexes of DMFU have only been reported with IPr and IMes, as described early in this chapter.[133] Attempts to synthesized DMFU complexes with either SIPr or IPr*OMe was particularly challenging, likely as a result of clashing with the NHC ligand bound to metal center. Although fumarate complexes of IPr*OMe could be ruled unlikely to form based purely on structural analysis of the NHC ligand, it was puzzling that DMFU complex of SIPr were not cleanly obtained. In the case of IPr*OMe-DMFU the reactions all decomposed after several hours and the crude NMR showed a complex mixture of products. In the case of SIPr small amounts of the desired complex could be seen by crude NMR analysis, but the major product appeared to be dimeric in nature, similar to **3-35**, and as a result the SIPr crude reaction mixtures were deep purple in color. Due to complexities of cleanly isolating a single well-defined complex we envisioned that this would not be a modular class of pre-catalysts and therefore fumarates were not investigated in for the larger NHC ligands.

**Synthesis and Structure of NHC–Ni Complexes with Large NHC Ligands**

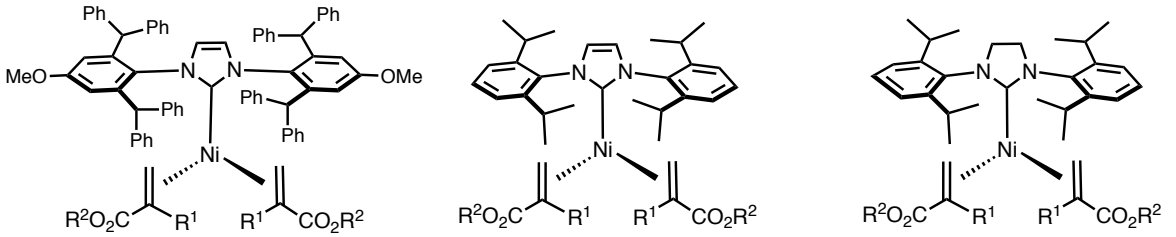


**3-42**: $R^1$= -H, $R^2$ = $-CH_3$, 85 %
**3-43**: $R^1$ = -H, $R^2$ = -Ph, 94 %

**3-44**: $R^1$= -H, $R^2$ = $-CH_3$, 92 %
**3-45**: $R^1$ = -H, $R^2$ = -Ph, 60 %
**3-46**: $R^1$ = $-CH_3$, $R^2$ = $-CH_3$, 81 %

**3-47**: $R^1$= -H, $R^2$ = $-CH_3$, 80 %
**3-48**: $R^1$ = -H, $R^2$ = -Ph, 51 %
**3-49**: $R^1$ = $-CH_3$, $R^2$ = $-CH_3$, 78 %

**Figure 3-21.** Synthesis of Large NHC-Ni(0) Complexes.

As a result of the observation discussed above, various acrylate and methacrylate ligands were tested for nickel complexes of the larger NHC ligands. Synthesizing the complexes in a similar way as described for the IMes series (Figure 3-12), rapid ligand substitution from $Ni(COD)_2$ with the respective acrylate followed by addition of the NHC ligand resulted in good yields of the desired complexes. Interestingly, IPr*OMe presented such a sterically hindered metal center that methacrylate ligands could not be used to make complexes of the empirical formula NHC:Ni:acrylate of 1:1:2. Instead, methacrylate ligands yielded yellow, air-sensitive, diamagnetic products which appeared to be a mixture of several different complexes by $^1H$ NMR. Attempts to crystallize or characterize these complexes further by X-ray diffraction was unsuccessful. Therefore the optimal ligand class for IPr*OMe was determined to be acrylates and complexes (IPr*OMe)Ni(methyl acrylate)$_2$ (**3-42**) and (IPr*OMe)Ni(phenyl acrylate)$_2$ (**3-43**) could be synthesized as highly crystalline yellow compounds. Qualitative evaluation of the air-stability of these complexes revealed that there was almost no discoloration of **3-43** after 24 hours on the bench exposed to ambient conditions. Furthermore X-ray quality crystals of complex **3-43** were obtained which provided some justification of steric constraints of IPr*OMe–Ni(0) subunit.

The X-ray structure of **3-43** has several interesting structural features that highlight metal-ligand interactions. The degree of back-bonding character of the Ni-acrylate interaction

can be seen in the increased bond length of the C–C double bond of the acrylate. Where in **3-43** the length of the C79-C80 double bond is measured at 1.404 Å; this is much longer than a typical C–C double bond, which is approximately 1.33 Å. The increase in bond length here is likely a result of back-bonding from the nickel d-orbitals into the π*-orbital of the acrylate weakening the C–C double bond. The Ni–$C^{NHC}$ bond length for **3-43** is 1.924 Å which is slightly longer than the Ni–$C^{NHC}$ bond length of (IPr*OMe)Ni(allyl)Cl (**3-7**, Figure 3-3) which is 1.899 Å. It difficult to assign the origin of the increased Ni–$C^{NHC}$ bond length for **3-43** since it unclear whether the increased steric demands of the phenyl acrylate ligands or the change in oxidation state of nickel (from Ni(0) in **3-43** to Ni(II) in **3-7**) is responsible.

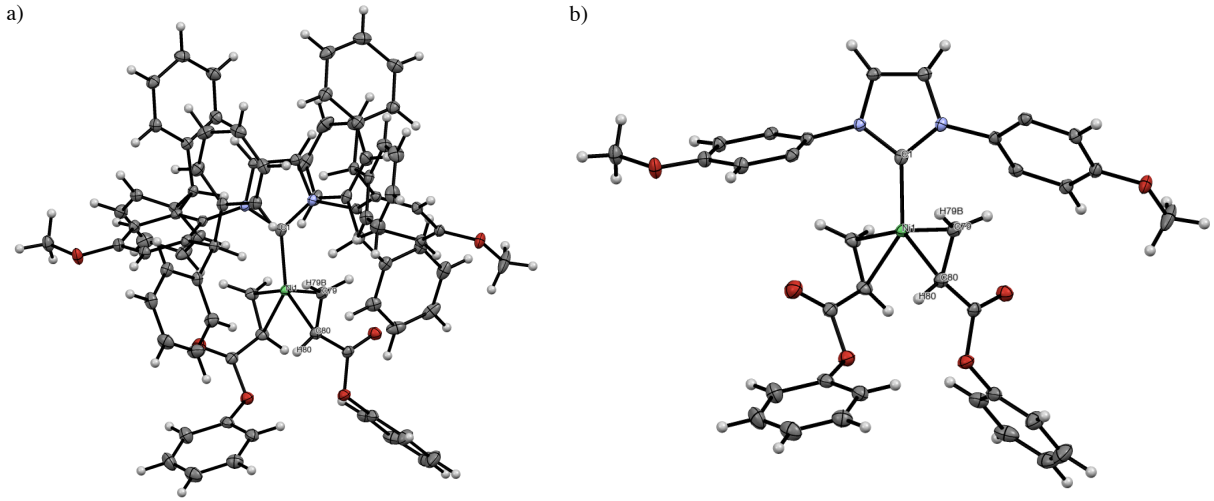


**Figure 3-22.** a) ORTEP of **3-43** b) The ortho-substituents on the N-aryl groups have been omitted for clarity. Both ORTEPs with thermal ellipsoids displayed at 50 % probability.

Analogous complexes of methyl acrylate and phenyl acrylate could also be accessed from $Ni(COD)_2$ for both IPr and SIPr (Figure 3-21). In addition to acrylate ligands being tolerated for IPr and SIPr, methyl methacrylate ligands could also be used as a result of less steric hindrance at the nickel center for these ligands. Although X-ray analysis was not done for these complexes, the

NMR data compared to that of **3-43** and the IMes series is consistent with the same general framework as shown in Figure 3-21.

**Reactivity Comparison for Amination Cross-Couplings**

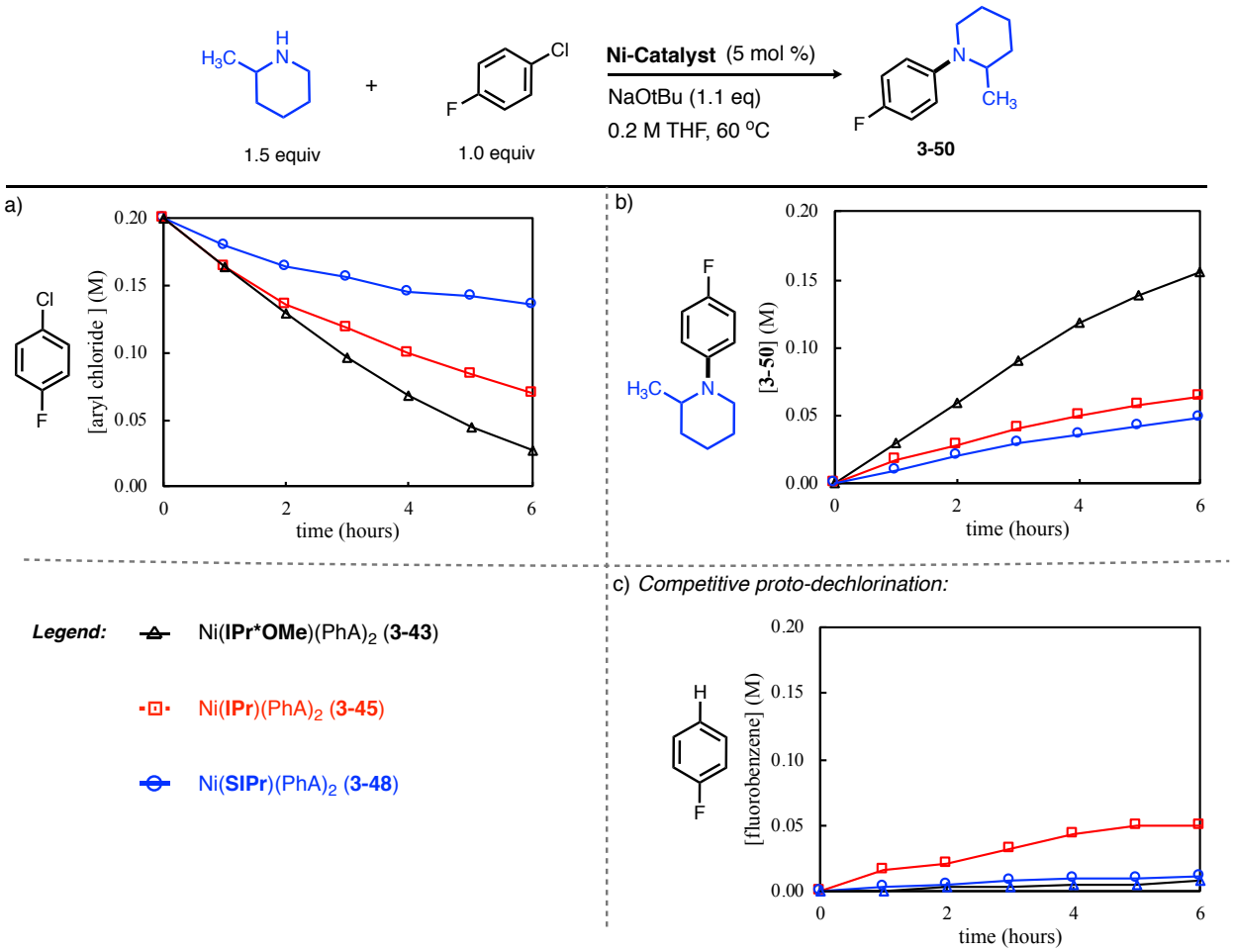


**Figure 3-23.** Reaction progress analysis of the amination shown at top of figure. The profiles shown above compare NHC ligand for N-arylation. a) Consumption of starting material. b) Product (**3-50**) formation. c) Proto-dechlorination byproduct formation. All reactions were monitored by $^{19}$F NMR using α, α, α-trifluorotoluene as an internal standard.

The N-arylation of 2-methylpiperidine with 4-fluorochlorobenzene was chosen as a model reaction for assessing the reactivity of each pre-catalysts. This specific reaction is challenging due to a sterically hindered nucleophilic coupling partner and therefore an appropriate reaction to benchmark the reactivity of each catalyst. It is important to note that although the electrophile is activated it serves as an NMR handle, allowing the reaction to be monitored by $^{19}$F NMR. By

evaluating the reaction profile insights could be obtained regarding initiation rates, rate of product formation and the production of undesired byproducts. A common byproduct in nickel-catalyzed cross-couplings is proto-dehalogenation, which could also be monitored over the course of the reaction. To compare the performance of each IPr, SIPr, and IPr*OMe the phenyl acrylate pre-catalyst of each respective NHC was tested as shown in Figure 3-23. Evaluation of the rate of product formation reveals that complex **3-43**, which contains IPr*OMe, is the superior pre-catalyst (Figure 3-23b). Interestingly, the rate of product formation appears to be independent of the concentration of substrate supported by the linear growth of product for the first 4 hours of the reaction. The overall pseudo-zero-order reaction profile is less pronounced for IPr (**3-45**) and SIPr (**3-48**), but the rate of product formation for both catalysts is significantly slower than **3-43**. As mentioned, real time monitoring of the reaction provides a more detailed assessment of the overall performance of each of pre-catalysts. For example, the initial rate of consumption of the 4-fluorochlorobenzene for **3-43** and **3-45** are near identical (Figure 3-23a), but after the first two hours of the reaction with **3-45** begins to slow down. Although the initial rates of starting material consumption are similar for **3-45** and **3-43**, the rate of product formation is quite different due to rapid proto-dechlorination catalyzed by **3-45** (Figure 3-23c).

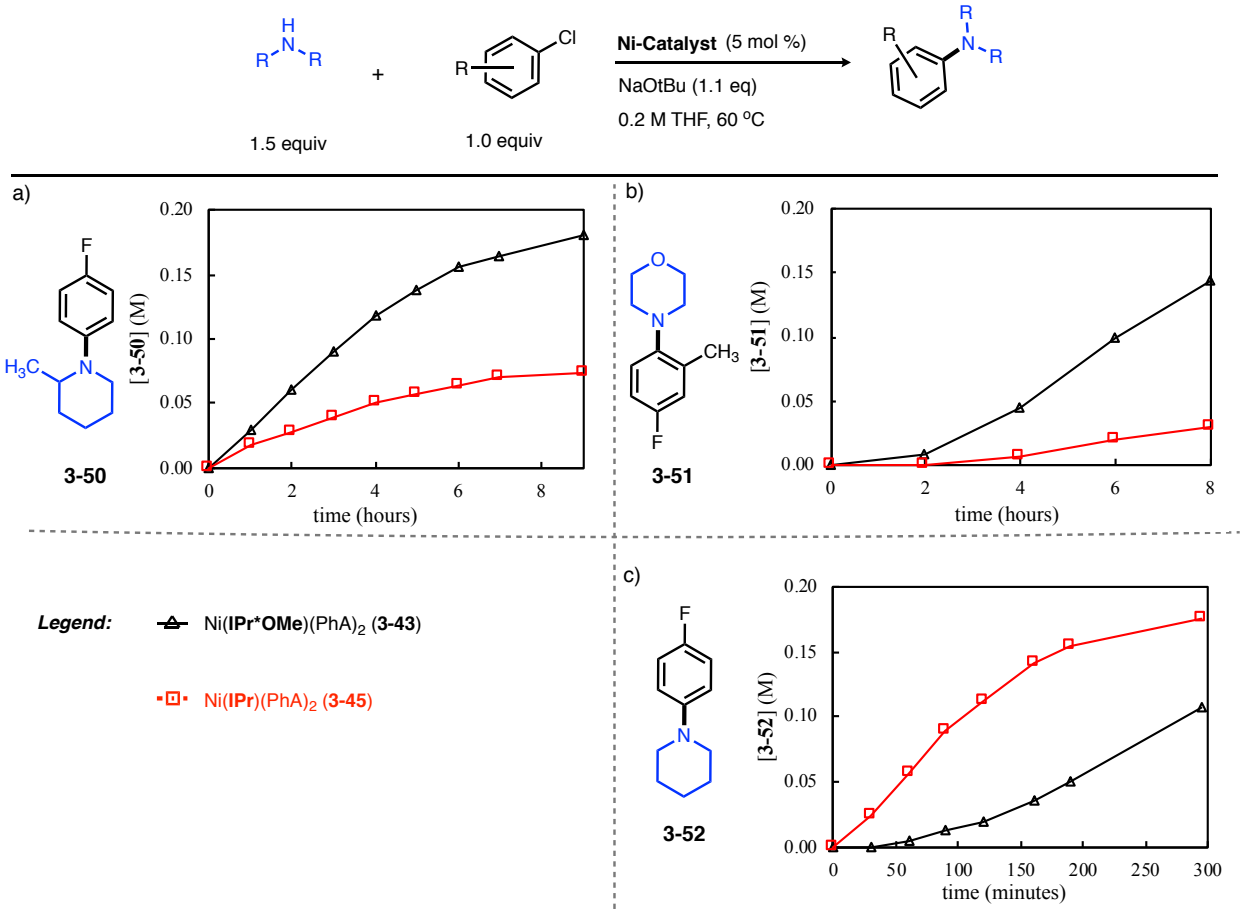


**Figure 3-24.** Reaction progression analysis of the amination shown at top of figure. The profiles shown above compare NHC ligand for N-arylation. All reactions were monitored by $^{19}F$ NMR using α, α, α-trifluorotoluene as an internal standard.

Some interesting phenomena were observed while investigating the substrate scope for the pre-catalysts. As shown in Figure 3-24 for coupling sterically hindered nucleophiles and unhindered electrophiles, IPr*OMe is the optimal ligand. Switching the sterically hindered coupling partner from the nucleophile to the electrophile shows that following a short induction period of about an hour, the reaction begins to form product in a linear fashion for both **3-43** and **3-45** (Figure 3-24b). Consistent with the previous coupling of 2-methylpiperidine, **3-43** is a much better pre-catalyst for this reaction. However, if piperidine, a much less hindered substrate, is coupled with an unhindered electrophile a very different conclusion is reached. Shown in Figure 3-24c, when both coupling partners are unhindered IPr (**3-45**) is a significantly better ligand for

N-arylation. There is no observed initiation period for **3-45** and similar to previously discuss kinetics, there rate of product formation seems to be independent of substrate concentration until later points in the reaction. Pre-catalyst **3-43** on the other hand is much slower with a profile that reveals the rate of product formation slowly increases over time, similar to a sigmoidal profile. The mechanistic implications of these results will be discussed later in this chapter.

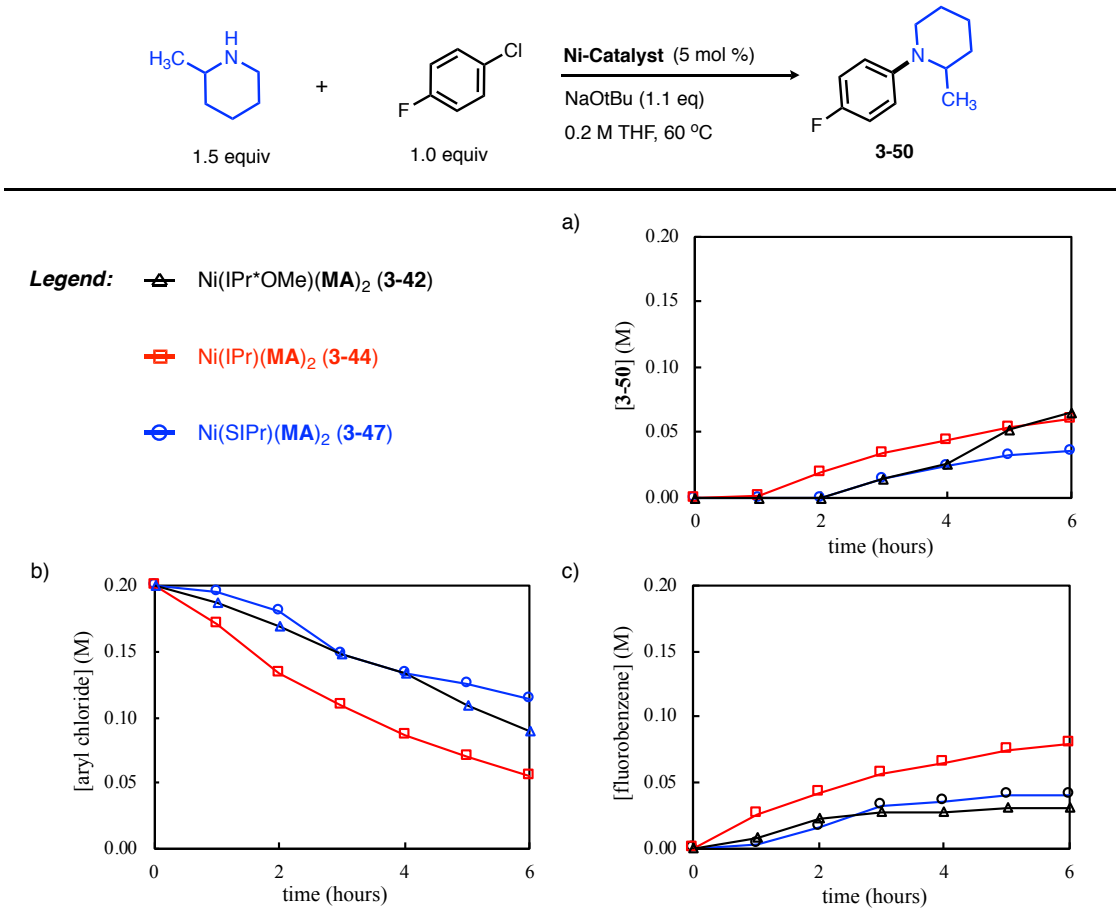


**Figure 3-25.** Reaction progression analysis of the amination shown at top of figure with the methyl acrylate pre-catalyst series. The profiles shown above compare acrylate ligands on the Ni-center All reactions were monitored by $^{19}F$ NMR using α, α, α-trifluorotoluene as an internal standard.

The phenyl acrylate-based pre-catalysts discussed thus far have proven to be highly active pre-catalysts for amination cross-couplings. The methyl acrylate series for IPr, SIPr, and IPr*OMe performed quite differently from the phenyl acrylate series and the reaction characteristics will be discussed here. Using the standard coupling of 2-methylpiperidine and 4-fluorochlorobenzene the

methyl acrylate catalysts were evaluated. As shown in Figure 3-25a, there appears to similarities between all of the pre-catalysts during early stages of the reaction. Long induction periods are observed for each of the catalysts where trace product and in some case no product (**3-50**) is formed during the first hour of the reaction. After the first hour the IPr-based pre-catalyst **3-44** starts to form product at a slow rate, but the other two pre-catalysts remain unproductive. The reactions containing IPr*OMe (**3-42**) and SIPr (**3-47**) do not begin to form product (**3-50**) until after the two-hour mark after which product slowly begins to form. The origin of the induction period associated with product formation becomes more complex with assessing the rate of starting material consumption and proto-dechlorination. Figure 3-25b shows the rate at which aryl chloride in consumed and surprisingly, there is no observed induction period. This artifact of the reaction profile is accounted for in the formation of fluorobenzene via undesired proto-dechlorination. Shown in Figure 3-25c is the formation of fluorobenzene for each of the respective catalysts and no induction period is observed for any of the pre-catalysts. It should be noted that for **3-43**, the phenyl acrylate based IPr*OMe pre-catalyst, discussed earlier there was only trace amounts of fluorobenzene formed over the entire course of the reaction (Figure 3-23) where **3-42** with methyl acrylate ligands forms an appreciable amount during the very early stages of the same reaction.

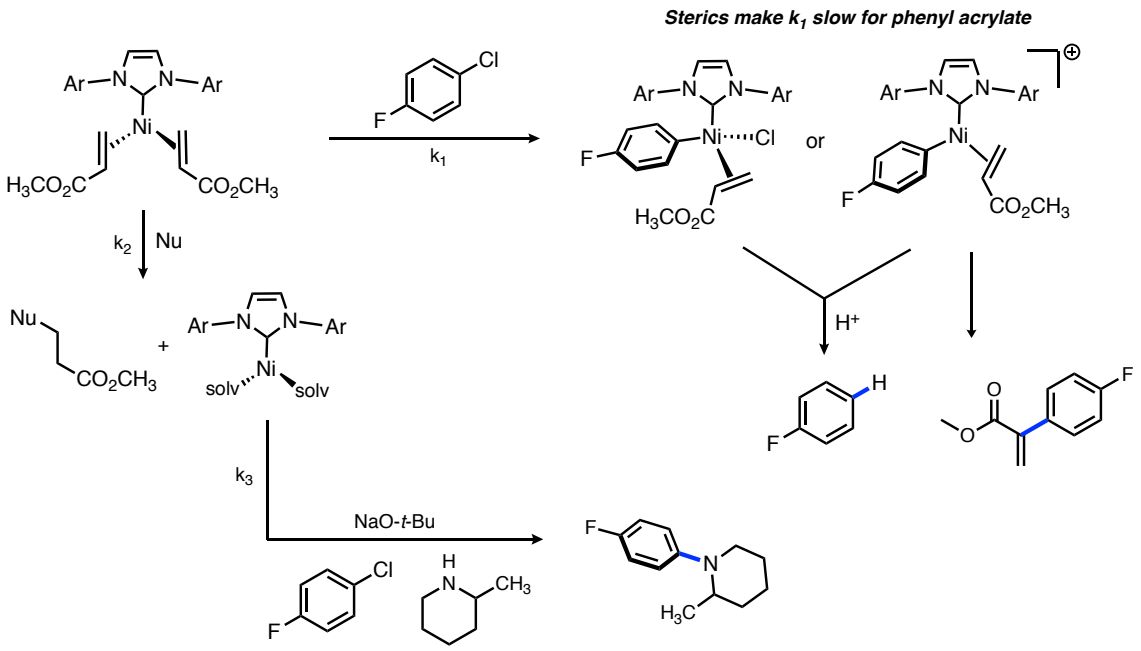


**Figure 3-26.** Proposal for differences between methyl and phenyl acrylate stabilized pre-catalysts.

Although more data is necessary to explain what is happening for the methyl acrylate pre-catalysts that is not observed with the phenyl acrylate, conclusions can be drawn from what is shown in Figure 3-25a-c. First, neither phenyl nor methyl acrylate have an induction period for the consumption of aryl chloride. Second, (IPr*OMe)Ni(phenyl acrylate)$_2$ (**3-43**) forms trace dechlorination and (IPr*OMe)Ni(methyl acrylate) (**3-42**) forms significant amounts. Third, methyl acrylate pre-catalysts have long flat induction periods and phenyl acrylate pre-catalysts do not. This could suggest that acrylate identity plays a crucial role in regulating product formation. Consumption of aryl chloride via dechlorination suggests that oxidative additions is operative, but transamination or reductive elimination is difficult. Since the amine does not change between Figure 3-23 and Figure 3-25, it could be that the smaller methyl acrylate is able to stabilize a σ-aryl nickel complex that would result from oxidative addition while phenyl acrylate is too large (Figure 3-26). One could envision proto-dechlorination becoming operative as this specie is built-up during the early stages of the reaction. Another potential scenario would be an analogous σ-

aryl species promoting Heck products with methyl acrylate. Furthermore, the long induction period for formation of product could signify that acrylate must be consumed via a side reaction in order to diminish the formation of an acrylate stabilized σ-aryl nickel complex, thus promoting product formation. Under the proposed mechanism just described, $k_1$ for proto-dechlorination is faster than $k_2$, which is consumption of methyl acrylate. The rate of product formation, $k_3$, is dependent on $k_2$ as a means of generating the active form of the catalyst and shutting down $k_1$ (Figure 3-27).

**Experiments Probing Pre-Catalyst Initiation**

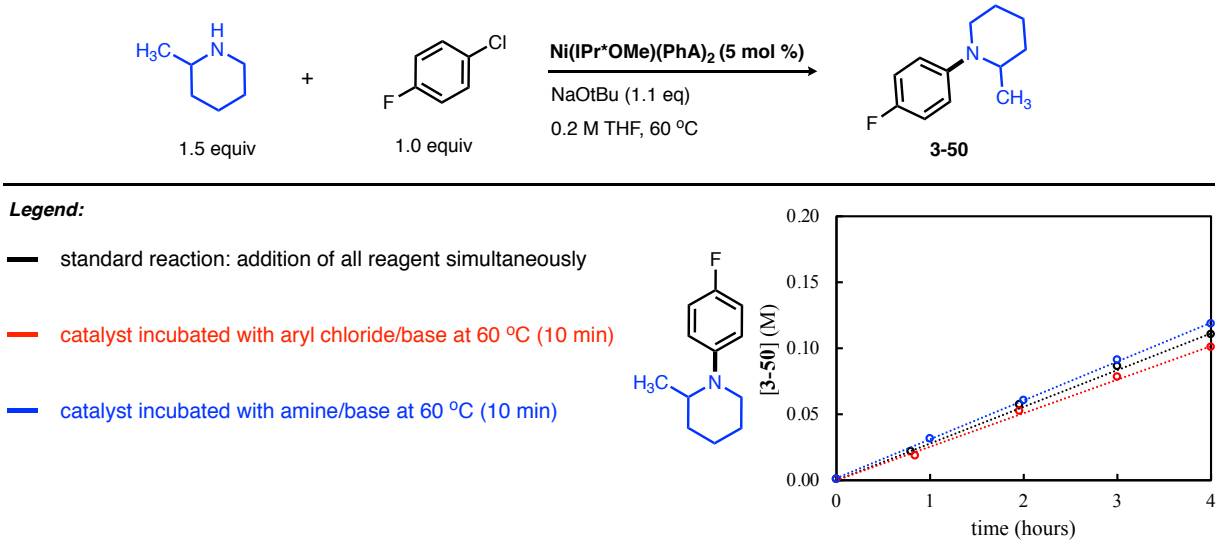


**Figure 3-27.** Probing pre-catalyst activation and fate of acrylate ligands. All reactions were monitored by $^{19}F$ NMR using α, α, α-trifluorotoluene as an internal standard.

Despite the interesting reaction profile features present in the methyl acrylate series of pre-catalysts, it is clear that phenyl acrylate is a superior stabilizer ligand. Additionally, IPr*OMe is the optimal ligand with the exception of sterically unhindered couplings, but these reactions go to completion after several hours, whereas IPr-based pre-catalysts are faster for small substrates. Considering all of the reaction features for **3-43** catalyzed N-arylation discussed in this chapter, the origin of pseudo-zero-order character of reaction profile remains a question. In order to probe the role that phenyl acrylate plays during the reaction, a series of incubation studies were

performed. We had hoped to gain insights into whether phenyl acrylate is consumed in the initial stages of the reaction releasing a much more active form of the catalyst or if the phenyl acrylate is present throughout the course of the reaction.

Two reactions were designed to gain information regarding the activation **3-43** under the reaction conditions. We envisioned that pre-stirring the catalyst with base and amine could potentially amidate the acrylate to release active catalyst. To test this, the reaction vessel was charged with 2-methyl piperidine, NaOtBu, and **3-43** and was stirred at 60 °C for 10 minutes prior to the addition of 4-fluorochlorobenzene, after which the reaction was monitored as usual. As shown in Figure 3-27, the rate of product formation for this experiment (blue) nearly overlays with the control (black). Furthermore, pre-stirring the pre-catalyst with aryl chloride and base following the same general protocol reveals the same observed rate of product formation. These reactions alone are by no means conclusive, but they do support the fact that an acrylate bound nickel specie could play an important role during catalysis.

If an acrylate bound species like **3-43** is present throughout the course of the reaction and it is playing a role during catalysis, it could offer a potential explanation as to why the reaction appears overall zero-order. It is possible that if **3-43** is the resting state for catalysis and the removal of two phenyl acrylate ligands is necessary to generate the turnover-limiting transition state that there would be an inverse second-order dependence in phenyl acrylate, or inverse first order in only one of the acrylates needs to leave the metal. The association of two components during the turnover-limiting step would result in a second-order rate dependence on substrates. The net rate law would be overall zero-order in this case. Again, it should be considered that these are speculations and more detailed experimental data is necessary to establish a complete reaction

mechanism for this class of pre-catalyst. The proposed mechanism based on the preliminary data presented herein is shown in Figure 3-28.

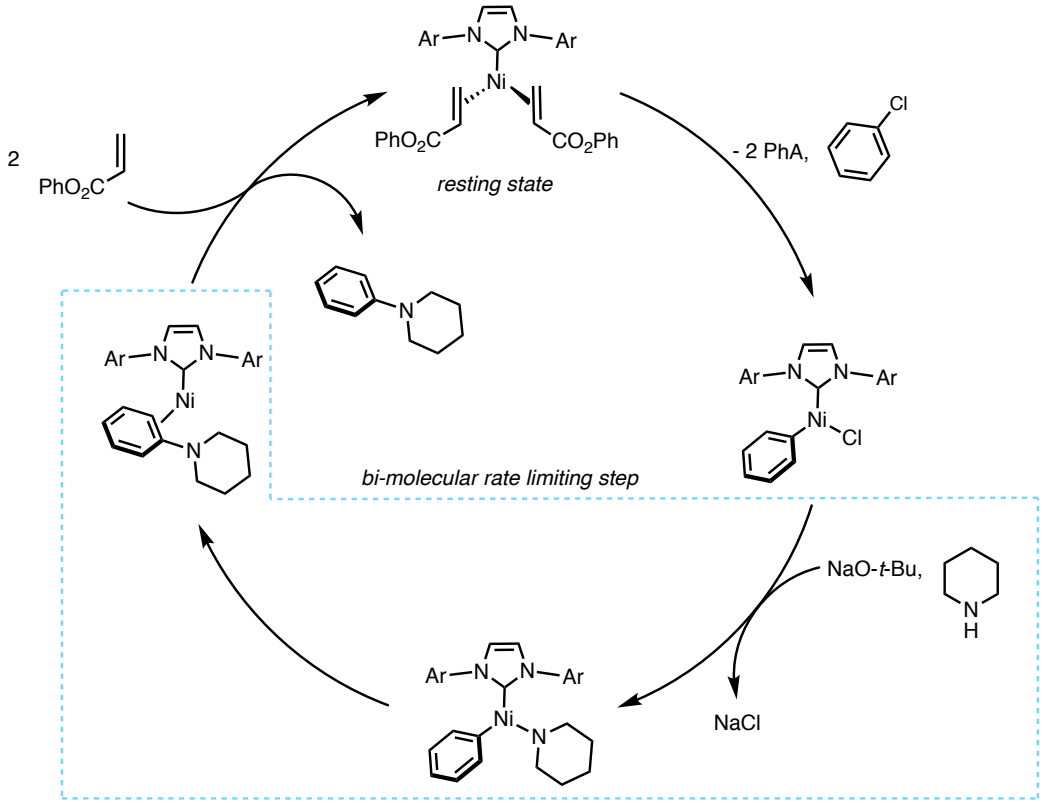


**Figure 3-28.** Preliminary proposed mechanism for N-arylation.

### Substrate Scope for Amination

Finally, to investigate the robustness of **3-43** as a broadly useful pre-catalyst for N-arylation of aryl chlorides the scope and limitations were investigated. A wide variety of electrophiles work in this chemistry including several heteroaryl chloride including pyridine (**3-53**) and quinolines (**3-54**). Pre-catalyst **3-43** is also able to couple highly sterically hindered coupling partners that are ortho-substituted (**3-55** and **3-56**). An example that highlights the selectivity of this catalyst is **3-59** which contains a methyl ketone which is known to undergo competitive α-arylation under similar reaction conditions. There are a variety of amine coupling partners that work well. Simple secondary amines work well for this reaction, as well as sterically hindered secondary amines like

the 2-pyridyl-pyrrolidine in **3-57** and **3-58** which comes from the core of nicotine. A hallmark of this pre-catalyst is the ability to efficiently couple amine substrates that lack β-hydrogens, like anilines and tert-butyl amine. These types of nucleophiles are rare in nickel-catalyzed amination reactions since it is proposed that the β-hydrogens are necessary to generate Ni(0) from well-defined Ni(II) pre-catalysts. In that vein, a variety of anilines work well for this reaction including hindered (**3-55**) and simple (**3-56** and **3-59**) anilines. The lability of this pre-catalyst for coupling anilines is highlighted in **3-56** where is it shown that it works quite well at room temperature as well.

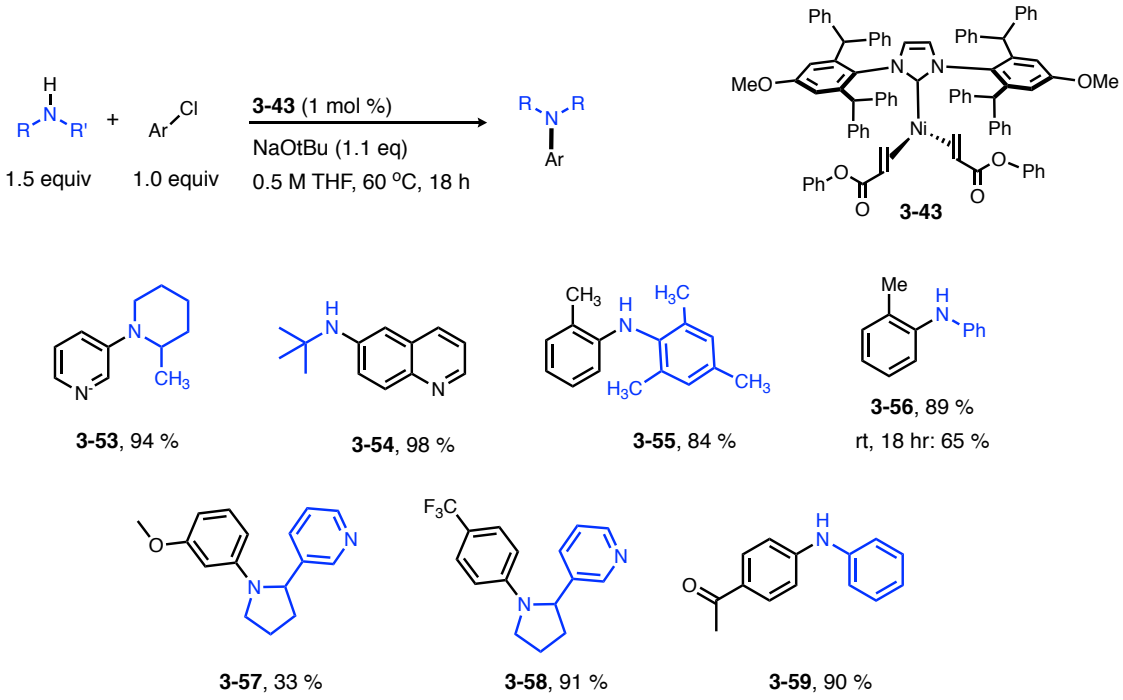


**Figure 3-29.** Substrate scope for N-arylation.

## Chapter 4 Conclusions and Future Outlook

Nickel-catalysis has yielded numerous synthetic advancements that have leveraged nickel-catalysis as a viable strategy for the development of many valuable synthetic methodologies. One of the greatest challenges in promoting the widespread use of these methods lies in the operational barriers of accessing nickel in a catalytically relevant state and reducing undesired reactivity. Chapters 2 and 3 have highlighted our efforts to understand how to diminish undesired activity in nickel catalyzed hydroarylations and to develop stable Ni(0) pre-catalysts that are readily activated under mild conditions. Although I believe that we have made significant advancements in both of these areas, the insight gained from these works will influence future developments in nickel catalysis. As stated by Fisher in 1912, *"This chapter on catalysis is unlimited and it is here that a systematic investigation promises to bring a rich reward."* This is still true today as many novel transformations are being reported that push the boundaries of what was is possible through nickel-catalysis.

### Recyclable C-H bonds: LLHT for Generating Reactive Organo-Nickel Species

The field of nickel-catalyzed C-H functionalization has seen many promising developments in recent years. This has provided several valuable bond disconnections via cross-couplings and hydroarylations, among other transformations that were not previously possible. A plethora of heterocyclic substrates can be tolerated under a variety of reaction manifolds exhibiting excellent C-H bond selectivity. Nickel's high selectivity for specific C-H bonds has been both a hallmark and a downfall since the scope of arene C-H bonds, regardless of the transformation, are

relatively similar. There has been little done to address this limitation due to the aforementioned challenges and so it is difficult to discern how to approach expanding the scope for C-H bonds that can be readily activated by nickel.

In hypothesizing how one might traverse the landscape of nickel-catalyzed C-H activation in search of new reactivity, it is important to recognize key mechanistic features that have been discovered through experimental and computational studies. Consider the alkyne hydroarylation mechanism discussed in chapter 2 (Figure 2-15). First, LLHT of an acidic arene C-H bond to an alkyne has a low barrier, which was determined to not be rate-limiting at room temperature. Secondly, rate-limiting reductive elimination produces a vinyl arene. It should be noted that all steps of this reaction are kinetically accessible at room temperature. Now, consider the formation of COD-based π-allyl complexes, which was also discussed in chapter 2 (Figure 2-5 and Figure 2-9). Similarly, low barrier LLHT takes place rapidly at room temperature, although reductive elimination is not observed. A more difficult reductive elimination could be attributed to either needing to break an $\eta^3$-allyl–Ni(II), or it is hindered by $sp^3$-character of the allyl ligand, or it is a combination thereof. Hartwig and Nakao overcame this issue for the hydroarylation of terminal olefins and in that case, temperatures exceeding 100 °C and extremely large NHC ligands (Figure 1-13) were used to facilitate C-C bond formation. One could envision the facile, reversible nature of the LLHT process and challenges with reductive elimination as an opportunity to generate organo-Ni(II) species and use them for orthogonal reactivity that ultimately regenerates the C-H bond cleaved initially. As an example, consider the reaction shown in Figure 4-1 where arene and propene are proposed to reversibly generate an alkyl- *in situ* (**4-4** to **4-2**, Figure 4-1). In the presence of an electrophile, like an aldehyde, the nickel-alkyl could undergo addition or migratory insertion into a carbonyl, which produces a nickel-alkoxy (**4-4**, Figure 4-1). It is important to

realize the similarities between **4-4** and **4-1**. Each contains a σ-bound arene and an alkyl/alkoxy ligand with a strong β-agostic interaction. Since the LLHT process is highly reversible, it could be envisioned that β-hydride elimination regenerates the C-H bond of the arene and forms ketone product. In this process, C-H activation is used a means of generating reactive organometallic nucleophiles but is never "functionalized." In this case, the C-H bond of the arene is recyclable in the same way a catalyst is. I believe that this chemistry is not limited to the simple example provided in Figure 4-1 and is a clever route to taking advantage of the challenges of nickel-catalyzed C-H functionalization for orthogonal reactivity. A few examples are highlighted in Figure 4-2.

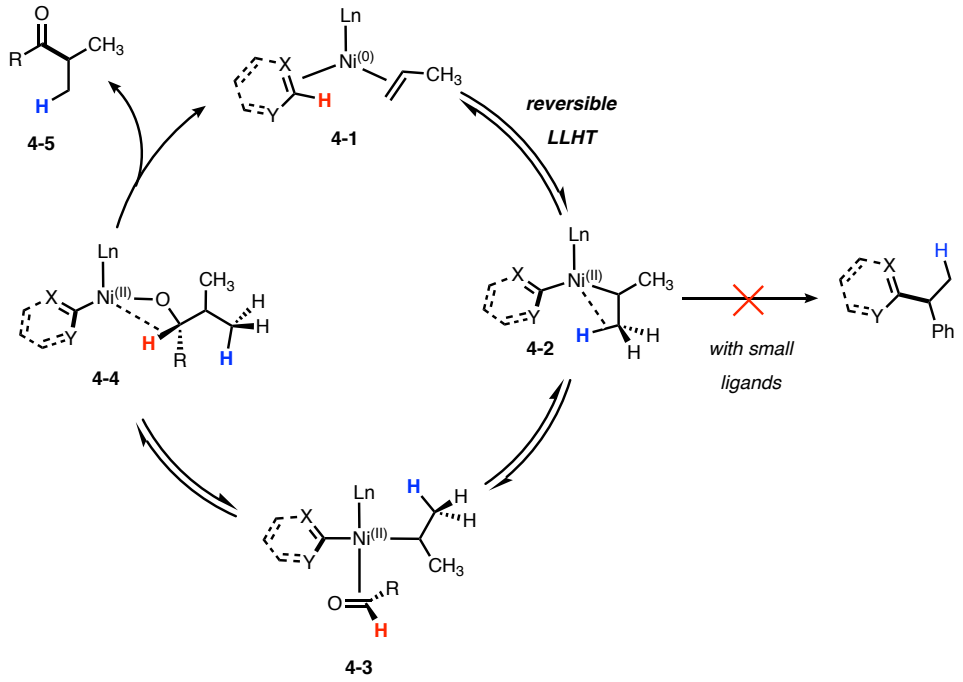


**Figure 4-1.** Recycle C-H bonds for olefin hydroacylation of olefins.

In Figure 4-2a, the recyclable C-H bond and Ni(0) are used to activate ethylene via LLHT. The low steric demands of ethylene as a ligand could allow for iterative insertions, which could be a route to accessing α-olefins in a mild way. Figure 4-2b shows a conjugate addition example

where the nickel-alkyl fragment, generated via LLHT, to ethylene in this case, could be added in a similar way that organo-cuprates perform 1,4-addition to α,β-unsaturated carbonyls. Furthermore, one could envision this being adapted for asymmetric catalysis. Finally, it is important to note that π-allyl complexes like **2-2** and **2-3** (Figure 2-5) could be targeted as catalytic intermediates in this fashion. Figure 4-2c shows an example where the nickel-allyl could potentially act as an electrophile in the presence of amines. In that case, an amine adds into the allyl generating anionic Ni(0)(Ar), which could be turned over via protonation by amine or conjugate base. Ultimately, this allows access to allylic amines from simple dienes. It could be envisioned that this could be operative for a variety of nucleophiles, similar to the broad scope of palladium-mediated allylic additions.

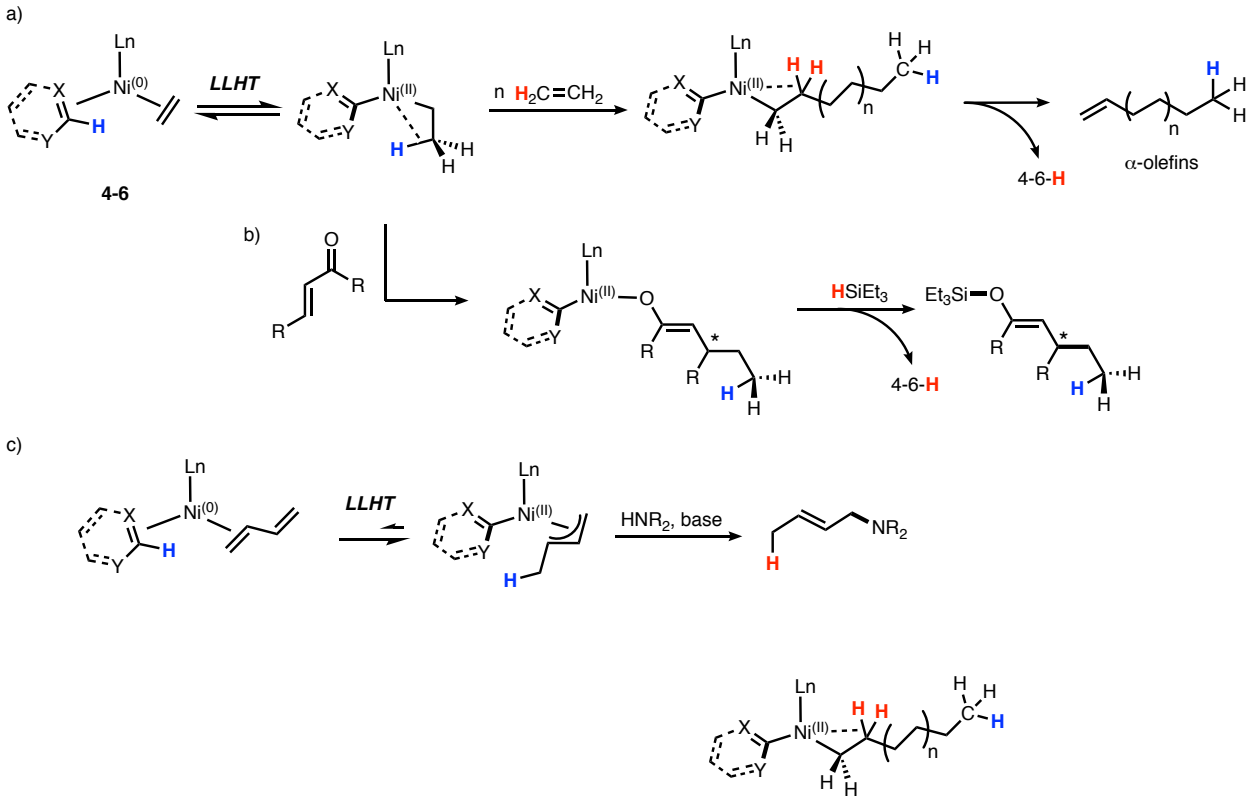


**Figure 4-2.** Potential transformations that utilize recyclable C-H bonds.

There are several mechanistic features that should contribute to the success of this chemistry. The use of small ligands, such as IMes, ITol, ItBu, IPr-BACC or monodenate phosphines, should provide a sufficient σ-donor to facilitate LLHT while hindering reductive elimination. We have demonstrated that undesirable outcomes associated with employing small NHCs can be avoided when a properly designed pre-catalyst is used. In this endeavor, our knowledge of stable pre-catalyst development, which was covered in chapter 3 would be helpful. In regard to the C-H bond used for this type reaction, a few issues could arise. The efficiency of highly active LLHT substrates like pentafluorobenzene or benzoxazole are proposed to be governed by the strength of the aryl-Ni(II) bond in the C-H activated complex. Therefore, more active, or acidic, C-H bonds are more thermodynamically favorable to cleave, which inherently suggests that reforming that C-H bond at the end of the reaction will be more difficult. Computational analysis, as described in chapter 2, could provide valuable insight into which types of arene C-H bond substrates will be best for this reaction. Finally, in reactions where the nickel-alkyl is added to an olefin there will exist a competitive path that involves insertion of the arene substrate. Fortunately, several intuitive methods exist to here mitigate this unproductive route for example, adding steric bulk to the arene substrate. Despite these few potential setbacks that could arise in achieving this type of reactivity, I do believe that these challenges can be confronted successfully, and this would open the door to transformations that were previously inaccessible under very mild conditions, thereby tolerating functional groups that are not typically allowed for analogous stoichiometric organometallic reagents, like Grignard reagents.

I believe the development of rapid computational screening will expedite exploration of this type of reactivity. The reaction scenarios described above highlight just a handful of potential transformations where recyclable C-H bonds could be used to generate reactive organometallic

reagents. It becomes apparent though that there may be a different combination of reagents, including ligand, arene, olefin acceptor, and potentially metal, necessary to promote a given transformation. Advancements in computational methods has provided the tools necessary for evaluating many reaction parameters in parallel, but regardless of how much data one can generate it lacks tractable meaning without experimentally supported structure-activity relationships. As a result, these processes are typically limited by the rate at which experimental data can be obtained. The work described herein provides an example where strong correlation can be drawn between straightforward computational descriptors and experimental data. Instances like these open the door for computational screening methods which can generate data much quicker than experimental techniques, for say a ligand screen. Tools developed by my colleagues in the Zimmerman lab demonstrate how ligand construction and evaluation can be automated which expands common ligand screens beyond commercially available compounds. I envision the extraction of meaningful data using these tools to expedite optimization of multivariable reactions like those mentioned previously in this section.

**Stable Ni(0) Pre-Catalysts**

Although there are many opportunities to apply the pre-catalysts discussed in chapter 3 to other transformations, I think it is more important that detailed mechanistic information regarding catalyst initiation be flushed out prior to further application. For example, in the IMes-series of pre-catalysts, which were used for reductive couplings, there seems to be a trend in the general shape of the reaction profiles where product formation overtime is sigmoidal (Figure 3-11). In these cases, the rate of product formation increases overtime until it reaches a maximum near 50 % conversion and then begins to slow down. This is true for all of the fumarate catalysts, but notably, this is also the case for methyl acrylate and not methyl methacrylate (Figure 3-11). This

indicates that placing an α-methyl on the acrylate impacts the mode of activation. In order to probe this further, lower catalyst loading should be tested to see if the overall shape of the reaction profile when using methyl methacrylate changes. Furthermore, analysis of by-products of pre-catalyst activation should be done and work is on-going in our lab regarding this.

In terms of the amination pre-catalysts, I think there are many opportunities for mechanistic inquiry. As mentioned, the pseudo zero-order nature of the amination reaction is interesting and could be a result of acrylate influencing the reaction kinetics (Figure 3-23). Experimental and computational analysis should be used to better characterize the mechanism for this transformation using pre-catalyst **3-43**. A more intriguing mechanistic feature of the amination pre-catalysts come from using the methyl acrylate stabilized complexes. A characteristic of these pre-catalysts are long induction periods where aryl chloride is consumed, but no product formation results in the early stages of the reaction (Figure 3-25). In some cases, induction periods of greater than 2 hours are observed. The consumption of aryl chloride without product formation suggests that oxidative addition is occurring, but other lower barrier pathways are operative early on in the reaction. Since the induction period seems to be dependent on the acrylate structure, it could imply that methyl acrylate is consumed prior to catalysis and phenyl acrylate-based pre-catalysts activate in a fundamentally different way.

Widespread use of nickel-catalyzed transformations rests on the ease of access to reactive Ni(0) species. Although the use of stable pre-catalysts could make this class of transition metal more accessible to groups that lack the capacity to perform air-free reactions, stable pre-catalysts are not crucial to designing new nickel-catalyzed transformations. I think that the greater impact that the use of stable pre-catalysts could have is on large scale applications of this chemistry where highly sensitive nickel precursors like $Ni(COD)_2$ present significant operational challenges.

Furthermore, using other Ni(II) based methods could lead to difficult catalyst initiations resulting in inconsistent performance. Additionally, our attempts to use this strategy has been outlined in chapter 3, but one could envision this technology being used for challenging oxidation states for other transition metal complexes. Obviously, it is likely that a new set of rules would apply given changes in metal or ligand, but systematic studies of structure activity relationships for a class of pre-catalyst could be valuable. The use of predictive computational models will be critical accelerating pre-catalyst optimization and should be considered as a crucial tool to advancing this field.

## Chapter 5 Experimental Section

### Experimental details for Chapter 2

### General Computational and Experimental Details

### Experimental Details

Unless otherwise stated, all operations were carried out under a nitrogen atmosphere in a glovebox or using standard Schlenk techniques. Deuterated benzene ($C_6D_6$), chloroform ($CDCl_3$), and tetrahydrofuran (THF-$d_8$) were obtained from Cambridge Isotopes and was freeze-pump-thawed prior to use. All aldehyde reagents were purchased and distill immediately prior to use. Liquid alkynes, amines, aryl chlorides, aryl fluorides, benzofuran, benzoxazole, 4,5-dimethylthiazole and benzothiazole were purchased and distilled prior to use. Sodium tert-butoxide was purchased and heat dried under vacuum and stored in glovebox. 1,3-Bis(2,4,6-trimethyphenyl)4,5-dihydroimidazol-2-ylidene and IPr*OMe were made according to reported procedure.[140,141] All other chemicals were purchased and used as received. All solvents were anhydrous and purchased from Sigma Aldrich and were freeze-pump-thawed prior to use. Unless otherwise noted, all other chemicals were used as purchased and used without further purification. **2-13** and **3-21** were prepared following published procedures. $^{1}H$ and $^{19}F$ NMR spectra were obtained in either THF, $CDCl_3$, THF-$d_8$, or $C_6D_6$ using a Varian Unity 500 or 700 MHz NMR. Elemental analysis was done by Atlantic Microlabs or Midwest Microlabs. High resolution mass

spectroscopy was collected on Agilent Q-TOF HPLC-MS for ESI+ and Micromass AutoSpec Ultima Magnetic Sector Mass Spectrometer for EI.

**Computational Details**

Density functional computations were carried out using the QChem 4.0 package.[142] All geometries were optimized using B3LYP hybrid density functional[143] and the LANL2DZ basis set.[144,145] The reaction discovery tools recently developed by the Zimmerman group[102–105] were used to probe potential reaction paths. These methods automatically hypothesize and evaluate plausible elementary reaction steps, providing atomistic descriptions of chemical structures and accurate thermodynamics. Kinetic information was obtained using the growing string method (GSM) with an exact transition-state (TS) search.[105] Vibrational frequency analysis was conducted at the B3LYP/LANL2DZ level for all stationary points. Stable intermediates were characterized by all real frequencies, and transition states were identified by a single imaginary frequency. Thermal corrections to the enthalpy (H) and gas phase entropy (S(g)) at catalytic conditions (298 K, 1 atm) were computed for all reported structures. To avoid inaccuracies inherent in the harmonic oscillator approximation, corrections for entropies were calculated by replacing low frequencies (below 50 $cm^{-1}$) with 50 $cm^{-1}$ .

The SMD implicit solvent model[146] in the GAMESS software package[147] was used to compute solvated free energies in toluene for all reaction intermediates and transition states. These computations were performed using the long-range corrected ωB97X-D functional[148] Correlation consistent basis sets of polarized, triple-ζ quality (cc-pVTZ)[149] were adopted for all atoms. Energies reported are solvent-phase Gibbs free energies.

**Synthesis of π-allyl complexes 2-2 and 2-3**

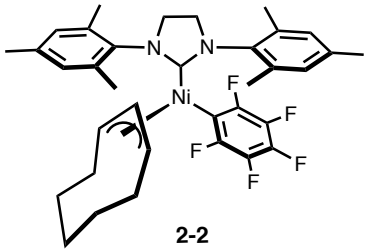


**2-2**

**2-1** (0.712g, 1.5 mmol) and $Ni(COD)_2$ (0.413g, 1.5 mmol) were dissolved in toluene. The yellow clear solution was heated to 60 °C, and over the course of 6 h the solution turned dark red, and was then allowed to cool to rt. Volatiles were pulled off in vacuo resulting in a red viscous oil. The crude was dissolved in a minimal amount of hexane and cooled to -78 °C. A yellow precipitate formed after several min, and the hexane was removed by cannula with a positive nitrogen pressure. The solid was washed twice with cold hexanes. Yield 0.702 g (73%).

**$^1$H NMR ($C_6D_6$, 500 MHz)**: δ 6.81 (2H, s), 6.69 (2H, s), 4.42 (1H, t, *J* = 12 Hz), 3.69 (1H, q, *J* = 10 Hz), 3.38 (1H, q, *J* = 10 Hz), 2.95 (4H, m), 2.28 (6H, s), 2.17 (6H, s), 1.98 (6H, s), 1.73-1.01 (10H, m).

**$^{13}$C NMR ($C_6D_6$, 125 MHz)**: δ 214.13, 138.01, 136.99, 135.50, 135.76, 129.64, 129.21, 128,29, 107.47, 72.08, 69.22, 51.10, 30.84, 29.91, 27.69, 27.64, 23.12, 20.99, 18.18, 17.64.

**$^{19}$F NMR ($C_6D_6$, 470MHz)**: δ -109.98 (1F, d, *J* = 47 Hz), -112.27 (1F, d, *J* = 52 Hz), -165.07 (1F, t, *J*=19 Hz), -165.74 (1F, m), -166.22 (1F, m).

**HRMS (ESI+) (m/z):** [M+Na] calcd for $C_{35}H_{39}F_5N_2NaNi$ 663.2285; found: 663.2289

**Anal calcd for** $C_{35}H_{39}F_5N_2Ni$: C (65.54 %), N (4.37 %), H (6.13 %); found: C (65.63 %), N (4.41 %), H (5.93 %).

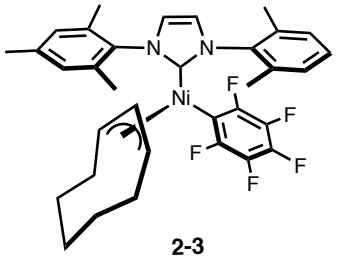


**2-3**

IMes (0.061g, 0.2 mmol) and $Ni(COD)_2$ (0.055g, 0.2 mmol) were dissolved in THF to form a dark brown solution. It was allowed to stir at rt for 30 min before the addition of pentafluorobenzene (23 μL, 0.21 mmol). The reaction mixture immediately turned red and was heated to 55 °C and allowed to stir for 3 h. The solution was cooled and THF was removed in vacuo. The product was extracted with pentane and filtered. The pentane solution was placed in a freezer at -20 °C, and an orange crystalline solid began to form. After filtration and washing with cold pentane, an orange solid was obtained. Yield 0.065 g (51 %).

**$^1$H NMR ($C_6D_6$, 500 MHz)**: δ 6.79 (2H, s), 6.63 (2H, s), 6.00 (2H, s), 4.58 (1H, t, *J* = 10 Hz), 3.57 (1H, q, *J* = 15 Hz), 3.43 (1H, q, *J* = 15 Hz), 2.19 and 2.17 (12H, overlapping singlets), 1.66 (6H, s), 1.65-1.24 (10H, m).

**$^{13}$C NMR ($C_6D_6$, 125 MHz)**: δ 185.11, 138.84, 136.89, 135.71, 134.87, 129.31, 128.82, 123.15, 107.16, 72.13, 68.02, 30.96, 30.15, 27.86, 27.56, 23.30, 21.00, 18.15, 17.68.

**$^{19}$F NMR ($C_6D_6$, 470 MHz)**: δ -110.12 (1F, d, *J* = 47 Hz), -112.25 (1F, d, *J* = 47 Hz), -165.17 (1F, t, *J*=24 Hz), -165.53 (1F, m), -166.02 (1F, m).

**Anal calcd for** $C_{35}H_{39}F_5N_2Ni$: C (65.75 %), N (4.38 %), H (5.83 %); found: C (65.75 %), N (4.93 %), H (6.11 %).

**General Alkenylation Procedure**

**General procedure using $Ni(COD)_2$/IMes as a catalyst**

$Ni(COD)_2$ (5.5 mg, 0.02 mmol) and IMes (6.0 mg. 0.02 mmol) were pre-stirred in 2 mL of toluene for 10 min. To the dark brown solution, substrate (0.20 mmol) was added, followed by addition of alkyne (0.30 mmol). The reaction mixture was stirred under a sealed nitrogen atmosphere. Upon completion, the reactions were quenched with methylene chloride and filtered through a silica plug eluting with methylene chloride.

**General procedure using IMes($C_6H_{10}$)Ni (2-13) as a catalyst.**

Complex **2-13** (4.5 mg, 0.01 mmol) was dissolved in 2.0 mL of toluene, followed by addition of substrate (0.20 mmol) and alkyne (0.30 mmol). The reaction mixture was stirred under a sealed nitrogen atmosphere. Upon completion, the reactions were quenched methylene chloride and filtered through a silica plug eluting with methylene chloride.

**Characterization**

Products from Figure 2-13 were purified by column chromatography. The yields for **2-19** and **2-20** were determined by $^1$H NMR with methylene bromide as an internal standard. $^1$H NMR spectra for the alkenylation products from Figure 2-13 (**2-12, 2-17,**[117] **2-18, 2-19, 2-20,**[60] **2-21**[150]) match those reported in the literature.

## Reaction Progression Monitored by $^{19}F$ NMR

All reactions progression profiles described in Figure 2-9 were monitored by $^{19}F$ NMR and yields were calculated using α,α,α-trifluorotoluene as an internal standard. A representative spectrum is shown below with labeled starting material, product and internal standard peaks.

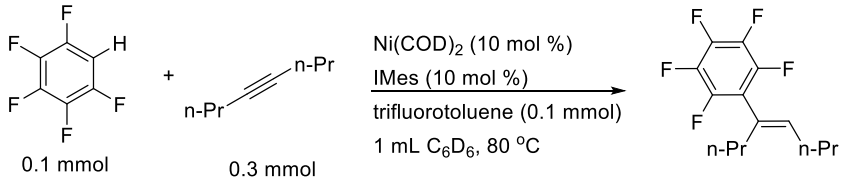


**30 second time point ($^{19}F$ NMR ($C_6D_6$, 470 MHz))**

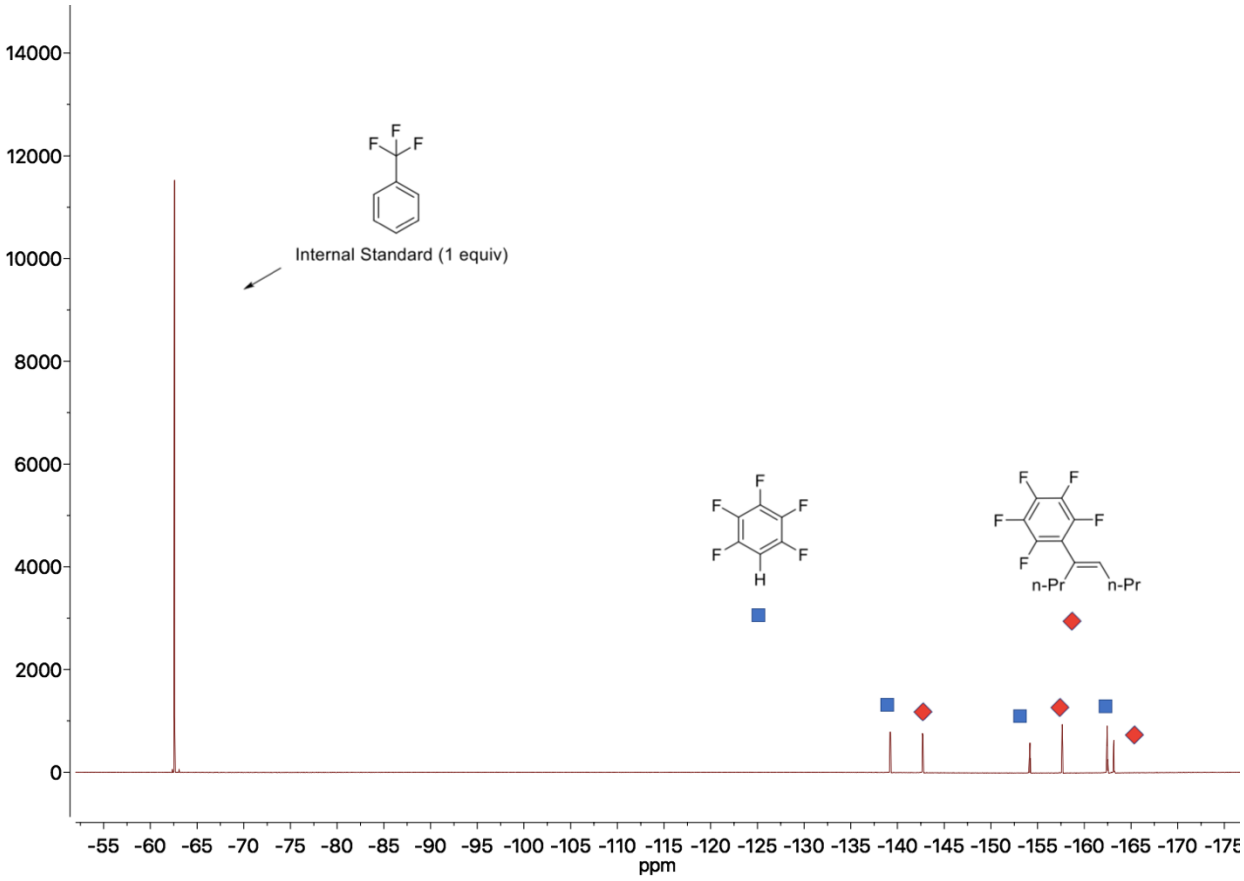


**Figure 5-1.** Example spectra for reaction progression analysis for hydroarylation of 4-octyne with pentafluorobenzene.

## Reaction Progression Analysis for Nickel-Catalyzed Hydroarylation

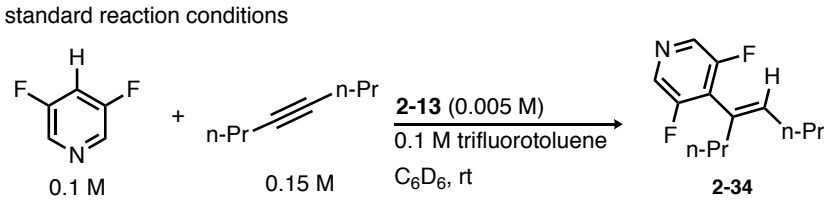


**Figure 5-2.** Model reaction and standard conditions used for RPKA.

**Technical Details:** All reactions were monitored in real time by $^{19}F$ NMR using screw-cap NMR tubes with septa caps. The typical delay between reagent addition and data collection is 30-45 seconds. All reactions were homogenous and did not require stirring. Automated data collection was used so that there was a fixed time interval of 12 seconds between each run. Each run was with a single scan with a relaxation delay of 5 seconds which was sufficient for accurate integration of both the internal standard, starting material and product. Reaction progression plots were generated by plotting the consumption of 3,5-difluoropyridine overtime using trifluorotoluene (0.1 M) as an internal standard.

**General Procedure (standard reaction conditions):** A solution of **2-13** (0.005 mmol) in 0.2 mL of $C_6D_6$ was added to an NMR tube and sealed with a septa cap. In a separate vial, a solution of 3,5-difluoropyridine (0.1 mmol) and 4-octyne (0.15 mmol) and 0.8 mL of $C_6D_6$ was prepared. Using a syringe the solution containing substrate was added to the NMR tube containing catalyst. The NMR tube was then carefully added to the NMR instrument and data collection began. All steps of the process were carried out under a nitrogen atmosphere.

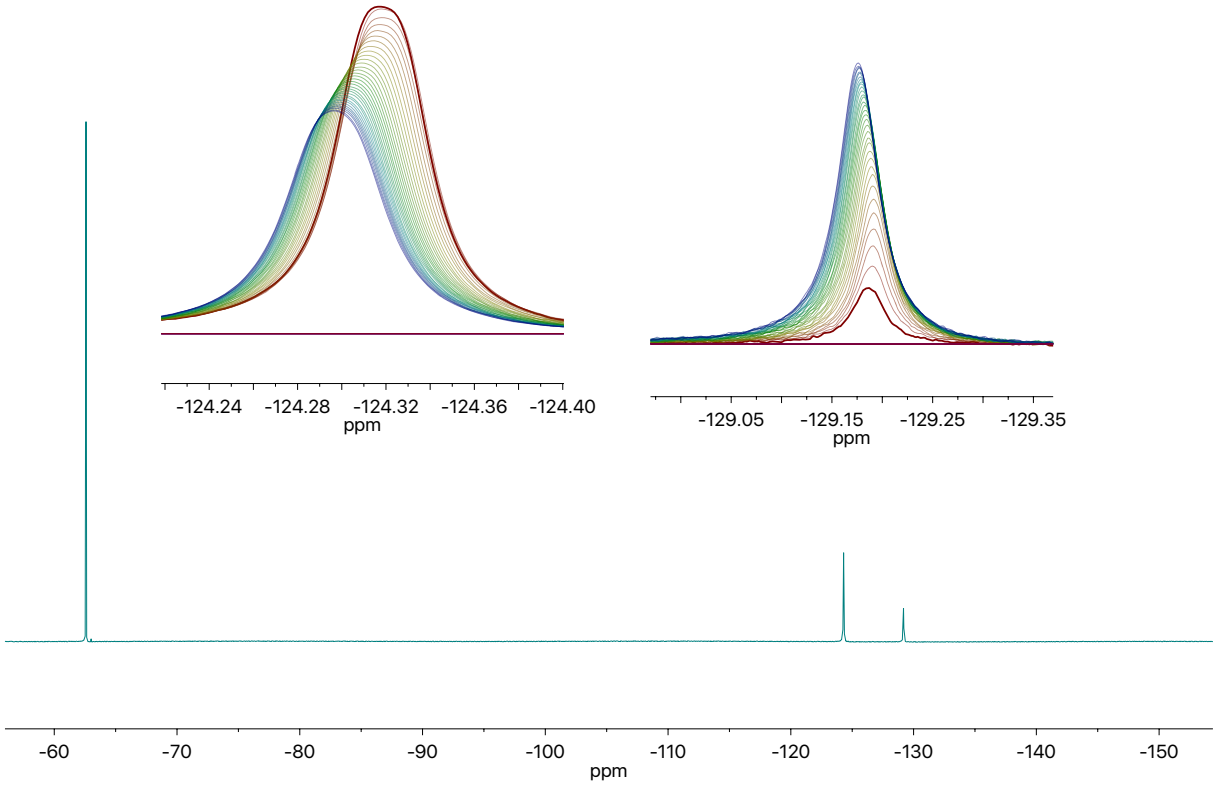


**Figure 5-3.** Example $^{19}F$ NMR spectra of the coupling of 3,5-difluoropyridine and 4-octyne.

**Reaction Progression Plots Varying Initial Concentration of 3,5-Difluoropyridine**

Initial concentrations of reagents for determining the effect of 3,5-difluoropyridine on the overall reaction progression.

| Entry | [**2-13**] (M) | **3,5-difluoropyridine (M)** | 4-octyne (M) |
|---|---|---|---|
| 1 | 0.005 | 0.05 | 0.15 |
| 2 | 0.005 | 0.10 | 0.15 |
| 3 | 0.005 | 0.15 | 0.15 |

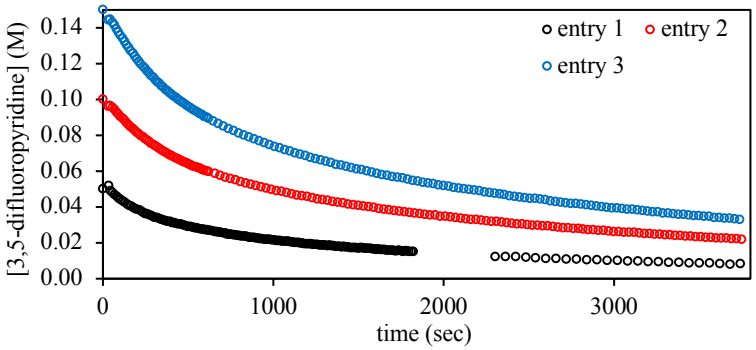


**Figure 5-4.** Reaction progression plot of the consumption of 3,5-difluoropyridine versus time for the hydroarylation of 4-octyne for different initial concentrations of 3,5-difluoropyridine.

**Reaction Progression Plots Varying Initial Concentration of 4-octyne**

Initial concentrations of reagents for determining the effect of 4-octyne on the overall reaction progression.

| Entry | [**2-13**] (M) | 3,5-difluoropyridine (M) | **4-octyne (M)** |
|---|---|---|---|
| 1 | 0.005 | 0.10 | 0.15 |
| 2 | 0.005 | 0.10 | 0.20 |
| 3 | 0.005 | 0.10 | 0.30 |

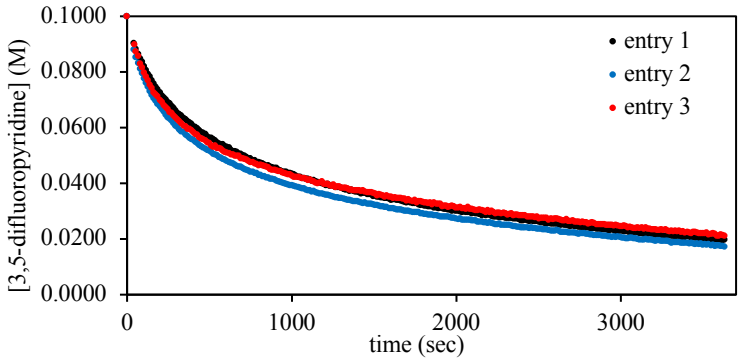


**Figure 5-5.** Reaction progression plot of the consumption of 3,5-difluoropyridine versus time for the hydroarylation of 4-octyne for different initial concentrations of 4-octyne.

**Reaction Progression Plots Varying Initial Concentration of Catalyst**

Initial concentrations of reagents for determining the effect of **2-13** on the overall reaction progression.

| Entry | **[2-13] (M)** | 3,5-difluoropyridine (M) | 4-octyne (M) |
|---|---|---|---|
| 1 | 0.010 | 0.10 | 0.15 |
| 2 | 0.005 | 0.10 | 0.15 |
| 3 | 0.0025 | 0.10 | 0.15 |
| 4 | 0.00125 | 0.10 | 0.15 |

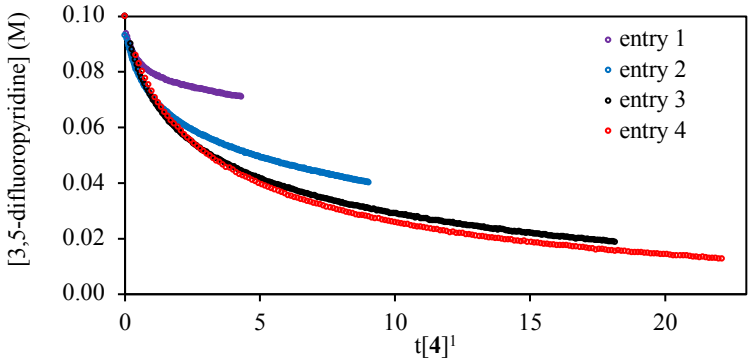


**Figure 5-6.** Plot of the consumption of 3,5-difluoropyridine. The *x*-axis is time normalized such that the correct catalyst order will cause the profiles to overlap.[11] In this case at high catalyst loading there is a first-order rate dependence in catalyst, but at low concentrations rapid catalyst decomposition causes the profiles to not overlap.

**Same Excess Experiments**

General procedure for reaction progression reactions with the initial concentration shown below.

For entry 3, product was synthesized following literature procedure.

Initial concentrations of reagents of 'same-excess' experiments.

| Entry | [**2-13**] (M) | 3,5-difluoropyridine (M) | 4-octyne (M) | **2-34** (M) |
|---|---|---|---|---|
| 1 | 0.005 | 0.10 | 0.15 | 0.0 |
| 2 | 0.005 | 0.05 | 0.10 | 0.0 |
| 3 | 0.0025 | 0.05 | 0.10 | 0.05 |

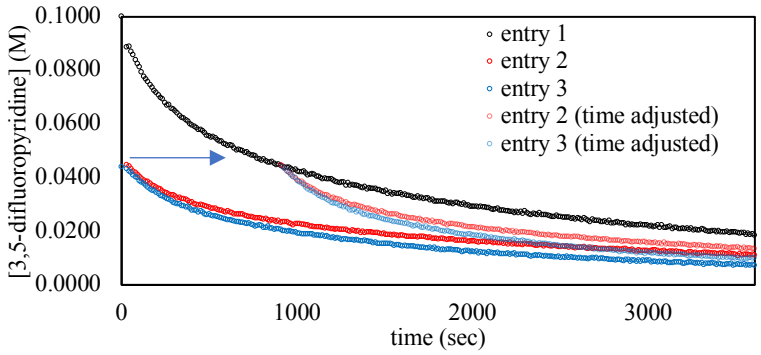


**Figure 5-7.** Plot of the consumption of 3,5-difluoropyridine versus time. The black profile is the standard reaction conditions. The red profile is a same excess experiment that does not contain added product. The blue profile is a same excess experiment that contains added product. An arrow indicates the time-shifted analysis which shows that both 'same excess' profiles are faster than the standard reaction profile.

**Initial Rates Analysis**

**Technical Details**: Following the same technical setup as the Reaction Progression Analysis, initial rates could be extracted by plotting the early time points of the reaction while the consumption of 3,5-difluoropyridine versus time was linear. The reported initial rates and standard deviations were generated from an average of three runs at each concentration. All rates were collected on a 500 MHz Varian NMR spectrometer.

**General Procedure**: For a given set of conditions two separate stock solutions were prepared (A and B).

**A:** Ni(IMes)(1,5-hexadiene) (2-13) (0.02 mmol) in $C_6D_6$.

**B**: 3,5-difluoropyridine,* 4-octyne,* and trifluorotoluene (0.0814 mmol) in $C_6D_6$.

Stock solution A was added to three separate NMR tubes for each set of conditions and sealed with a septa cap. Stock solution B was added to three separate 1 dram vials for each set of concentrations and each was sealed with a septa cap. Solution B was added to the NMR tube containing A with a syringe that was flushed with $N_2$, marking t = 0. One of the NMR tubes was used to lock, shim, and gain the instrument and was kinetics were not collected. The other three samples began data collection after the addition of B to the NMR tube. The initial rates are reported as an average, and respective standard deviation, of three runs and is reported below.

*Concentrations are noted in the Tables below.

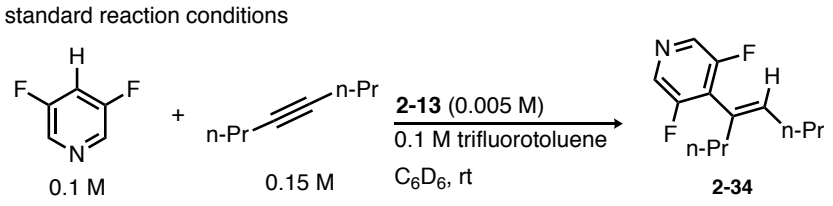


**Figure 5-8.** Standard reaction concentrations. Reaction order in each substrate was determined by varying the concentration of a single substrates while maintaining the concentrations shown.

## Initial Rates as Function of 3,5-difluoropyridine

**Table 5-1.** Initial rates as a function of the initial concentration of 3,5-difluoropyridine.

| initial [3,5-difluoropyridine] | Δ [**2-34**]/Δt x $10^{-4}$ (M/s) | average (Δ [**2-34**]/Δt x $10^{-4}$ (M/s) |
|---|---|---|
| 0.05 | 0.80 | 0.77 ± 0.06 |
| | 0.80 | |
| | 0.70 | |
| 0.10 | 1.07 | 1.06 ± 0.02 |
| | 1.07 | |
| | 1.04 | |
| 0.15 | 1.62 | 1.60 ± 0.05 |
| | 1.63 | |
| | 1.54 | |
| 0.20 | 1.91 | 2.07 ± 0.14 |
| | 2.11 | |
| | 2.18 | |

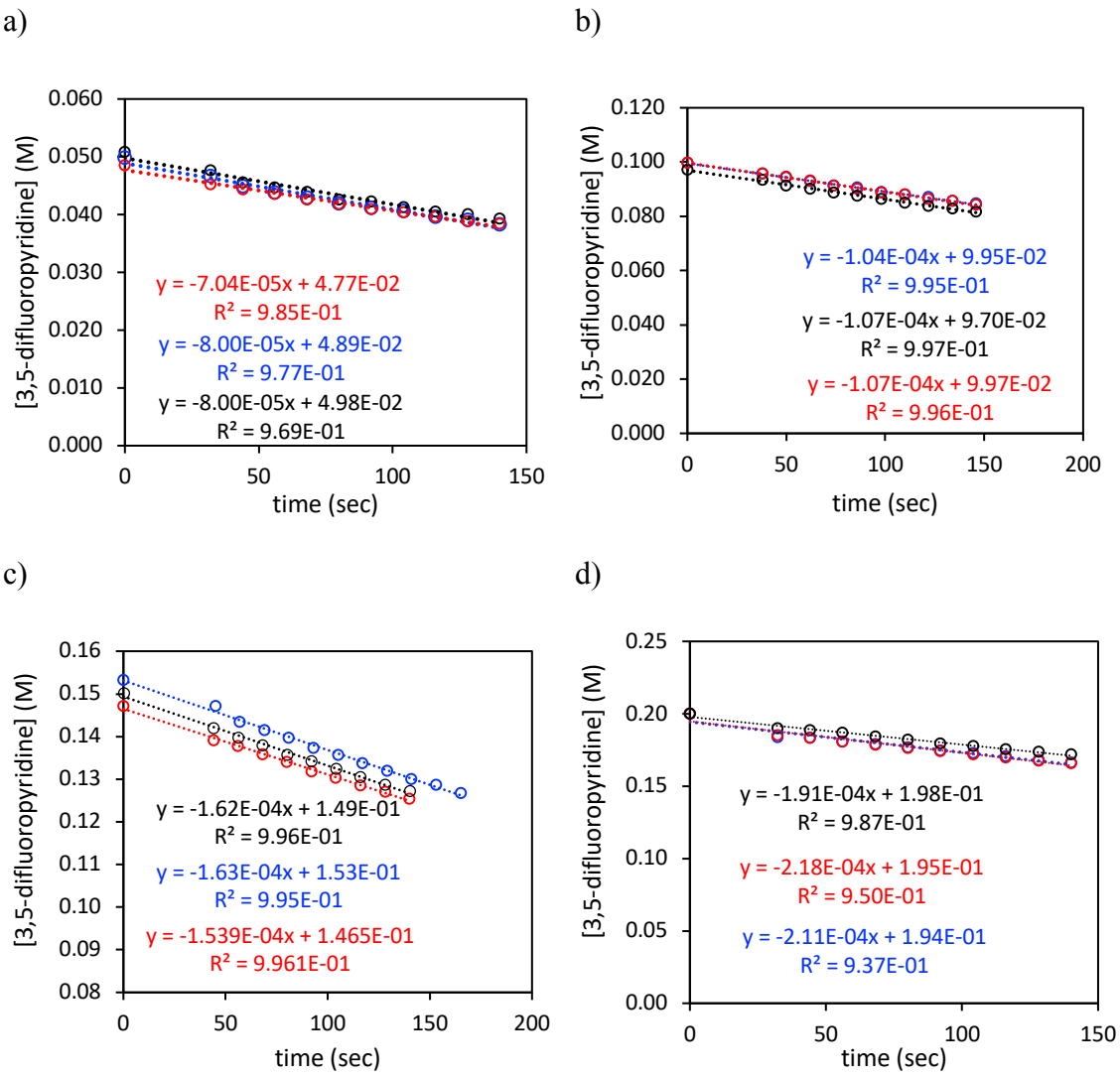


**Figure 5-9.** Initial rate plots varying the initial concentration of 3,5-difluoropyridine. Initial 3,5-difluoropyridine concentrations are: a) 0.05 M, b) 0.10 M, c) 0.15 M, d) 0.20 M.

## Initial Rates as a Function of 4-octyne

**Table 5-2.** Initial rates as a function of the initial concentration of 4-octyne.

| initial [4-octyne] | $\Delta$ [**2-34**]/$\Delta$t x $10^{-4}$ (M/s) | average ($\Delta$ [**2-34**]/$\Delta$t x $10^{-4}$ (M/s) |
|---|---|---|
| a) 0.10 | 0.87 | 0.92 ± 0.06 |
| | 0.90 | |
| | 0.99 | |
| b) 0.15 | 1.07 | 1.06 ± 0.02 |
| | 1.07 | |
| | 1.04 | |
| c) 0.20 | 1.11 | 1.11 ± 0.02 |
| | 1.14 | |
| | 1.10 | |
| d) 0.25 | 1.09 | 1.13 ± 0.04 |
| | 1.14 | |
| | 1.16 | |
| e) 0.30 | 1.157 | 1.159 |
| | 1.157 | |
| | 1.157 | |

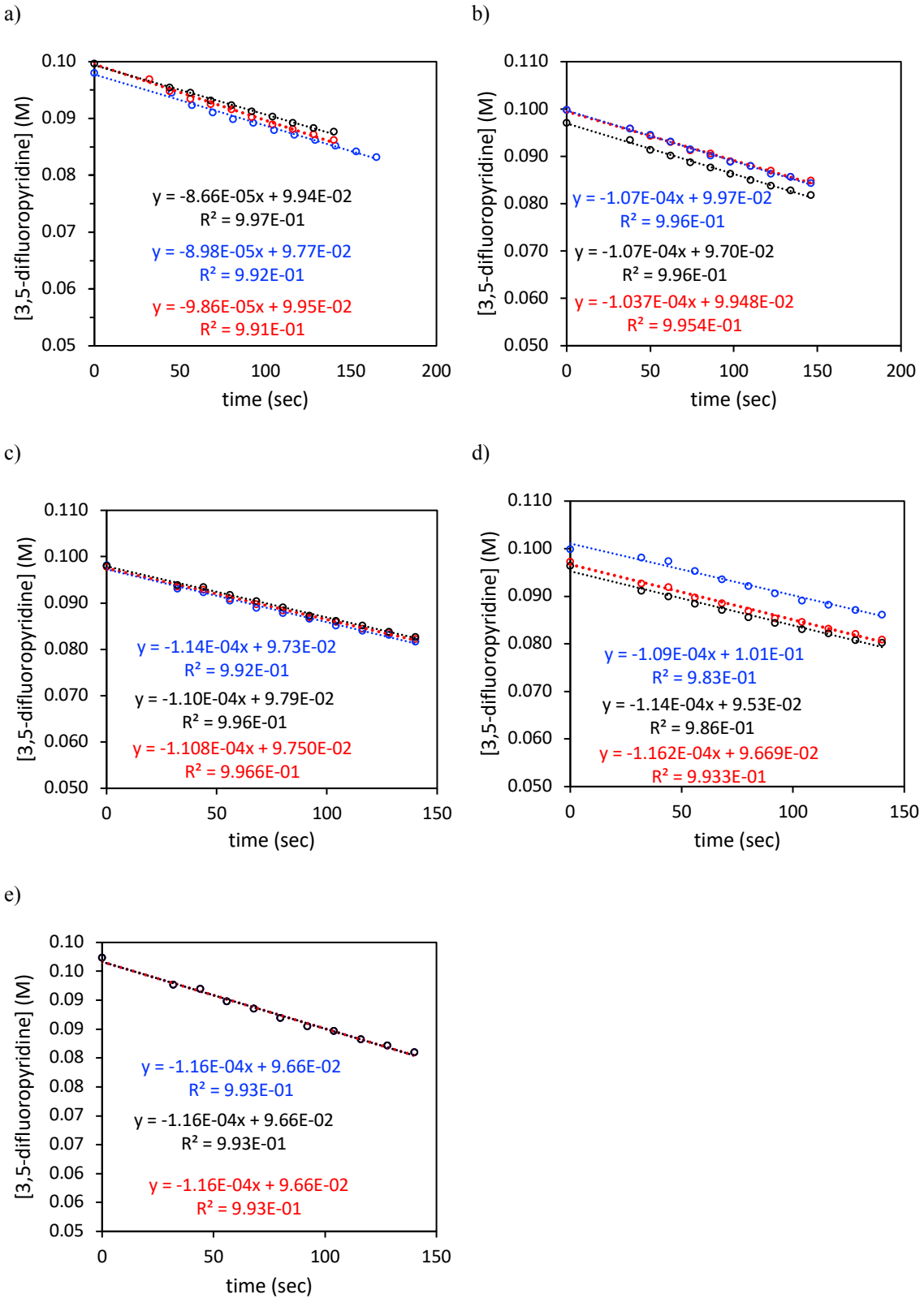


**Figure 5-10.** Initial rate plots varying the initial concentration of 4-octyne. Initial 4-octyne concentrations are: a) 0.10 M, b) 0.15 M, c) 0.20 M, d) 0.25 M, e) 0.30 M.

**Table 5-3.** Initial rates as a function of the initial concentration of 2-13.

| initial [**5**] | Δ [**2-34**]/Δt x $10^{-4}$ (M/s) | average (Δ [**2-34**]/Δt x $10^{-4}$ (M/s) |
|---|---|---|
| a) 0.00125 | 0.39<br>0.38<br>0.39 | 0.387 ± 0.007 |
| b) 0.0025 | 0.72<br>0.83<br>0.78 | 0.78 ± 0.05 |
| c) 0.0050 | 1.0<br>1.1<br>1.1 | 1.06 ± 0.02 |
| d) 0.010 | 2.1<br>2.0<br>2.0 | 2.00 ± 0.06 |

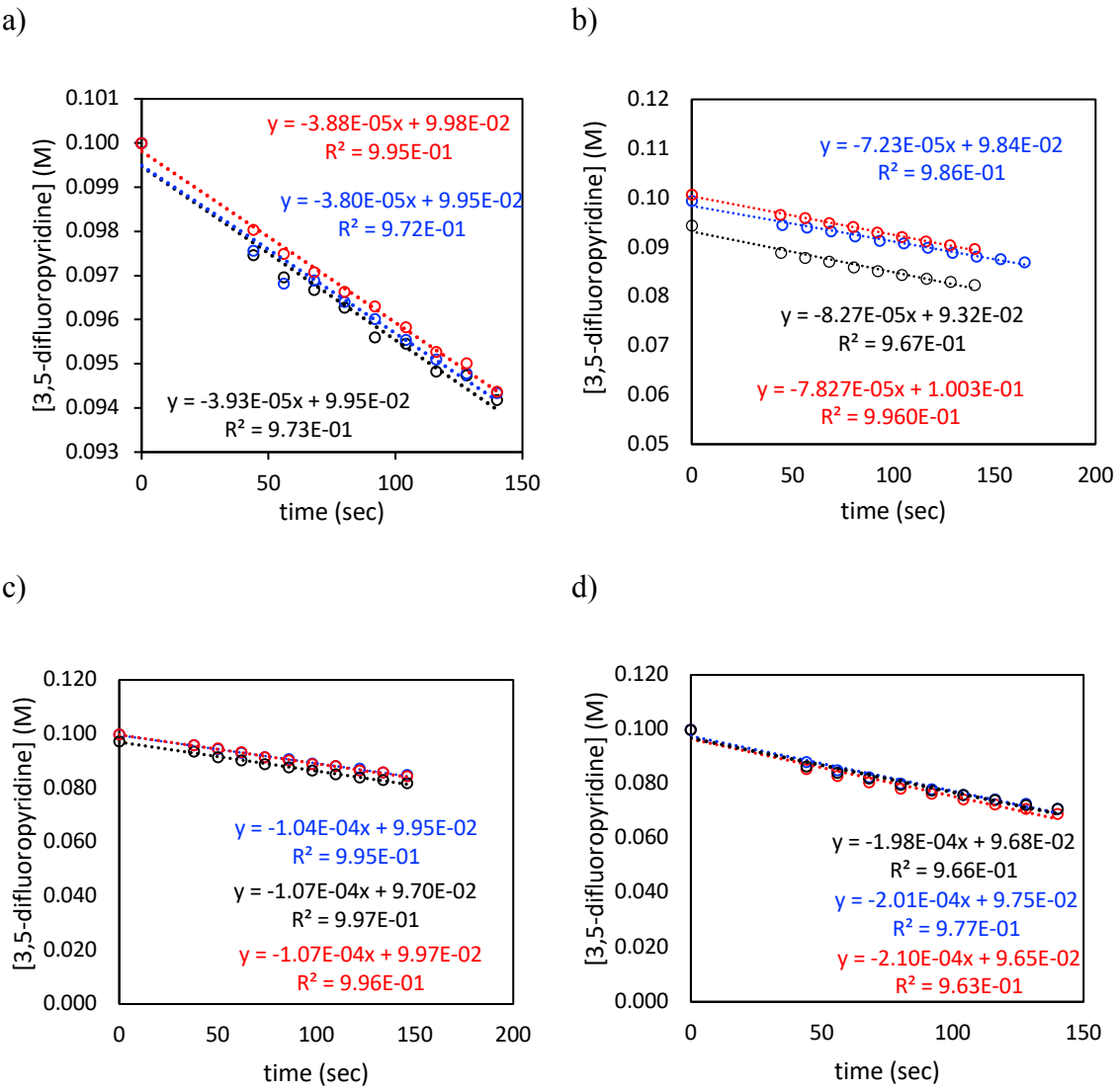


**Figure 5-11.** Plots of 3,5-difluoropyridine versus time as a function of initial concentration of 2-13.

**Order of Addition**

**Technical Details**: Same NMR setup as the Reaction Progression Analysis.

**General procedure A**: A solution of $Ni(COD)_2$ and IMes was prepared in 0.75 mL of $C_6D_6$ and was allowed to stir for 15 minutes. It was then transferred to an NMR tube with a septa cap. In a separate solution, pentafluorobenzene, 4-octyne, and trifluorotoluene were dissolved in 0.25 mL of $C_6D_6$. The reagent solution was added to the catalyst solution via syringe. Reaction was monitored by $^{19}F$ NMR.

**General Procedure B**: A solution of $Ni(COD)_2$ and IMes was prepared in 0.75 mL of $C_6D_6$ and was allowed to stir for 15 minutes. The additive was then added the resulting solution was transferred to an NMR tube with a septa cap. In a separate solution, the remaining reagents pentafluorobenzene, 4-octyne, and trifluorotoluene were dissolved in 0.25 mL of $C_6D_6$. The final concentrations of each reagent was the same regardless of the amount and identity of early additive. The reagent solution was added to the catalyst solution via syringe. NOTE: The final concentrations of each reagent was the same regardless of the amount or identity of early additive. Reaction was monitored by $^{19}F$ NMR.

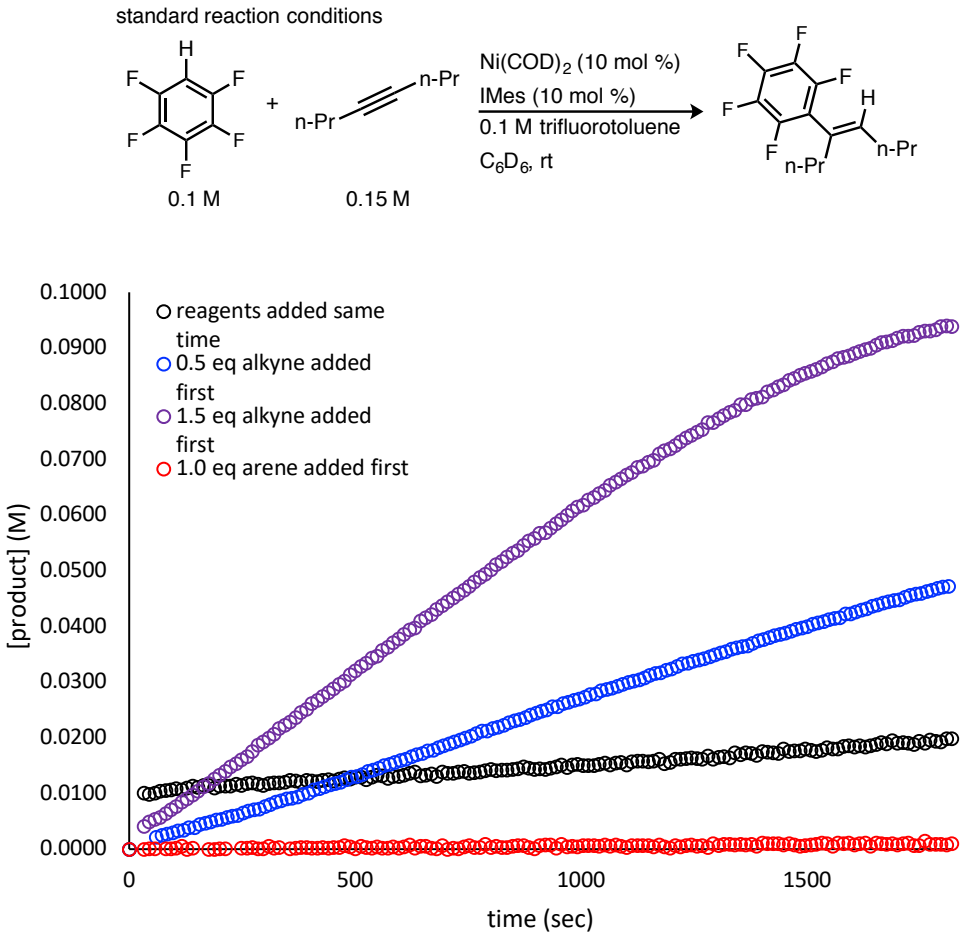


**Figure 5-12.** Monitoring the product formation of the hydroarylation of 4-octyne with pentafluorobenzene as a function of order of addition. General Procedure A was for black, and General Procedure B was used for blue, red, and purple with noted early additive.

**Initial Rates from Table 2-2**

**Technical Details:** Following the same technical setup as the Reaction Progression Analysis, initial rates could be extracted by plotting the early time points of the reaction while the formation the respective product is linear versus time. The reported initial rates and standard deviations were generated from an average of three runs at each concentration. All rates were collected on a 500 MHz Varian NMR spectrometer.

**General Procedure**: For a given substrates two separate stock solutions were prepared (**A** and **B**).

**A**: Ni(IMes)(1,5-hexadiene) (**5**) (0.02 mmol) in 0.8 mL of $C_6D_6$

**B**: Arene (0.4 mmol), 4-octyne (0.6 mmol) and internal standard (X mmol)* in 3.2 mL of $C_6D_6$.

0.2 mL of stock solution **A** was added to three separate NMR tubes and sealed with a septa cap. 0.8 mL of stock solution **B** was added to three separate 1 dram vials and each was sealed with a septa cap. Solution **B** was added to the NMR tube containing **A** with a syringe that was flushed with $N_2$, marking t = 0. One of the NMR tubes was used to lock, shim, and gain the instrument and was kinetics were not collected. The other two samples began data collection after the addition of **B** to the NMR tube. The initial rate is reported as an average and respective standard deviation of these two runs was reported in Table 1.

*The amount and identity of the internal standard is noted below for each entry.

**pentafluorobenzene -** *internal standard: trifluorotoluene (0.1 mmol)*

a)

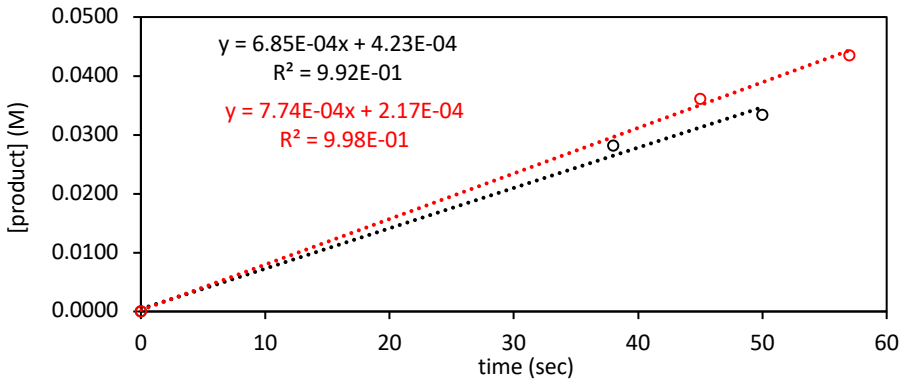


b)

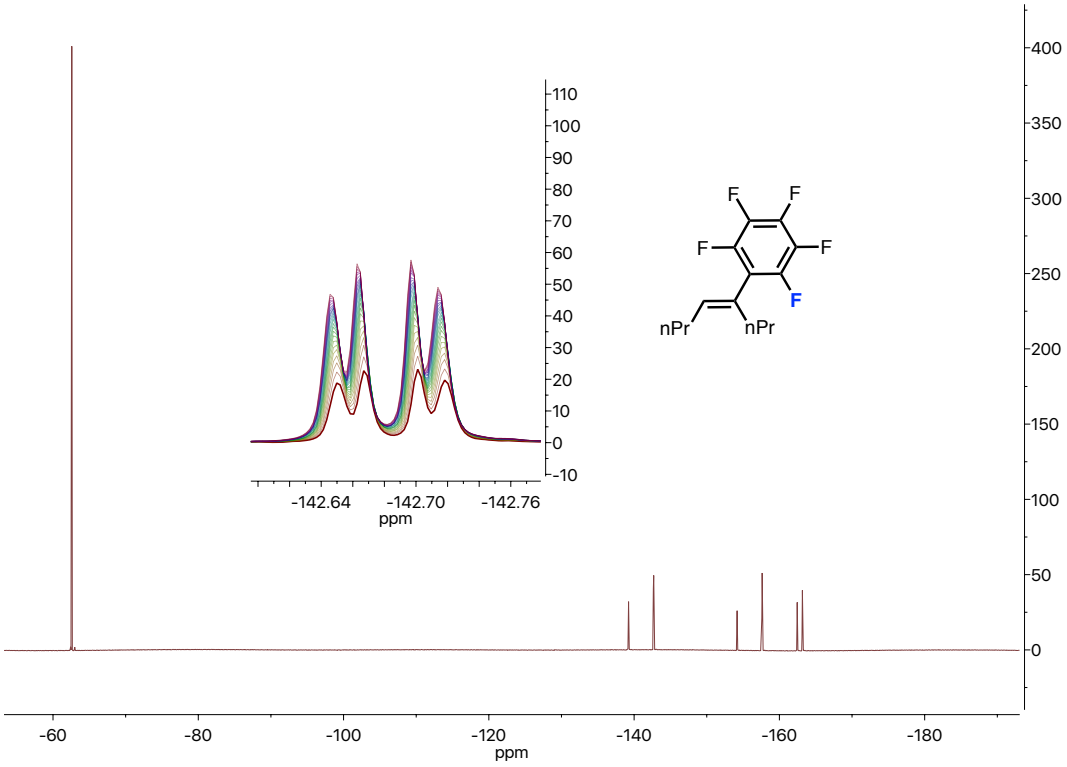


**Figure 5-13.** a) Plot of early product formation versus time for the hydroarylation of 4-octyne with pentafluorobenzene. b) Sample $^{19}F$ NMR spectra for data collection of the initial rate for pentafluorobenzene. The inlay shows the fluorine in the product that was integrated to measure the progress of the reaction.

**1,2,4,5-tetrafluorobenzene -** *internal standard: trifluorotoluene (0.1 mmol)*

a)

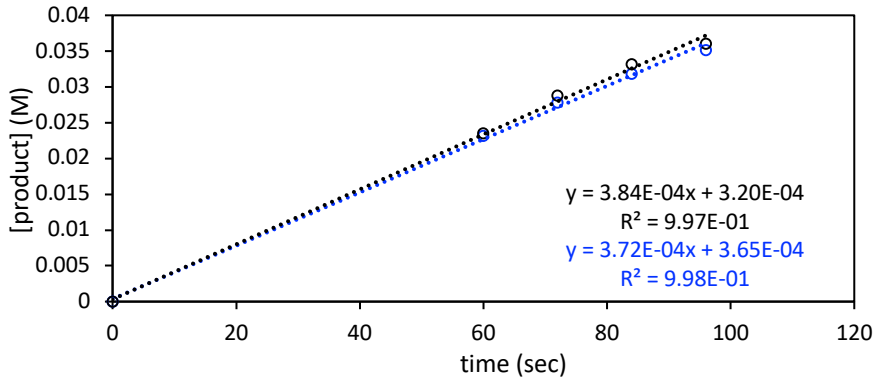


b)

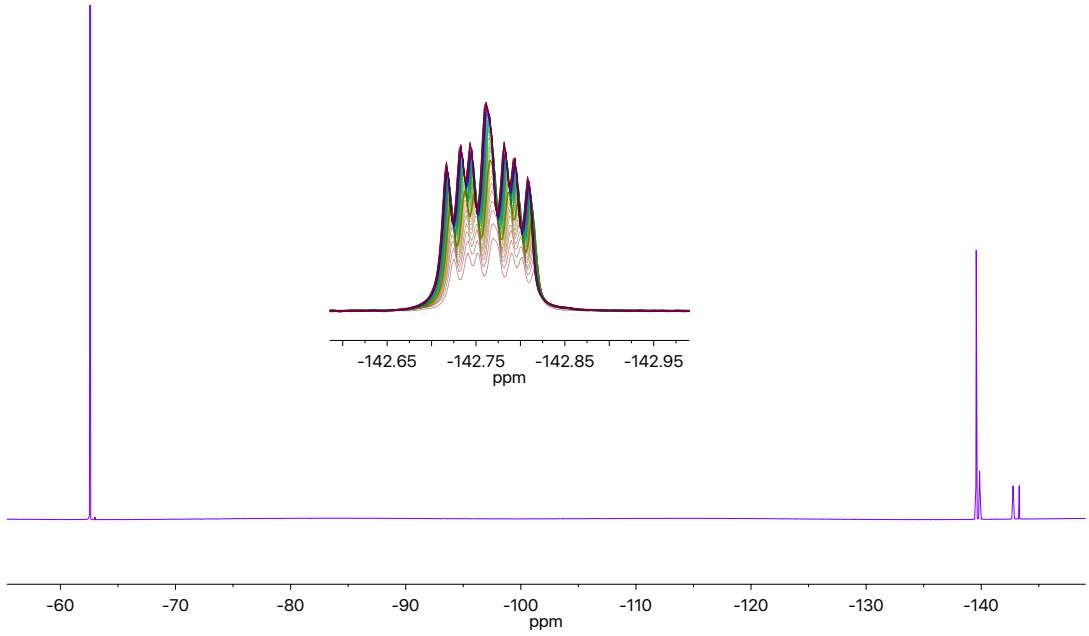


**Figure 5-14.** a) Plot of early product formation versus time for the hydroarylation of 4-octyne with 1,2,4,5-tetrafluorobenzene. b) Sample $^{19}F$ NMR spectra for data collection of the initial rate for 1,2,4,5-tetrafluorobenzene. The inlay shows the fluorine in the product that was integrated to measure the progress of the reaction.

**3,5-difluoropyridine -** *internal standard: trifluorotoluene (0.1 mmol)*

a)

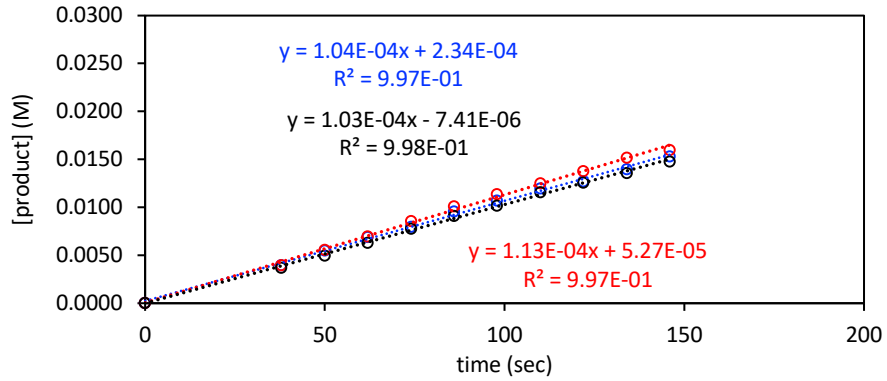


b)

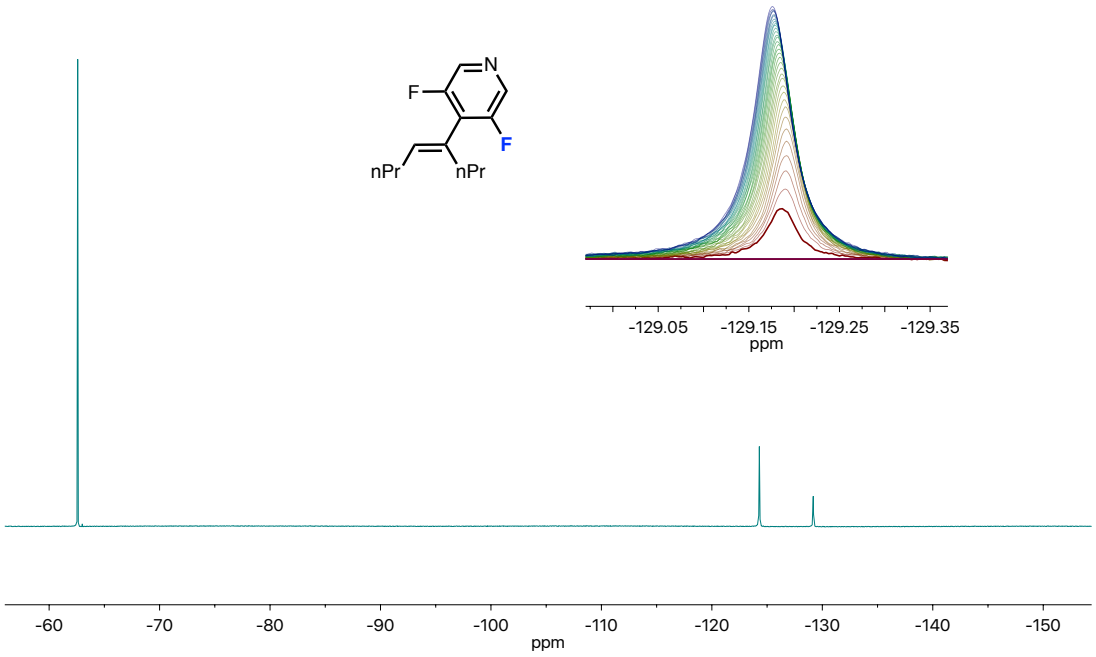


**Figure 5-15.** a) Plot of early product formation versus time for the hydroarylation of 4-octyne with 3,5-difluoropyridine. b) Sample $^{19}F$ NMR spectra for data collection of the initial rate for 3,5-difluoropyridine. The inlay shows the fluorine in the product that was integrated to measure reaction progress.

**1,3-dimethyluracil -** *internal standard: trifluoroanisole (0.1 mmol)*

a)

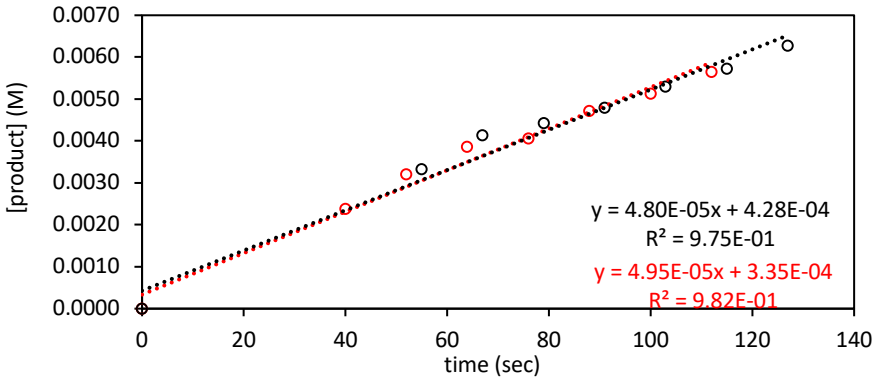


b)

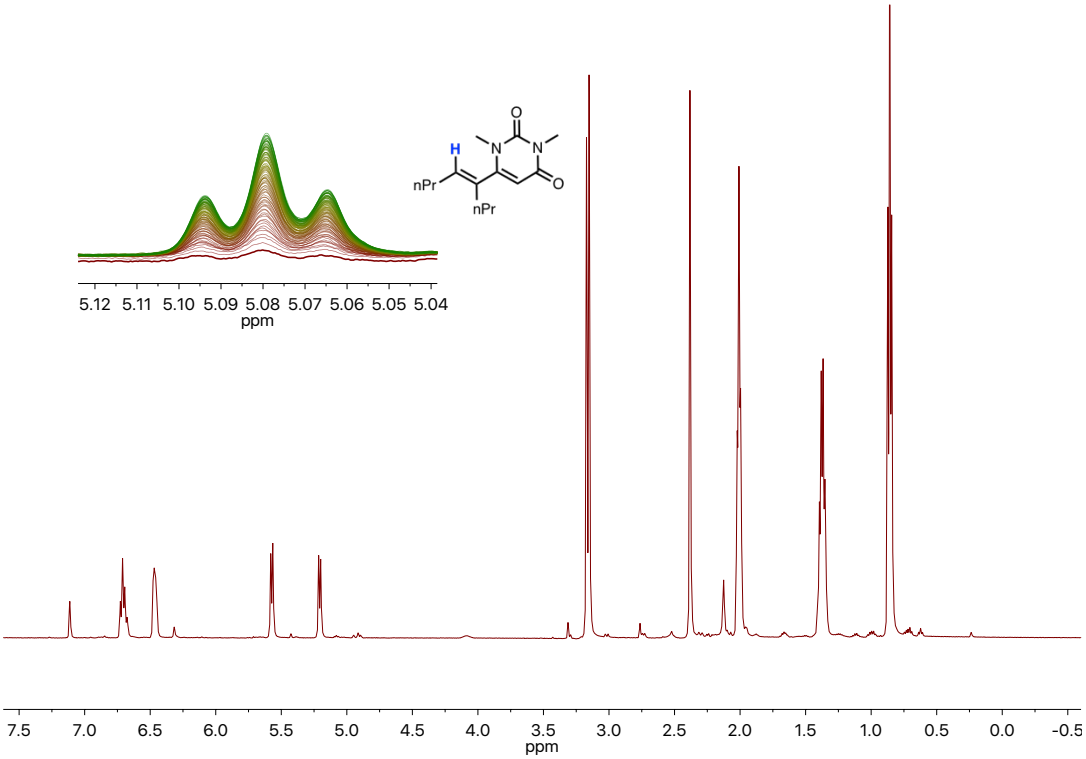


**Figure 5-16.** a) Plot of early product formation versus time for the hydroarylation of 4-octyne with 1,3-dimethyluracil. b) Sample $^{1}$H NMR spectra for data collection of the initial rate for 1,3-dimethyluracil. The inlay shows the alkenyl proton in the product that was integrated to measure the progress of the reaction.

**4,5-dimethylthiazole** - *internal standard: trimethoxybenzene (0.033 mmol)*

a)

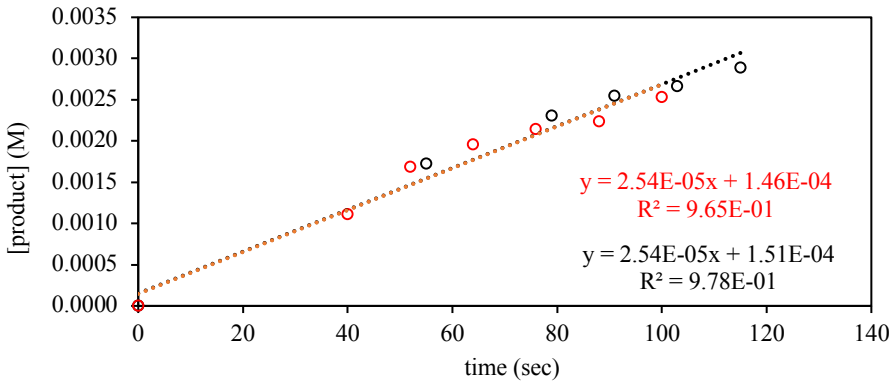


b)

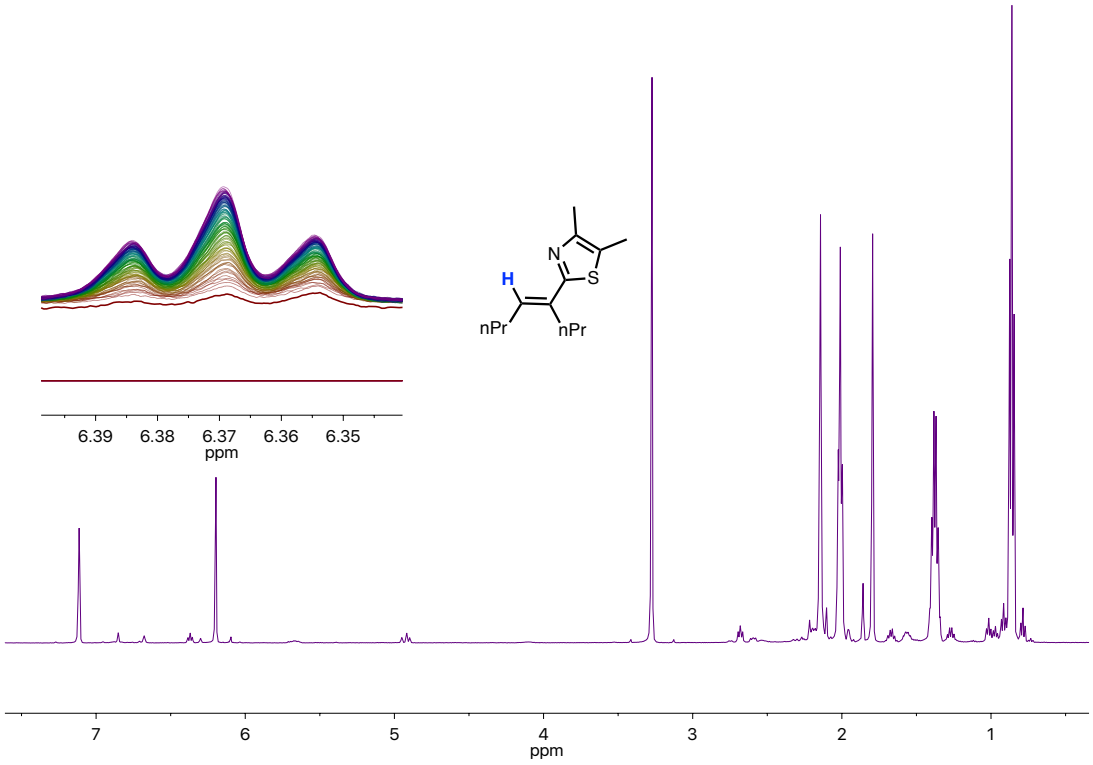


**Figure 5-17.** a) Plot of early product formation versus time for the hydroarylation of 4-octyne with 4,5-dimethylthiazole. b) Sample $^{1}$H NMR spectra for data collection of the initial rate for 4,5-dimethylthiazole. The inlay shows the alkenyl proton in the product that was integrated to measure the progress of the reaction.

**benzofuran -** *internal standard: trimethoxybenzene (0.033 mmol)*

**a)**

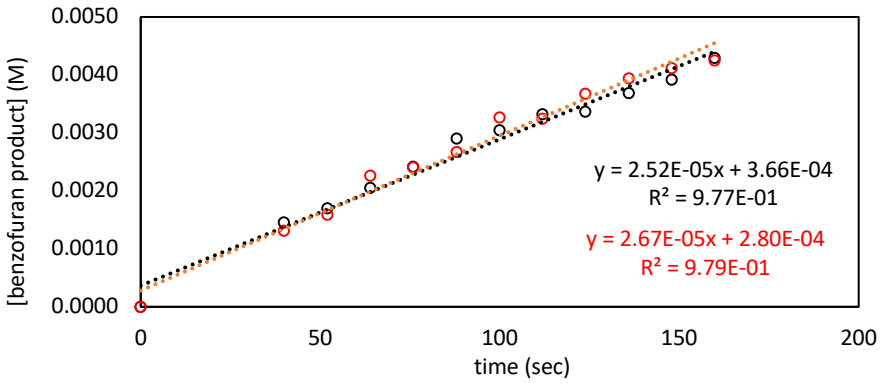


**b)**

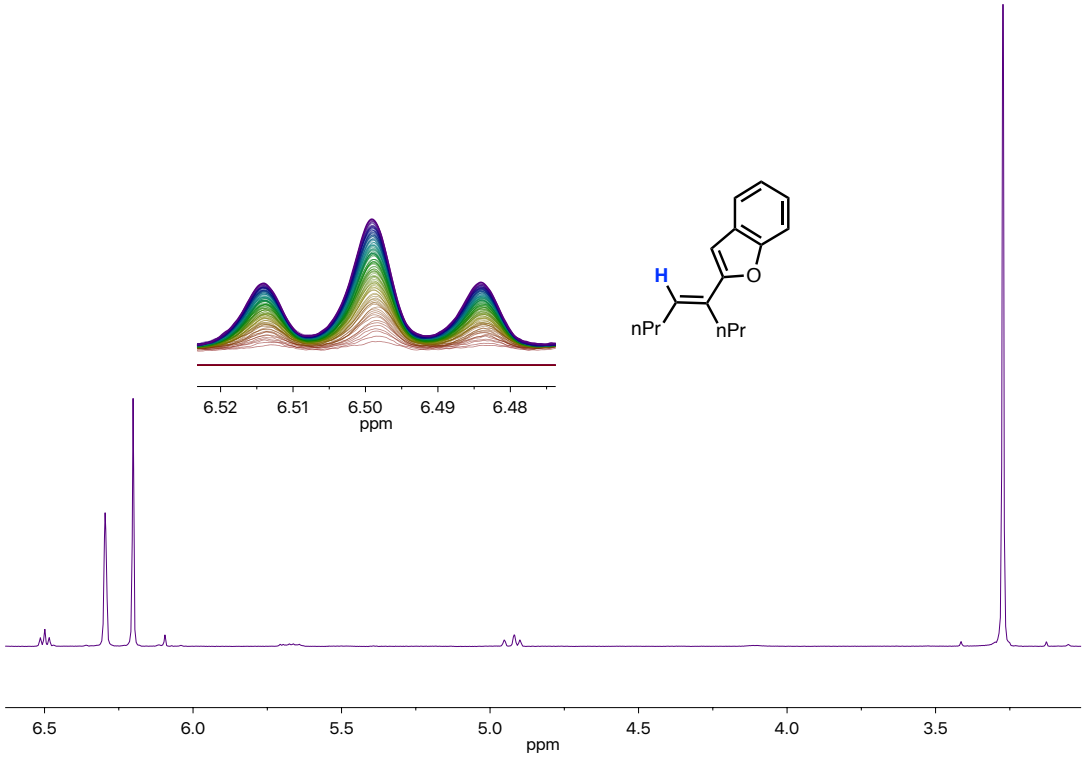


**Figure 5-18.** a) Plot of early product formation versus time for the hydroarylation of 4-octyne with benzofuran. b) Sample $^{1}$H NMR spectra for data collection of the initial rate for benzofuran. The inlay shows the alkenyl proton in the product that was integrated to measure the progress of the reaction.

**1,2,3.4-tetrafluorobenzene-** *internal standard: trifluorotoluene (0.033 mmol)*

a)

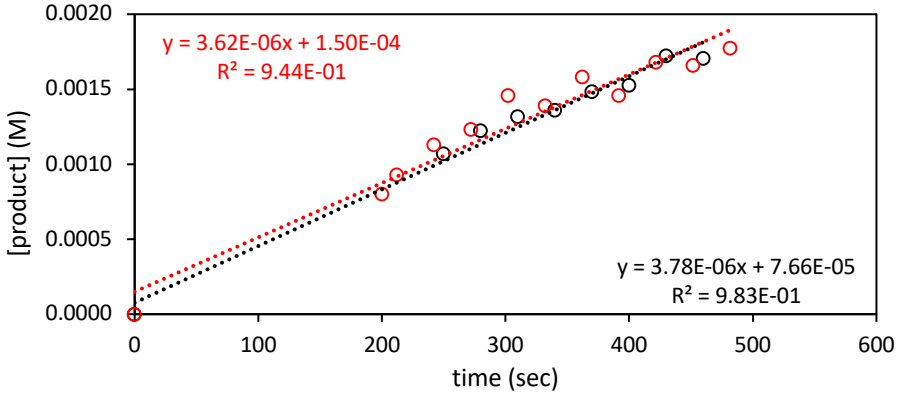


b)

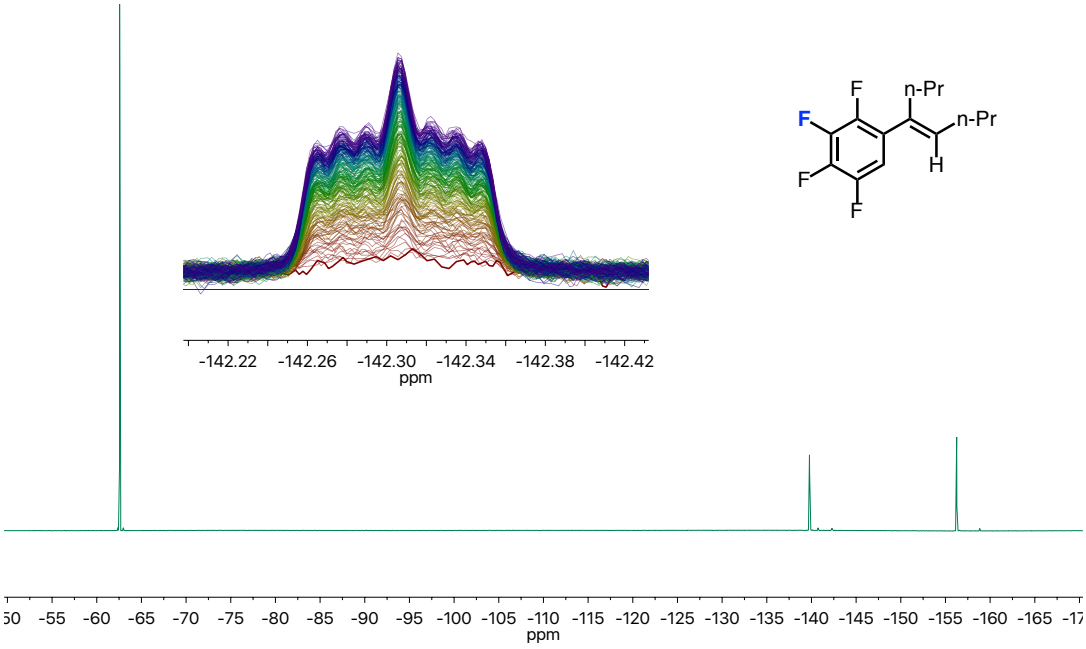


**Figure 5-19.** a) Plot of early product formation versus time for the hydroarylation of 4-octyne with 1,2,3,4-tetrafluorobenzene. b) Sample $^{1}$H NMR spectra for data collection of the initial rate for benzofuran. The inlay shows the alkenyl proton in the product that was integrated to measure the progress of the reaction.

**benzothiophene -** *internal standard: trimethoxybenzene (0.033 mmol)*

a)

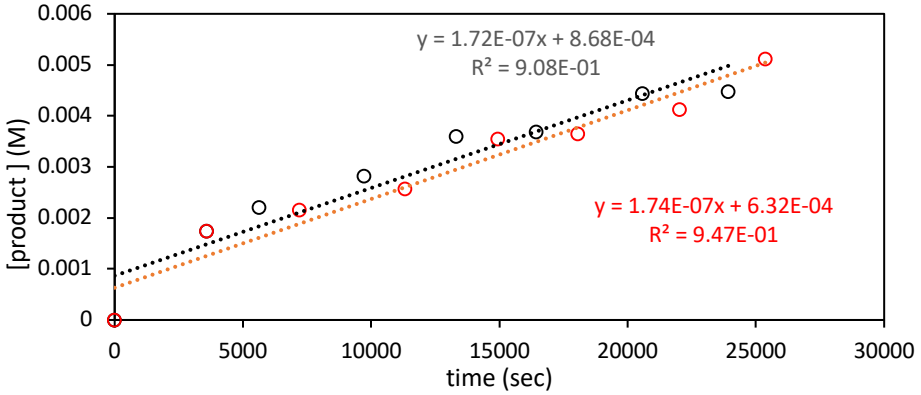


b)

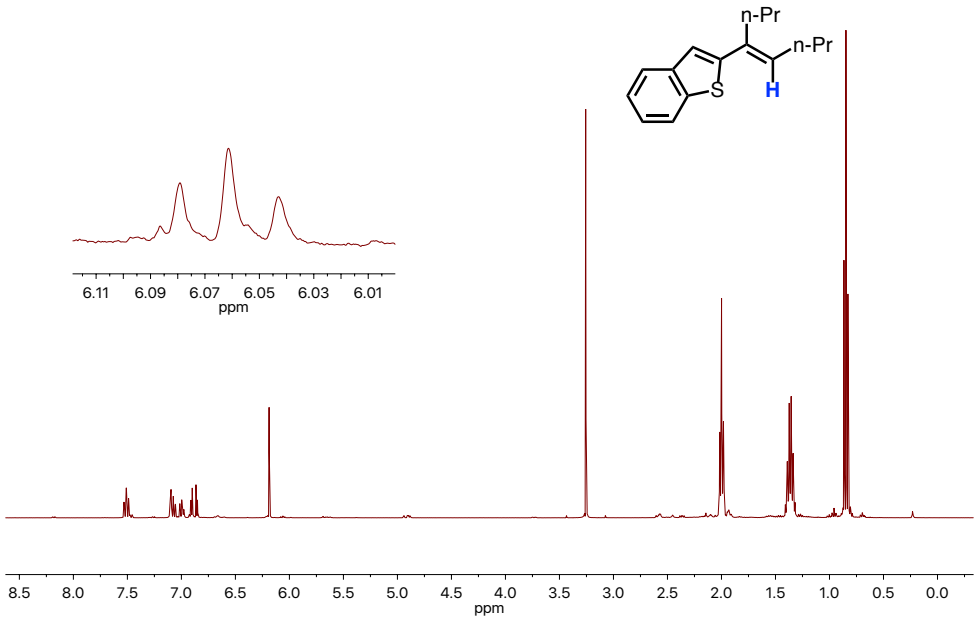


**Figure 5-20.** a) Plot of early product formation versus time for the hydroarylation of 4-octyne with benzothiophene. b) Sample $^{1}$H NMR spectra for data collection of the initial rate for benzofuran. The inlay shows the alkenyl proton in the product that was integrated to measure the progress of the reaction. The spectra for benzothiophene were not collected using automated timing and data collection due to the slow rate of the reaction.

**Experimental Details for Chapter 3**

**General protocol for fumarate synthesis**

An oven dried round bottom was charged with a stir bar, alcohol (2.0 equiv), triethylamine (2.0 equiv), and THF (0.15 M). The solution was cooled to 0 °C and fumaryl chloride (1.0 equiv) was slowly added. A precipitate formed immediately, and the solution was allowed to warm to room temperature and stirred overnight. The reaction was quenched with the addition of a small amount of triethylamine. The reaction crude was absorbed onto silica which was added on top of a small plug of silica. The silica plug was rinsed with dichloromethane and was subsequently concentrated. In most cases the product crystallized out upon the addition of pentane. In the case where the product was an oil it was purified by column chromatography using ethyl acetate/hexanes.

**Diethyl fumarate (3-13).**

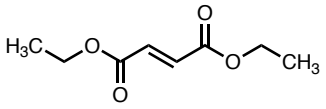

Following the general procedure: anhydrous ethanol (0.58 mL, 10 mmol), triethylamine (1.4 mL, 10 mmol), and fumaryl chloride (0.54 mL, 5 mmol) produced 686 mg of **3-13** (2.0 mmol, 40 % yield). The product was purified by column chromatography using ethyl acetate/hexane.

Spectral data as previously reported.[151]

**Diisopropyl fumarate (3-14).**

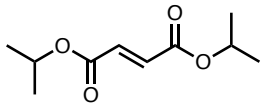

Following the general procedure: anhydrous isopropanol (1.52 mL, 20 mmol), triethylamine (2.8 mL, 20 mmol), and fumaryl chloride (1.1 mL, 10 mmol) produced 875 mg of **3-14** (4.4 mmol, 44 % yield). The product was purified by column chromatography using ethyl acetate/hexane.

**$^{1}$H NMR (700 MHz, $CDCl_3$)** δ 6.80 (s, 2H), 5.10 (hept, *J* = 6.1 Hz, 2H), 1.28 (d, *J* = 6.3 Hz, 12H).

**$^{13}$C NMR (176 MHz, $CDCl_3$)** δ 164.55, 133.86, 68.87, 21.72.

**Diisobutyl fumarate (3-15).**

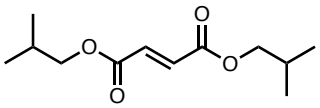

Following the general procedure: anhydrous isobutanol (0.92 mL, 10 mmol), triethylamine (1.4 mL, 10 mmol), and fumaryl chloride (0.54 mL, 5.0 mmol) produced 360 mg of **3-15** (0.8 mmol, 16 % yield). The product was purified by column chromatography using ethyl acetate/hexane.

Spectral data as previously reported.[152]

**Di-tert-butyl fumarate (3-16)**

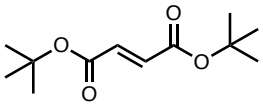

Following an adapted general procedure: anhydrous tert-butanol (7.2 mL, 75 mmol), n-butyl lithium (30 mL, 2.5 M), and fumaryl chloride (4.0 mL, 37.5 mmol). Tert-butanol and THF (3.75 M) were added to a round bottom and cooled to -78 °C and n-butyl lithium was added dropwise. The resulting solution stirred at -78 °C for 2 hr. The reaction was warmed to 0 °C and fumaryl chloride was slowly added and the reaction stirred room temperature overnight. The product was recrystallized from pentane at -78 °C and filtered. 6.215 g of **3-16** (27 mmol, 72 % yield).

Spectral data as previously reported.[153]

**Bis(2-phenylpropan-2-yl) fumarate (3-17)**.

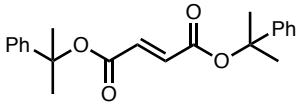

Following an adapted general procedure: 2-phenylpropan-2-ol (5.0 g, 36.7 mmol), n-butyl lithium (14.6 mL, 2.5 M), and fumaryl chloride (2.0 mL, 18.4 mmol). 2-phenylpropan-2-ol and THF (3.75 M) were added to a round bottom and cooled to -78 °C and n-butyl lithium was added dropwise. The resulting solution was warmed to room temperature and stirred at for 2 hr. The reaction was warmed to 0 °C and fumaryl chloride was slowly added and the reaction stirred room temperature overnight. The product was purified by column chromatography in ethyl acetate/hexane. 2.675 g of **3-17** (7.5 mmol, 41 % yield).

**$^1$H NMR (700 MHz, $CDCl_3$)** δ 7.36 (m, 8H), 7.27 (t, $J$ = 7.3 Hz, 2H), 6.79 (s, 2H), 1.83 (s, 12H).

**$^{13}$C NMR (176 MHz, $CDCl_3$)** δ 163.69, 145.04, 134.49, 128.36, 127.21, 124.27, 82.94, 28.53.

**HRMS (ESI+) (m/z)**: $[M+Na]^+$ calcd for $C_{22}H_{24}O_4Na$ 375.1567; found 375.1569.

**Bis(4-(methoxycarbonyl)phenyl) fumarate (3-18).**

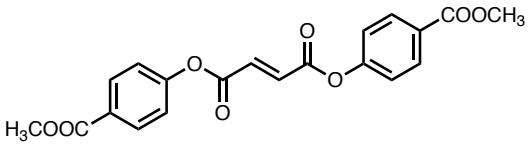


Following the general procedure: methyl 4-hydroxybenzoate (919 mg, 6.0 mmol), triethylamine (0.84 mL, 6.0 mmol), and fumaryl chloride (0.33 mL, 3.0 mmol) produced 2.374 g of **3-18** (4.3 mmol, 71 % yield). The product was recrystallized from DCM/pentane.

**$^1$H NMR (700 MHz, $CDCl_3$)** δ 8.12 (d, $J$ = 8.2 Hz, 4H), 7.35 – 7.21 (m, 4H + chloroform-d), 3.93 (s, 6H).

**$^{13}$C NMR (176 MHz, $CDCl_3$)** δ 166.10, 162.40, 153.67, 134.46, 131.31, 128.30, 121.26, 52.28.

**HRMS (ESI+) (m/z)**: $[M+H]^+$ calcd for $C_{20}H_{17}O_8$ 385.0918; found 385.0928.

**Di-*o*-tolyl fumarate (3-19).**

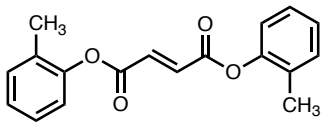

Following the general procedure: o-cresol (919 mg, 6.0 mmol), triethylamine (0.84 mL, 6.0 mmol), and fumaryl chloride (0.33 mL, 3.0 mmol) produced 2.374 g of **3-18** (4.3 mmol, 71 % yield). The product was recrystallized from DCM/pentane.

**$^{1}$H NMR (700 MHz, $CDCl_3$)** δ 7.30 – 7.27 (m, 2H + chloroform-d), 7.26 (t, *J* = 7.7 Hz, 2H), 7.21 (t, *J* = 7.4 Hz, 2H), 7.10 (d, *J* = 7.9 Hz, 2H), 2.24 (s, 6H).

**$^{13}$C NMR (176 MHz, $CDCl_3$)** δ 162.91, 148.87, 134.24, 131.32, 129.91, 127.08, 126.52, 121.54, 16.19.

**HRMS (ESI+) (m/z)**: $[M+H]^+$ calcd for $C_{18}H_{17}O_4$ 297.1121; found 297.1123.

**Bis(4-methoxyphenyl) fumarate (3-20)**.

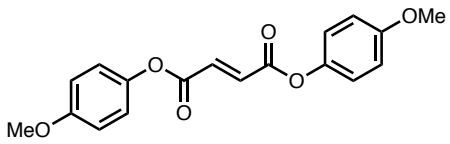

Following the general procedure: methyl 4-methoxyphenol (1.241 g, 10 mmol), triethylamine (1.4 mL, 10 mmol), and fumaryl chloride (0.54 mL, 5.0 mmol) produced 3.071 g of **3-20** (4.7 mmol, 94 % yield). The product was recrystallized from DCM/pentane.

**$^{1}$H NMR (700 MHz, $CDCl_3$)** δ 7.21 (s, 2H), 7.09 (d, *J* = 8.9 Hz, 4H), 6.92 (d, *J* = 8.9 Hz, 4H), 3.82 (s, 6H).

**$^{13}$C NMR (176 MHz, $CDCl_3$)** δ 163.52, 157.56, 143.74, 134.33, 122.00, 114.55, 55.61.

**HRMS (ESI+) (m/z)**: $[M+H]^+$ calcd for $C_{18}H_{17}O_4$ 329.1020; found 329.1022.

**Reductive Coupling Pre-catalysts**

**General Procedure for Synthesizing Reductive Coupling Pre-Catalysts:** A vial was charged with a stir bar and $Ni(COD)_2$ (1.0 equiv). A solution of fumarate (2.2 equiv) or acrylate (4.0 equiv) in THF was added dropwise directly to the vial containing $Ni(COD)_2$. The resulting solution was bright red and stirred for 15 minutes. Then a solution of IMes (1.0 equiv) was added and the reaction stirred overnight. Volatiles were removed *en vacuo* and desired product was either extracted with pentane and isolated by crystallization at -20 °C or precipitated out with the addition of pentane and was isolated by filtration.

**Ni(IMes)(diethyl fumarate)$_2$ (3-22).**

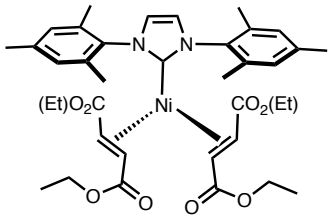


Following the general procedure: $Ni(COD)_2$ (137 mg, 0.5 mmol), IMes (152 mg, 0.5 mmol), di-ethyl fumarate (189 mg, 1.1 mmol) the product precipitated from the crude reaction mixture following the addition of pentane. A red solid was isolated by filtration. 284 mg (0.40 mmol), 80 % yield.

**$^1$H NMR (400 MHz, $C_6D_6$)** δ 6.96 (s, 2H), 6.88 (s, 2H), 6.32 (s, 2H), 4.59 (d, *J* = 11.0 Hz, 2H), 4.20 – 3.99 (m, 2H), 3.94 (d, *J* = 10.9 Hz, 2H), 3.90 – 3.71 (m, 6H), 2.41 (s, 6H), 2.13 (s, 6H), 1.99 (s, 6H), 0.98 (t, *J* = 7.0 Hz, 6H), 0.87 (t, *J* = 7.1 Hz, 6H).

**$^{13}$C NMR (100 MHz, $C_6D_6$)** δ 187.13, 170.90, 168.37, 138.01, 136.35, 135.60, 134.51, 130.04, 129.13, 124.25, 63.42, 59.33, 58.95, 56.61, 20.74, 19.08, 18.03, 14.25, 13.89.

Anal calcd for $C_{37}H_{48}N_2NiO_8$ : C (62.81 %), N (3.96 %), H (6.84 %); found: C (62.52 %), N (3.80 %), H (6.79 %).

**Ni(IMes)(di-*iso*-propyl fumarate)$_2$ (3-23)**

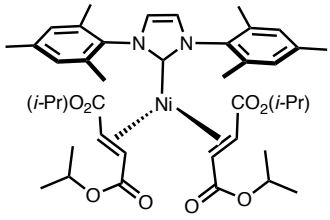


Following the general procedure: Ni(COD)$_2$ (137 mg, 0.5 mmol), IMes (152 mg, 0.5 mmol), and di-isopropyl fumarate (220 mg, 1.1 mmol). Product was extracted from crude reaction mixture with hot pentane and a red crystalline solid was isolated via recrystallization at -20 °C. 302 mg (0.40 mmol), 79 % yield.

**$^1$H NMR (500 MHz, $C_6D_6$)** δ 7.09 (s, 2H), 6.93 (s, 1H), 6.40 (s, 2H), 5.07 (hept, *J* = 6.3 Hz, 2H), 4.87 (hept, *J* = 6.2 Hz, 2H), 4.57 (d, *J* = 11.0 Hz, 2H), 4.04 (d, *J* = 11.0 Hz, 2H), 2.48 (s, 6H), 2.18 (s, 6H), 2.14 (s, 6H), 1.29 (d, *J* = 6.3 Hz, 6H), 1.08 (d, *J* = 6.3 Hz, 6H), 1.04 – 0.95 (m, 12H).

**$^{13}$C NMR (176 MHz, $C_6D_6$)** δ 188.35, 171.41, 168.83, 138.58, 136.92, 136.26, 134.84, 130.79, 129.74, 128.33, 124.78, 66.80, 63.63, 57.79, 22.63, 22.38, 22.09, 21.34, 19.95, 19.11.

Anal calcd for $C_{41}H_{56}N_2NiO_8$ : C (64.49 %), N (3.67 %), H (7.39 %); found: C (64.72 %), N (3.67 %), H (7.47 %).

**Ni(IMes)(di-*i*-butyl fumarate)$_2$ (3-24).**

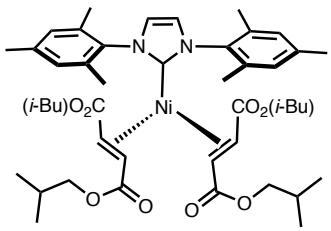

Following the general procedure: $Ni(COD)_2$ (137 mg, 0.5 mmol), IMes (152 mg, 0.5 mmol), and di-iso-butyl fumarate (251 mg, 1.1 mmol). Product was extracted from crude reaction mixture with hot pentane and a red crystalline solid was isolated via recrystallization at -20 °C. 385 mg (0.47 mmol), 94 % yield.

**$^1$H NMR (500 MHz, $C_6D_6$)** δ 7.10 (s, 2H), 6.97 (s, 1H), 6.40 (s, 2H), 4.65 (d, *J* = 10.9 Hz, 2H), 4.07 (d, *J* = 11.0 Hz, 2H), 3.98 (dd, *J* = 10.6, 6.7 Hz, 2H), 3.85 – 3.67 (m, 5H), 2.50 (s, 6H), 2.21 (s, 6H), 2.12 (s, 6H), 1.84 (d, *J* = 58.9 Hz, 1H), 0.89 (d, *J* = 6.7 Hz, 6H), 0.86 (d, *J* = 6.7 Hz, 6H), 0.77 (overlapping doublets, 12H).

**$^{13}$C NMR (176 MHz, $C_6D_6$)** δ 187.68, 171.41, 168.93, 138.52, 136.78, 136.16, 134.84, 130.68, 129.52, 128.35, 128.06, 124.72, 70.40, 70.13, 63.58, 57.16, 28.15, 21.22, 19.65, 19.54, 19.50, 19.40, 19.39, 18.68.

Anal calcd for $C_{45}H_{64}N_2NiO_8$ : C (65.94 %), N (3.42 %), H (7.87 %); found: C (66.18%), N (3.46 %), H (7.76 %).

**Ni(IMes)(di-*t*-butyl fumarate)$_2$ (3-25).**

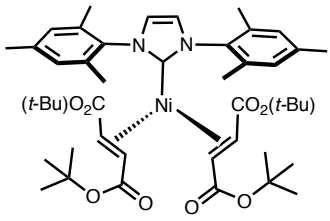


Following the general procedure: $Ni(COD)_2$ (137 mg, 0.5 mmol), IMes (152 mg, 0.5 mmol), and di-tert-butyl fumarate (251 mg, 1.1 mmol). Product was extracted from crude reaction mixture with hot pentane and a red crystalline solid was isolated via recrystallization at -20 °C. 283 mg (0.35 mmol), 69 % yield.

**$^1$H NMR (500 MHz, $C_6D_6$)** δ 7.05 (s, 2H), 6.90 (s, 2H), 6.41 (s, 2H), 4.51 (d, *J* = 11.1 Hz, 2H), 3.79 (d, *J* = 11.1 Hz, 2H), 2.35 (s, 6H), 2.19 (s, 6H), 2.14 (s, 6H), 1.48 (s, 18H), 1.28 (s, 18H).

**$^{13}$C NMR (176 MHz, $C_6D_6$)** δ 189.02, 171.78, 168.36, 137.99, 136.48, 136.00, 133.91, 130.49, 129.12, 124.14, 78.73, 78.59, 65.37, 58.26, 28.24, 20.87, 20.13, 19.99.

Anal calcd for $C_{45}H_{64}N_2NiO_8$ : C (65.94 %), N (3.42 %), H (7.87 %); found: C (65.99%), N (3.46 %), H (7.89 %).

**Ni(IMes)(di- (2-phenylpropan-2-yl) fumarate)$_2$ (3-26)**

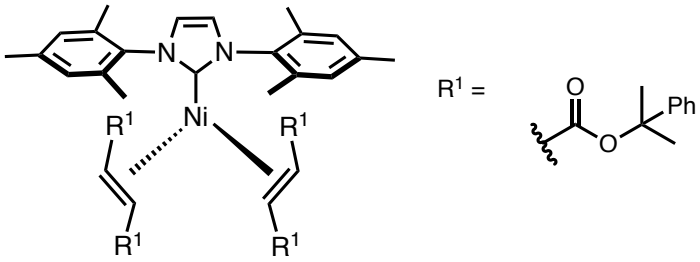


Following the general procedure: Ni(COD)$_2$ (55 mg, 0.2 mmol), IMes (61 mg, 0.2 mmol), and di-4-methyoxyphenyl fumarate (70 mg, 0.4 mmol). Product was precipitated from crude as an orange solid and the filtrate was purple. Orange precipitate collected via filtration and dried. Filtrate likely contained dimeric materials indicated by the purple color. 51 mg (0.05 mmol), 24 % yield.

**$^1$H NMR (500 MHz, $C_6D_6$)** δ 7.52 (d, *J* = 7.4 Hz, 4H), 7.21 (d, *J* = 7.4 Hz, 4H), 7.09 (m, 9H), 7.02 (t, *J* = 7.4 Hz, 4H), 6.98 (s, 2H), 6.79 (s, 2H), 6.33 (s, 2H), 4.91 (d, *J* = 11.0 Hz, 2H), 3.83 (d, *J* = 11.0 Hz, 2H), 2.15 (s, 6H), 2.13 (s, 6H), 2.04 (s, 6H), 1.90 (s, 6H), 1.81 (s, 6H), 1.66 (s, 8H), 1.65 (s, 6H).

**$^{13}$C NMR (176 MHz, $C_6D_6$)** δ 187.91, 171.16, 167.33, 147.66, 146.60, 137.90, 136.28, 135.53, 133.59, 130.33, 129.05, 126.50, 126.01, 124.84, 124.63, 124.06, 81.28, 81.02, 65.36, 57.95, 30.09, 27.92, 27.70, 26.72, 20.73, 20.01, 19.38.

**Ni(IMes)(di-o-tolyl fumarate)$_2$ (3-27).**

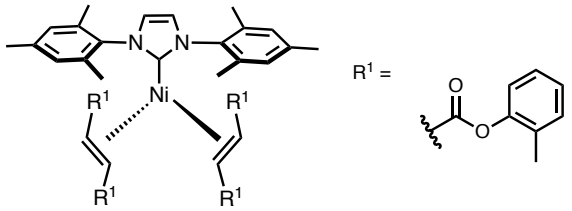

Following the general procedure: Ni(COD)$_2$ (200 mg, 0.73 mmol), IMes (222 mg, 0.73 mmol), and di-o-tolyl fumarate (432 mg, 1.46 mmol). Product was precipitated out as a dark red crystalline solid from reaction crude with the addition of pentane. Product was isolated by filtration and dried. 1.45 mg (0.51 mmol), 70 % yield.

**$^1$H NMR (500 MHz, $C_6D_6$)** δ 7.29 (d, *J* = 7.8 Hz, 2H), 7.00 (t, *J* = 7.5 Hz, 2H), 6.90 (dt, *J* = 14.6, 6.7 Hz, 4H), 6.83 – 6.76 (m, 4H), 6.71 (t, *J* = 7.8 Hz, 2H), 6.66 (t, *J* = 7.7 Hz, 2H), 6.41 (s, 2H), 6.36 (s, 2H), 5.20 (d, *J* = 11.1 Hz, 2H), 4.41 (d, *J* = 11.1 Hz, 2H), 2.39 (s, 6H), 2.16 (s, 6H), 2.03 (s, 6H), 1.93 (s, 6H), 1.89 (s, 6H).

**$^{13}$C NMR (176 MHz, $C_6D_6$)*** δ 184.62, 169.11, 166.91, 150.05, 149.94, 138.40, 136.14, 135.39, 134.29, 131.09, 130.83, 130.26, 130.12, 129.79, 129.03, 126.38, 126.13, 125.30, 124.98, 124.74, 123.02, 122.01, 64.40, 56.62, 20.53, 19.54, 19.18, 16.46, 15.90.

Anal calcd for $C_{57}H_{56}N_2NiO_8$ : C (71.63 %), N (2.93 %), H (5.91 %); found: C (71.97 %), N (2.83 %), H (6.39 %).

* Synthesized my me, but NMR data was collected by Alexander W. Rand.

**Ni(IMes)(di-*p*-anisole) fumarate)$_2$ (3-28).**

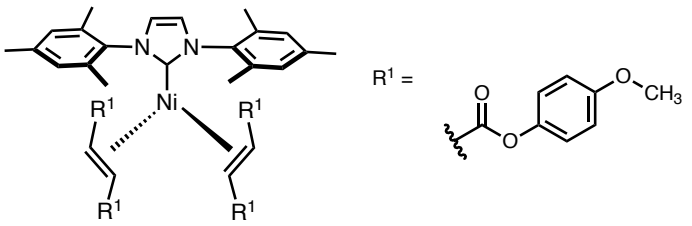

Following the general procedure: $Ni(COD)_2$ (28 mg, 0.1 mmol), IMes (30 mg, 0.1 mmol), and di-4-methyoxyphenyl fumarate (66 mg, 0.2 mmol). Product was precipitated from crude with the addition of pentane and collected by filtration. Product was recrystallized from THF/pentane at room temperature as a dark red crystalline solid. 71 mg (0.07 mmol), 71 % yield.

**$^1$H NMR (500 MHz, $C_6D_6$)** δ 7.03 (d, *J* = 9.0 Hz, 4H), 6.97 (d, *J* = 9.0 Hz, 4H), 6.88 (d, *J* = 2.0 Hz, 2H), 6.68 – 6.59 (m, 6H), 6.46 (d, *J* = 9.0 Hz, 4H), 6.38 (s, 2H), 5.20 (d, *J* = 11.0 Hz, 2H), 4.34 (d, *J* = 11.1 Hz, 2H), 3.20 (s, 6H), 3.09 (s, 6H), 2.44 (s, 6H), 2.10 (s, 6H), 2.00 (s, 6H).

**$^{13}$C NMR (126 MHz, $C_6D_6$)** δ 170.08, 167.80, 157.27, 157.23, 145.29, 145.14, 138.74, 136.44, 135.77, 134.60, 130.66, 129.50, 124.99, 123.58, 122.92, 114.29, 114.22, 64.51, 57.15, 54.97, 54.83, 21.03, 19.52, 19.47.

**Ni(IMes)(dimethylbenzoate fumarate)$_2$ (3-29).**

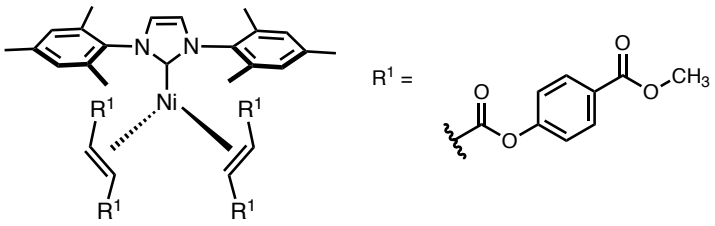

Following the general procedure: $Ni(COD)_2$ (28 mg, 0.1 mmol), IMes (30 mg, 0.1 mmol), and di-p-methyl benzoate fumarate (77 mg, 0.2 mmol). Product was precipitated out as a dark red crystalline solid from reaction crude with the addition of pentane. Product was isolated by filtration and dried. 101 mg (0.09 mmol), 90 % yield.

**$^1$H NMR (400 MHz, $C_6D_6$)** δ 8.05 (d, *J* = 8.7 Hz, 3H), 7.87 (d, *J* = 8.7 Hz, 3H), 7.04 (d, *J* = 8.7 Hz, 3H), 6.99 (d, *J* = 8.7 Hz, 3H), 6.87 (d, *J* = 2.0 Hz, 2H), 6.50 – 6.43 (m, 2H), 6.29 (s, 2H), 5.06 (d, *J* = 10.9 Hz, 2H), 4.29 (d, *J* = 10.9 Hz, 2H), 3.47 (s, 5H), 3.40 (s, 5H), 2.38 (s, 5H), 1.98 (s, 6H), 1.88 (s, 6H).

**$^{13}$C NMR (176 MHz, $C_6D_6$)** δ 183.23, 168.54, 166.01, 165.55, 165.53, 154.64, 154.50, 138.80, 135.79, 135.12, 134.22, 130.71, 130.54, 130.10, 129.19, 124.94, 122.25, 121.32, 121.11, 65.50, 63.48, 56.51, 51.24, 51.07, 22.31, 20.64, 18.82, 18.48, 15.18.

**Ni(IMes)(methyl acrylate)$_2$ (3-31).**

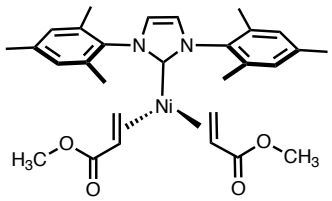


Following the general procedure: Ni(COD)$_2$ (137 mg, mmol), IMes (152 mg, 0.5 mmol), methyl acrylate (0.18 mL, 2.0 mmol). Product precipitated from the crude reaction mixture following the addition of pentane. A yellow/orange solid was isolated by filtration and recrystallized from THF/pentane at -20 °C. 228 mg (0.43 mmol), 85 % yield.

**$^1$H NMR (700 MHz, $C_6D_6$)** - *Peaks for major isomer are reported although NMR suggests the presence of higher symmetry diastereomers:* δ 6.76 (s, 2H), 6.64 (s, 2H), 6.25 (s, 2H), 3.59 (dd, *J* = 12.4, 8.9 Hz, 2H), 3.34 (s, 6H), 2.50 (d, *J* = 8.8 Hz, 2H), 2.36 (s, 6H+2H from minor diastereomer), 2.01 (s, 6H), 1.95 (s, 6H).

**$^{13}$C NMR (176 MHz, $C_6D_6$)** - *Major and minor isomers are reported together:* δ 195.43, 194.67, 173.31, 172.66, 138.63, 137.03, 136.34, 135.62, 134.86, 129.71, 129.35, 128.89, 128.35, 128.06, 123.39, 123.30, 58.91, 57.36, 52.25, 50.28, 50.09, 20.95, 18.43, 18.31.

Anal calcd for $C_{29}H_{36}N_2NiO_4$ : C (65.07 %), N (5.23 %), H (6.78 %); found: C (65.24%), N (5.05 %), H (6.70 %).

**Ni(IMes)(methyl methacrylate)$_2$ (3-32).**

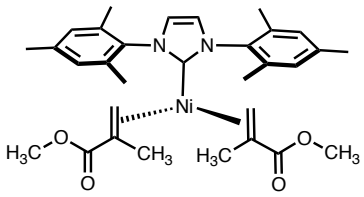

Following the general procedure, $Ni(COD)_2$ (137 mg, mmol), IMes (152 mg, mmol), methyl methacrylate (0.21 mL, 2.0 mmol). Product precipitated from the crude reaction mixture following the addition of pentane. A yellow/orange solid was isolated by filtration and recrystallized from THF/pentane at -20 °C. 215 mg (0.38 mmol), 77 % yield.

**$^1$H NMR (700 MHz, $C_6D_6$)** - *Peaks for major isomer are reported although NMR suggests the presence of higher symmetry diastereomers:* δ 6.69 (s, 2H), 6.62 (s, 2H), 6.22 (s, 2H), 3.53 (s, 2H), 3.36 (s, 6H), 3.21 (s, 2H), 2.47 (s, 2H), 2.21 (s, 6H), 2.00 (s, 6H+1H from minor diastereomer), 1.97 (s, 6H+1H from minor diastereomer), 1.32 (s, 6H).

**$^{13}$C NMR (176 MHz, $C_6D_6$)** - *Major and minor isomers are reported together:* δ 198.18, 197.67, 173.64, 173.49, 138.45, 137.10, 135.99, 134.88, 129.54, 129.35, 129.09, 128.35, 128.06, 123.33, 64.57, 64.32, 58.09, 58.04, 50.37, 50.15, 20.92, 19.02, 18.58, 18.50, 18.07.

Anal calcd for $C_{31}H_{40}N_2NiO_4$: C (66.09 %), N (4.97 %), H (7.16 %); found: C (66.03%), N (4.88 %), H (6.99 %).

**Ni(IMes)(phenyl acrylate)$_2$ (3-33).**

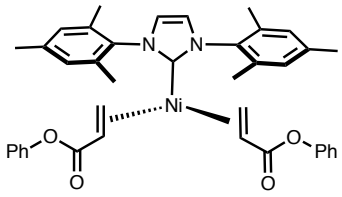

Following the general procedure: $Ni(COD)_2$ (55 mg, 0.2 mmol), IMes (61 mg, 0.2 mmol), and phenyl acrylate (0.08 mL, 0.6 mmol). Product precipitated from the crude reaction mixture following the addition of pentane. An orange solid was isolated by filtration and recrystallized from THF/pentane at room temperature. 55 mg (0.08 mmol), 42 % yield.

**$^1$H NMR (500 MHz, $C_6D_6$)** δ 7.04 (d, *J* = 7.8 Hz, 4H), 6.95 (t, *J* = 7.9 Hz, 4H), 6.82 (t, *J* = 7.3 Hz, 2H), 6.60 (s, 2H), 6.55 (s, 2H), 6.21 (s, 2H), 3.87 (dd, *J* = 12.4, 8.9 Hz, 2H), 3.44 (d, *J* = 12.5 Hz, 2H), 2.66 (d, *J* = 8.8 Hz, 2H), 2.23 (s, 6H), 1.97 (s, 6H), 1.92 (s, 6H).

**$^{13}$C NMR (176 MHz, $C_6D_6$)** δ 194.01, 169.83, 152.01, 138.30, 136.34, 135.59, 134.24, 129.42, 128.98, 128.62, 128.58, 124.16, 123.09, 122.45, 122.27, 58.66, 52.69, 20.52, 20.49, 18.07, 17.92, 17.87.

**Ni(IMes)(phenyl methacrylate)$_2$ (3-34).**

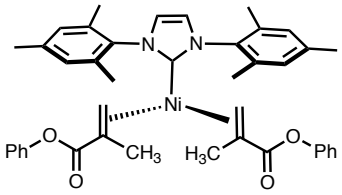

Following an adapted general procedure: $Ni(COD)_2$ (275 mg, 1.0 mmol), IMes (304 mg, 1.0 mmol), potassium tert-butoxide (134 mg, 1.2 mmol), and phenyl methacrylate (0.62 mL, and 4.0 mmol). Product precipitated from the crude reaction mixture following the addition of pentane. An orange solid was isolated by filtration and recrystallized from THF/pentane at room temperature. 497 mg (0.72 mmol), 72 % yield.

**$^1$H NMR (500 MHz, $C_6D_6$)** -*Peaks for major isomer are reported although NMR suggests the presence of higher symmetry diastereomers:* δ 7.25 (d, *J* = 8.0 Hz, 4H), 7.05 (t, *J* = 7.9 Hz, 4H), 6.86 (t, *J* = 7.4 Hz, 2H), 6.63 (s, 4H), 6.25 (s, 2H), 3.51 – 3.17 (m, 2H), 2.88 – 2.60 (m, 2H), 2.19 (s, 6H), 2.02 (s, 6H), 1.96 (s, 6H), 1.57 (s, 6H).

**$^{13}$C NMR (126 MHz, $C_6D_6$)** - *Major and minor isomers are reported together:* δ 196.23, 171.62, 152.64, 138.65, 136.80, 135.65, 134.65, 129.60, 129.40, 129.20, 128.93, 128.51, 124.41, 124.28, 123.78, 123.49, 122.87, 63.77, 58.81, 20.80, 19.40, 18.81, 18.53, 18.48, 18.39.

**[Ni(IMes)(dimethyl mesaconate]$_2$ (3-35).**

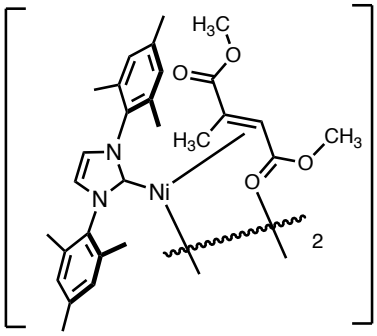


Following the general procedure: $Ni(COD)_2$ (55 mg, 0.2 mmol), IMes (61 mg, 0.2 mmol), and mesaconate (64 mg, and 0.4 mmol). Product was extracted from crude reaction mixture with hot pentane and a red crystalline solid was isolated via recrystallization at -20 °C. 82 mg (0.13 mmol of monomer), 66 % yield. X-ray quality crystals were grown from pentane at -20 °C.

**$^1$H NMR (401 MHz, $C_6D_6$)** δ 6.99 (d, *J* = 2.0 Hz, 2H), 6.77 (s, 2H), 6.18 (s, 2H), 3.63 (s, 3H), 3.28 (s, 3H), 3.11 (s, 1H), 2.61 (s, 6H), 2.19 (s, 6H), 1.94 (s, 6H), 0.53 (s, 3H).

**$^{13}$C NMR (176 MHz, $C_6D_6$)** δ 193.81, 178.24, 175.03, 137.73, 137.67, 137.22, 135.89, 135.38, 128.80, 128.79, 121.50, 49.88, 49.79, 42.41, 34.04, 34.00, 22.34, 20.79, 18.17, 18.11, 17.67, 15.35, 13.90.

**General Protocol for Reaction Progress Analysis for IMes-based Pre-Catalysts:** A vial was charged with the respective pre-catalyst (0.00625 mmol) and 0.25 mL of THF and added to a septa cap NMR tube. A separate vial was prepared with 4-fluorobenzaldehyde (0.125 mmol), 1-phenyl-1-propyne (0.125 mmol), triethylsilane (0.25 mmol), trifluorotoluene (0.0417 mmol), and 0.25 mL of THF. The solution containing reagents and standard was added to the NMR tube and real time monitoring of the reaction was doen using $^{19}F$ NMR which was collected at fixed time intervals. A sample $^{19}F$ NMR spectra is shown below in Figure 5-3.

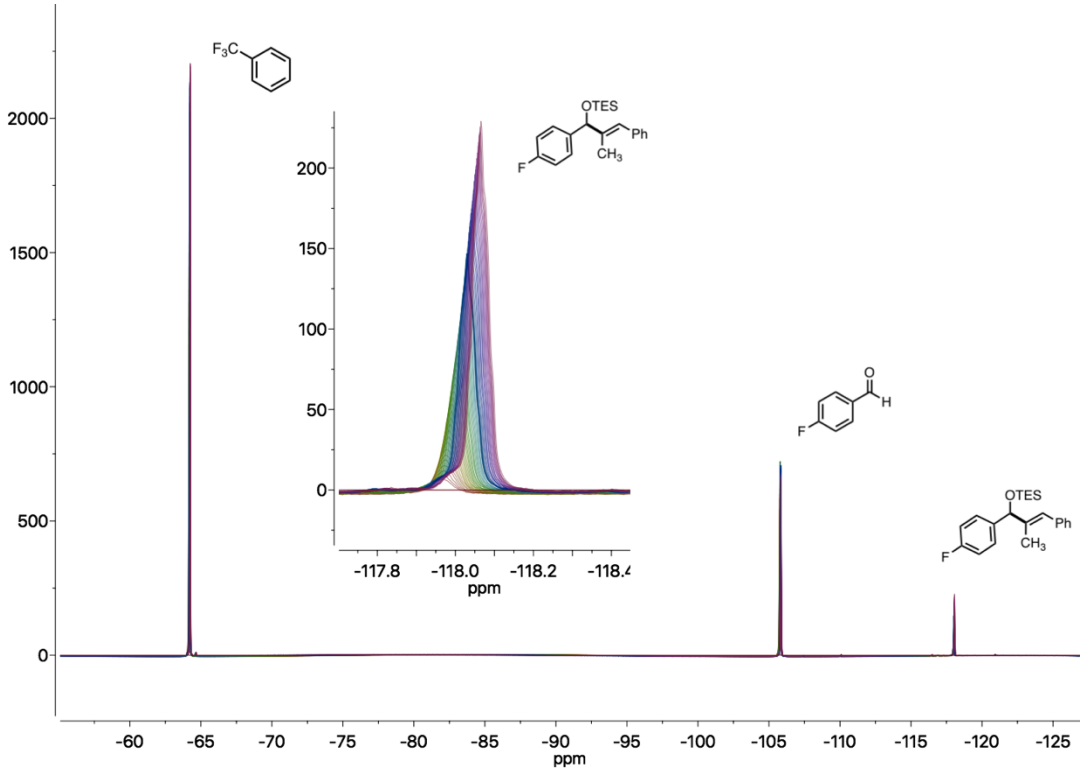


**Figure 5-21.** $^{19}F$ NMR spectra for reaction progression analysis of reductive couplings.

**General Procedure for Reductive Couplings**

In the glovebox, a 1-dram vial was charged with **3-25** (0.02 equiv) and THF (0.5 M). Then silane (2.0 equiv), alkyne (1.2 equiv) and aldehyde (1.0 equiv) were added sequentially. The reaction stirred for 18 hours at room temperature. It was quenched by pushing through a plug of silica and rinsed with dichloromethane. Regioselectivity was determined by GCMS analysis of the crude reaction mixture and product were purified by silica column chromatography.

**Characterization of Silyl-Protected Allylic Alcohols**

***Tert*-butyl (*E*)-4-(3-methyl-4-phenyl-2-((triethylsilyl)oxy)but-3-en-1-yl)piperidine-1-carboxylate (3-36).**

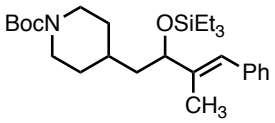


Following the general procedure for reductive couplings: Ni(IMes)(di-tert-butyl fumarate (**3-25**) (8.2 mg, 0.01 mmol), *N*-Boc-4-piperidineacetaldehyde (114 mg, 0.5 mmol), 1-phenyl-1propyne (75 μL, 0.6 mmol), and triethylsilane (0.160 mL, 1.0 mmol) produced 202 mg (0.44 mmol, 88 % yield) of **3-36** in a 98:2 regioisomeric mixture. Product was purified by silica column chromatography using ethyl acetate/hexane and isolated as a single regioisomer.

**$^1$H NMR (500 MHz, $CDCl_3$)** δ 7.35 (t, *J* = 7.6 , 2H), 7.26 (d, 2H, overlapping with $CDCl_3$ signal), 7.23 (t, *J* = 7.3 Hz, 1H), 6.43 (s, 1H), 4.25 (t, *J* = 6.4 Hz, 1H), 4.08 (s, 2H), 2.69 (t, *J* = 12.3 Hz, 2H), 1.84 (s, 3H), 1.72 (t, *J* = 15.1 Hz, 2H), 1.57 (m, 2H), 1.47 (s, 9H), 1.15 (td, *J* = 12.3, 3.9 Hz, 2H), 0.97 (t, *J* = 7.9 Hz, 9H), 0.62 (q, *J* = 7.9 Hz, 6H).

**$^{13}$C NMR (176 MHz, $CDCl_3$)** δ 154.88, 140.97, 137.77, 128.84, 128.10, 126.28, 125.16, 79.15, 76.06, 44.31, 43.62, 43.23, 32.72, 32.43, 32.10, 28.46, 13.01, 6.89, 4.88.

**HRMS (ESI+) (m/z)**: $[M+Na]^+$ calcd for $C_{27}H_{45}NO_3Si$ 482.3061; found 482.3056

**Triethyl(((*E*)-4-((tetrahydro-2*H*-pyran-2-yl)oxy)-1-(4-(trifluoromethyl)phenyl)but-2-en-1-yl)oxy)silane (3-37).**

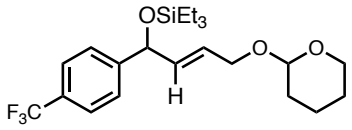


Following the general procedure for reductive couplings: Ni(IMes)(di-tert-butyl fumarate (**3-25**) (8.2 mg, 0.01 mmol), 4-(trifluoromethyl)benzaldehyde (68 μL, 0.5 mmol), tetrahydro-2-(2-propyn-1-yloxy)-2H-pyran (84 μL, 0.6 mmol), and triethylsilane (0.160 mL, 1.0 mmol) produced 161 mg (0.38 mmol, 75 % yield) of **3-37** in a >98:2 regioisomeric mixture. Product was purified by silica column chromatography using ethyl acetate/hexane and isolated as a single regioisomer.

**$^1$H NMR (700 MHz, $CDCl_3$)** δ 7.57 (d, *J* = 7.9 Hz, 2H), 7.46 (d, *J* = 7.9 Hz, 2H), 5.96 – 5.69 (m, 2H), 5.23 (t, *J* = 5.2 Hz, 1H), 4.62 – 4.50 (m, 1H), 4.22 (ddd, *J* = 13.6, 9.1, 4.4 Hz, 1H), 3.98 (ddd, *J* = 13.1, 7.3, 5.8 Hz, 1H), 3.84 (t, *J* = 9.9 Hz, 1H), 3.53 – 3.41 (m, 1H), 1.91 – 1.77 (m, 1H), 1.70 (t, *J* = 11.4 Hz, 1H), 1.63 – 1.41 (m, 2H), 1.53 – 1.46 (m, 2H), 0.92 (t, *J* = 8.0 Hz, 9H), 0.66 – 0.53 (m, 6H).

**$^{13}$C NMR (176 MHz, $CDCl_3$) -** *reported as a mixture of diastereomers* - δ 147.85, 134.95, 134.90, 129.14, 127.03, 126.87, 126.23, 126.22, 125.13, 97.93, 97.88, 74.37, 74.27, 66.71, 66.70, 62.18, 62.16, 30.57, 30.55, 25.42, 19.43, 19.40, 6.74, 4.85.

**HRMS (ESI+) (m/z)**: $[M+Na]^+$ calcd for $C_{22}H_{33}F_3O_3SiNa$: 453.2048; found 453.2045

**Di-*tert*-butyl(((*E*)-4-((tetrahydro-2*H*-pyran-2-yl)oxy)-1-(4-(trifluoromethyl)phenyl)but-2-en-1-yl)oxy)silane (3-38).**

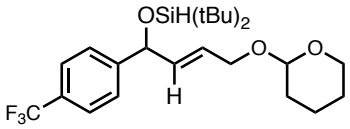


Following the general procedure for reductive couplings: Ni(IMes)(di-tert-butyl fumarate (**3-25**) (8.2 mg, 0.01 mmol), 4-(trifluoromethyl)benzaldehyde (68 μL, 0.5 mmol), tetrahydro-2-(2-propyn-1-yloxy)-2H-pyran (84 μL, 0.6 mmol), and di-tert-butylsilane (0.198 mL, 1.0 mmol) produced 202 mg (0.44 mmol, 88 % yield) of **3-38** in a >98:2 regioisomeric mixture. Product was purified by silica column chromatography using ethyl acetate/hexane and isolated as a single regioisomer.

**$^1$H NMR (500 MHz, $CDCl_3$)** δ 7.60 (d, *J* = 8.1 Hz, 2H), 7.48 (d, *J* = 8.0 Hz, 2H), 5.88 – 5.72 (m, 2H), 5.30 (dd, *J* = 6.0, 3.1 Hz, 1H), 4.63 (dt, *J* = 10.7, 3.5 Hz, 1H), 4.30 – 4.19 (m, 1H), 4.08 (d, *J* = 2.2 Hz, 1H), 4.05 – 3.94 (m, 1H), 3.90 – 3.80 (m, 1H), 3.55 – 3.44 (m, 1H), 1.89 – 1.77 (m, 1H), 1.77 – 1.64 (m, 1H), 1.65 – 1.46 (m, 3H), 1.06 (s, 9H), 0.91 (s, 9H).

**$^{13}$C NMR (176 MHz, $CDCl_3$)** - *reported as a mixture of diastereomers* - δ 147.19, 134.37, 127.73, 127.57, 126.58, 125.15, 97.80, 97.78, 78.01, 66.56, 62.16, 30.53, 27.37, 27.15, 25.42, 20.14, 19.94, 19.39.

**HRMS (ESI+) (m/z)**: [M-tBu] calcd for $C_{20}H_{28}F_3O_3Si$: 401.1760; found: 401.1780.

**(*E*)-((1-(4-Chlorophenyl)-2-phenylpenta-2,4-dien-1-yl)oxy)triethylsilane ) (3-39).**

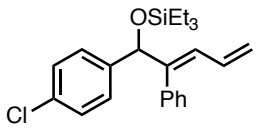


Following the general procedure for reductive couplings: : Ni(IMes)(di-tert-butyl fumarate (**3-25**) (8.2 mg, 0.01 mmol), 4-chlorobenzaldehyde (70 mg, 0.5 mmol), 1-phenyl-1-butyne-3-ene (77 mg, 0.6 mmol), and triethylsilane (0.160 mL, 1.0 mmol) produced 77 mg (0.20 mmol, 40 % yield) of

**3-39** in a >98:2 regioisomeric mixture. Product was purified by silica column chromatography using ethyl acetate/hexane and isolated as a single regioisomer.

**$^1$H NMR (700 MHz, $CDCl_3$)** δ 7.22 – 7.20 (m, 2H), 7.16 (d, *J* = 8.2 Hz, 2H), 7.09 (d, *J* = 8.2 Hz, 2H), 6.90 (d, *J* = 5.9 Hz, 2H), 6.52 (d, *J* = 11.0 Hz, 1H), 6.20 (dt, *J* = 17.0, 10.6 Hz, 1H), 5.36 (s, 1H), 5.31 (d, *J* = 16.9 Hz, 1H), 5.04 (d, *J* = 10.2 Hz, 1H), 0.91 (t, *J* = 7.9 Hz, 9H), 0.59 (q, *J* = 7.9 Hz, 6H).

**$^{13}$C NMR (176 MHz, $CDCl_3$)** δ 145.67, 141.51, 137.74, 133.96, 132.56, 129.55, 127.96, 127.93, 127.73, 127.03, 126.89, 118.19, 77.77, 77.17, 6.77.

**HRMS (EI) (m/z)**: [M+] calcd for $C_{23}H_{29}ClOSi$ 384.1676; found 384.1663.

**2,2-Di-*tert*-butyl-5-(4-chlorophenyl)-4-phenyl-3-vinyl-2,5-dihydro-1,2-oxasilole (3-40).**

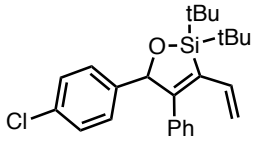


Following the general procedure for reductive couplings: : Ni(IMes)(di-tert-butyl fumarate (**3-25**) (8.2 mg, 0.01 mmol), 4-chlorobenzaldehyde (70 mg, 0.5 mmol), 1-phenyl-1-butyne-3-ene (77 mg, 0.6 mmol), and di-tert-butylsilane (0.198 mL, 1.0 mmol) produced 201 mg (0.49 mmol, 98 % yield) of **3-40** as a single regioisomer. Product was purified by silica column chromatography using ethyl acetate/hexane.

**$^1$H NMR (700 MHz, $CDCl_3$)** δ 7.28 (t, *J* = 7.6 Hz, 2H), 7.20 – 7.17 (m, 1H), 7.15 (d, *J* = 8.3 Hz, 2H), 7.11 (d, *J* = 8.3 Hz, 2H), 6.91 (d, *J* = 8.0 Hz, 2H), 6.56 – 6.47 (m, 1H), 5.85 (s, 1H), 5.33 (d, *J* = 17.5 Hz, 1H), 5.22 (d, *J* = 10.6 Hz, 1H), 1.22 (s, 9H), 1.14 (s, 9H).

**$^{13}$C NMR (176 MHz, $CDCl_3$)** δ 158.76, 139.90, 137.09, 136.01, 134.88, 133.13, 129.08, 128.63, 128.13, 128.03, 127.35, 119.88, 86.37, 28.39, 27.68, 22.91, 20.55.

**HRMS (EI) (m/z)**: [M] calcd for $C_{25}H_{31}ClOSi$ 410.1832; found 410.1813

**(*E*)-2-(4-cyclohexyl-3-methyl-4-((triethylsilyl)oxy)but-2-en-1-yl)isoindoline-1,3-dione (3-41).**

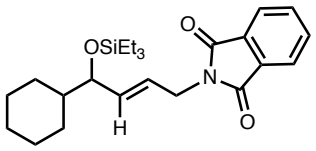


Following the general procedure for reductive couplings: Ni(IMes)(di-tert-butyl fumarate (**3-25**) (8.2 mg, 0.01 mmol), cyclohexanecarboxaldehyde (61 μL, 0.5 mmol), *N*-propargylphthalimide (111 mg, 0.6 mmol), and triethylsilane (0.160 mL, 1.0 mmol) produced 128 mg (0.31 mmol, 62 % yield) of **3-41** in a >98:2 regioisomeric mixture. Product was purified by silica column chromatography using ethyl acetate/hexane and isolated as a single regioisomer.

**$^1$H NMR (700 MHz, $CDCl_3$)** δ 7.85 (dd, *J* = 4.9, 3.2 Hz, 2H), 7.71 (dd, *J* = 5.1, 3.1 Hz, 2H), 5.67 (dd, *J* = 15.5, 6.8 Hz, 1H), 5.60 (dt, *J* = 15.4, 5.9 Hz, 1H), 4.38 – 4.16 (m, 2H), 3.76 (t, *J* = 6.6 Hz, 1H), 1.79 (d, *J* = 12.7 Hz, 1H), 1.69 (t, *J* = 12.3 Hz, 2H), 1.60 (t, *J* = 13.4 Hz, 2H), 1.34 – 1.23 (m, 1H), 1.23 – 1.04 (m, 4H), 0.91 – 0.80 (m, 10H), 0.51 (q, *J* = 7.8 Hz, 6H).

**$^{13}$C NMR (176 MHz, $CDCl_3$)** δ 167.80, 136.44, 133.86, 132.15, 123.64, 123.20, 77.30, 44.35, 39.01, 28.76, 28.70, 26.59, 26.20, 26.17, 6.81, 4.94.

**HRMS (ESI+) (m/z)**: $[M+Na]^+$ calcd for $C_{24}H_{35}NO_3SiNa$: 436.2278; found 436.2281.

**Buchwald-Hartwig Pre-Catalysts**

**General Procedure for synthesis of Pre-Catalysts for Buchwald-Hartwig Couplings:** A vial was charged with a stir bar and $Ni(COD)_2$ (1.0 equiv). A solution of acrylate (4.0 equiv) in THF

was added dropwise directly to the vial containing $Ni(COD)_2$. The resulting solution was bright red and stirred for 15 minutes. Then a solution of NHC (1.0 equiv) was added and the reaction stirred overnight. Volatiles were removed *en vacuo* and desired product was either extracted with pentane and isolated by crystallization at -20 °C or precipitated out with the addition of pentane and was isolated by filtration.

**Ni(IPr*OMe)(methyl acrylate)$_2$ (3-42)**.

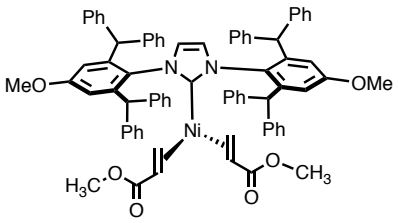


Following general procedure, $Ni(COD)_2$ (137 mg, 0.5 mmol), IPr*OMe (473 mg, 0.5 mmol), and methyl acrylate (0.18 mL, mmol). Product precipitated from the crude reaction mixture following the addition of pentane. A yellow/orange solid was isolated by filtration and recrystallized from THF/pentane at -20 °C. 502 mg (0.43 mmol), 85 % yield.

**$^1$H NMR (700 MHz, $C_6D_6$)** δ 7.36 (d, *J* = 7.6 Hz, 8H), 7.15 – 6.76 (m, 51H), 6.72 (t, 3H), 6.69 (d, *J* = 2.9 Hz, 2H), 6.31 (s, 2H), 5.50 (s, 2H), 5.42 (s, 2H), 3.77 (dd, *J* = 12.8, 8.8 Hz, 2H), 3.53 (d, *J* = 12.8 Hz, 2H), 3.41 (s, 6H), 3.14 (d, *J* = 8.8 Hz, 2H), 3.03 (s, 6H).

**$^{13}$C NMR (176 MHz, $C_6D_6$)** δ 197.49, 172.92, 159.90, 145.05, 144.68, 144.08, 143.71, 143.58, 142.21, 132.18, 130.49, 130.34, 129.84, 129.61, 128.89, 128.82, 128.57, 128.43, 128.35, 128.31, 127.06, 126.98, 126.90, 126.70, 124.18, 115.86, 115.62, 61.04, 55.03, 54.69, 52.73, 52.03, 50.52. Anal calcd for $C_{77}H_{68}N_2NiO_6$ : C (78.64 %), N (2.38 %), H (5.83 %); found: C (78.00 %), N (2.65 %), H (5.68 %).

**Ni(IPr*OMe)(phenyl acrylate)$_2$ (3-43)**.

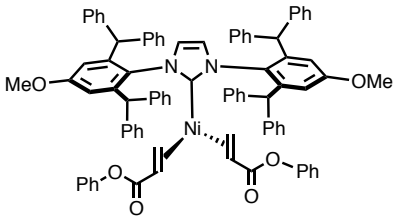


Following general procedure, Ni(COD)$_2$ (137 mg, 0.5 mmol), IPr*OMe (473 mg, 0.5 mmol), and phenyl acrylate (0.28 mL, 2.0 mmol). Product precipitated from the crude reaction mixture following the addition of pentane. A yellow/orange solid was isolated by filtration and recrystallized from THF/pentane at -20 °C. 609 mg (0.47 mmol), 94 % yield.

**$^1$H NMR (400 MHz, $C_6D_6$)** δ 7.38 (d, 8H,), 7.18 – 6.69 (m, 40H), 6.65 (d, *J* = 2.9 Hz, 2H), 6.16 (s, 2H), 5.56 (s, 2H), 5.53 (s, 2H), 3.95 (dd, *J* = 12.7, 8.8 Hz, 2H), 3.65 (d, *J* = 12.8 Hz, 2H), 3.19 (d, *J* = 8.7 Hz, 2H), 2.91 (s, 6H).

**$^{13}$C NMR (176 MHz, $C_6D_6$)** δ 195.79 (N-C-N), 170.83(-C=O), 159.62 , 152.17, 144.66, 144.25, 144.00, 143.09, 142.83, 141.53, 131.42, 130.05, 129.96, 129.37, 129.22, 128.71, 128.50, 128.43, 128.23, 128.18, 128.07, 127.93, 127.89, 127.78, 127.71, 127.64, 127.56, 127.50, 126.65, 126.62, 126.54, 126.36, 124.38, 124.15 (N-HC=CH-N), 122.60, 115.80, 115.06, 59.07 (=CH-, acrylate), 55.44 ($H_2C$=, acrylate), 54.26 (-O-$CH_3$, NHC), 52.43 (-CH-$Ph_2$), 51.81 (-CH-$Ph_2$).

Anal calcd for $C_{87}H_{72}N_2NiO_6$: C (80.37 %), N (2.15 %), H (5.58 %); found: C (79.41%), N (2.21 %), H (5.51 %).

**Ni(IPr)(methyl acrylate)$_2$ (3-44)**.

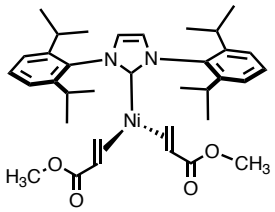

Following general procedure, $Ni(COD)_2$ (137 mg, 0.5 mmol), IPr (194 mg, 0.5 mmol), and methyl acrylate (0.18 mL, 0.5 mmol). Product precipitated from the crude reaction mixture following the addition of pentane. A yellow/orange solid was isolated by filtration and recrystallized from THF/pentane at 25 °C. 57 mg (0.09 mmol), 92 % yield.

**$^1$H NMR (700 MHz, THF-$d_8$)** - *Peaks for major isomer are reported although NMR suggests the presence of higher symmetry diastereomers:* δ 7.44 – 7.36 (m, 5H), 7.32 – 7.25 (m, 3H), 7.23 (d, *J* = 7.7 Hz, 2H), 3.22 (s, 4H), 3.04 (hept, *J* = 6.7 Hz, 2H), 2.83 (hept, *J* = 6.6, 6.1 Hz, 2H), 2.70 (dd, *J* = 13.0, 8.7 Hz, 2H), 2.54 (d, *J* = 12.8 Hz, 2H), 2.36 (d, *J* = 8.9 Hz, 2H), 1.71 (s, 18H), 1.40 (d, *J* = 6.8 Hz, 6H), 1.24 (d, *J* = 6.7 Hz, 6H), 1.08 (d, *J* = 6.8 Hz, 6H), 1.05 (d, *J* = 6.9 Hz, 7H).

**$^{13}$C NMR (176 MHz, THF- $d_8$)** - *Major and minor isomers are reported together:* δ 197.45, 172.42, 146.41, 145.99, 137.49, 130.08, 130.02, 125.91, 125.79, 124.58, 124.46, 124.42, 124.06, 59.97, 57.94, 53.60, 49.71, 29.38, 29.19, 28.88, 26.52, 26.06, 22.88, 22.64, 22.20.

Anal calcd for $C_{35}H_{48}N_2NiO_4$: C (67.86 %), N (4.52 %), H (7.81 %); found: C (67.00%), N (4.50 %), H (7.69 %).

**Ni(IPr)(phenyl acrylate)$_2$ (3-45).**

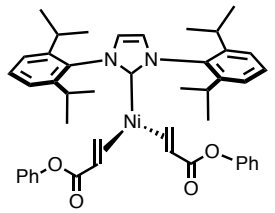

Following general procedure, $Ni(COD)_2$ (137 mg, 0.5 mmol), IPr (194 mg, 0.5 mmol), and phenyl acrylate (0.28 mL, 2.0 mmol). Product precipitated from the crude reaction mixture following the addition of pentane. A yellow/orange solid was isolated by filtration and recrystallized from THF/pentane at -20 °C. 223 mg (0.30mmol), 60 % yield.

**$^1$H NMR (700 MHz, $C_6D_6$)** δ 7.19 (d, 4H), 7.15 – 7.07 (m, 4H), 7.01 (d, *J* = 7.8, 1.4 Hz, 2H), 6.97 – 6.89 (m, 7H), 6.77 (t, *J* = 7.4 Hz, 2H), 6.59 (s, 2H), 3.68 (dd, *J* = 12.8, 9.0 Hz, 2H), 3.09 (d, *J* = 12.8 Hz, 2H), 3.04 (m, 2H), 2.84 (d, *J* = 8.6 Hz, 2H), 2.82 – 2.71 (m, 2H), 1.38 (d, *J* = 6.8 Hz, 6H), 1.04 (d, *J* = 6.9 Hz, 6H), 1.02 (d, *J* = 6.8 Hz, 6H), 0.90 (d, *J* = 6.9 Hz, 6H).

**$^{13}$C NMR (176 MHz, $C_6D_6$)** δ 196.73, 170.98, 152.44, 145.80, 145.23, 136.58, 130.27, 129.03, 124.79, 124.71, 124.64, 124.25, 122.81, 59.24, 54.68, 29.02, 28.64, 26.64, 25.63, 22.89, 22.27.

Anal calcd for $C_{45}H_{52}N_2NiO_4$: C (72.68 %), N (3.77 %), H (7.05 %); found: C (72.98%), N (3.73 %), H (7.12 %).

**Ni(IPr)(methyl methacrylate)$_2$ (3-46)**

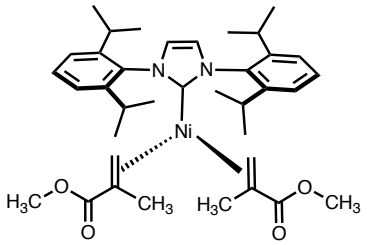


Following general procedure, $Ni(COD)_2$ (137 mg, 0.5 mmol), IPr (194 mg, 0.5 mmol), and methyl methacrylate (0.21 mL, 2.0 mmol). Product precipitated from the crude reaction mixture following the addition of pentane. A yellow/orange solid was isolated by filtration and recrystallized from THF/pentane at -20 °C. 261 mg (0.40 mmol), 81 % yield.

**$^1$H NMR (700 MHz, $C_6D_6$)** - $^1$H NMR contained diastereomers that were in thermal equilibrium with one another. Complete resolution of the different complexes could not be achieved and peak

numbers reflect NMR spectra at 25 °C which is included in this document. δ 7.09 – 7.04, 7.02 – 6.98, 6.62 – 6.57, 3.44, 3.32, 3.14 – 3.04, 3.02 – 2.86, 2.68 – 2.55, 1.40, 1.35, 1.26 – 1.20, 1.03 – 0.90.

**$^{13}$C NMR (176 MHz, $C_6D_6$)** δ 200.63, 173.03, 172.94, 145.76, 145.23, 136.71, 129.56, 124.23, 124.18, 123.84, 123.77, 123.68, 65.08, 58.04, 50.21, 49.79, 28.49, 28.37, 25.86, 22.01, 21.94, 21.84, 18.25, 17.49.

Anal calcd for $C_{45}H_{64}N_2NiO_8$ : C (68.63 %), N (4.33 %), H (8.09 %); found: C (68.43%), N (4.04 %), H (8.04 %).

**Ni(SIPr)(methyl acrylate)$_2$ (3-47)**

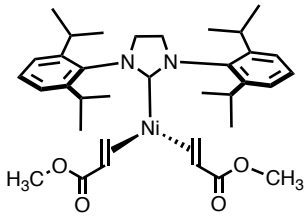


Following adapted general procedure, Ni(COD)$_2$ (137 mg, 0.5 mmol), SIPr•HBF$_4$ (239 mg, 0.5 mmol), sodium tert-butoxide (53 mg, 0.55 mmol) and methyl acrylate (0.18 mL, 2.0 mmol). Note: SIPr•HBF$_4$ and sodium tert-butoxide were stirred for 15 min in 5 mL of THF prior to being added to a solution of Ni(COD)$_2$ and methyl acrylate. Product precipitated from the crude reaction mixture. A yellow powder was collected on a frit and dried. Product was extracted with hot THF and crystallized upon cooling to room temperature. A yellow solid was isolated by filtration. 247 mg (0.40 mmol), 80 % yield.

**$^1$H NMR (700 MHz, THF-*d*$_8$)** *Peaks for major isomer are reported although NMR suggests the presence of higher symmetry diastereomers:* δ 7.31 (t, *J* = 7.6 Hz, 2H), 7.26 (d, *J* = 7.7 Hz, 2H), 7.16 (d, *J* = 7.6 Hz, 2H), 4.07 – 3.95 (m, 2H + 2H from minor diastereomers), 3.44 (hept, *J* = 6.3

Hz, 2H), 3.21 (hept, $J$ = 6.9 Hz, 2H), 3.13 (s, 6H), 2.55 (dd, $J$ = 12.5, 9.3 Hz, 2H), 2.47 (m, 2H + 2H from minor diastereomers), 1.50 (d, $J$ = 6.7 Hz, 6H), 1.35 (d, $J$ = 6.8 Hz, 6H), 1.18 (d, $J$ = 6.8 Hz, 6H), 0.95 (d, $J$ = 6.8 Hz, 6H).

**$^{13}$C NMR (176 MHz, THF-$d_8$)** δ 225.47, 171.88, 146.74, 146.61, 145.89, 137.00, 128.38, 124.32, 124.05, 123.91, 59.58, 57.49, 54.23, 53.43, 52.94, 48.97, 28.36, 28.23, 27.93, 25.91, 25.61, 24.74, 24.63, 22.61, 22.26.

Anal calcd for $C_{35}H_{50}N_2NiO_4$ : C (67.64 %), N (4.51 %), H (8.11 %); found: C (67.38%), N (4.37 %), H (7.90 %).

**Ni(SIPr)(phenyl acrylate)$_2$ (3-48).**

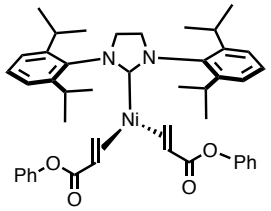


Following general procedure, Ni(COD)$_2$ (mg, mmol), SIPr•HBF$_4$ (239 mg, 0.5 mmol), sodium tert-butoxide (53 mg, 0.55 mmol), and phenyl acrylate (0.28 mL, 2.0 mmol). Note: SIPr•HBF$_4$ and sodium tert-butoxide were stirred for 15 min in 5 mL of THF prior to being added to a solution of Ni(COD)$_2$ and phenyl acrylate. Product precipitated from the crude reaction mixture following the addition of pentane. A yellow/orange solid was isolated by filtration and recrystallized from THF/pentane at 25 °C.189 mg (0.26 mmol), 51 % yield.

**$^1$H NMR (700 MHz, $C_6D_6$)** δ 7.18 (d, $J$ = 8.3 Hz, 4H), 7.07 (t, 2H), 7.02 – 7.00 (m, 2H), 6.93 (t, 4H), 6.88 (d, $J$ = 7.7 Hz, 2H), 6.77 (td, $J$ = 7.4, 1.3 Hz, 2H), 3.61 – 3.56 (m, 2H), 3.48 – 3.39 (m, 4H), 3.32 (p, $J$ = 6.9 Hz, 2H), 3.18 (p, $J$ = 6.9 Hz, 2H), 3.00 (d, $J$ = 12.9 Hz, 2H), 2.91 (d, $J$ = 8.9

Hz, 2H), 1.45 (d, *J* = 6.6 Hz, 6H), 1.12 (d, *J* = 6.8 Hz, 6H), 0.99 (d, *J* = 6.8 Hz, 6H), 0.95 (d, *J* = 6.8 Hz, 6H).

**$^{13}$C NMR (176 MHz, $C_6D_6$)** δ 225.26, 170.67, 151.98, 146.53, 145.38, 136.51, 129.09, 128.56, 124.95, 124.19, 124.07, 122.41, 59.06, 54.76, 53.92, 28.43, 28.10, 26.35, 26.06, 23.04, 22.68.

Anal calcd for $C_{45}H_{54}N_2NiO_4$: C (72.49 %), N (3.76 %), H (7.30 %); found: C (72.77%), N (3.81 %), H (7.37 %).

**Ni(SIPr)(methyl methacrylate)$_2$ (3-49)**

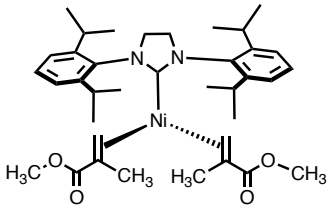


Following an adpated general procedure, Ni(COD)$_2$ (mg, mmol), SIPr (mg, mmol), potassium bis(trimethylsilyl)amide (100 mg, 0.5 mmol) and methyl methacrylate (0.21 mL, 2.0 mmol). Note: SIPr•HBF$_4$ and potassium bis(trimethylsilyl)amide were stirred in 5 mL toluene for 15 min and filtered. The filtrate was added directly to a solution of Ni(COD)$_2$ and methyl methacrylate. Product precipitated from the crude reaction mixture following the addition of pentane. A pale-yellow solid was isolated by filtration and recrystallized from THF/pentane at -20 °C. 254 mg (0.39 mmol), 78 % yield.

**$^{1}$H NMR (500 MHz, $C_6D_6$)** -*Peaks for major isomer are reported although NMR suggests the presence of higher symmetry diastereomers:* δ 7.10 – 6.90 (m, 6H), 3.51 (m, 4H), 3.40 (s, 3H), 3.33 (s, 3H), 3.13 (s, 1H), 3.10 (s, 1H), 2.68 (s, 2H), 1.48 (d, *J* = 6.7 Hz, 3H), 1.44 (d, *J* = 6.7 Hz, 3H), 1.33 (d, *J* = 6.7 Hz, 3H), 1.29 (s, 3H), 1.24 (d, *J* = 6.7 Hz, 3H), 1.11 (d, *J* = 6.8 Hz, 3H), 1.08 (d, *J* = 6.8 Hz, 3H), 1.07 – 1.05 (m, 6H), 1.03 (d, *J* = 6.8 Hz, 3H).

**$^{13}$C NMR (126 MHz, $C_6D_6$)** -*Major and minor isomers are reported together:* δ 229.61, 229.47, 173.03, 172.96, 147.21, 146.70, 146.65, 146.25, 137.19, 137.11, 136.96, 128.90, 128.84, 128.57, 124.33, 124.29, 124.13, 124.07, 65.66, 65.46, 57.71, 54.11, 53.57, 53.10, 50.21, 49.74, 28.41, 28.39, 28.22, 26.89, 26.69, 26.51, 26.47, 22.79, 22.72, 22.69, 22.54, 17.94, 17.26.

Anal calcd for $C_{37}H_{54}N_2NiO_4$: C (68.42 %), N (4.31 %), H (8.38 %); found: C (68.64 %), N (4.32 %), H (8.39 %).

**Reaction Progression Analysis for Amination Cross-Couplings**

General protocol: General protocol: In the glovebox, a 1-dram vial was charged with respective catalyst (5.0 x 10-3 mmol), NaOtBu (0.12 mmol) and 0.5 mL THF. Then amine (0.15 mmol), α, α, α-trifluorotoluene (3.0 x 10-2 mmol), 4-fluorochloroarene (0.10 mmol) were added sequentially. The reaction mixture was then transferred to an NMR tube and the reaction was placed in an oil bath at 60 °C. At each time point the sample was removed from the oil bath and placed in an ice water solution for 2 minutes. Since the reaction does not proceed or is very slow at room temperature, a $^{19}F$ NMR spectrum could be obtained for each time point at room temperature then placed back in the 60 °C oil bath until the next time point needed to be taken. For each spectrum a 5 second relaxation delay was used which was sufficient relaxation for 4-fluorochlorobenzene, α, α, α-trifluorotoluene, and amination product.

**Sample spectra for** Figure 3-23 **and** Figure 3-24**:**

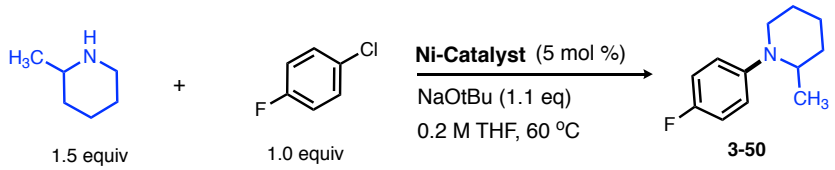


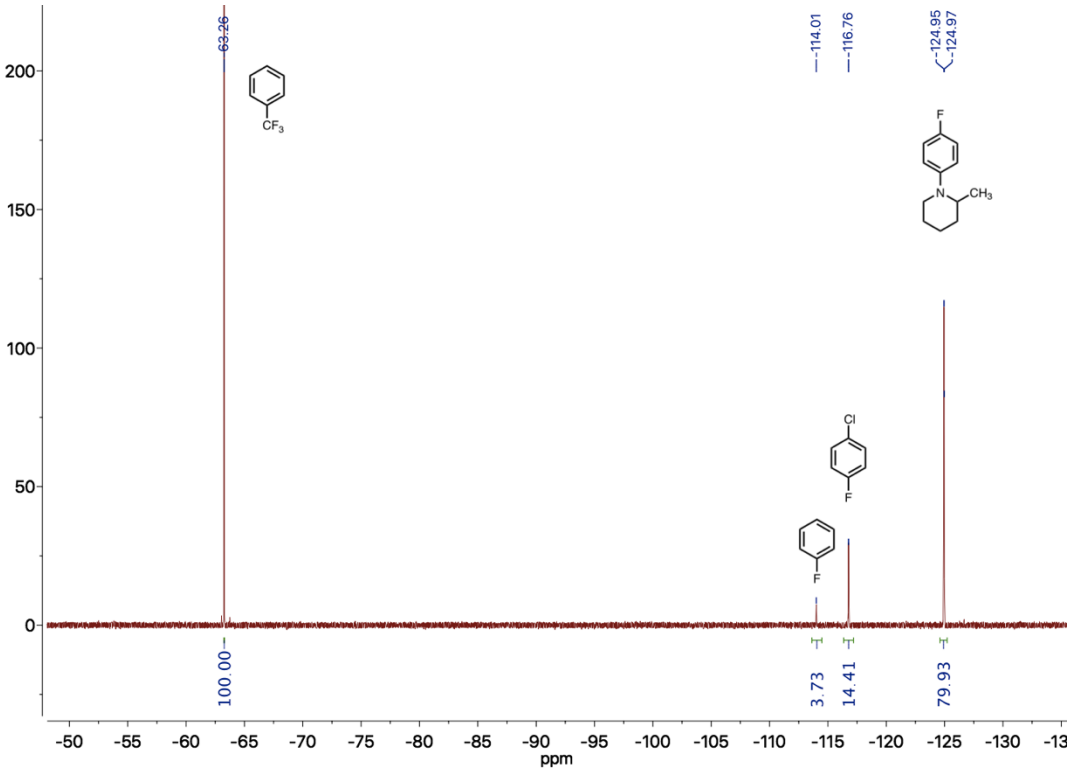


**Figure 5-22.** $^{19}$F NMR spectra for 6 hour time point using Ni(IPr*OMe)(PhA)$_2$ as a pre-catalyst.

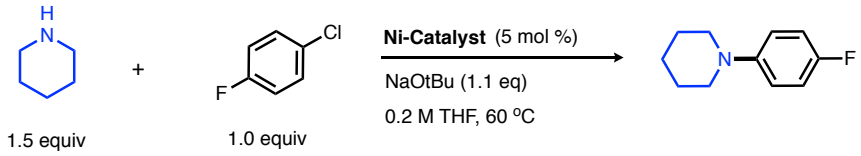


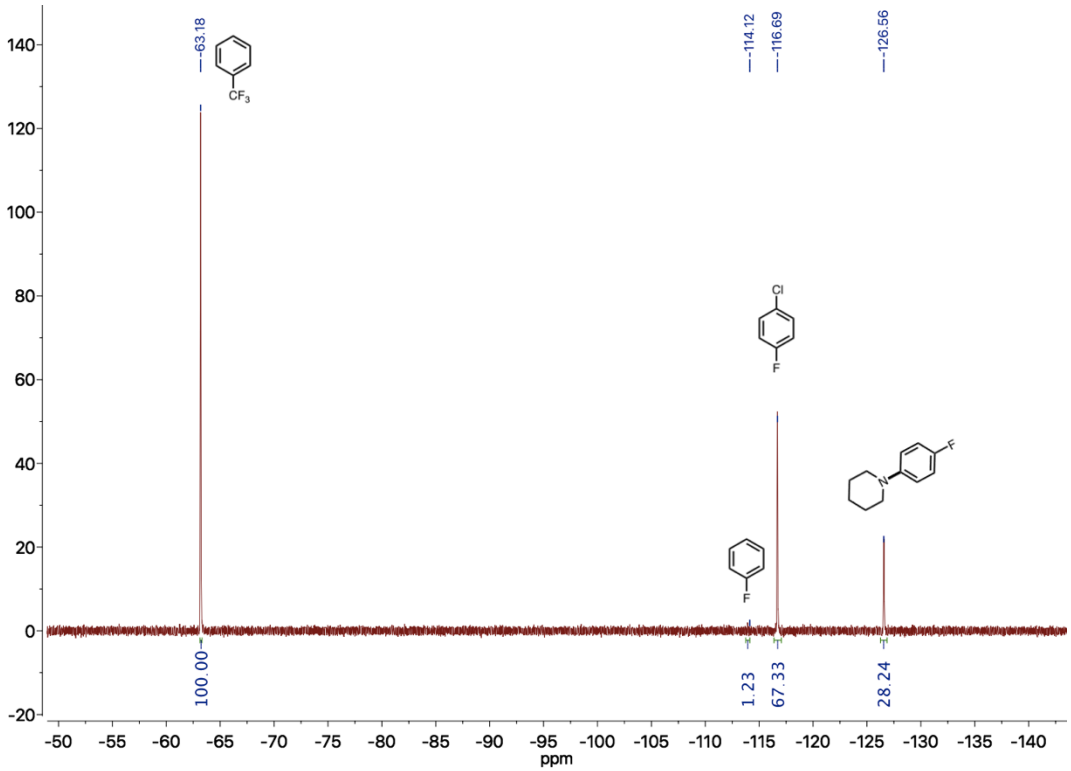


**Figure 5-23.** $^{19}F$ NMR spectra for 60 minute time point of reaction above using $Ni(IPr)(PhA)_2$ as a pre-catalyst.

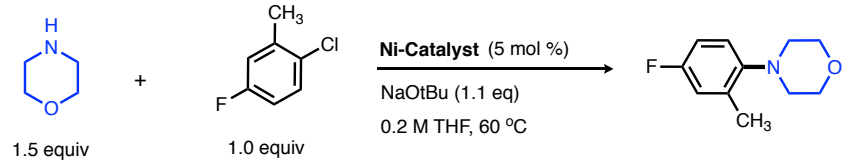


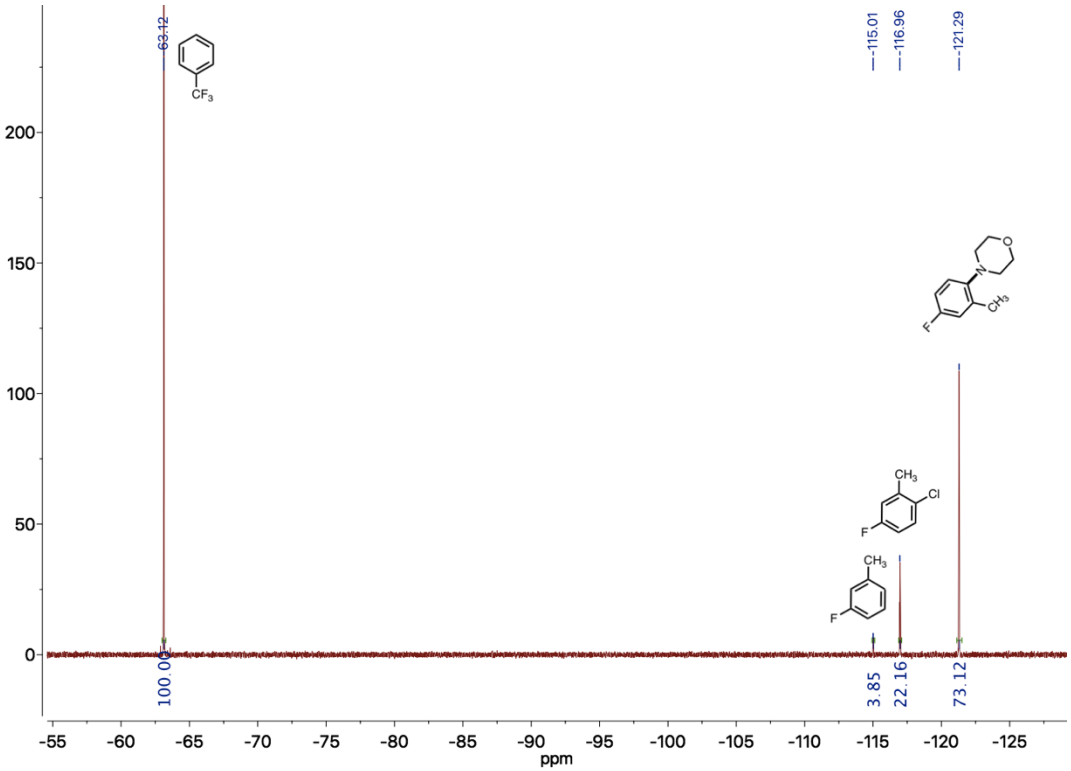


**Figure 5-24.** $^{19}F$ NMR spectra for 8 hour time point of reaction above using Ni(IPr*OMe)$(PhA)_2$ as a pre-catalyst.

**General Procedure for Amination Cross-Coupling**

In the glovebox, a 1-dram vial was charged with respective catalyst (1.0 mol %), NaO$^t$Bu (1.1 equiv) and THF (0.20 M). Then amine (0.15 mmol) and arylchloride (1.0 equiv) were added sequentially. The reaction vial was sealed and placed in an aluminum heating block at 60 °C for 18 hours. The reaction was then quenched upon exposure to air, passed through a plug of silica and rinsed with 10 % methanol in dicholoromethane. **16b-h** were purified by column chromatography with hexanes and ethyl acetate as indicated for each compound.

**Characterization of N-Arylated Products**

**3-(2-methylpiperidin-1-yl)pyridine (3-53)**

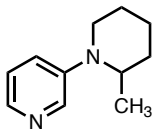


Following the general procedure for amination: Ni(IPr*OMe)(phenyl acrylate)$_2$ (**3-43**) (2.5 mg, 0.002 mmol), 3-chloropyridine (23 μL, 0.2 mmol), 2-methylpiperidine (27 μL, 0.3 mmol), and sodium tert-butoxide (21 mg, 0.22 mmol) produced 34 mg (0.19 mmol, 94 % yield) of **3-53** as a single regioisomer. Product was purified by silica column chromatography using ethyl acetate/hexane.

**$^1$H NMR (500 MHz, $CDCl_3$)** δ 8.30 (s, 1H), 8.05 (d, *J* = 4.4 Hz, 1H), 7.23 – 7.11 (m, 2H), 4.04 – 3.95 (m, 1H), 3.29 (dt, *J* = 11.7, 4.1 Hz, 1H), 3.02 – 2.93 (m, 1H), 1.93 – 1.83 (m, 1H), 1.83 – 1.75 (m, 1H), 1.76 – 1.57 (m, 4H), 1.04 (d, *J* = 6.6 Hz, 3H).

**$^{13}$C NMR (176 MHz, $CDCl_3$)** δ 146.90, 139.78, 139.56, 123.48, 123.25, 77.20, 50.68, 43.71, 31.31, 25.82, 19.17, 13.54.

**HRMS (ESI+)** $[M+H]^+$ m/z Calcd for $C_{11}H_{17}N_2$: 177.139173. Found: 177.1401

***N*-(*tert*-butyl)quinolin-6-amine (3-54)**

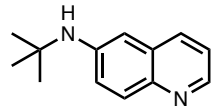

Following the general procedure for amination: Ni(IPr*OMe)(phenyl acrylate)$_2$ (**3-43**) (2.5 mg, 0.002 mmol), 6-chloroquinoline (33 mg, 0.2 mmol), tert-butylamine (32 μL, 0.3 mmol), and sodium tert-butoxide (21 mg, 0.22 mmol) produced 37 mg (0.19 mmol, 93 % yield) of **3-54** as a single regioisomer. Product was purified by silica column chromatography using ethyl acetate/hexane.

**$^1$H NMR (700 MHz, $CDCl_3$)** δ 8.60 (d, *J* = 4.3 Hz, 1H), 7.91 (d, *J* = 8.2 Hz, 1H), 7.84 (d, *J* = 8.9 Hz, 1H), 7.25 – 7.21 (m, 1H), 7.07 (d, *J* = 9.1 Hz, 1H), 6.90 (s, 1H), 3.90 (s, 2H), 1.44 (s, 7H).

**$^{13}$C NMR (176 MHz, $CDCl_3$)** δ 146.20, 144.67, 142.91, 133.94, 129.96, 129.79, 123.93, 121.25, 106.63, 51.44, 29.66.

**HRMS (ESI+)** $[M+H]^+$ m/z Calcd for $C_{13}H_{17}N_2$: 201.1386. Found: 201.1387.

**2,4,6-trimethyl-*N*-(*o*-tolyl)aniline (3-55)**

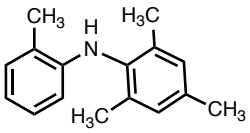

Following the general procedure for amination: Ni(IPr*OMe)(phenyl acrylate)$_2$ (**3-43**) (2.5 mg, 0.002 mmol), 2-chlorotoluene (23 μL, 0.2 mmol), 2,4,6-trimethylaniline (42 μL, 0.3 mmol), and sodium tert-butoxide (21 mg, 0.22 mmol) produced 38 mg (0.17 mmol, 84 % yield) of **3-56** as a

single regioisomer. Product was purified by silica column chromatography using ethyl acetate/hexane.

**$^{1}$H NMR (700 MHz, $CDCl_3$)** δ 7.12 (d, *J* = 7.4 Hz, 1H), 6.99 – 6.90 (m, 3H), 6.68 (t, *J* = 7.3 Hz, 1H), 6.13 (d, *J* = 8.0 Hz, 1H), 4.86 (s, 1H), 2.32 (s, 3H), 2.31 (s, 3H), 2.14 (s, 6H), .

**$^{13}$C NMR (176 MHz, $CDCl_3$)** δ 144.45, 135.95, 135.56, 135.13, 130.15, 129.17, 126.89, 122.08, 117.70, 111.39, 76.81, 20.89, 18.08, 17.59.

Reported in: Hill, L. K.; Crowell, J. L.; Tutwiler, S. T.; Massie, N. L.; Hines, C. C.; Griffin, S. T.; Rogers, R. D.; Shaughnessy, K. H. *J. Org. Chem.*, **2010**, *75*, 6477–6488.

**2-methyl-*N*-phenylaniline (3-56)**

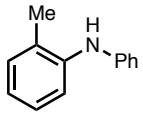


Following the general procedure for amination: Ni(IPr*OMe)(phenyl acrylate)$_2$ (**3-43**) (2.5 mg, 0.002 mmol), 2-chlorotoluene (23 μL, 0.2 mmol), aniline (27 μL, 0.3 mmol), and sodium tert-butoxide (21 mg, 0.22 mmol) produced 33 mg (0.18 mmol, 89 % yield) of **3-56** as a single regioisomer. Product was purified by silica column chromatography using ethyl acetate/hexane.

**$^{1}$H NMR (500 MHz, $CDCl_3$)** δ 7.32 – 7.26 (m, 3H), 7.23 (d, *J* = 7.4 Hz, 1H), 7.17 (t, *J* = 7.7 Hz, 1H), 6.99 (d, *J* = 8.6 Hz, 2H), 6.97 – 6.88 (m, 2H), 5.40 (s, 1H), 2.29 (s, 3H).

**$^{13}$C NMR (176 MHz, $CDCl_3$)** δ 143.97, 141.20, 130.94, 129.30, 128.30, 126.75, 121.98, 120.46, 118.79, 117.44, 17.90.

Matches spectra from: Hill, L. K.; Crowell, J. L.; Tutwiler, S. T.; Massie, N. L.; Hines, C. C.; Griffin, S. T.; Rogers, R. D.; Shaughnessy, K. H. *J. Org. Chem.*, **2010**, *75*, 6477–6488.

**3-(1-(3-methoxyphenyl)pyrrolidin-2-yl)pyridine (3-57)**

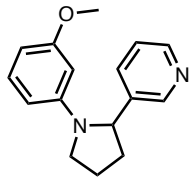

Following the general procedure for amination: Ni(IPr*OMe)(phenyl acrylate)$_2$ (**3-43**) (2.5 mg, 0.002 mmol), 3-chloroanisole (24 μL, 0.2 mmol), 3-(2-pyrrolidinyl)pyridine (44 mg, 0.3 mmol), and sodium tert-butoxide (21 mg, 0.22 mmol) produced 17 mg (0.07 mmol, 33 % yield) of **3-57** as a single regioisomer. Product was purified by silica column chromatography using ethyl acetate/hexane.

**$^1$H NMR (500 MHz, CDCl3)** δ 8.64 – 8.38 (m, 2H), 7.50 (d, *J* = 7.8 Hz, 1H), 7.21 (dd, *J* = 7.9, 4.8 Hz, 1H), 7.07 (t, *J* = 8.2 Hz, 1H), 6.26 (ddd, *J* = 8.2, 2.4, 0.8 Hz, 1H), 6.11 (ddd, *J* = 8.2, 2.4, 0.8 Hz, 1H), 6.05 (t, *J* = 2.4 Hz, 1H), 4.77 (dd, *J* = 8.4, 2.2 Hz, 1H), 3.84 – 3.60 (m, 4H), 3.43 (q, *J* = 8.6 Hz, 1H), 2.54 – 2.34 (m, 1H), 2.12 – 1.84 (m, 3H).

**$^{13}$C NMR (176 MHz, CDCl$_3$)** δ 160.58, 148.21, 148.16, 148.14, 139.79, 133.55, 129.79, 123.40, 105.74, 101.20, 99.00, 60.79, 55.01, 49.19, 35.85, 23.02.

**HRMS (ESI+)** $[M+H]^+$ m/z Calcd for $C_{16}H_{19}N_2O$: 255.1497 Found: 255.1491.

**3-(1-(4-(trifluoromethyl)phenyl)pyrrolidin-2-yl)pyridine (3-58)**

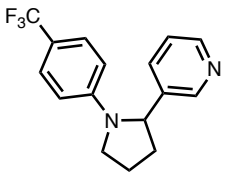

Following the general procedure for amination: Ni(IPr*OMe)(phenyl acrylate)$_2$ (**3-43**) (2.5 mg, 0.002 mmol), 4-chlorobenzotrifluoride (27 μL, 0.2 mmol), 3-(2-pyrrolidinyl)pyridine (44 mg, 0.3

mmol), and sodium tert-butoxide (21 mg, 0.22 mmol) produced 52 mg (0.18 mmol, 91 % yield) of **3-58** as a single regioisomer. Product was purified by silica column chromatography using ethyl acetate/hexane.

**$^1$H NMR (500 MHz, $CDCl_3$)** δ 8.55 – 8.49 (m, 2H), 7.46 (dt, *J* = 7.8, 1.7 Hz, 2H), 7.38 (d, *J* = 8.6 Hz, 2H), 7.24 (dd, *J* = 7.8, 4.8 Hz, 1H), 6.49 (d, *J* = 8.6 Hz, 2H), 4.84 (dd, *J* = 8.3, 2.1 Hz, 1H), 3.81 – 3.71 (m, 1H), 3.49 (td, *J* = 9.0, 7.1 Hz, 1H), 2.63 – 2.39 (m, 1H), 2.17 – 1.89 (m, 3H).

**$^{13}$C NMR (176 MHz, $CDCl_3$)** δ 148.71, 148.56, 148.06, 138.69, 133.40, 126.41, 126.39, 126.36, 123.50, 111.84, 60.66, 49.06, 35.80, 22.91.

**HRMS (ESI+)** $[M+H]^+$ m/z Calcd for $C_{16}H_{16}F_3N_2$: 293.1265. Found: 293.1263.

**1-(4-(phenylamino)phenyl)ethan-1-one (3-59)**

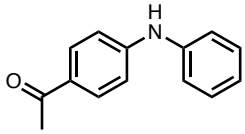


Following the general procedure for amination: Ni(IPr*OMe)(phenyl acrylate)$_2$ (**3-43**) (2.5 mg, 0.002 mmol), 4′-Chloroacetophenone (26 μL, 0.2 mmol), aniline (27 μL, 0.3 mmol), and sodium tert-butoxide (21 mg, 0.22 mmol) produced 38 mg (0.18 mmol, 89 % yield) of **3-59** as a single regioisomer. Product was purified by silica column chromatography using ethyl acetate/hexane.

**$^1$H NMR (500 MHz, $CDCl_3$)** δ 7.89 (d, *J* = 8.8 Hz, 2H), 7.36 (tt, *J* = 8.5, 7.3 Hz, 2H), 7.23 – 7.17 (m, 3H), 7.14 – 7.07 (m, 1H), 7.01 (d, *J* = 8.8 Hz, 2H), 6.10 (s, 1H), 2.55 (s, 3H).

**$^{13}$C NMR (176 MHz, $CDCl_3$)** δ 196.37, 148.29, 140.55, 130.61, 129.53, 129.04, 123.36, 120.67, 114.39, 26.18.

Reported in: Rao, H.; Fu, H.; Jiang, Y.; Zhao, Y. *J. Org. Chem.*, **2005**, *70*, 8107–8109.

## $^{1}H$ and $^{13}C$ NMR Spectra

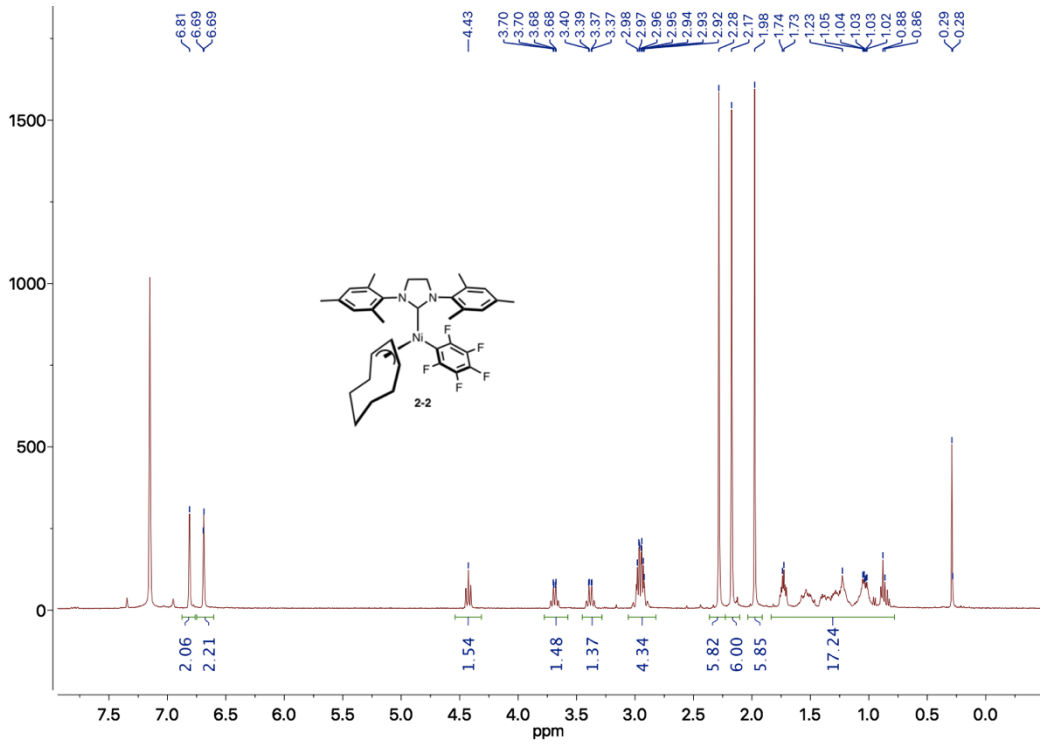


**Figure 5-25.** 2-2 - $^{1}H$ NMR ($C_6D_6$, 500 MHz)

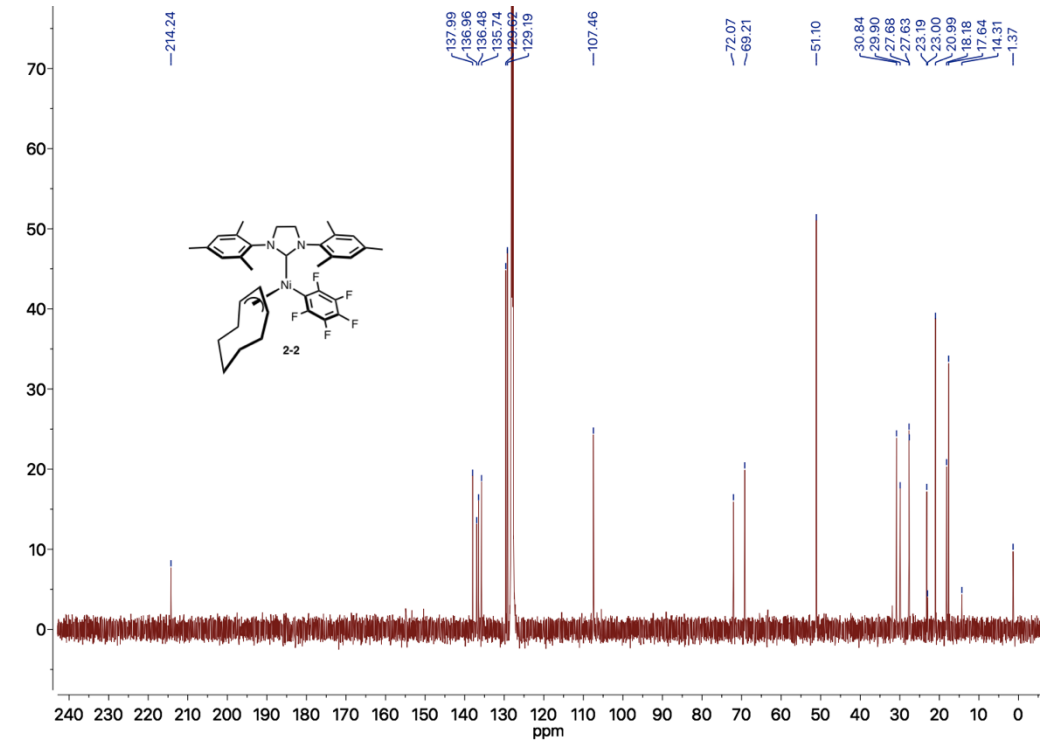


**Figure 5-26.** 2-2 - $^{13}C$ NMR ($C_6D_6$, 125 MHz)

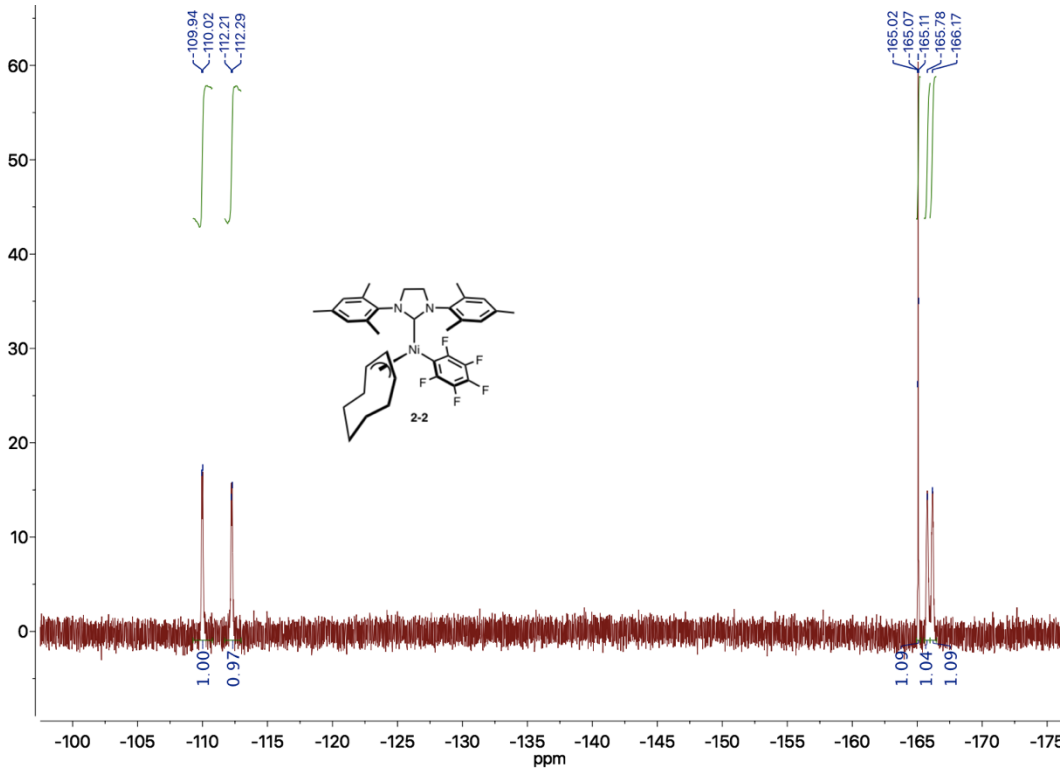


**Figure 5-27.** 2-2 - **$^{19}$F NMR ($C_6D_6$, 470 MHz)**

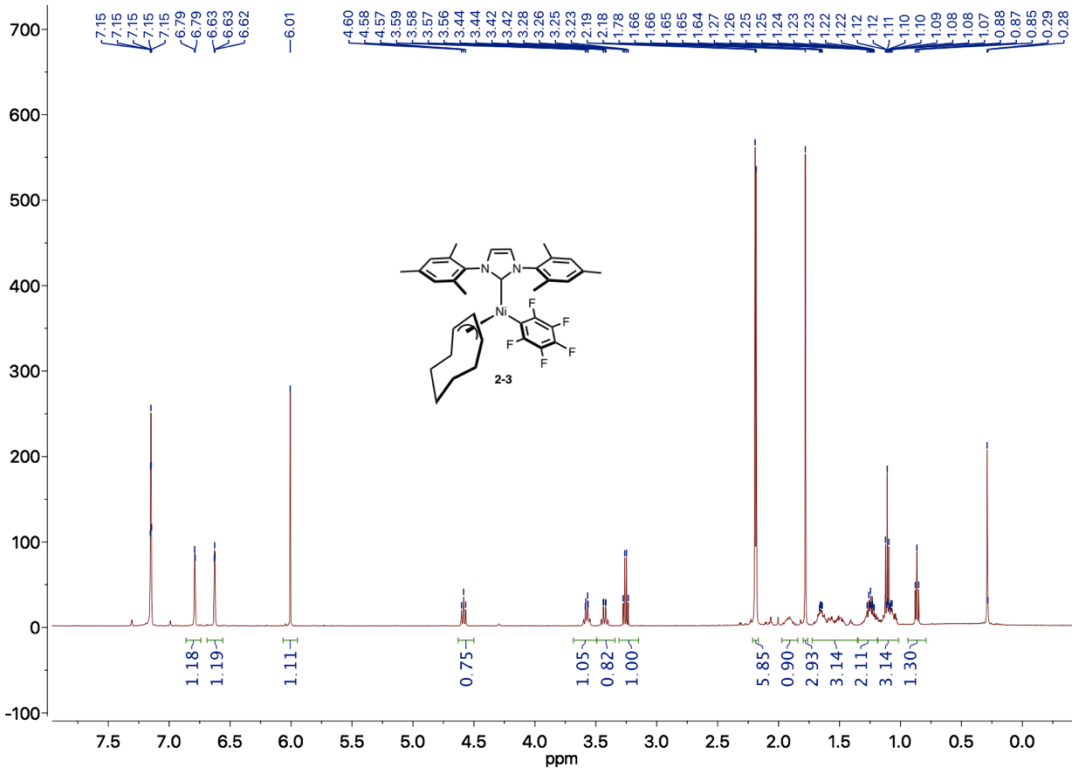


**Figure 5-28.** 2-3 - $^{1}$H NMR ($C_6D_6$, 500 MHz)

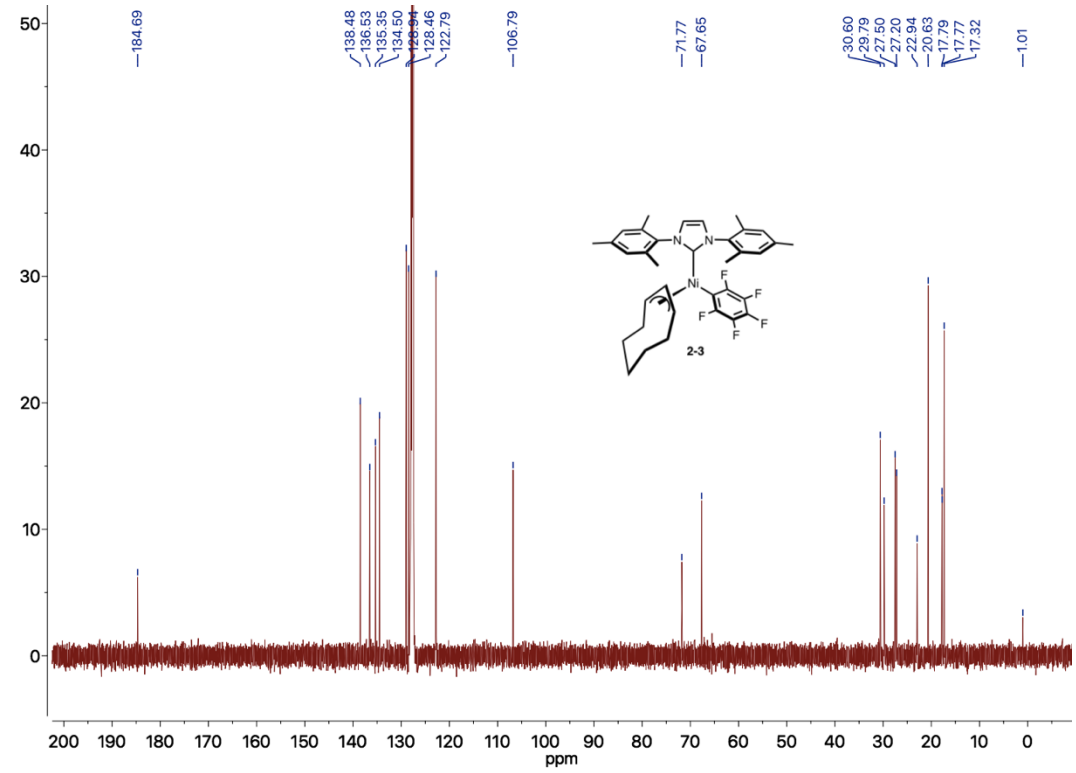


**Figure 5-29.** 2-3 - $^{13}$C NMR ($C_6D_6$, 125 MHz)

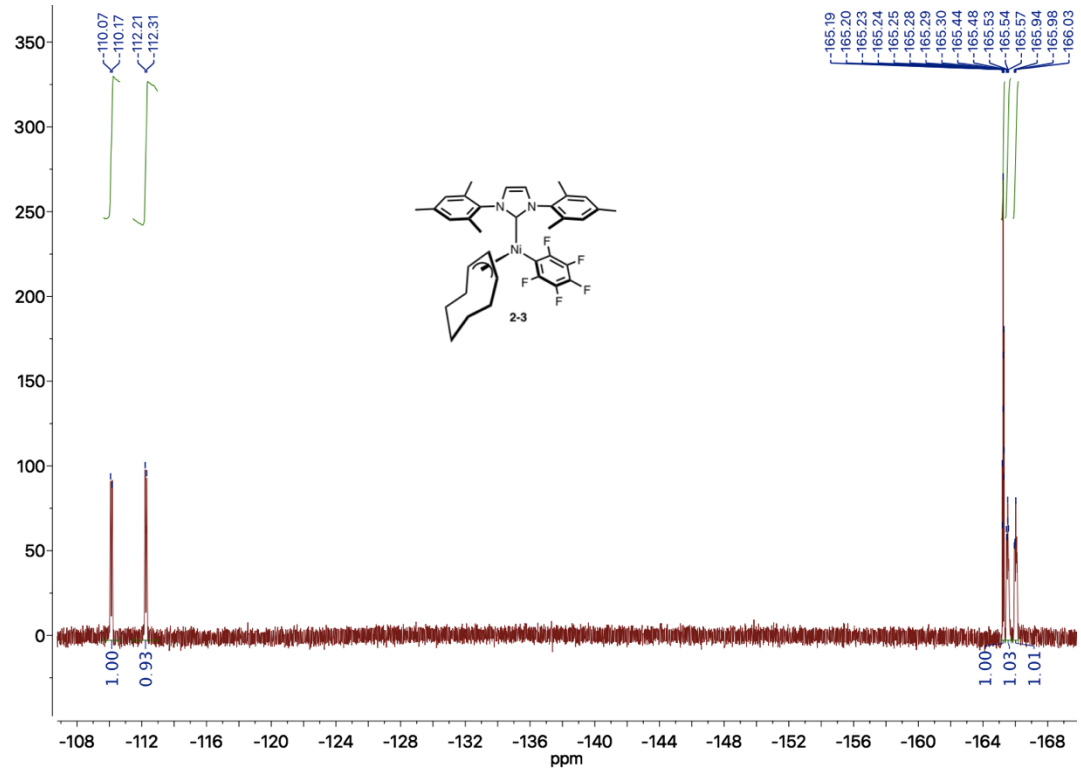


**Figure 5-30.** 2-3 - **$^{19}$F NMR ($C_6D_6$, 470 MHz)**

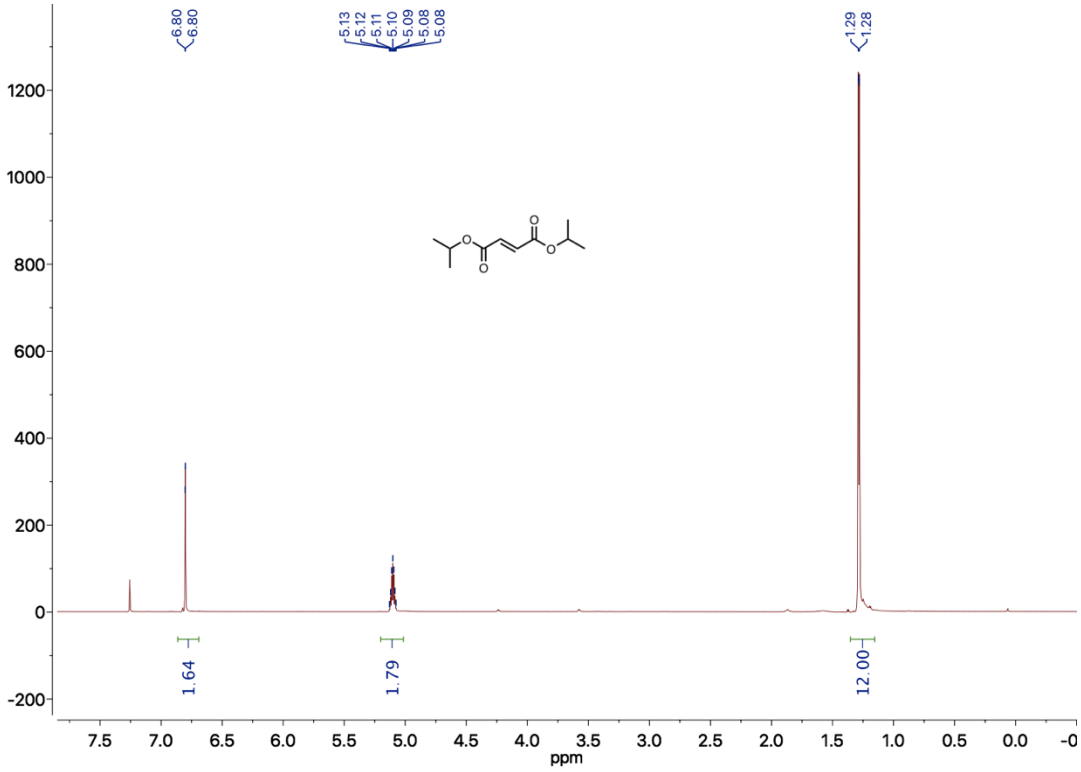


**Figure 5-31.** 3-14 - **$^{1}$H NMR (700 MHz)**

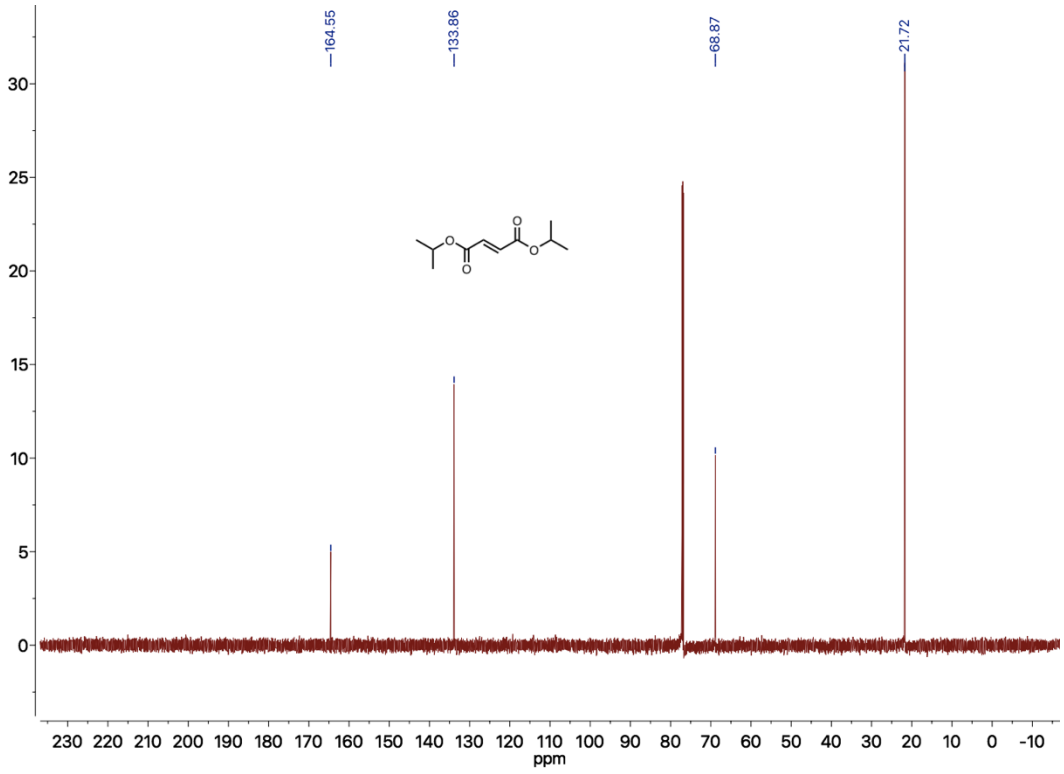


**Figure 5-32.** 3-14 - **$^{13}$C NMR (176 MHz)**

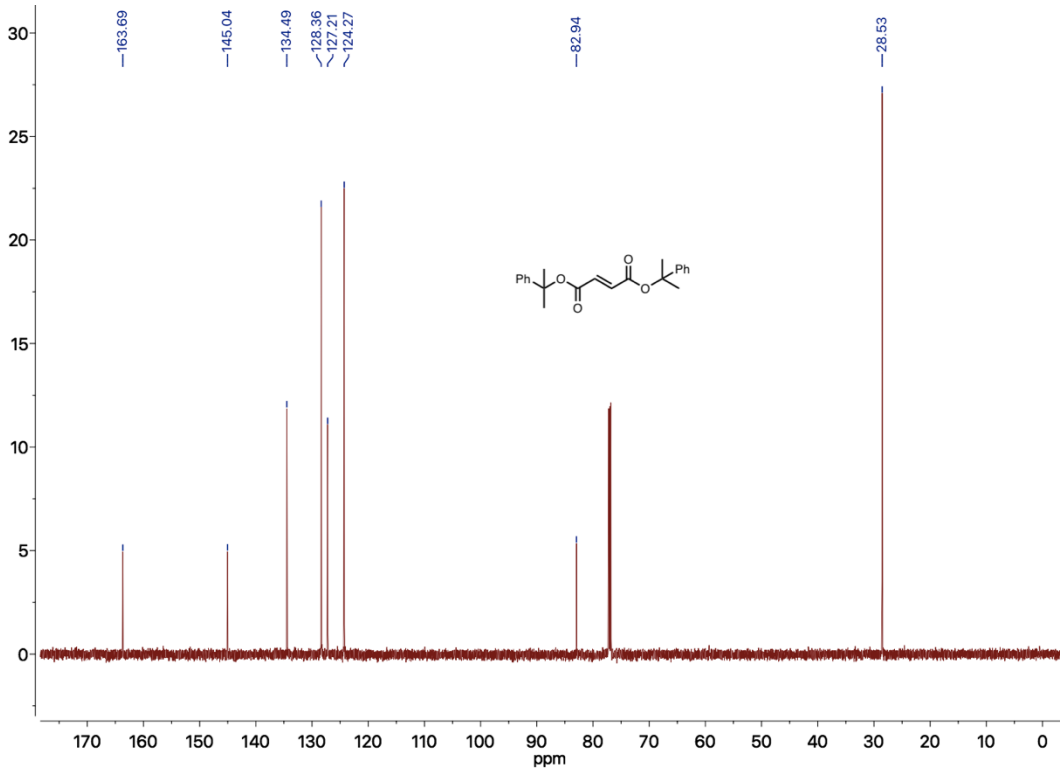


**Figure 5-33.** 3-17 - **$^{1}$H NMR (700 MHz)**

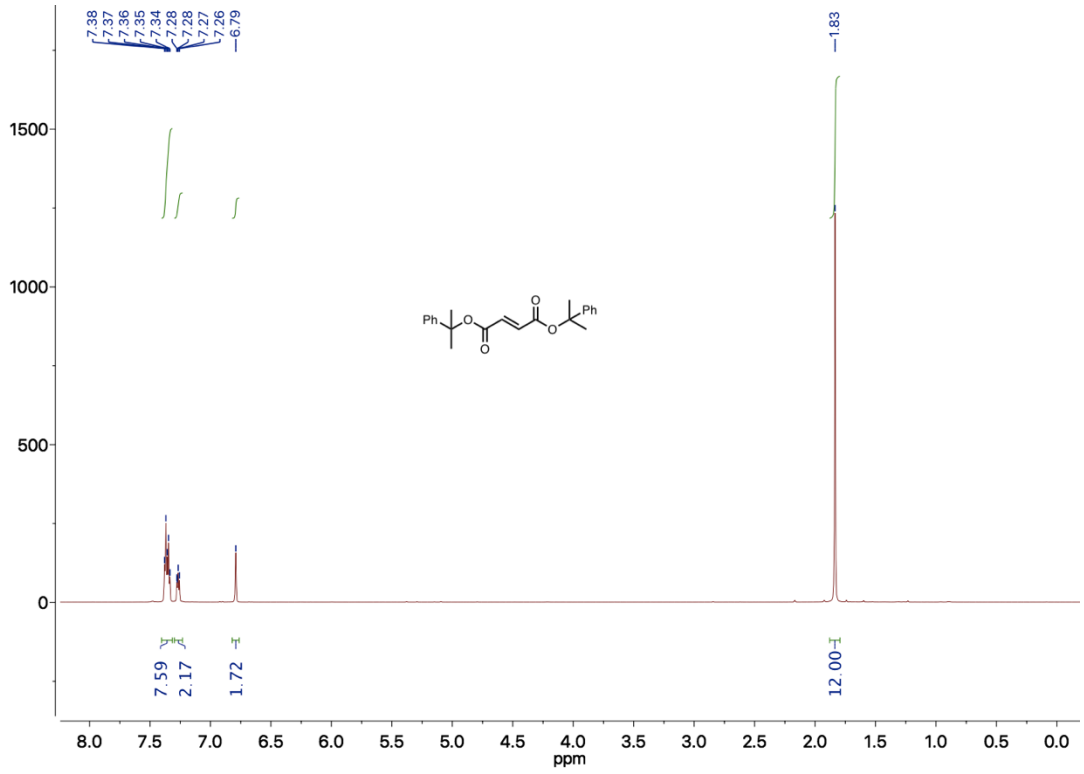


**Figure 5-34.** 3-17 - **$^{13}$C NMR (176 MHz)**

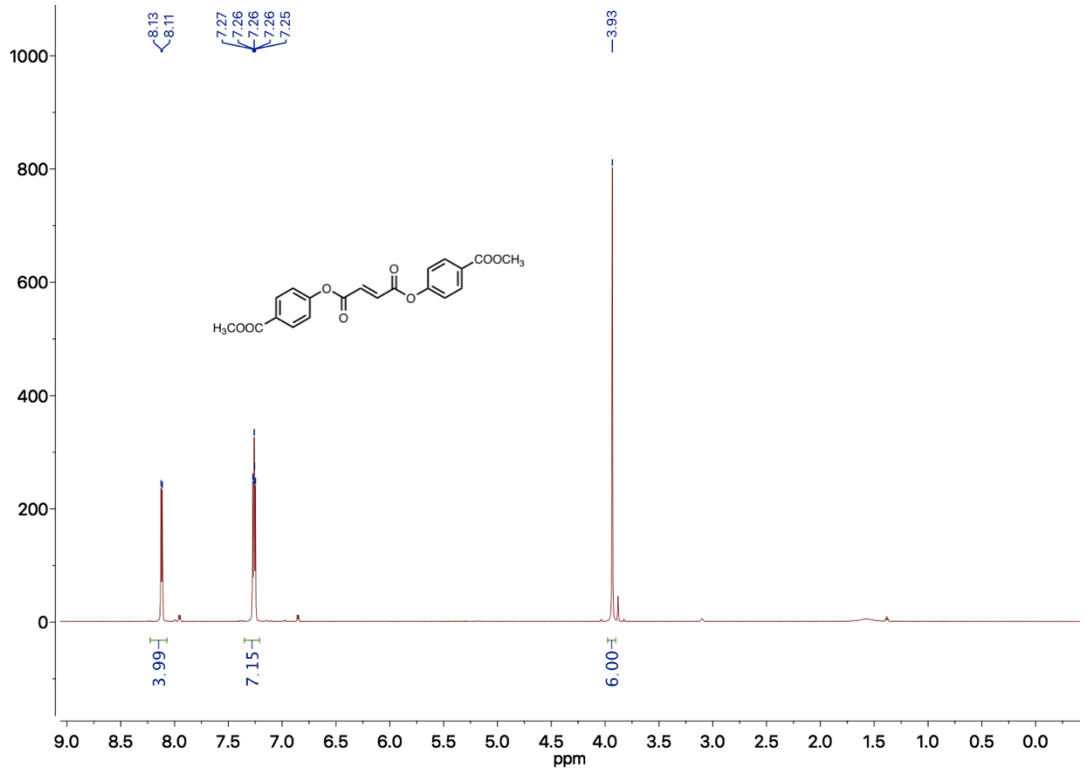


**Figure 5-35.** 3-18 - **$^{1}$H NMR (700 MHz)**

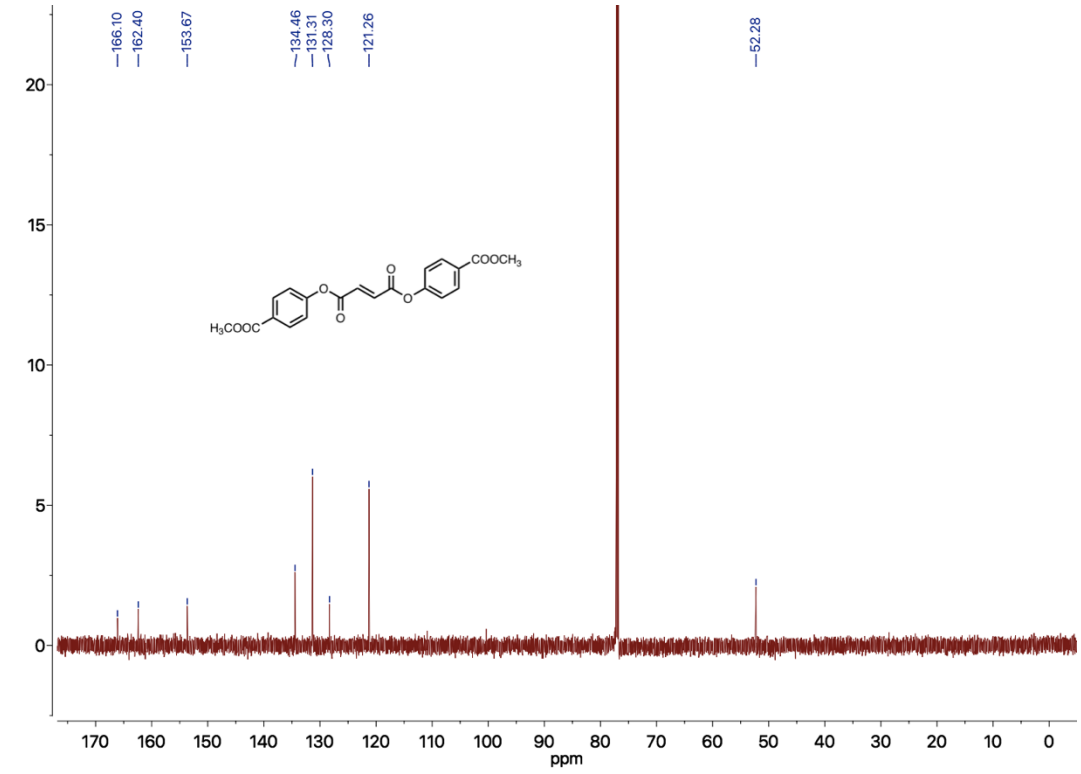


**Figure 5-36.** 3-18 - **$^{13}$C NMR (176 MHz)**

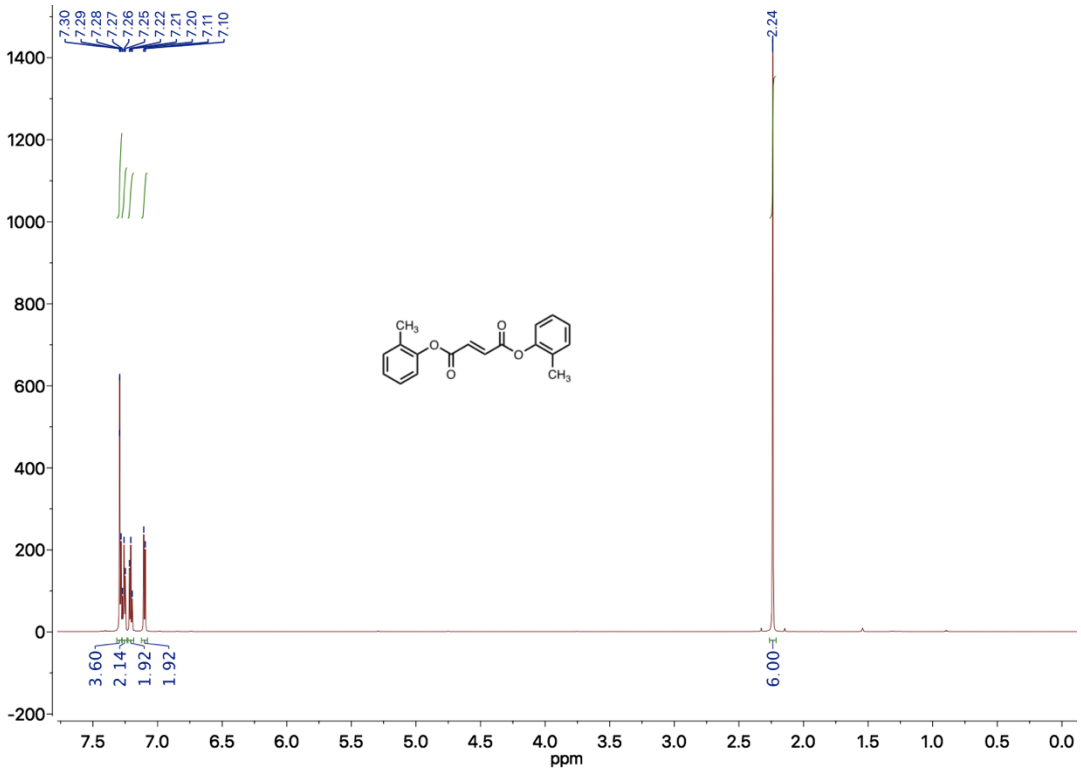


**Figure 5-37.** 3-19 - **$^{1}$H NMR (700 MHz)**

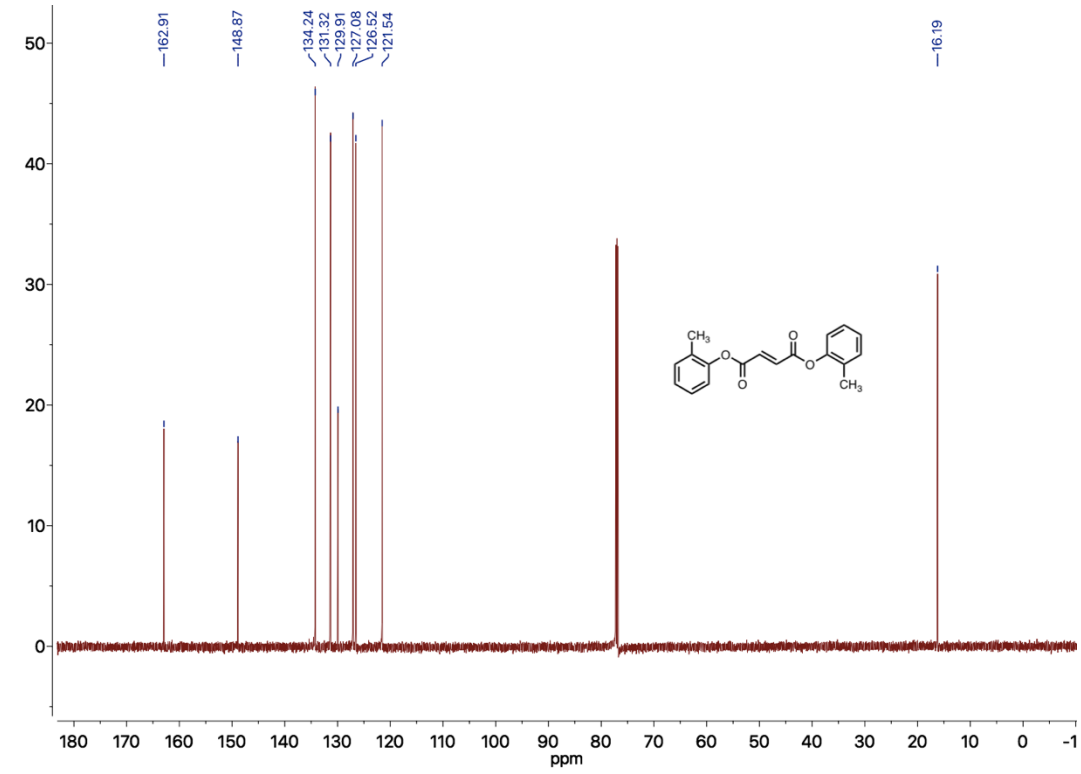


**Figure 5-38.** 3-19 - **$^{13}$C NMR (176 MHz)**

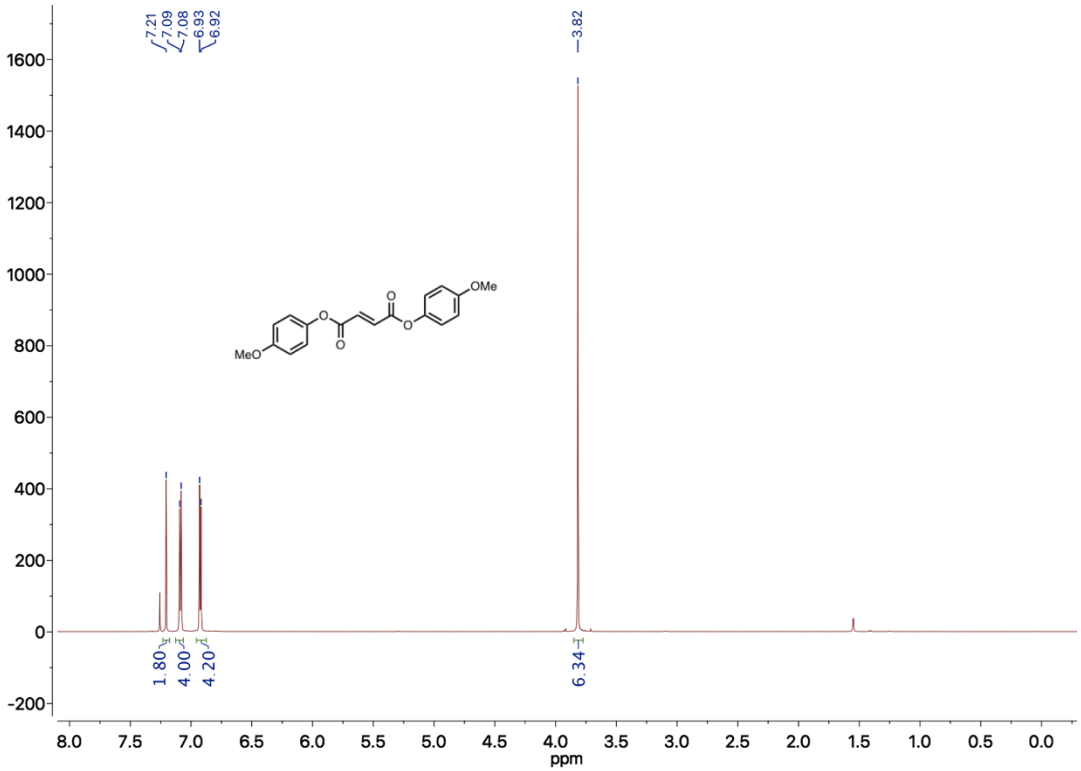


**Figure 5-39.** 3-20 - **$^{1}$H NMR (700 MHz)**

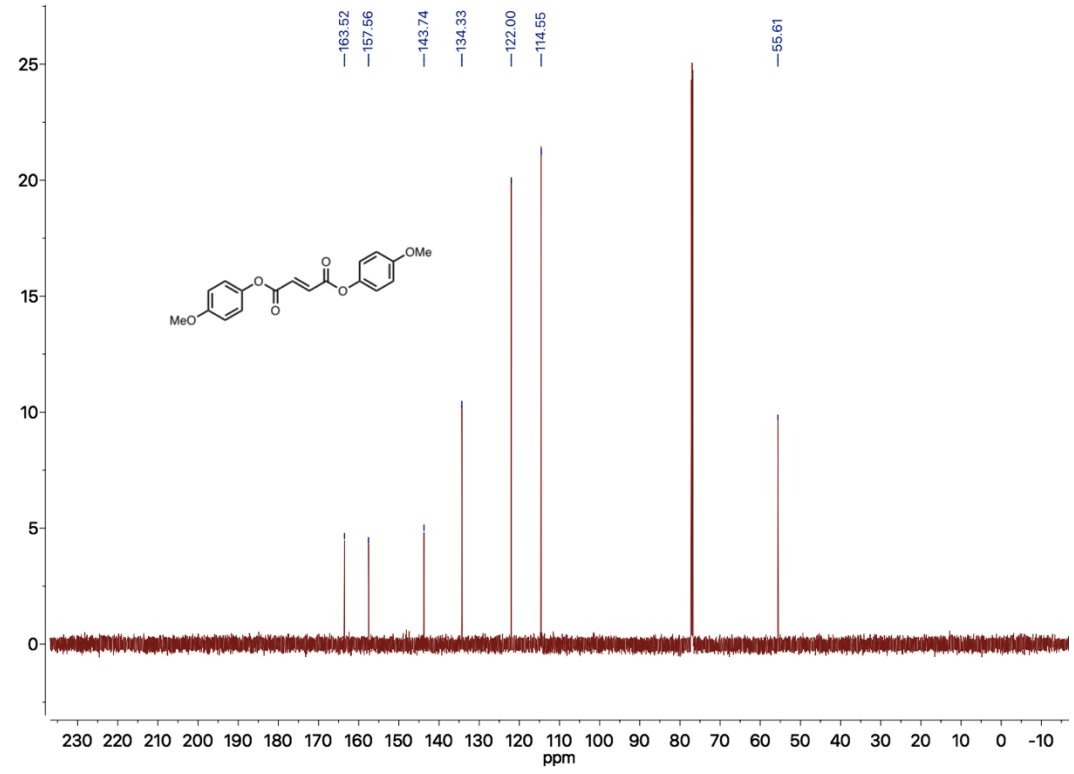


**Figure 5-40.** 3-20 - **$^{13}$C NMR (176 MHz)**

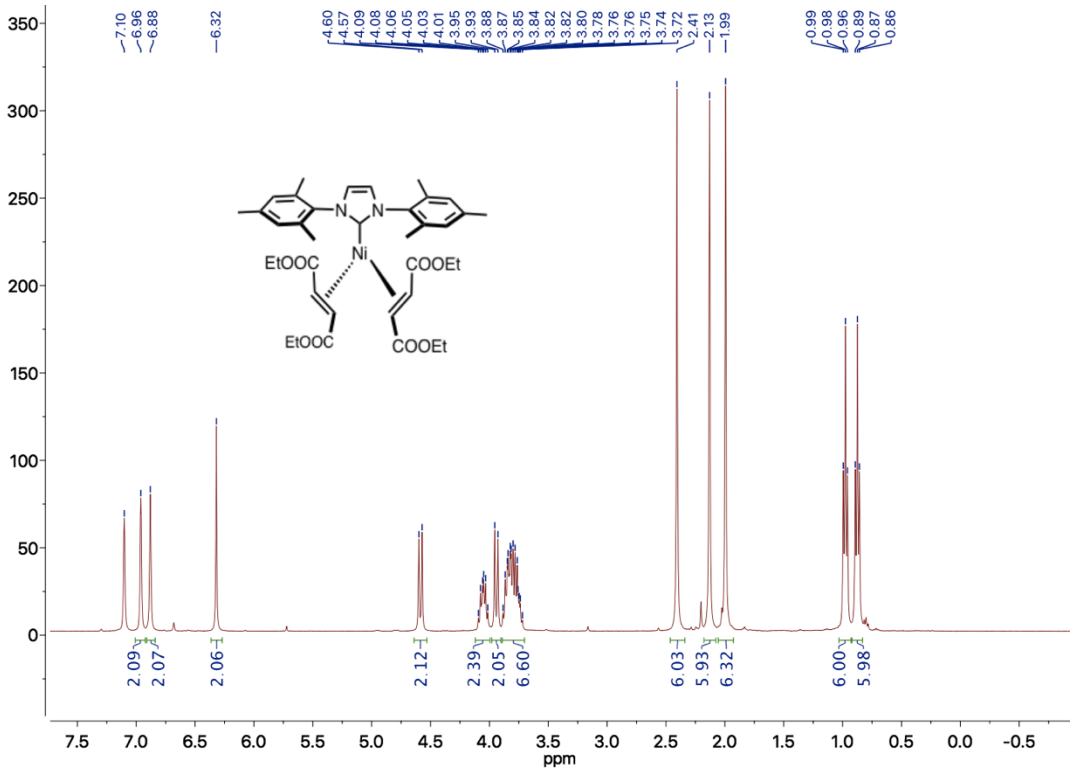


**Figure 5-41.** 3-22 - **$^{1}$H NMR (400 MHz)**

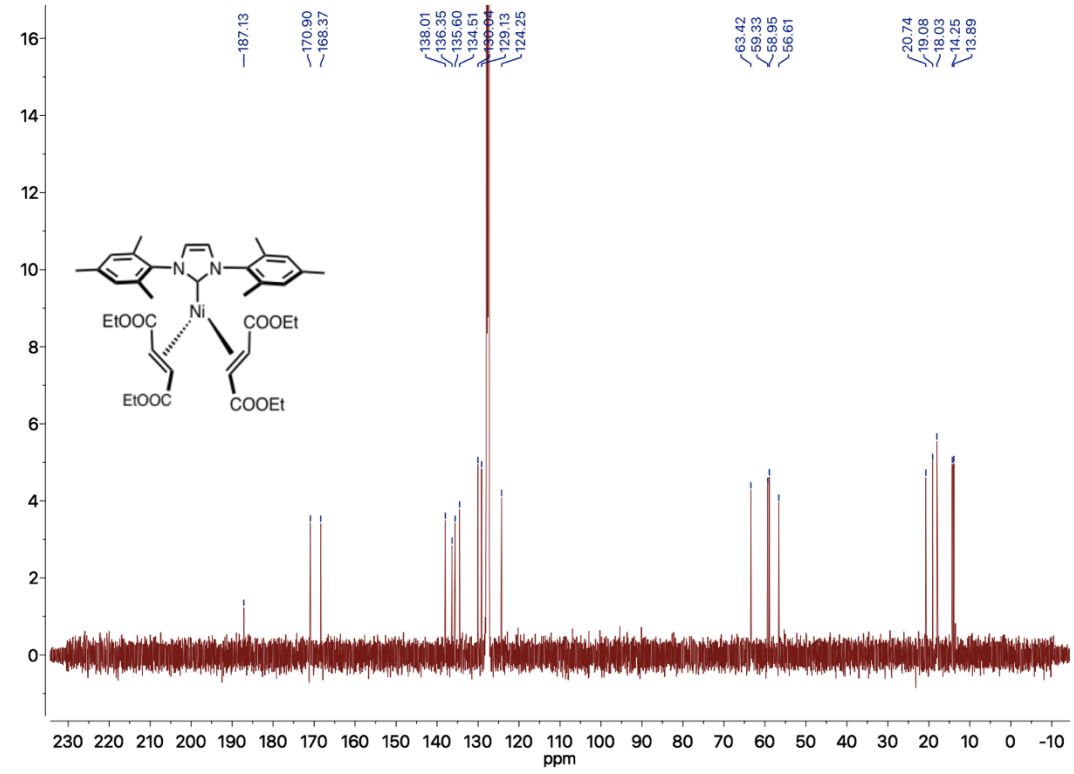


**Figure 5-42.** 3-22 - **$^{13}$C NMR (100 MHz)**

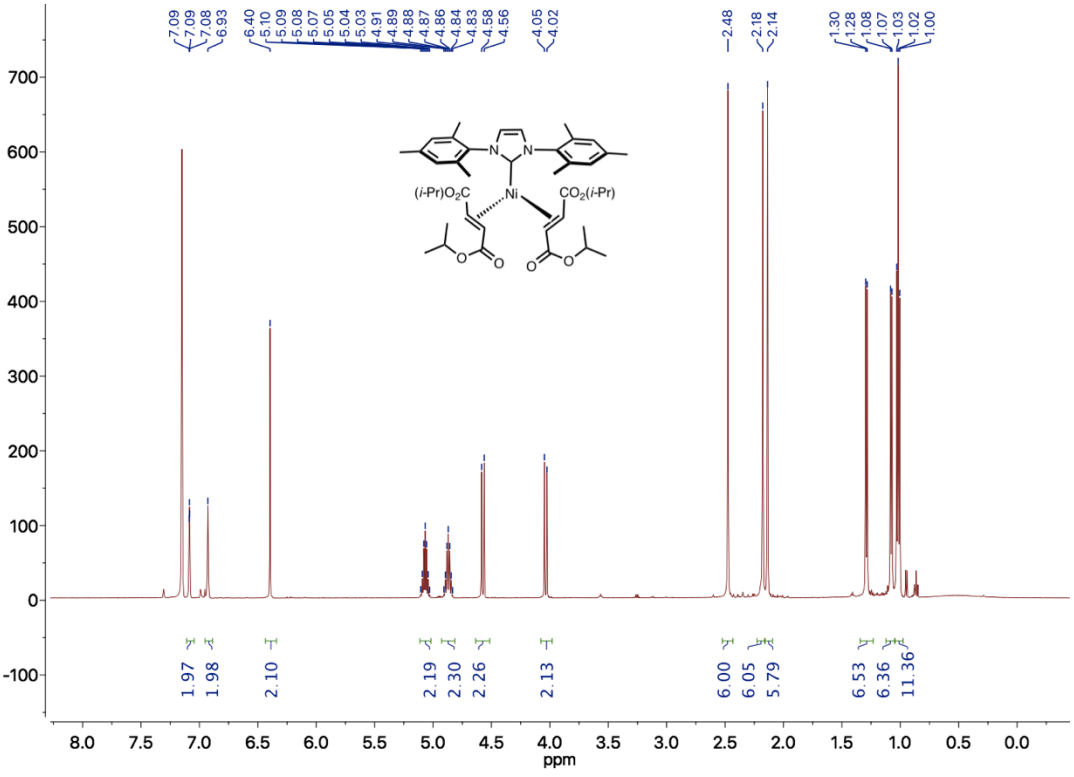


**Figure 5-43.** 3-23 - **$^{1}$H NMR (500 MHz)**

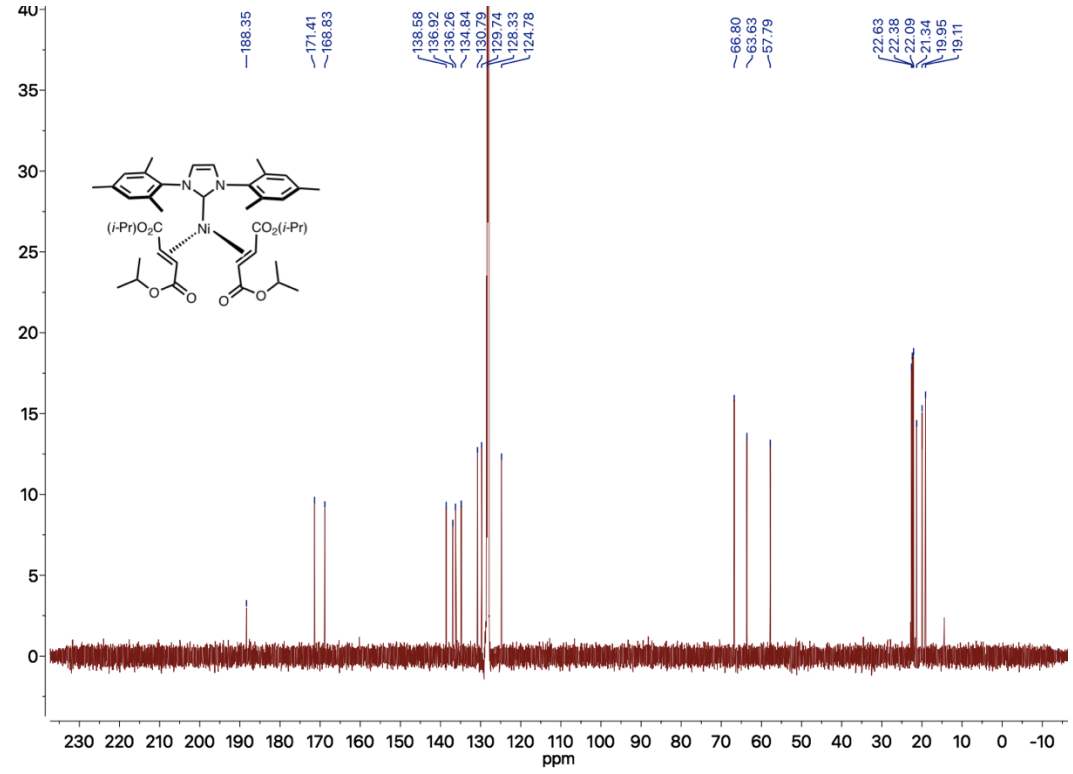


**Figure 5-44.** 3-23 - **$^{13}$C NMR (176 MHz)**

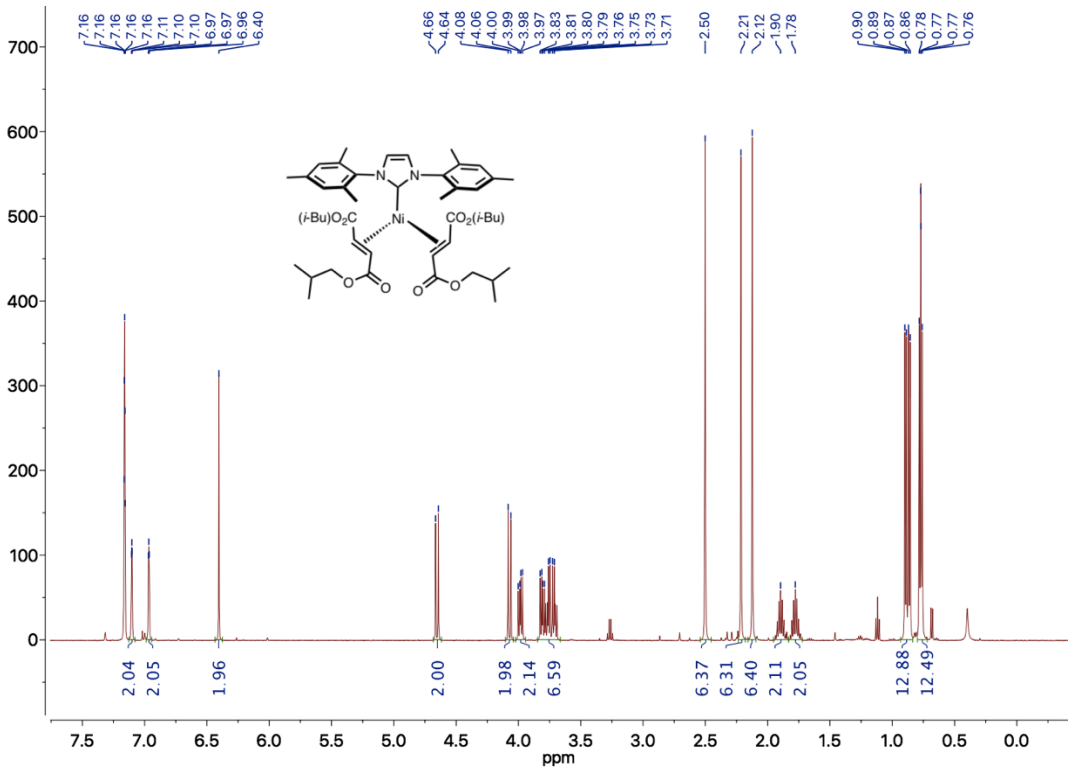


**Figure 5-45.** 3-24 - **$^{1}$H NMR (500 MHz)**

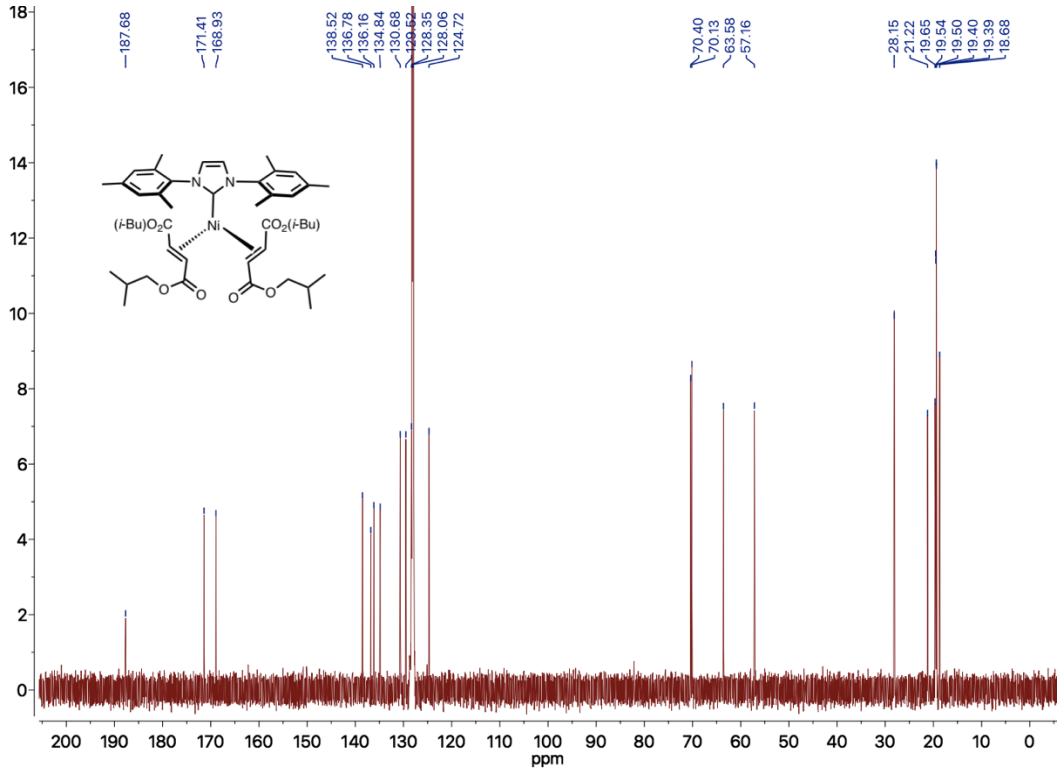


**Figure 5-46.** 3-24 - **$^{13}$C NMR (176 MHz)**

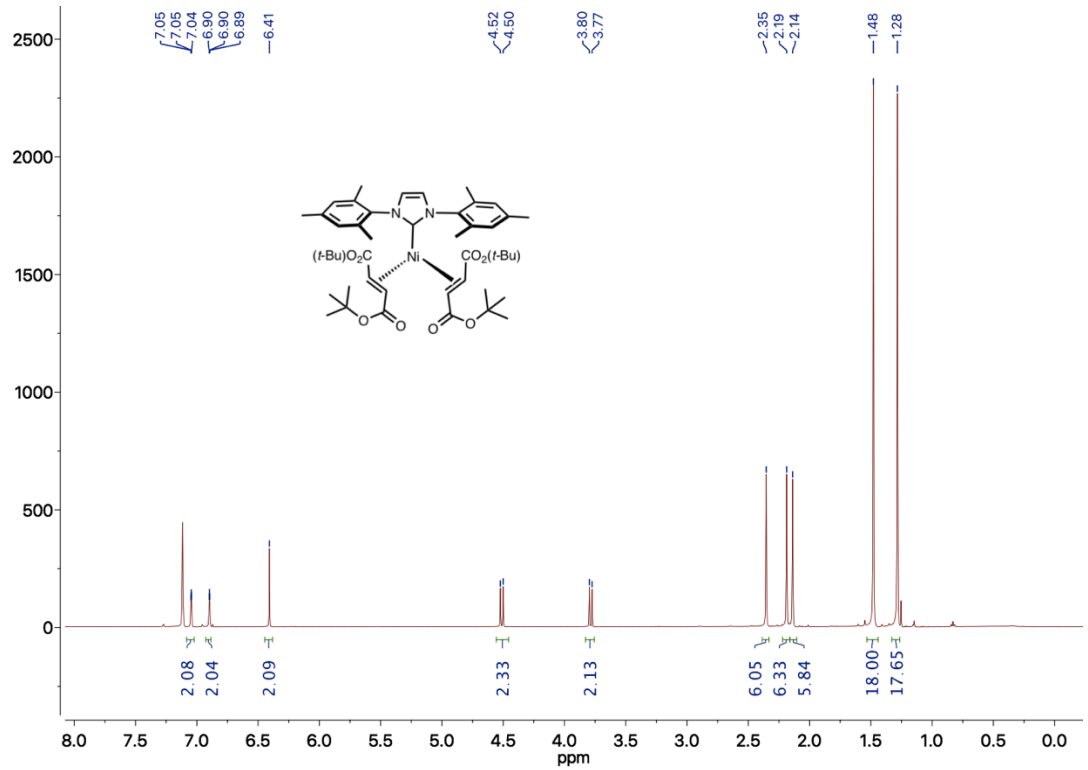


**Figure 5-47.** 3-25 - **$^{1}$H NMR (500 MHz)**

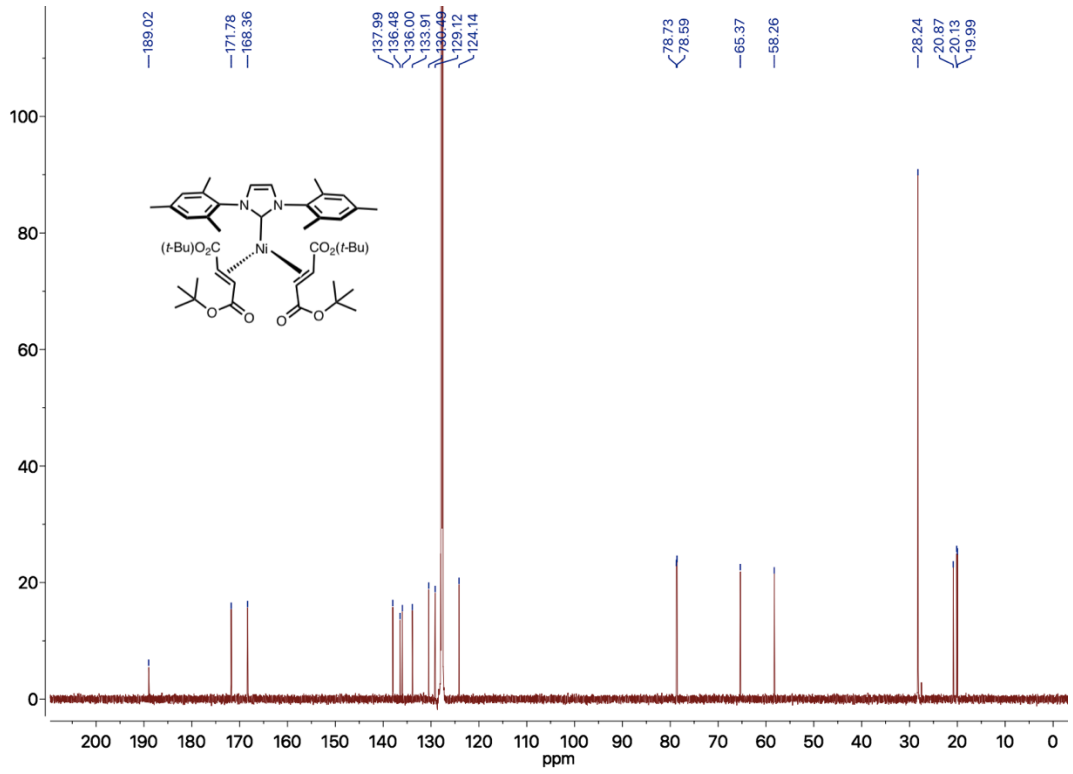


**Figure 5-48.** 3-25 - $^{13}$C NMR (176 MHz)

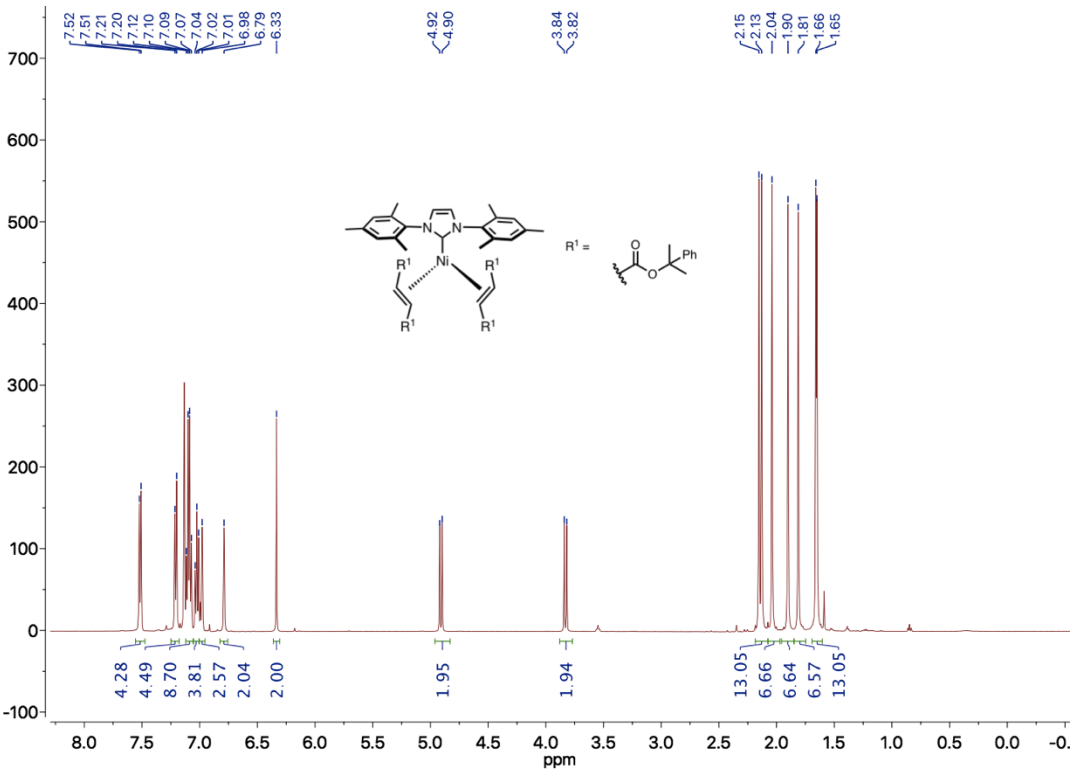


**Figure 5-49.** 3-26 - $^{1}$H NMR (500 MHz)

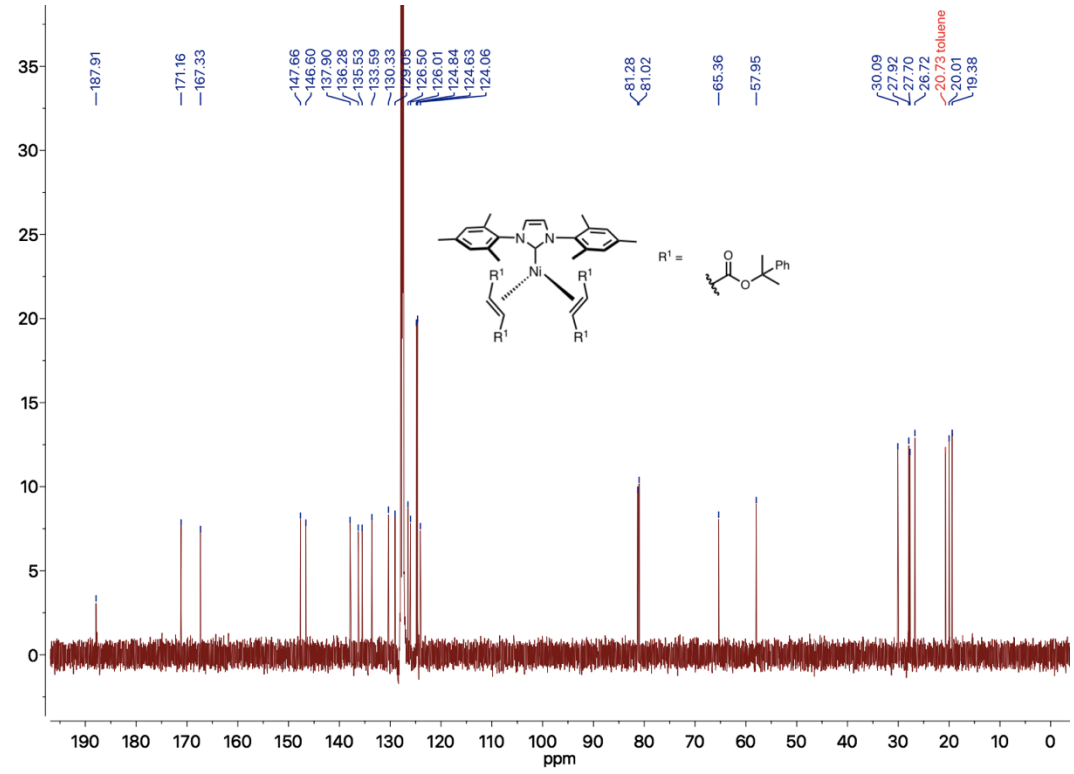


**Figure 5-50.** 3-26 - **$^{13}$C NMR (176 MHz)**

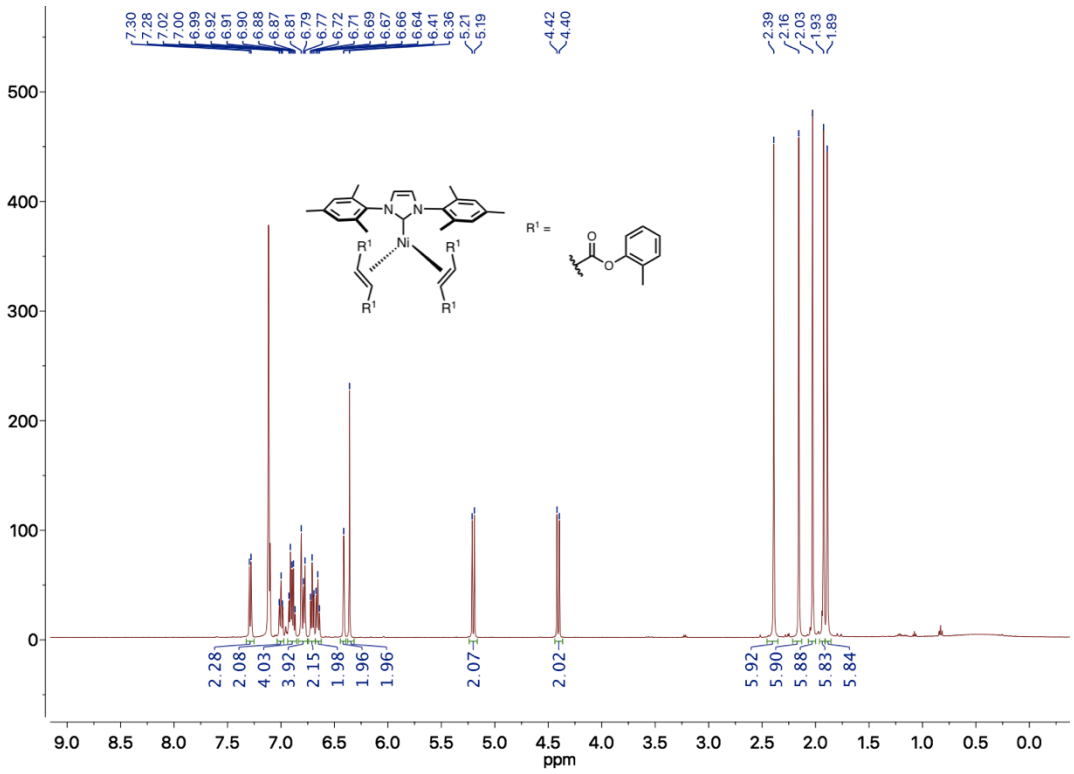


**Figure 5-51**. 3-27 - **$^{1}$H NMR (500 MHz)**

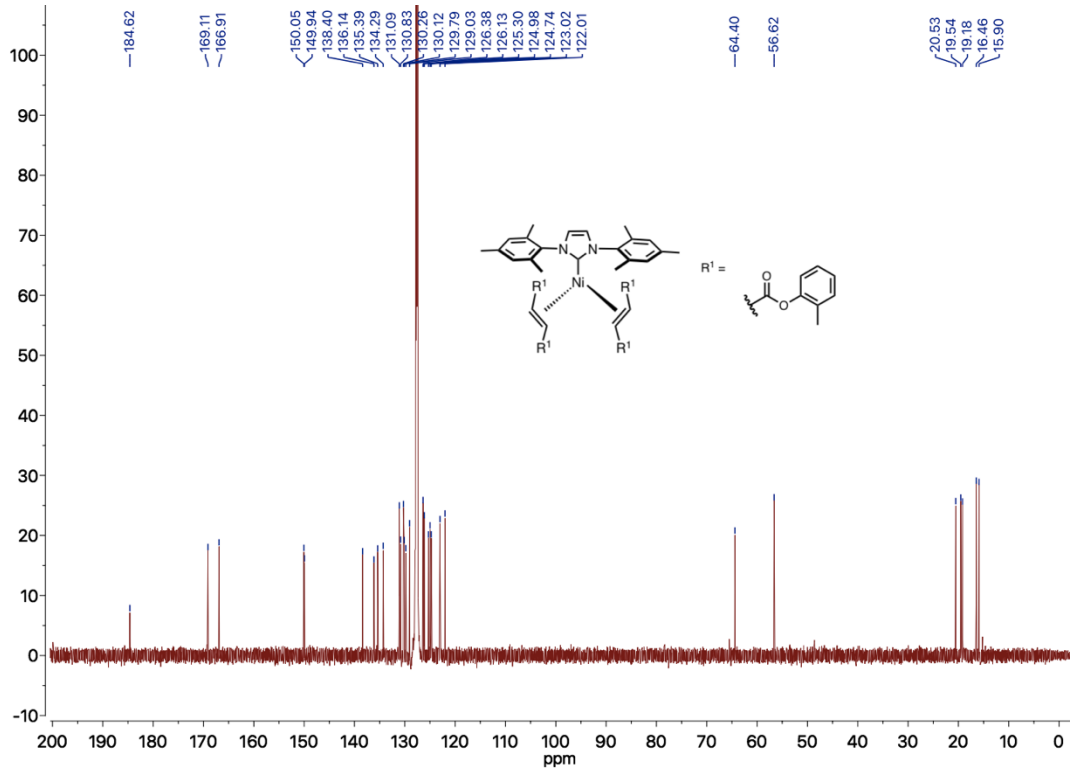


**Figure 5-52.** 3-27 - **$^{13}$C NMR (176 MHz)**

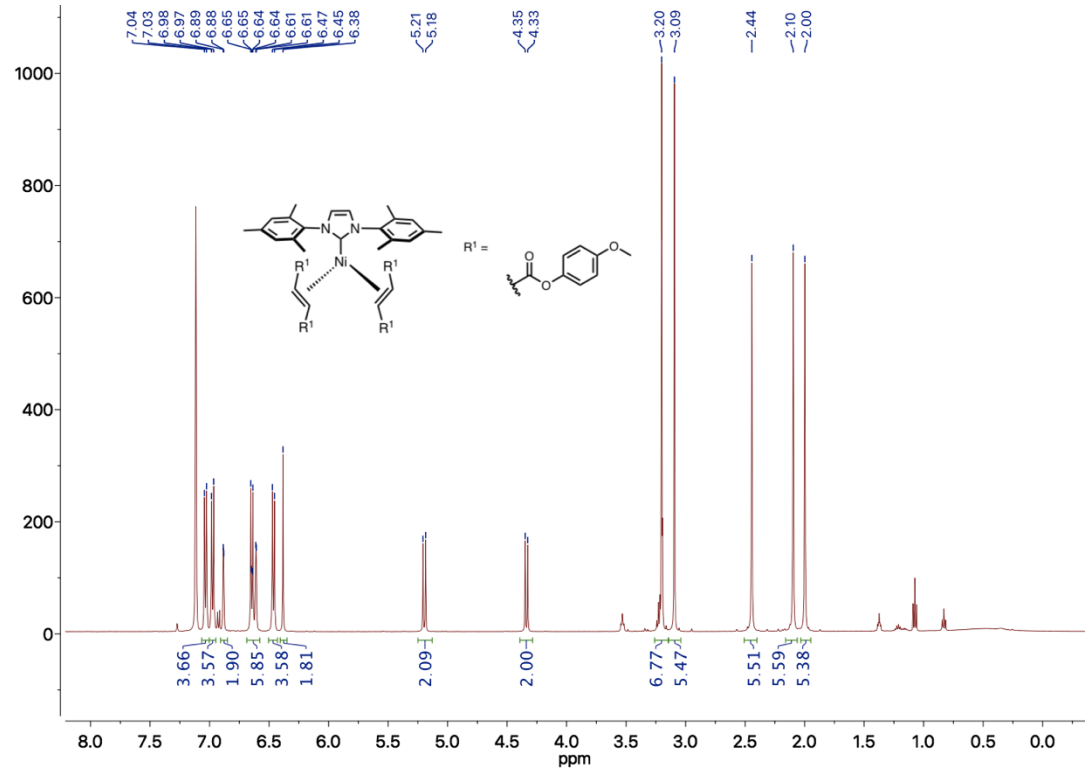


**Figure 5-53.** 3-28 - **$^{1}$H NMR (500 MHz, $C_6D_6$)**

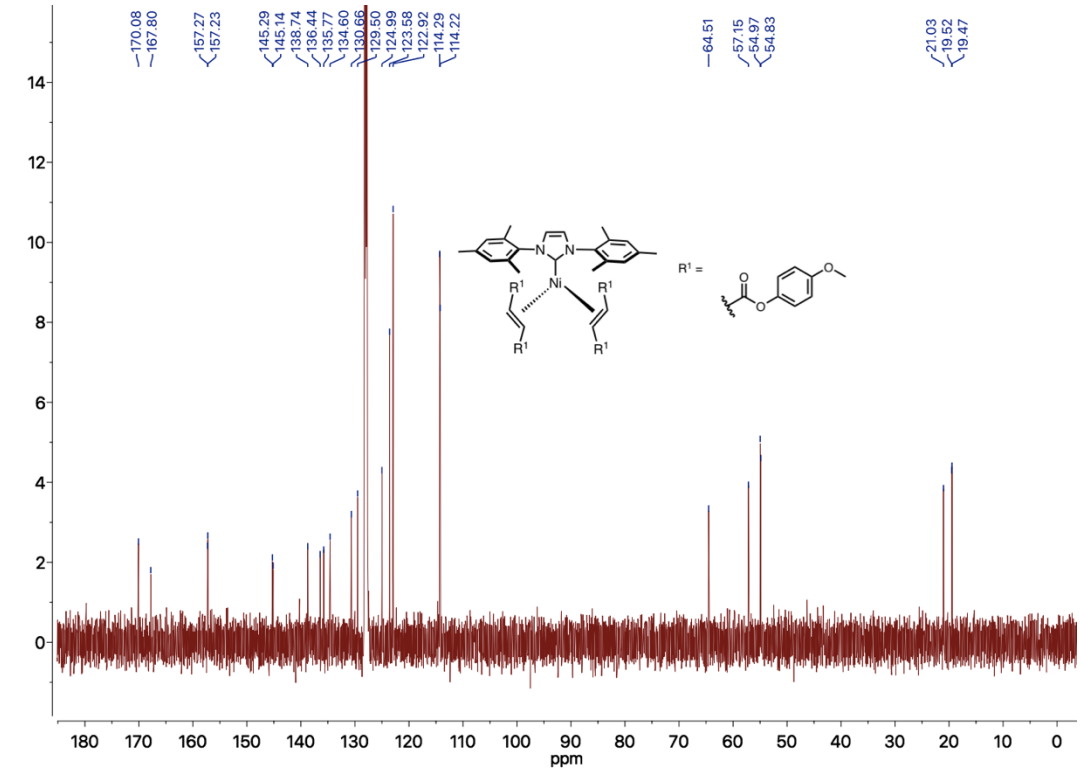


**Figure 5-54.** 3-28 - **$^{13}$C NMR (126 MHz, $C_6D_6$)**

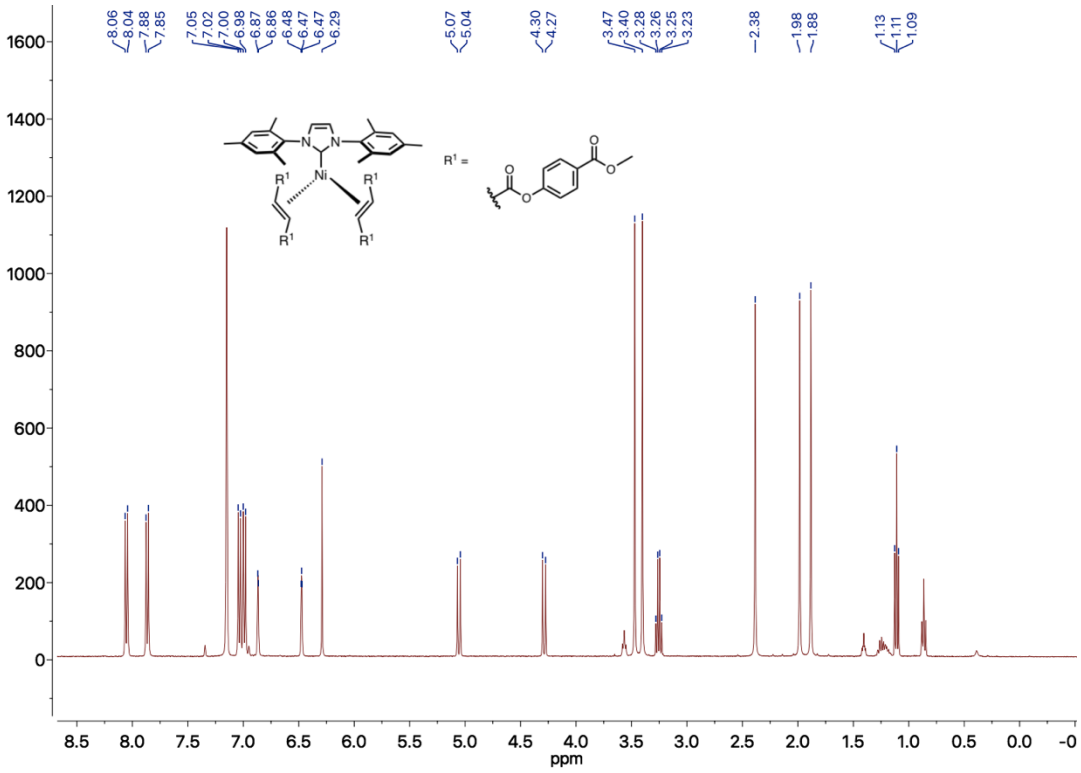


**Figure 5-55**. 3-29 - **$^{1}$H NMR (400 MHz)**

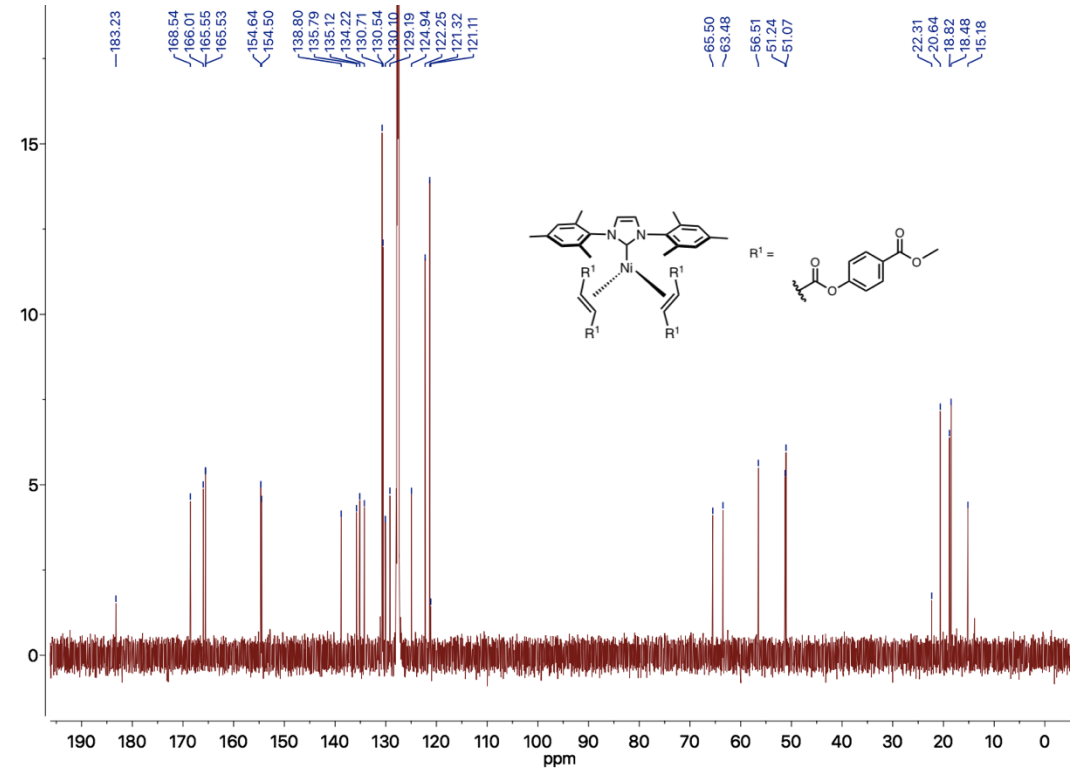


**Figure 5-56.** 3-29 - **$^{13}$C NMR (176 MHz)**

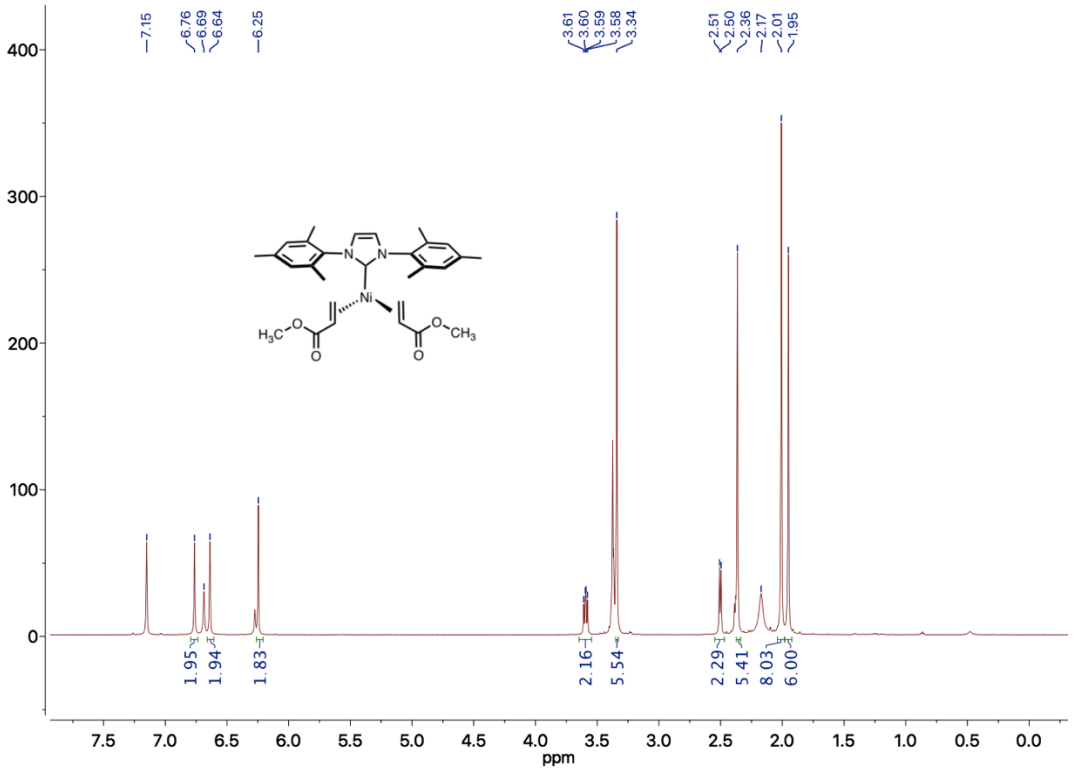


**Figure 5-57.** 3-31 - **$^{1}$H NMR (700 MHz)**

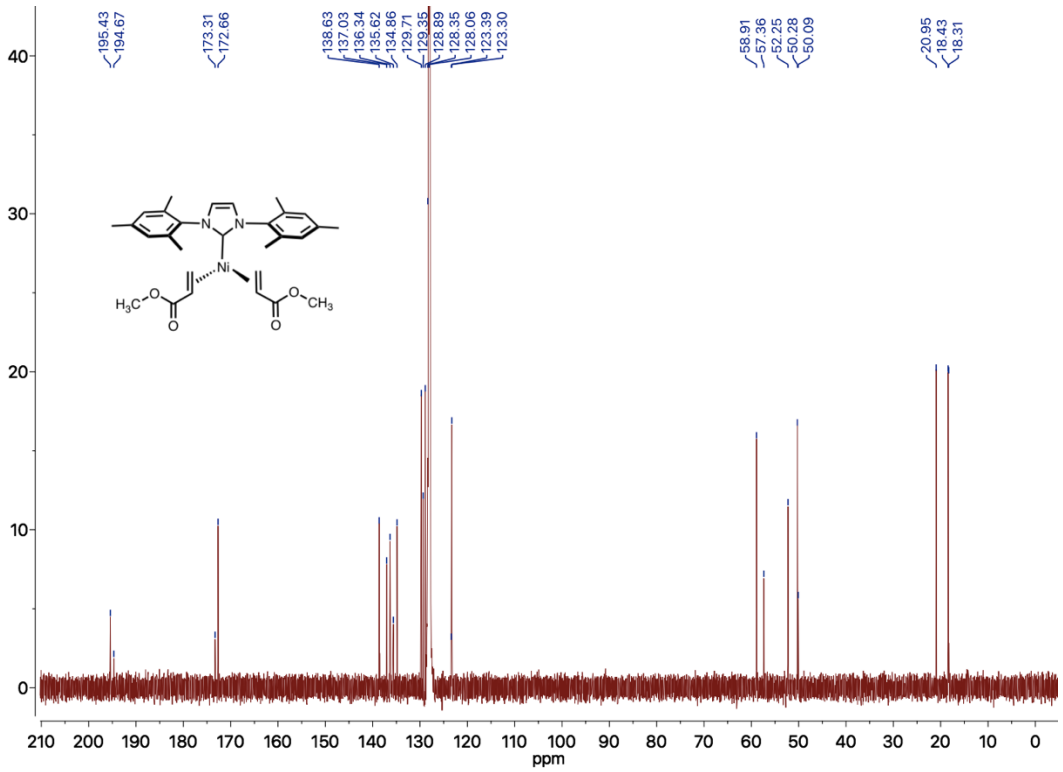


**Figure 5-58.** 3-31 - **$^{13}$C NMR (176 MHz)**

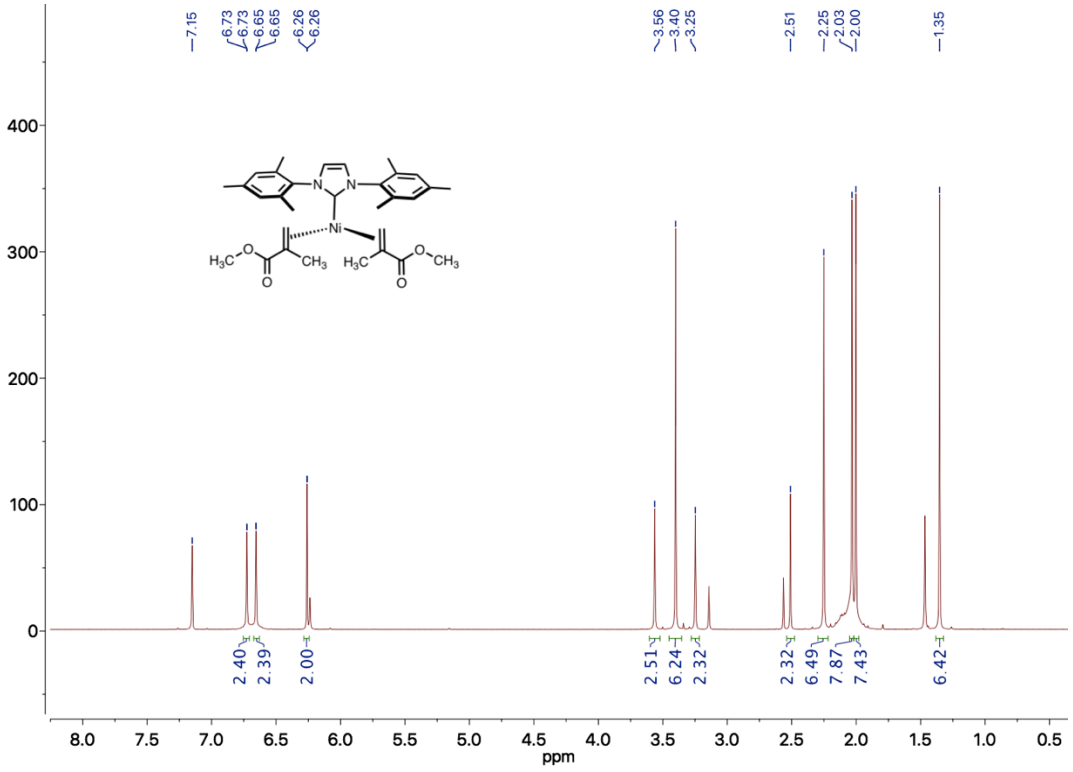


**Figure 5-59.** 3-32 - **$^{1}$H NMR (700 MHz)**

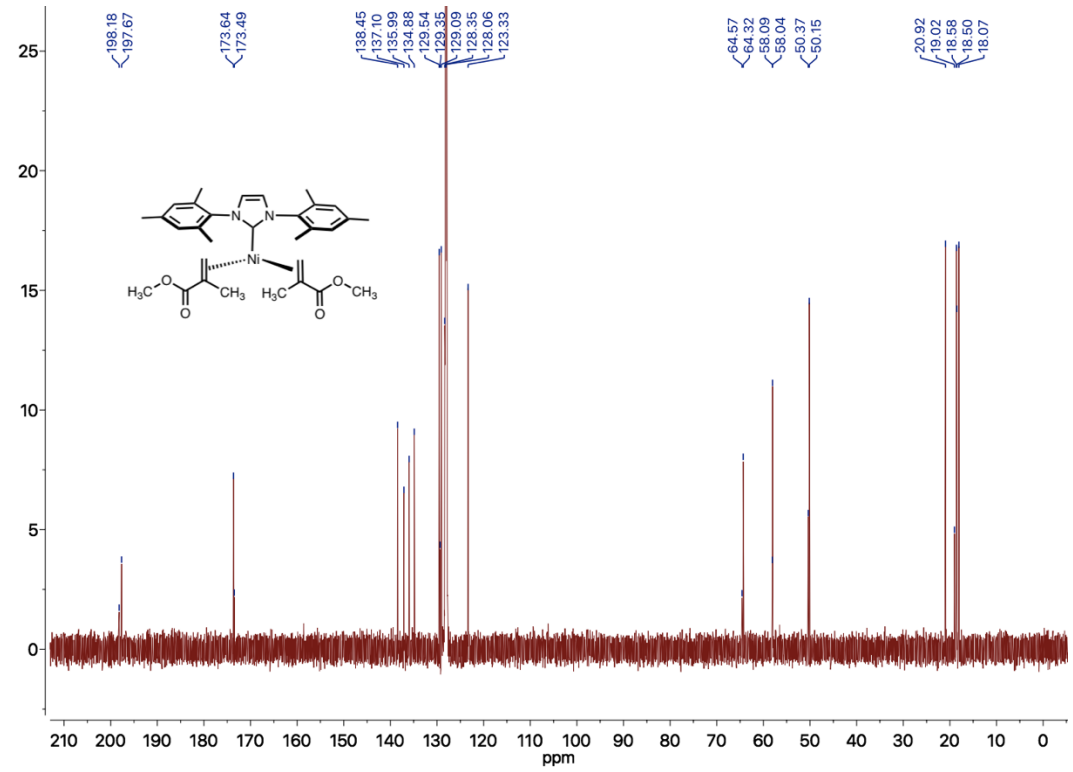


**Figure 5-60.** 3-32 - **$^{13}$C NMR (176 MHz)**

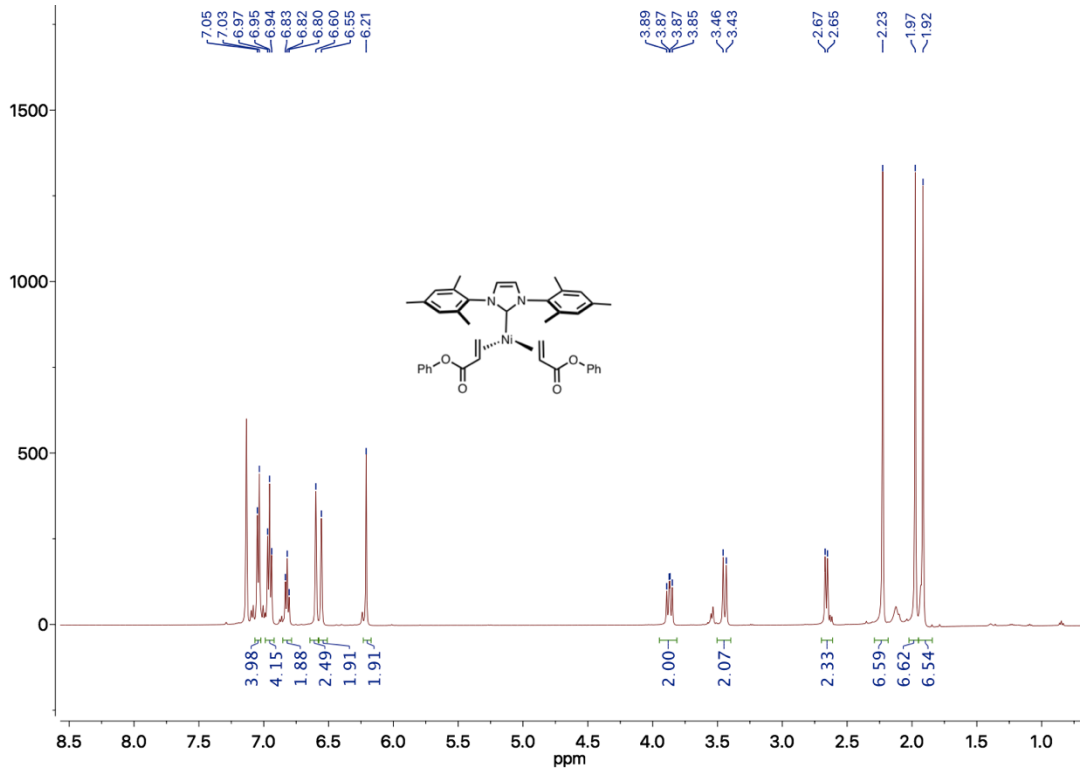


**Figure 5-61.** 3-33 - **$^{1}$H NMR (500 MHz)**

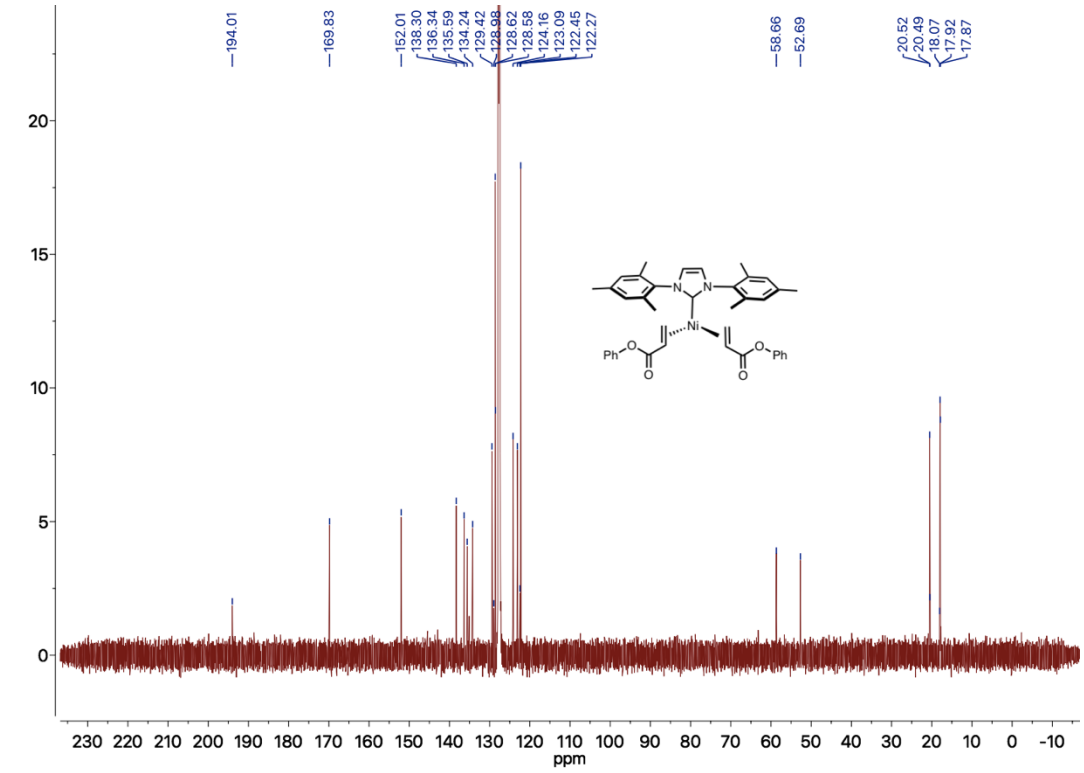


**Figure 5-62.** 3-33 - **$^{13}$C NMR (176 MHz)**

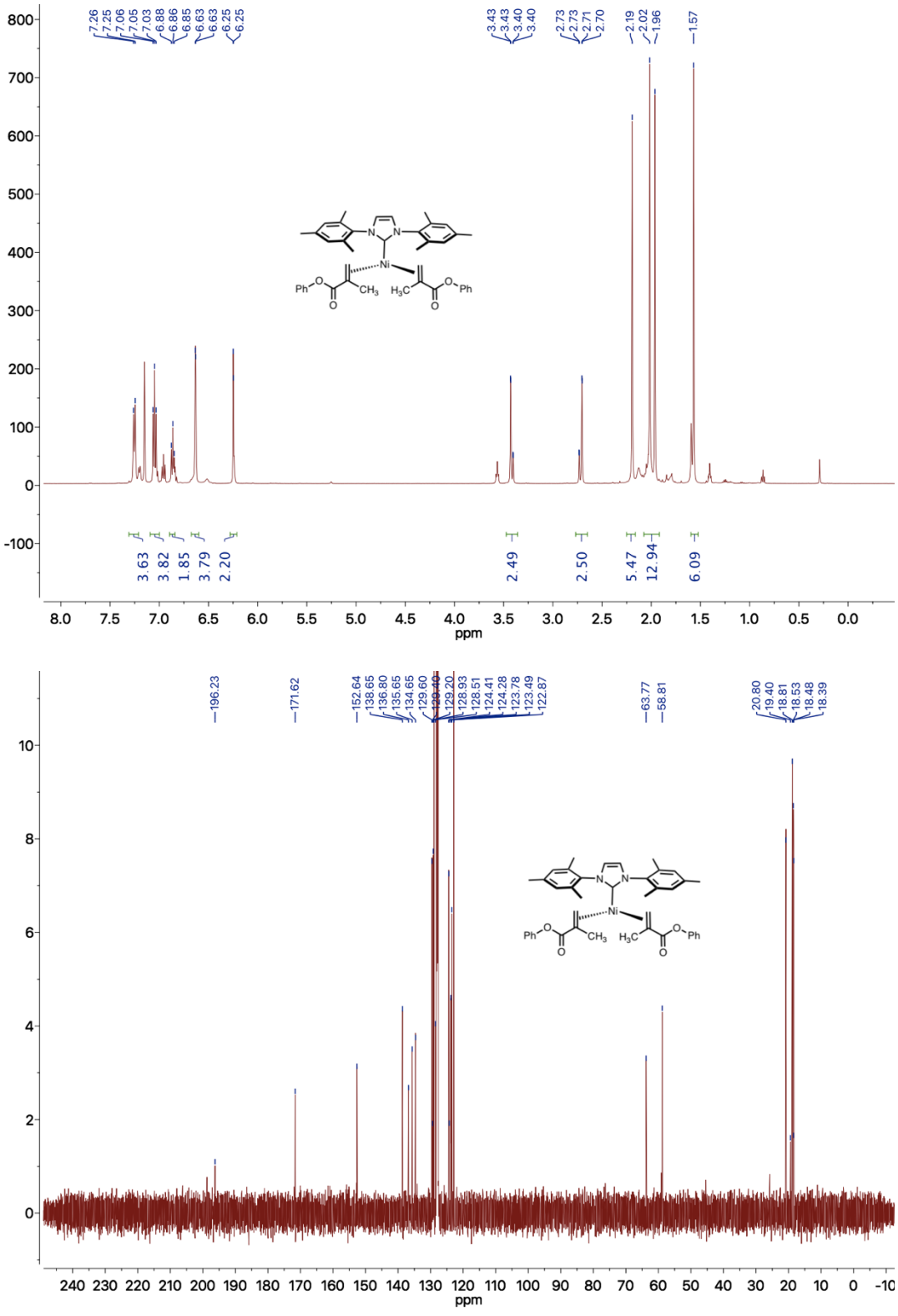


**Figure 5-63**. 3-34 - **$^{13}$C NMR (126 MHz, $C_6D_6$)** 3-34 - **$^{1}$H NMR (500 MHz)**

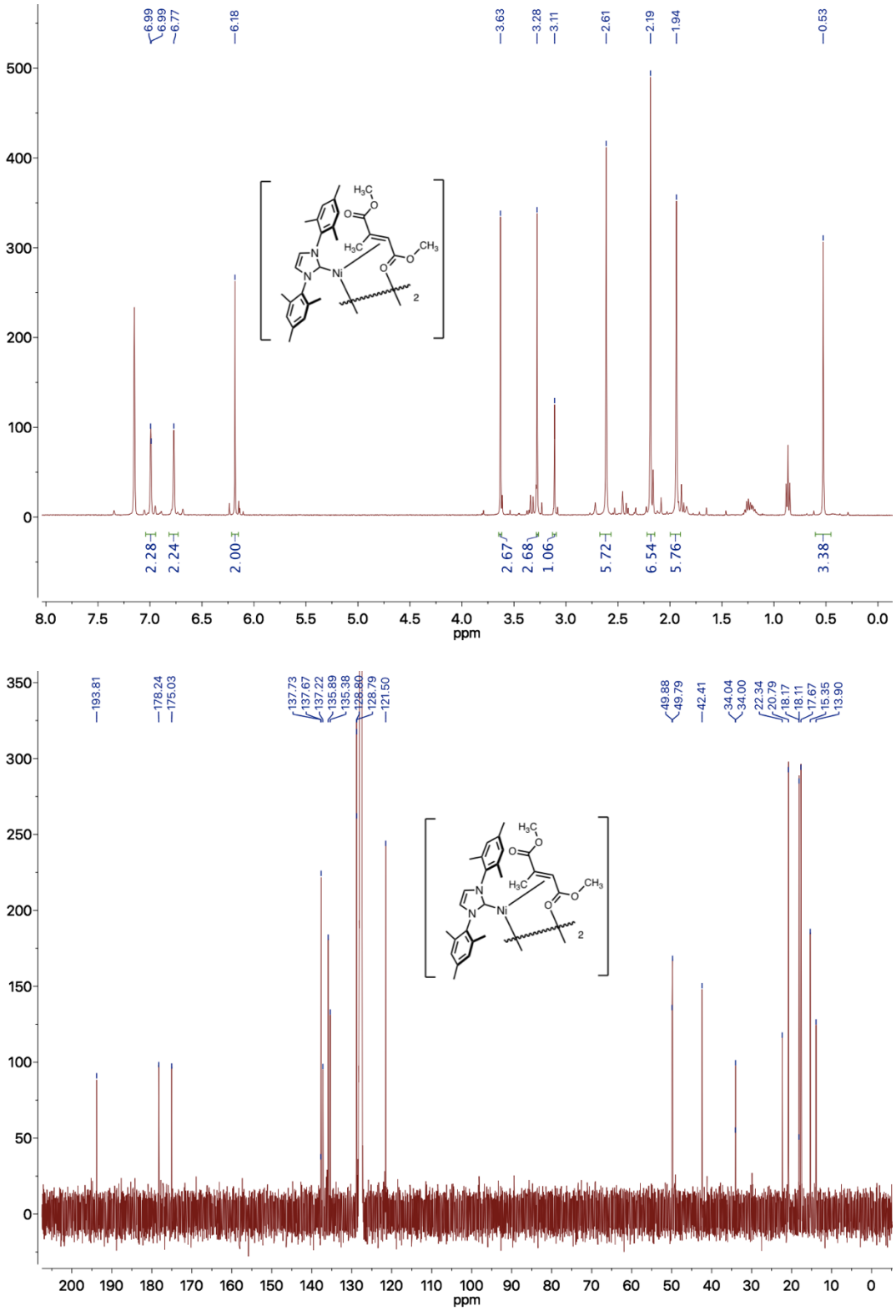


**Figure 5-64.** 3-35 - $^{13}$C NMR (176 MHz, $C_6D_6$), $^{1}$H NMR (401 MHz, $C_6D_6$)

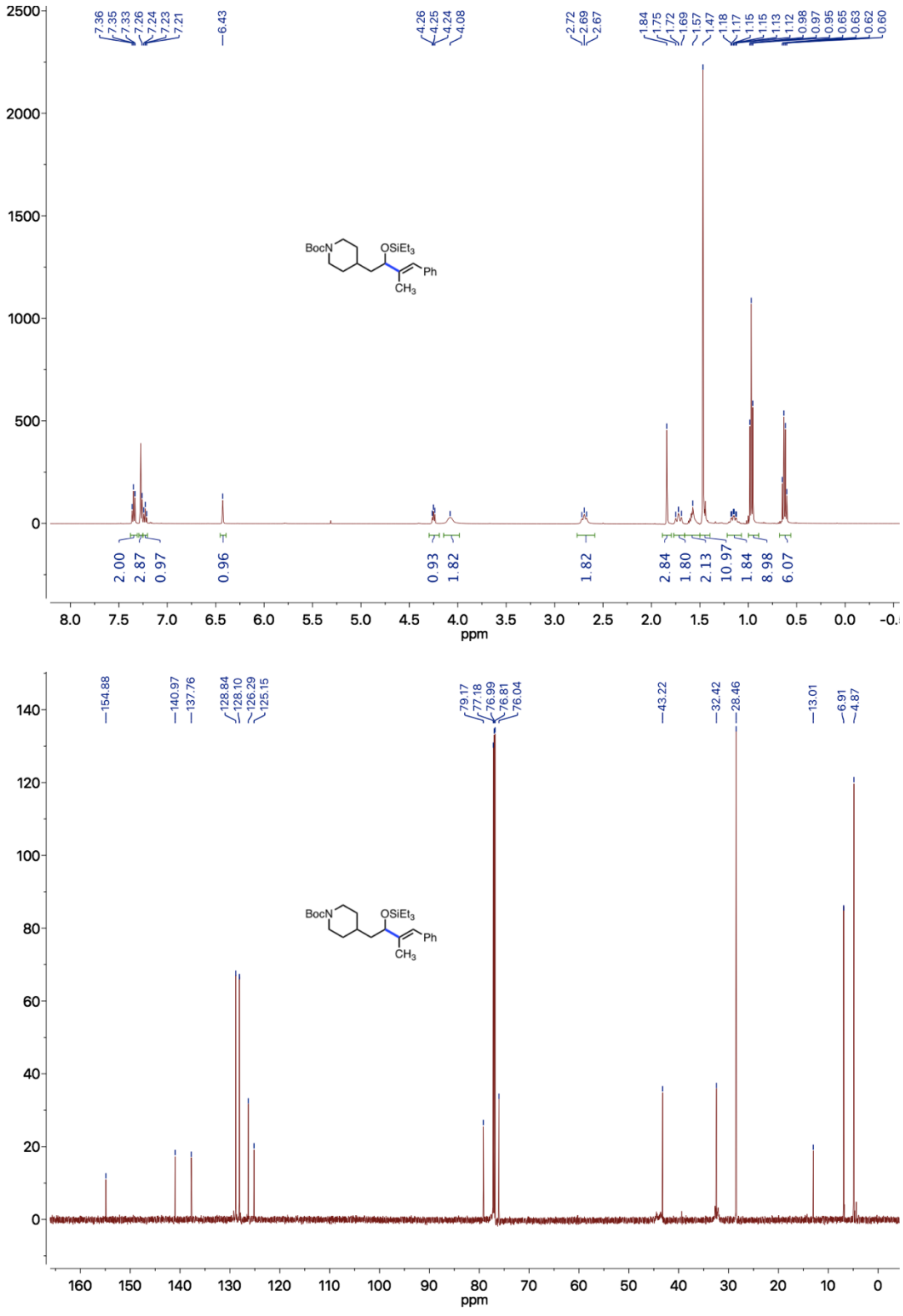


**Figure 5-65.** 3-36 - **$^{1}$H NMR (500 MHz), $^{13}$C NMR (176 MHz)**

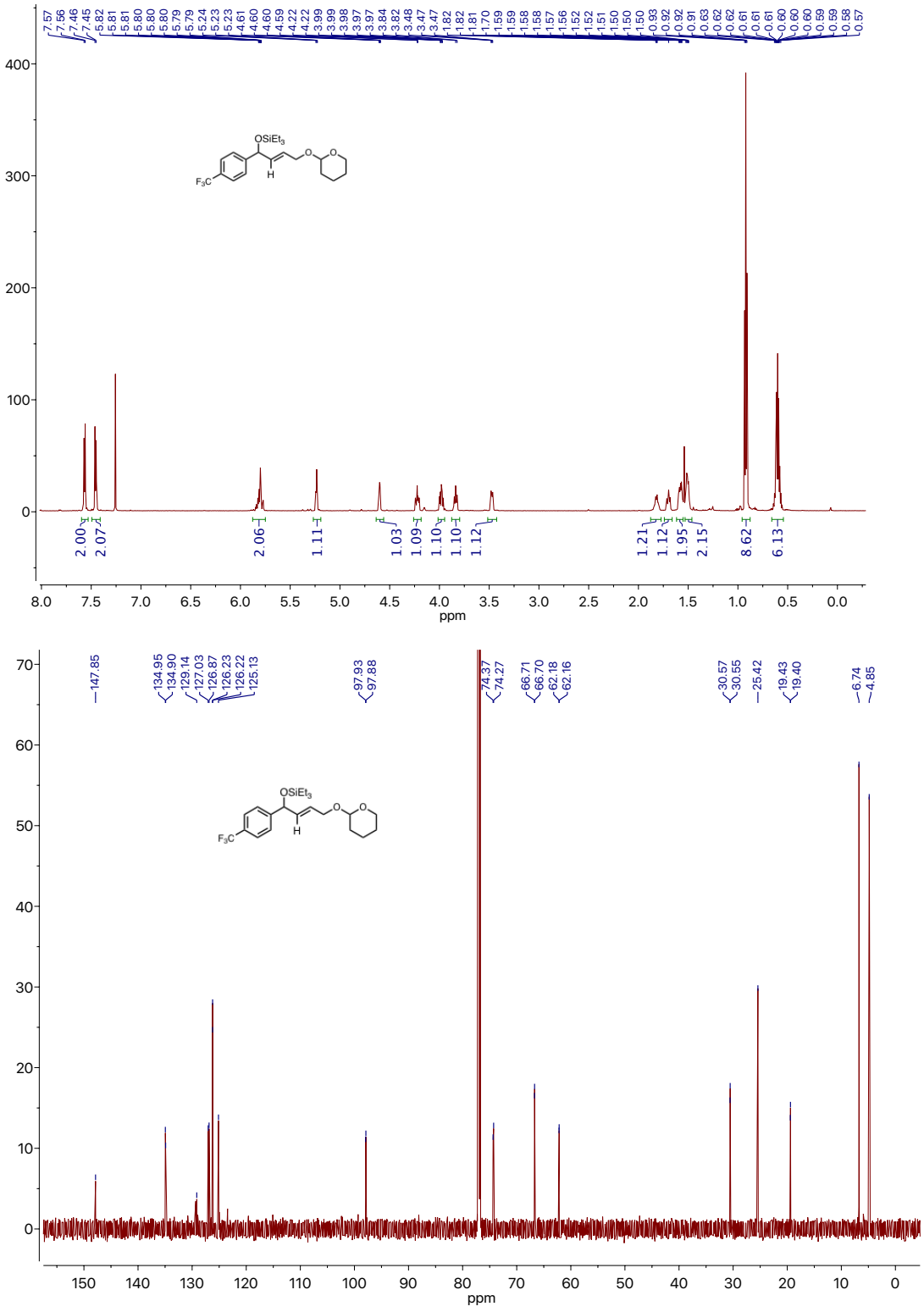


**Figure 5-66.** 3-37 **- $^{1}$H NMR (700 MHz), $^{13}$C NMR (176 MHz)**

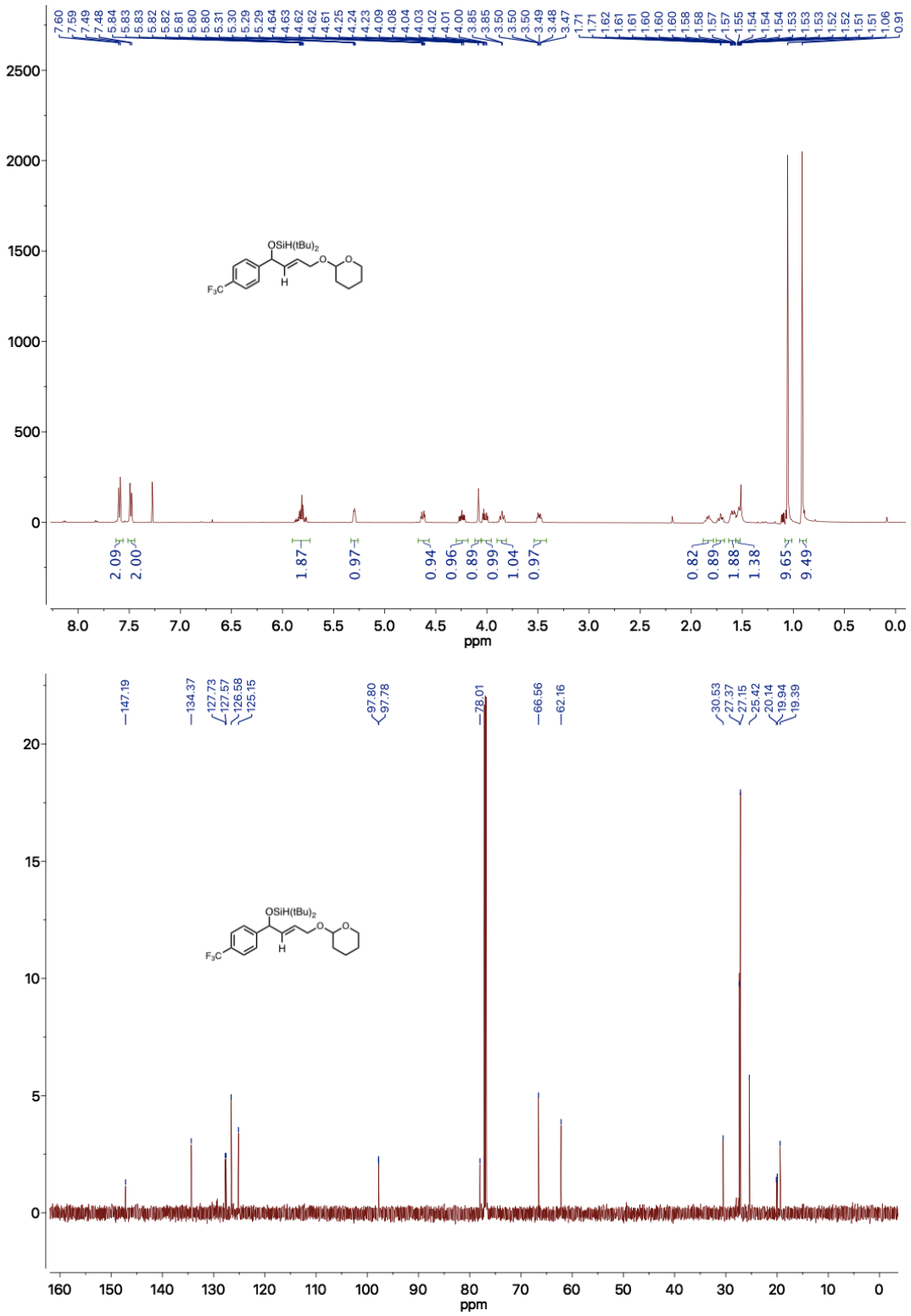


**Figure 5-67.** 3-38 - **$^{1}$H NMR (700 MHz) - $^{13}$C NMR (176 MHz)**

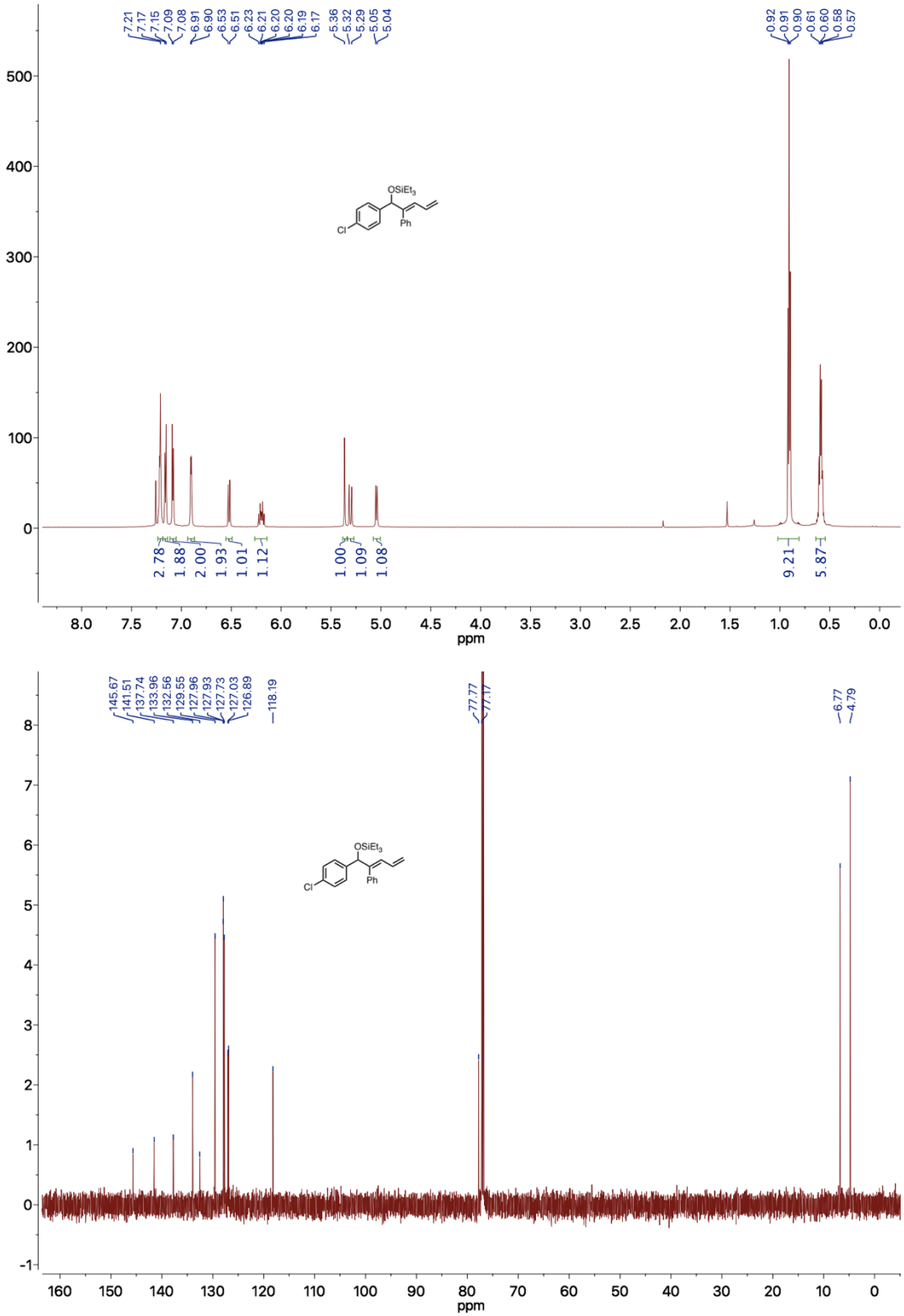


**Figure 5-68.** 3-39 - **$^{1}$H NMR (700 MHz), $^{13}$C NMR (176 MHz)**

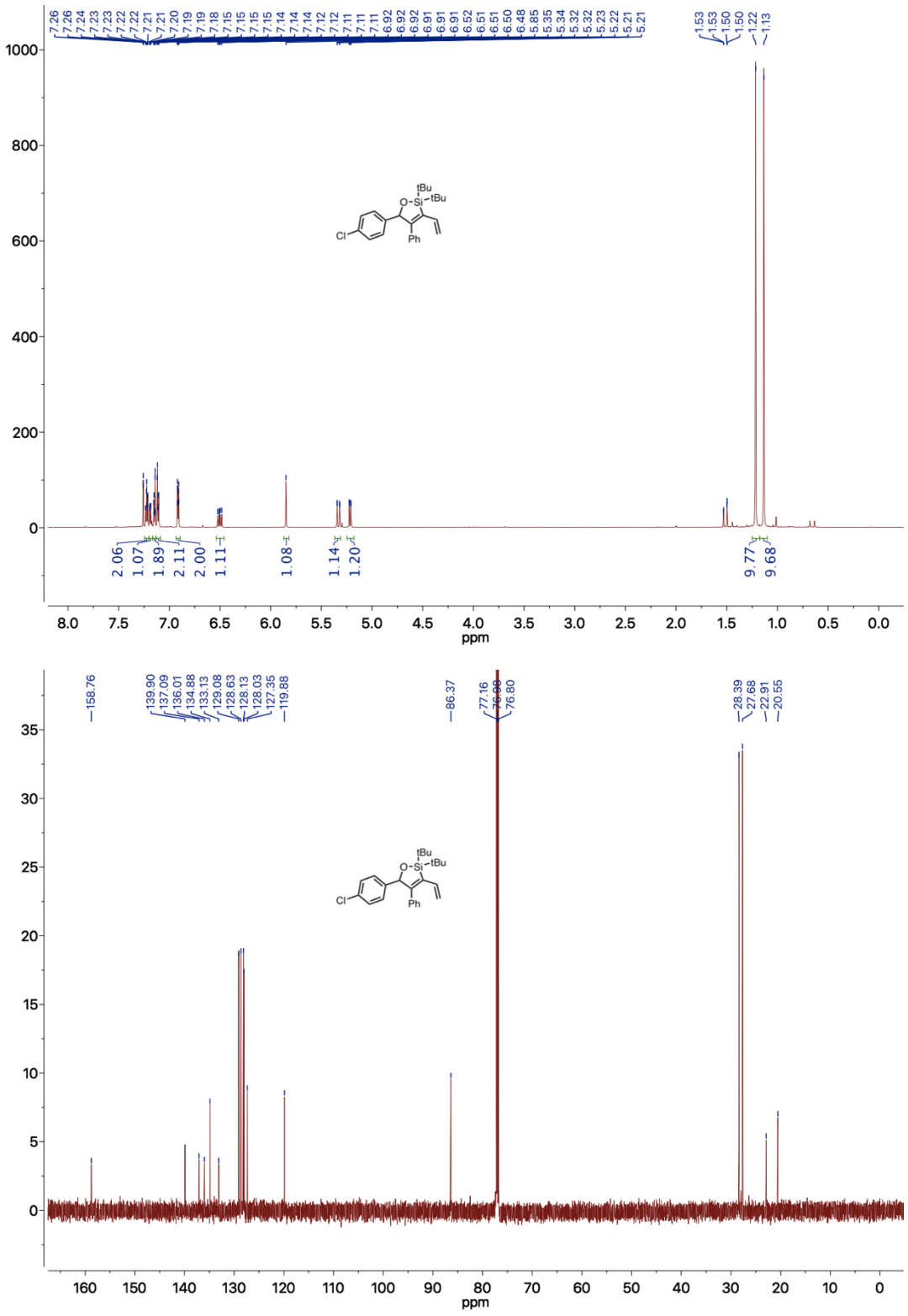


**Figure 5-69.** 3-40 - **$^{1}$H NMR (700 MHz)$^{13}$C NMR (176 MHz)**

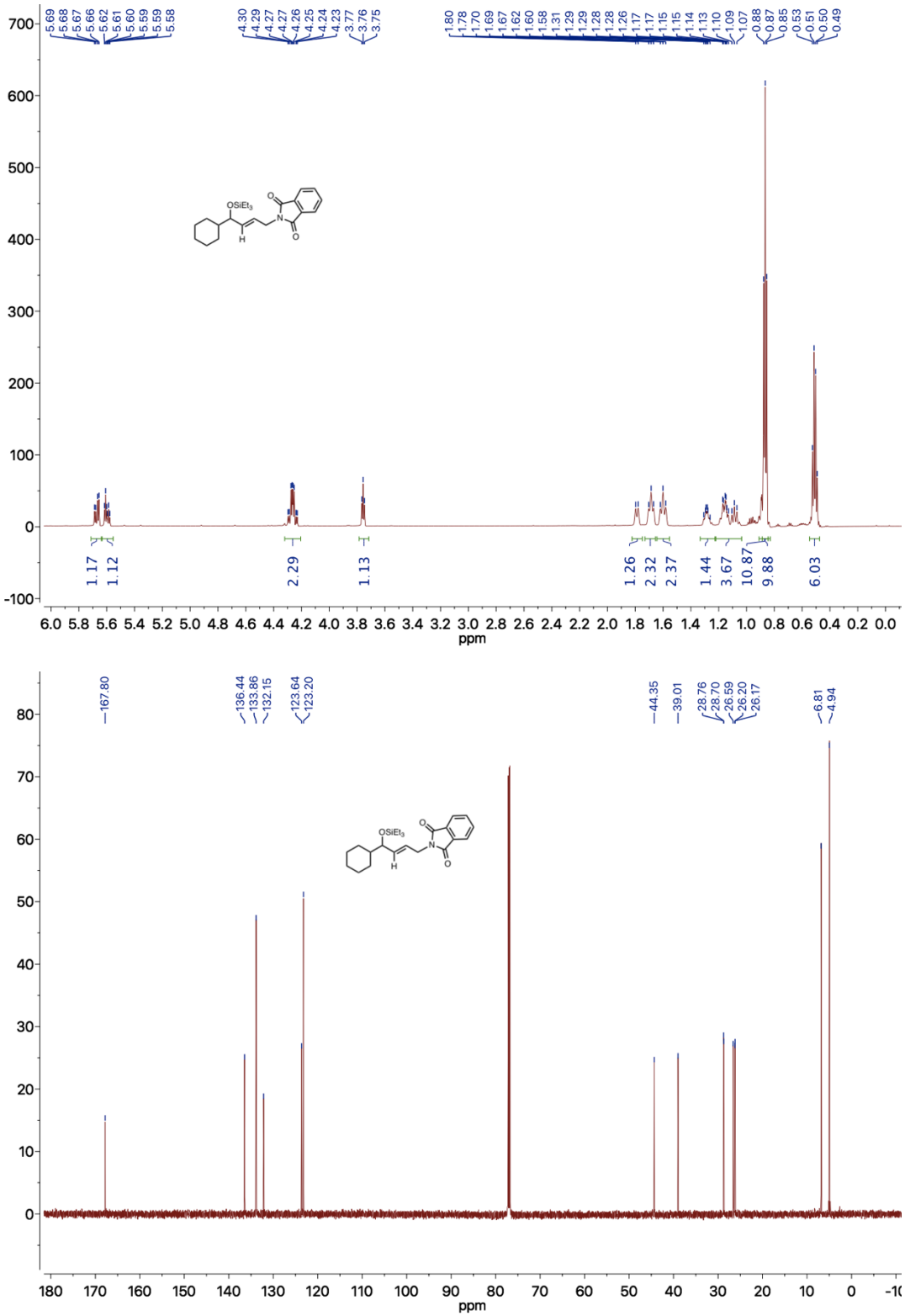

**Figure 5-70.** 3-41 - **$^{1}$H NMR (700 MHz), $^{13}$C NMR (176 MHz)**

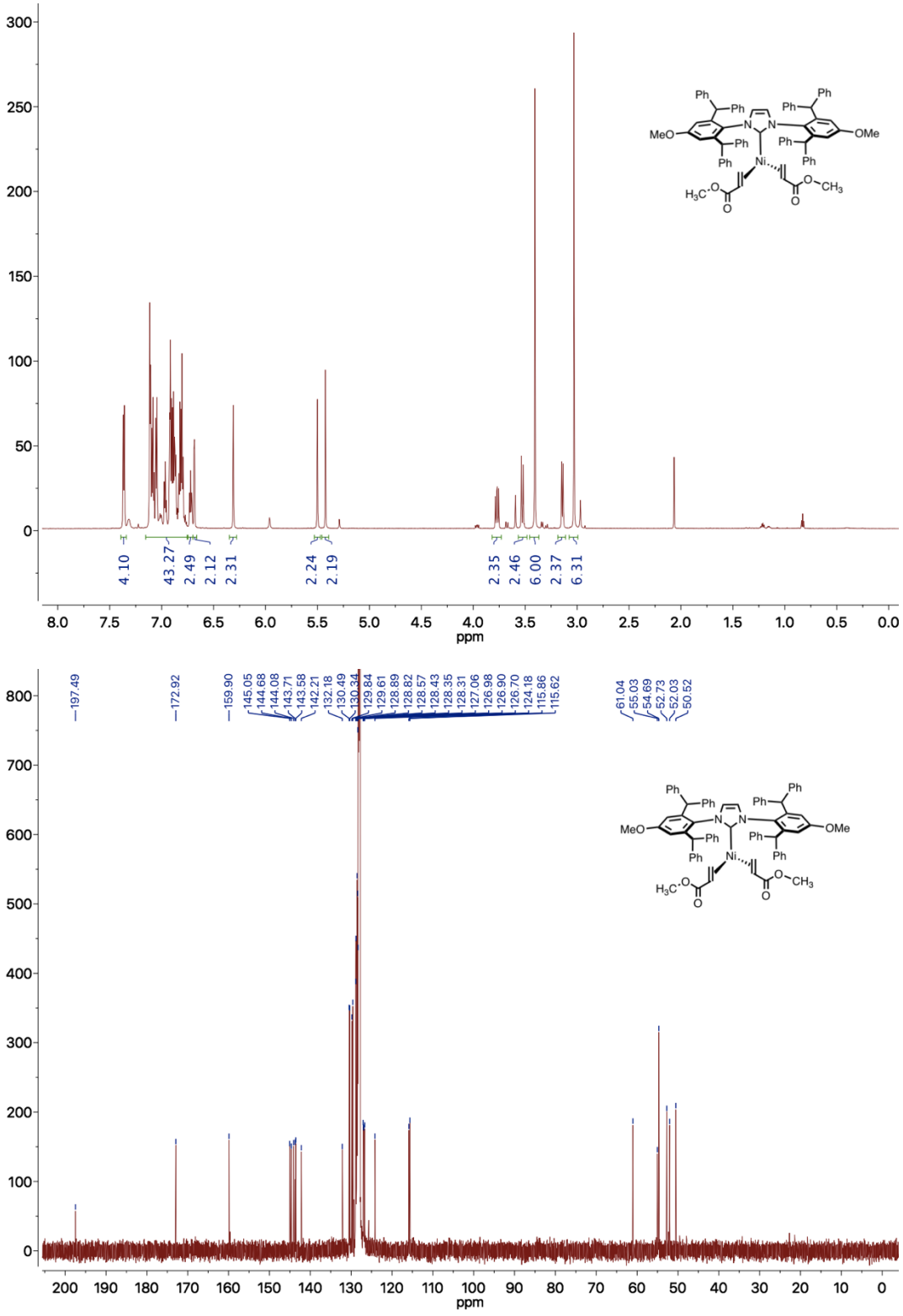


**Figure 5-71.** 3-42 - **$^{1}$H NMR (700 MHz), $^{13}$C NMR (176 MHz)**

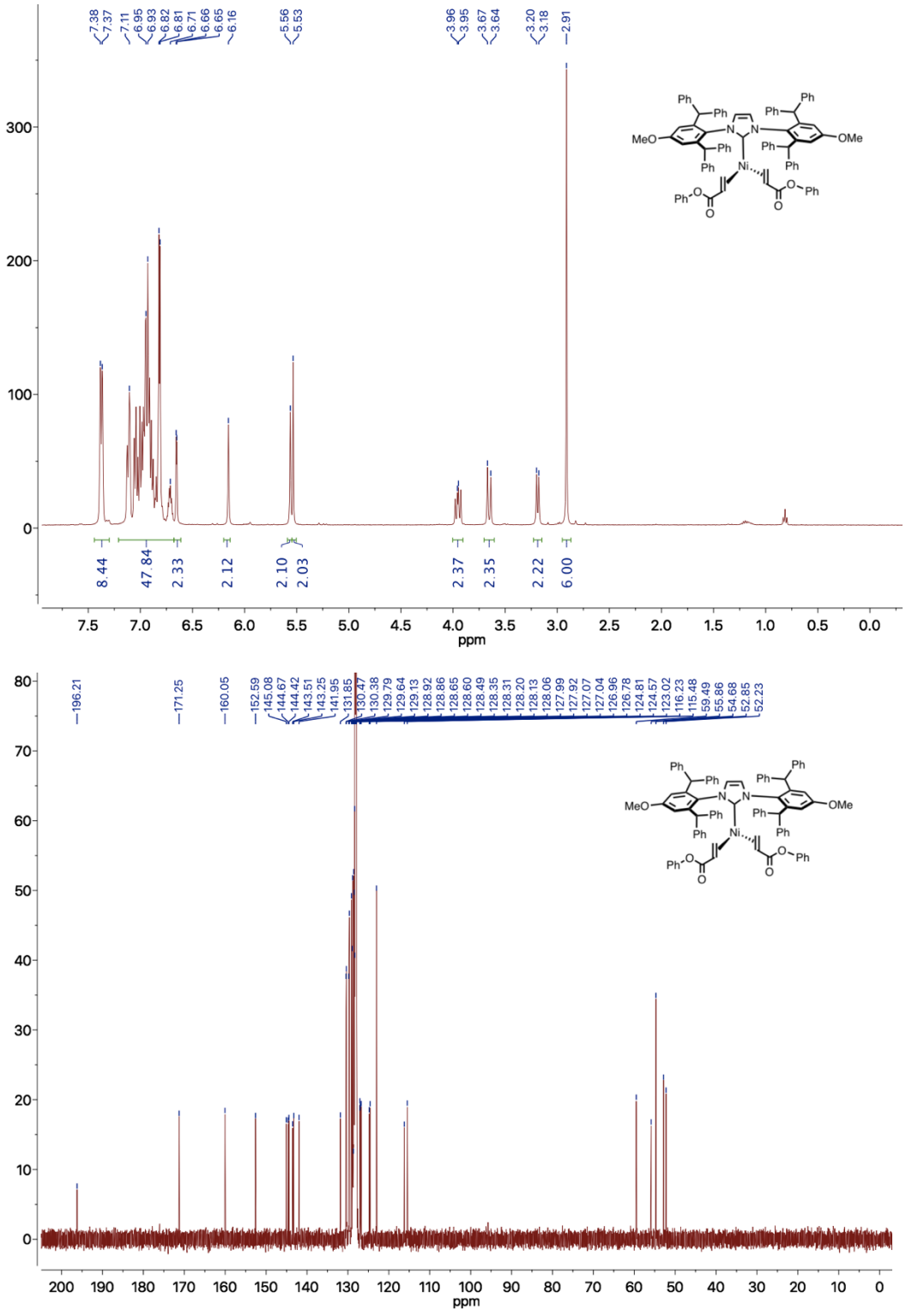


**Figure 5-72.** 3-43 - **$^{1}$H NMR (400 MHz)$^{13}$C NMR (176 MHz)**

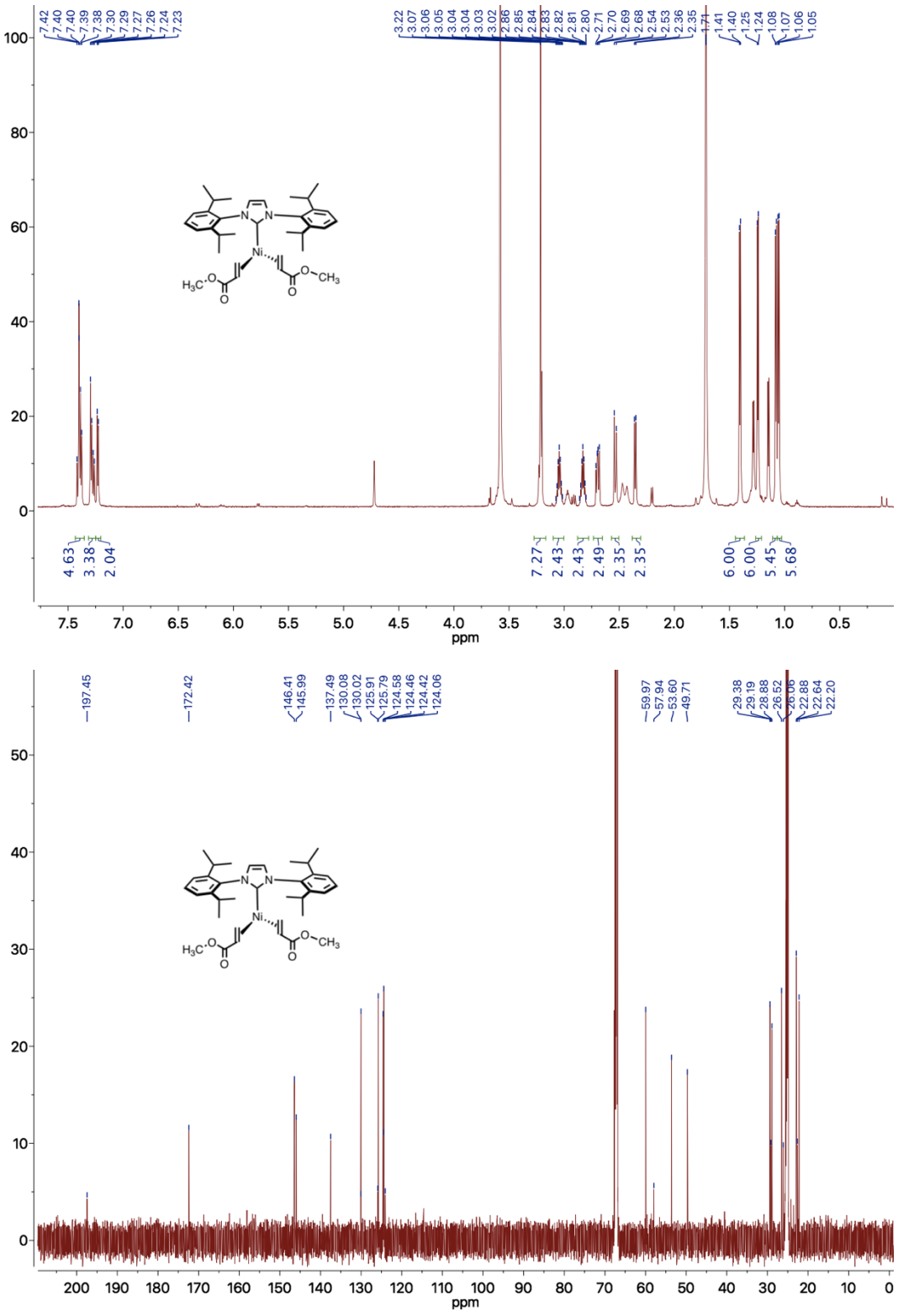


**Figure 5-73.** 3-44 - **$^{1}$H NMR (700 MHz), $^{13}$C NMR (176 MHz)**

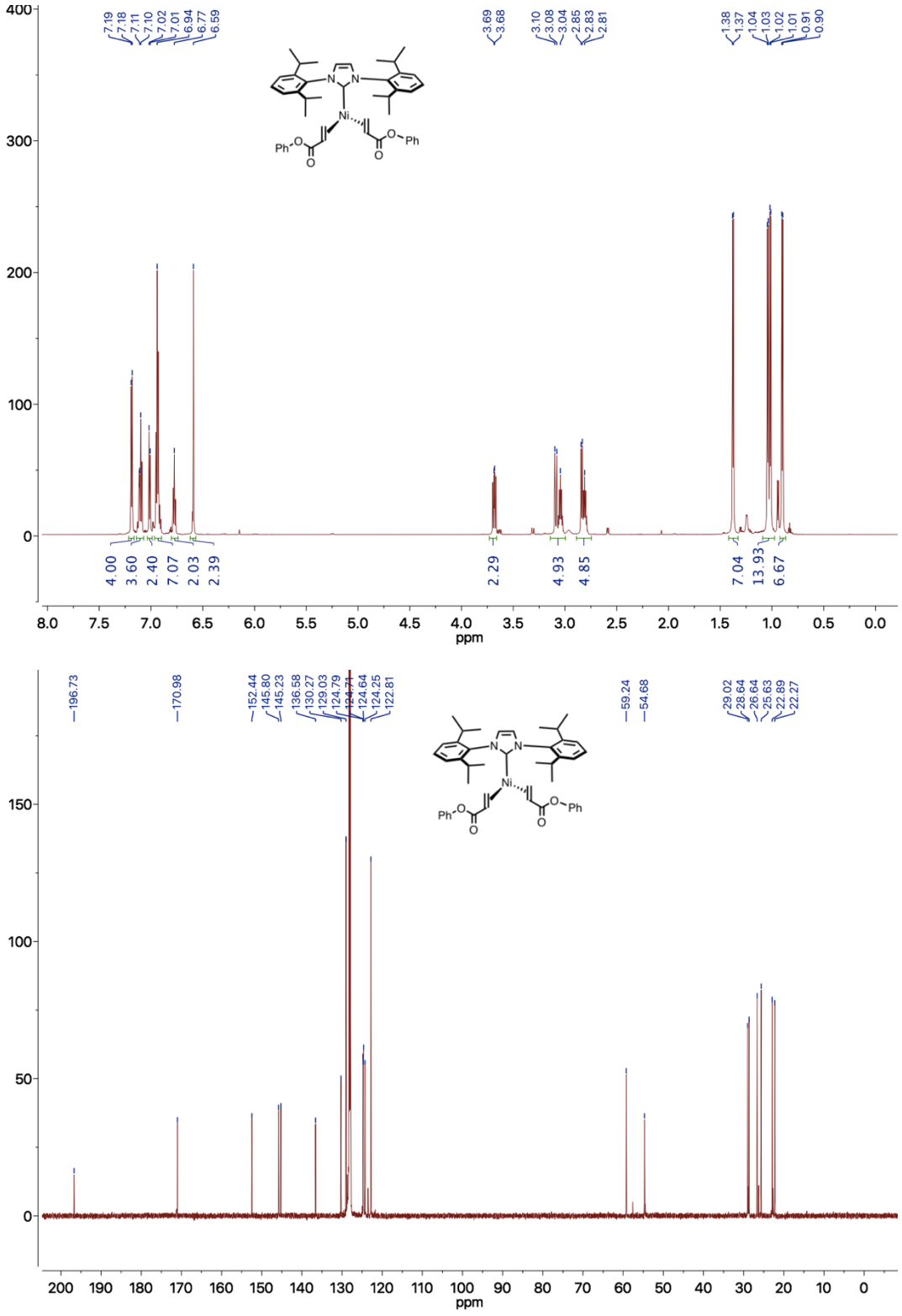


**Figure 5-74.** 3-45 - **$^{1}$H NMR (700 MHz), $^{13}$C NMR (176 MHz)**

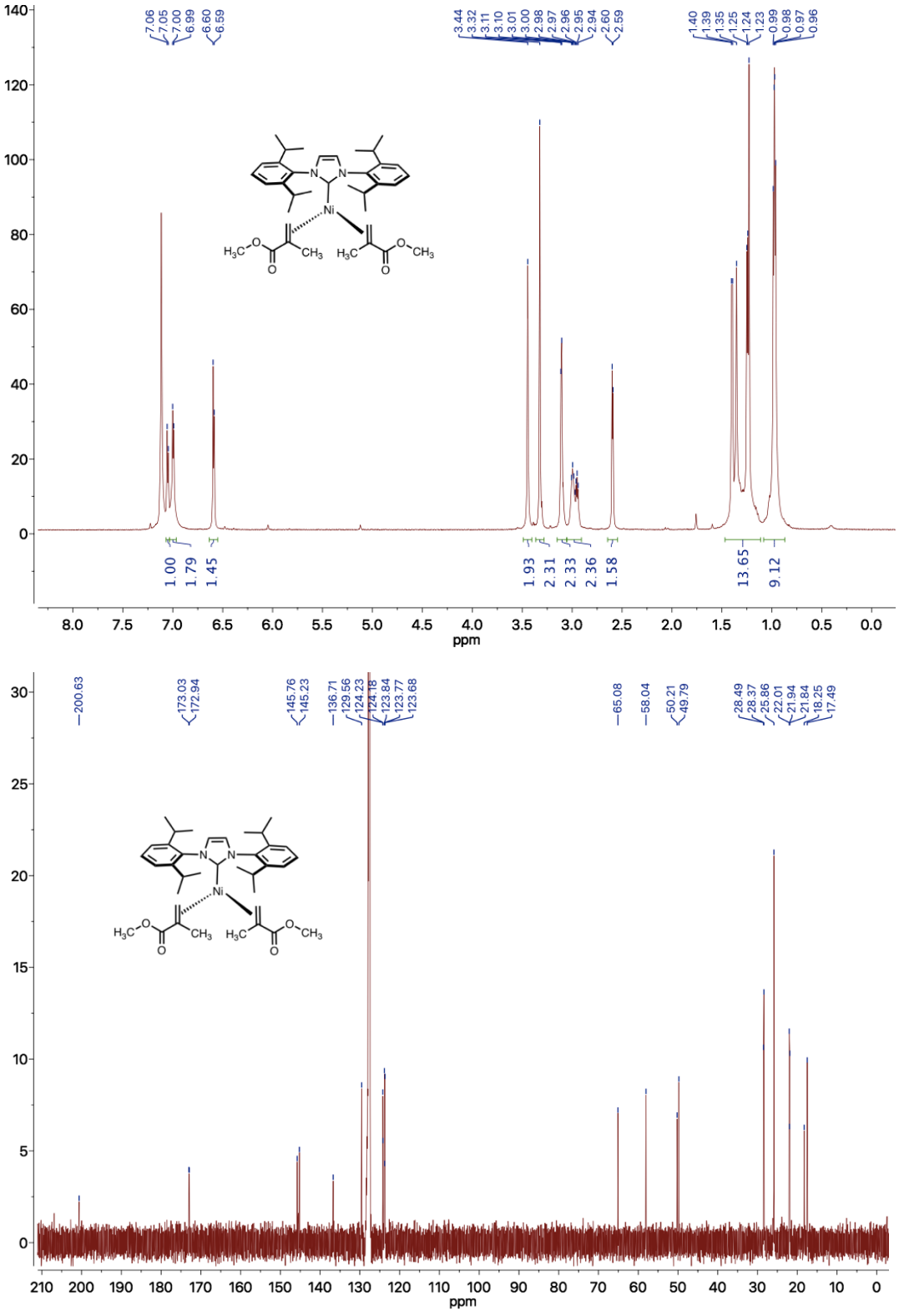


**Figure 5-75.** 3-46 - **$^{1}$H NMR (700 MHz), $^{13}$C NMR (176 MHz)**

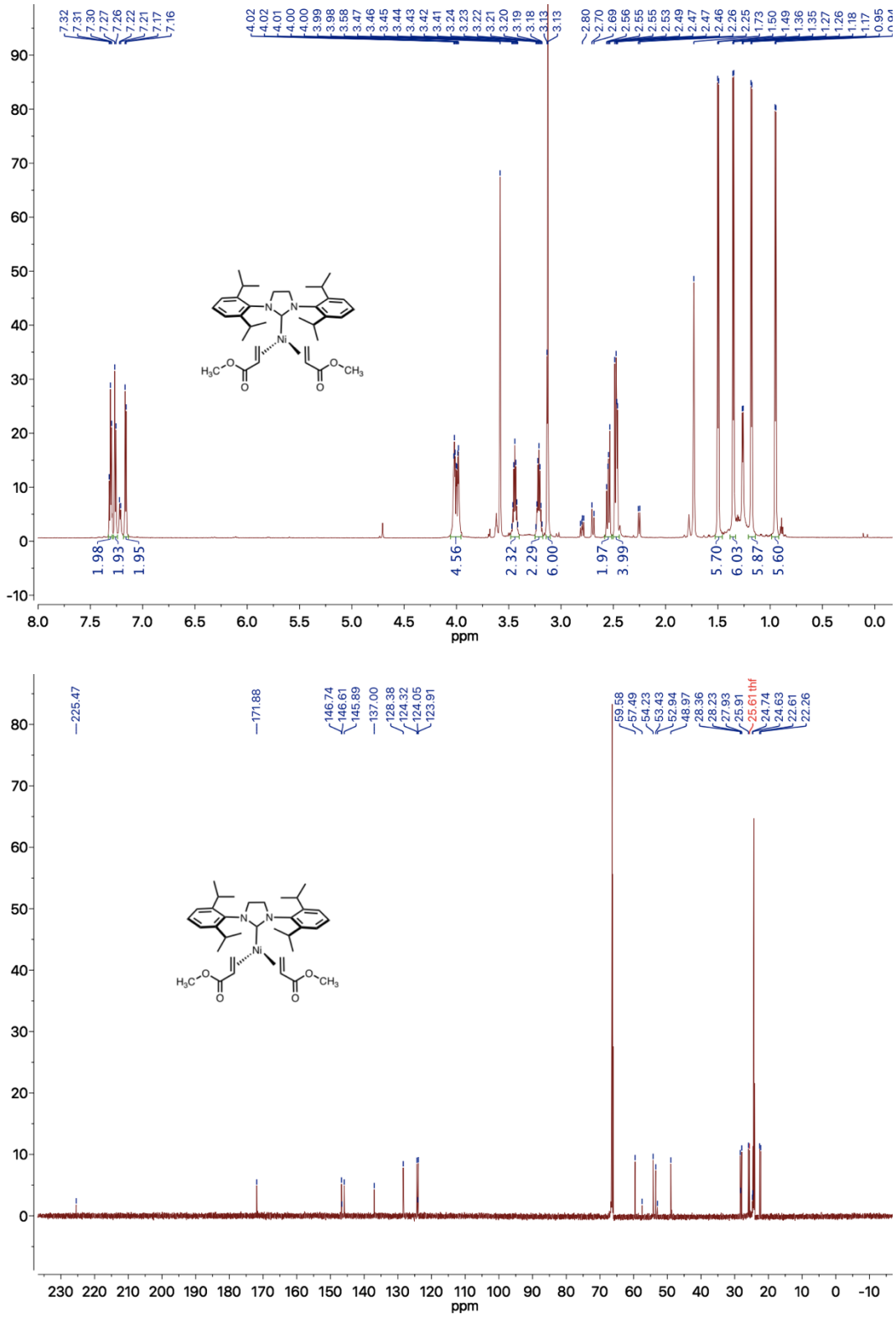


**Figure 5-76.** 3-47 - **$^{1}$H NMR (700 MHz) , $^{13}$C NMR (176 MHz)**

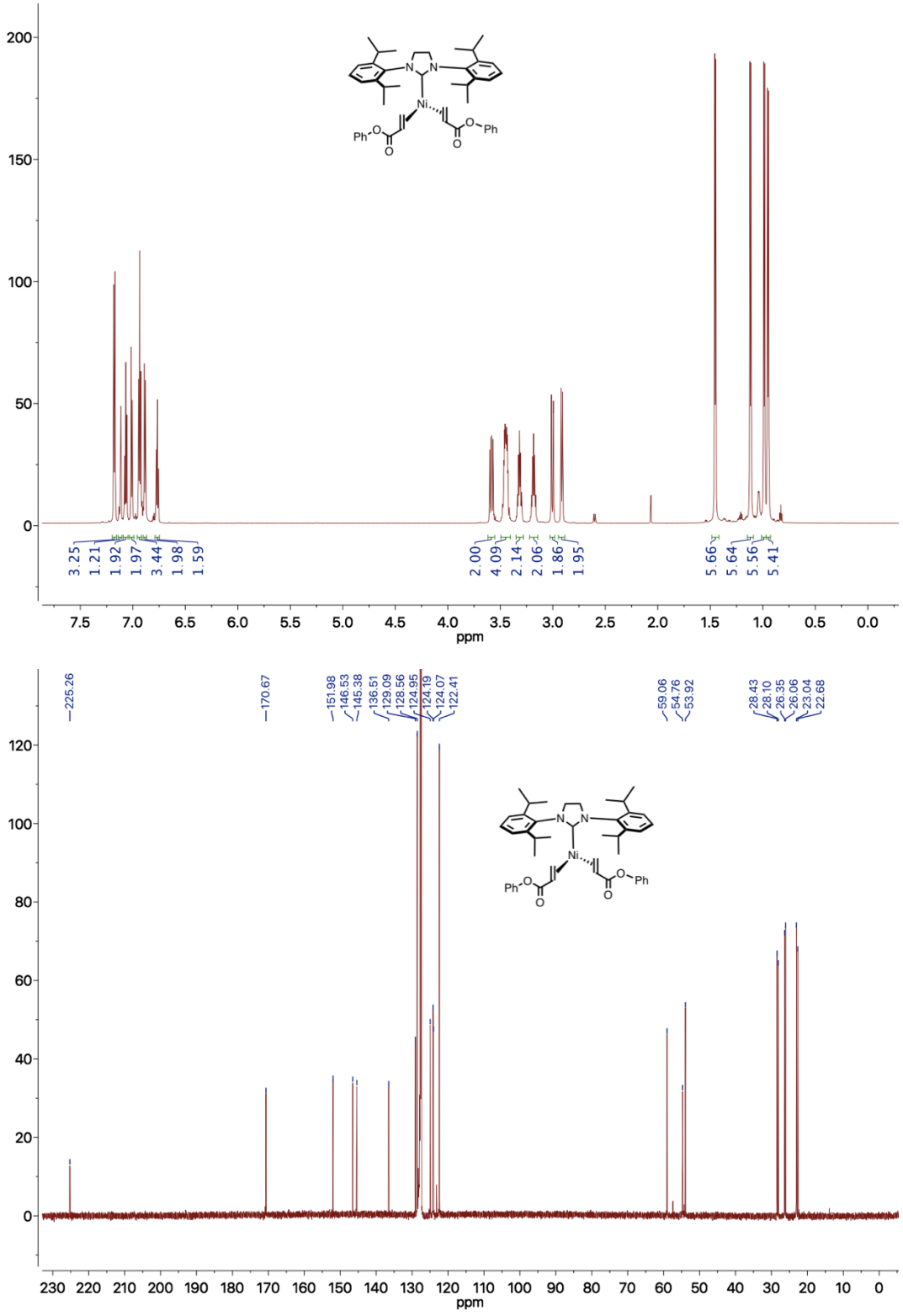


**Figure 5-77.** 3-48 - **$^{1}$H NMR (700 MHz), $^{13}$C NMR (176 MHz)**

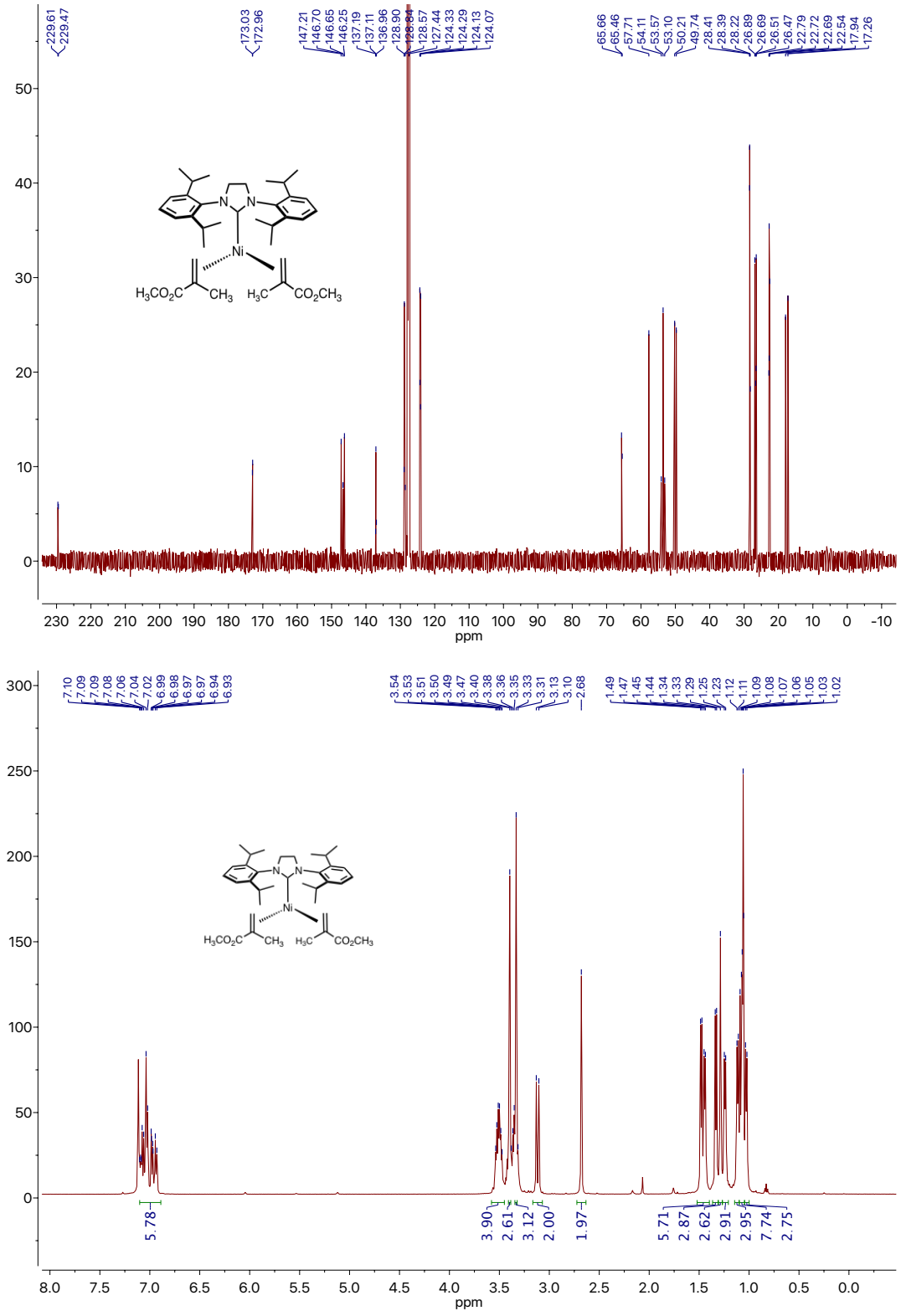


**Figure 5-78.** 3-49 - **$^{1}$H NMR (700 MHz), $^{13}$C NMR (176 MHz)**

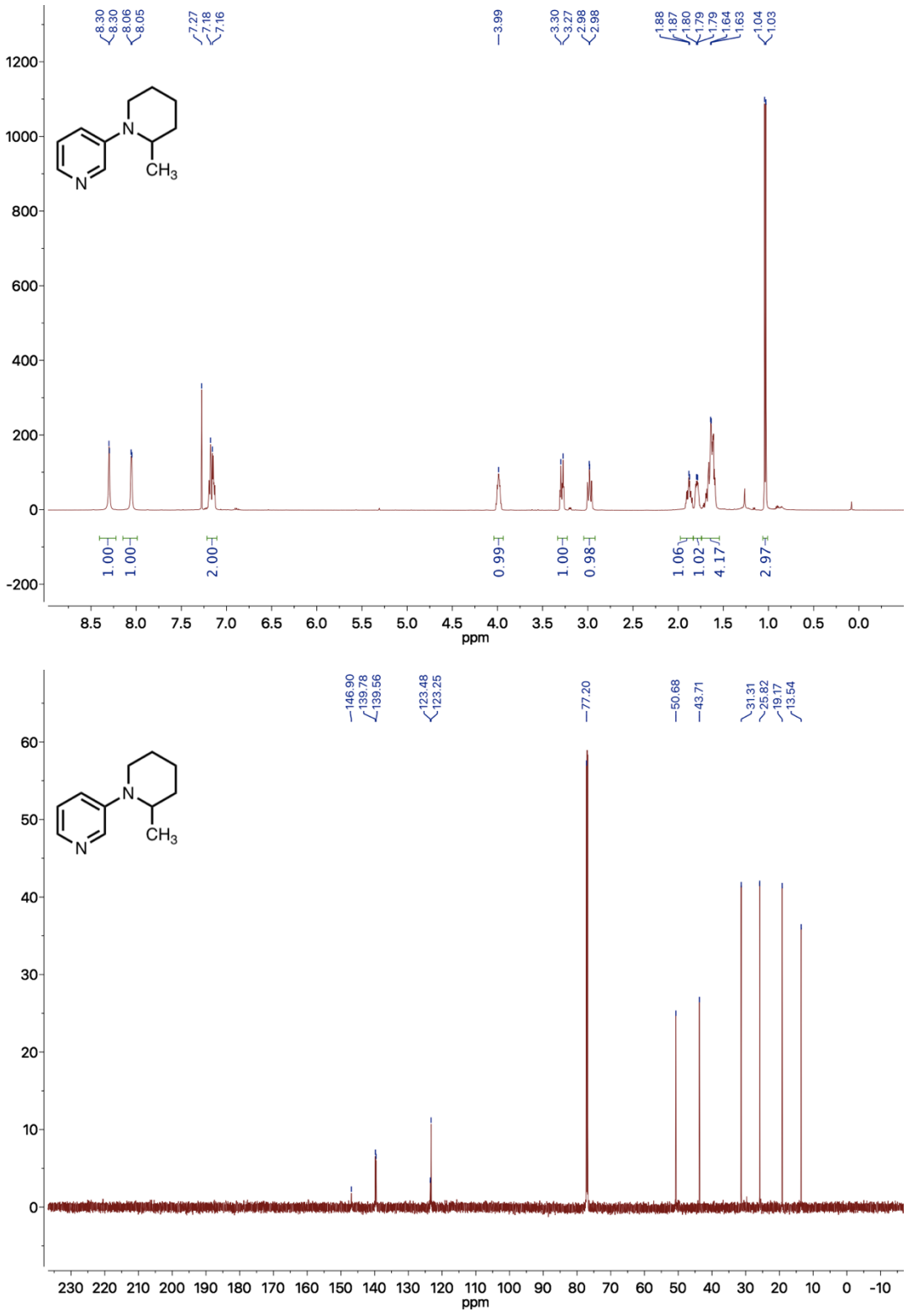


**Figure 5-79.** 3-53 - **$^{1}$H NMR (500 MHz), $^{13}$C NMR (176 MHz)**

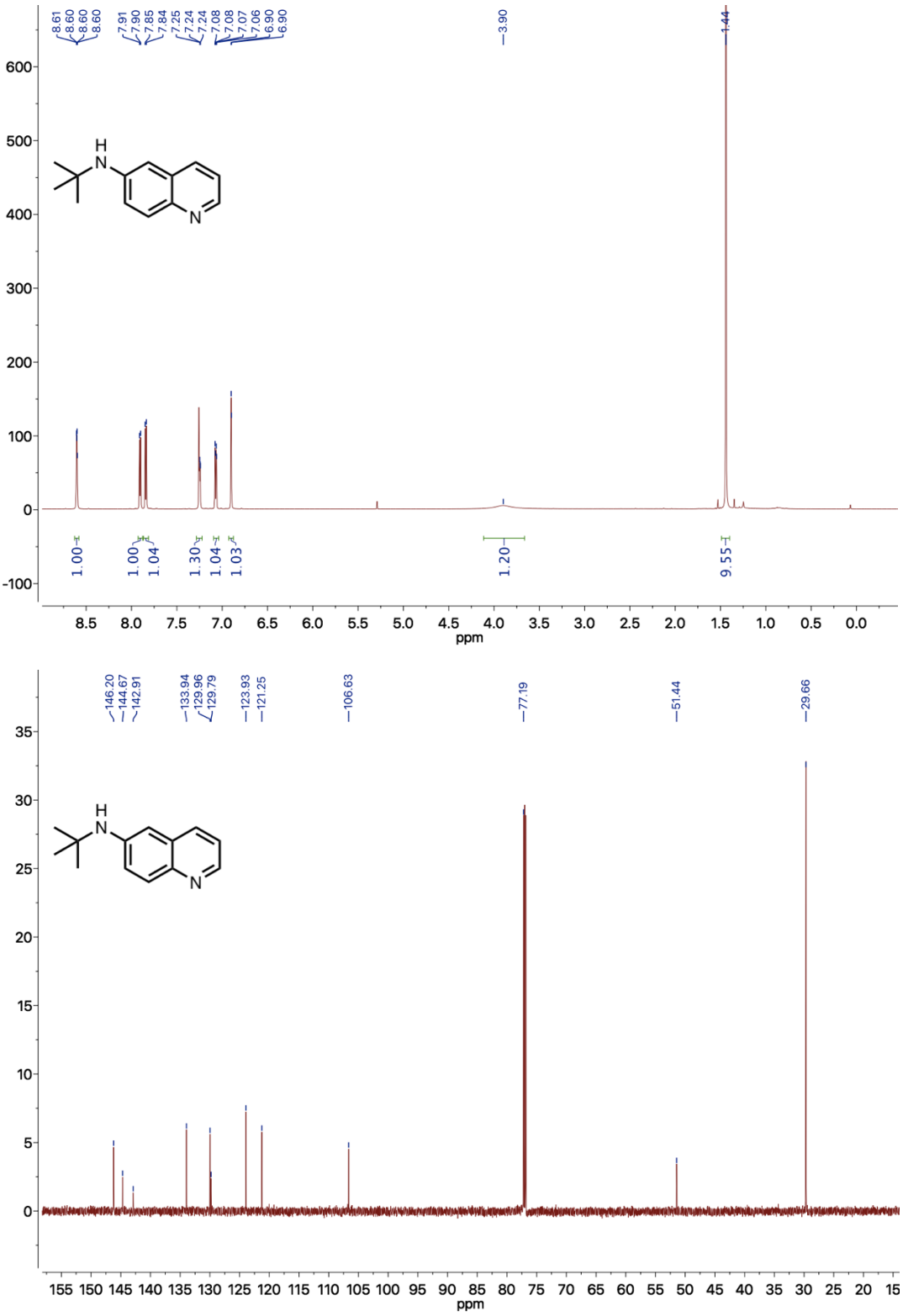


**Figure 5-80.** 3-54 - **$^{1}$H NMR (700 MHz), $^{13}$C NMR (176 MHz)**

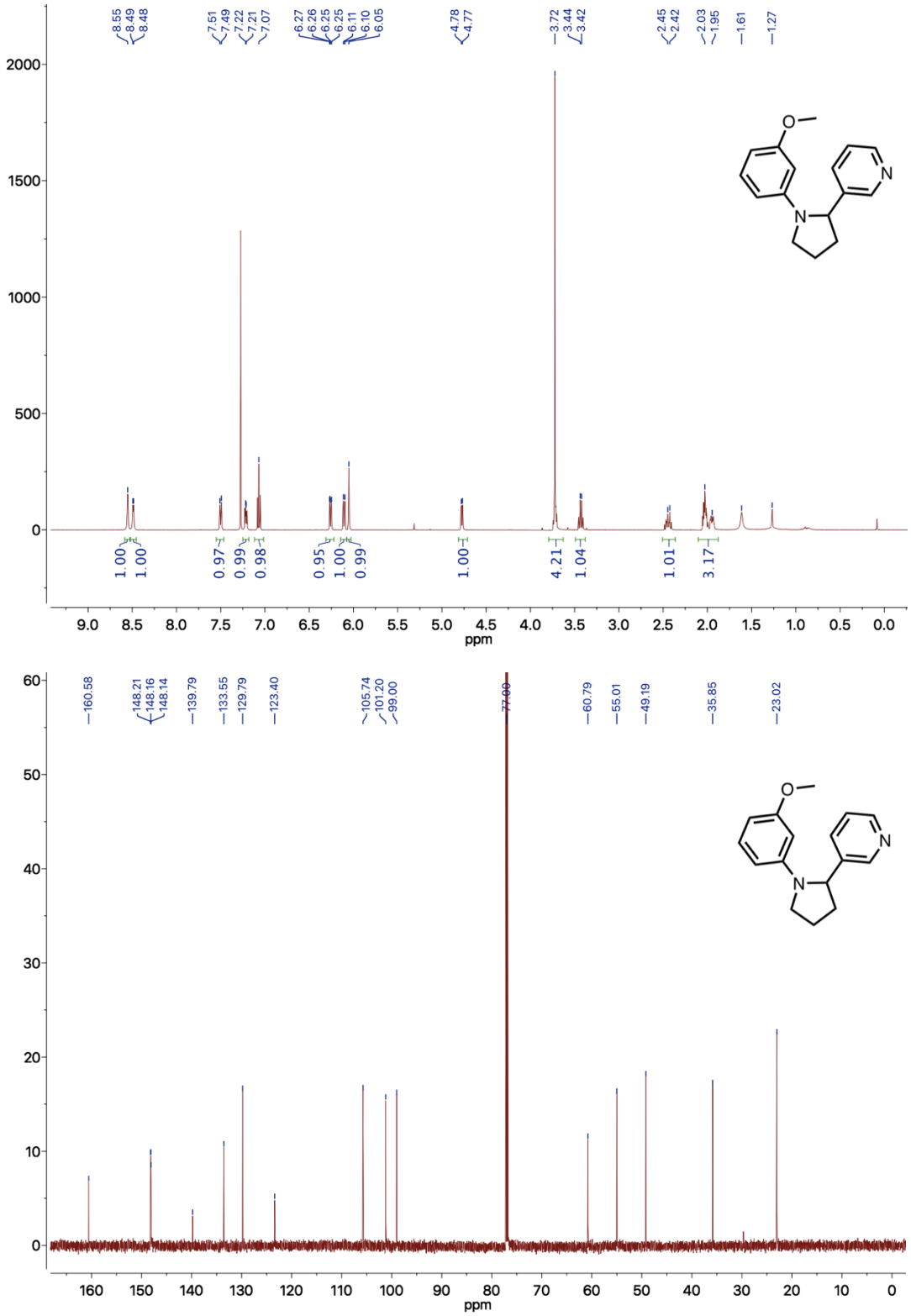


**Figure 5-81.** 3-57 - **$^{1}$H NMR (500 MHz), $^{13}$C NMR (176 MHz)**

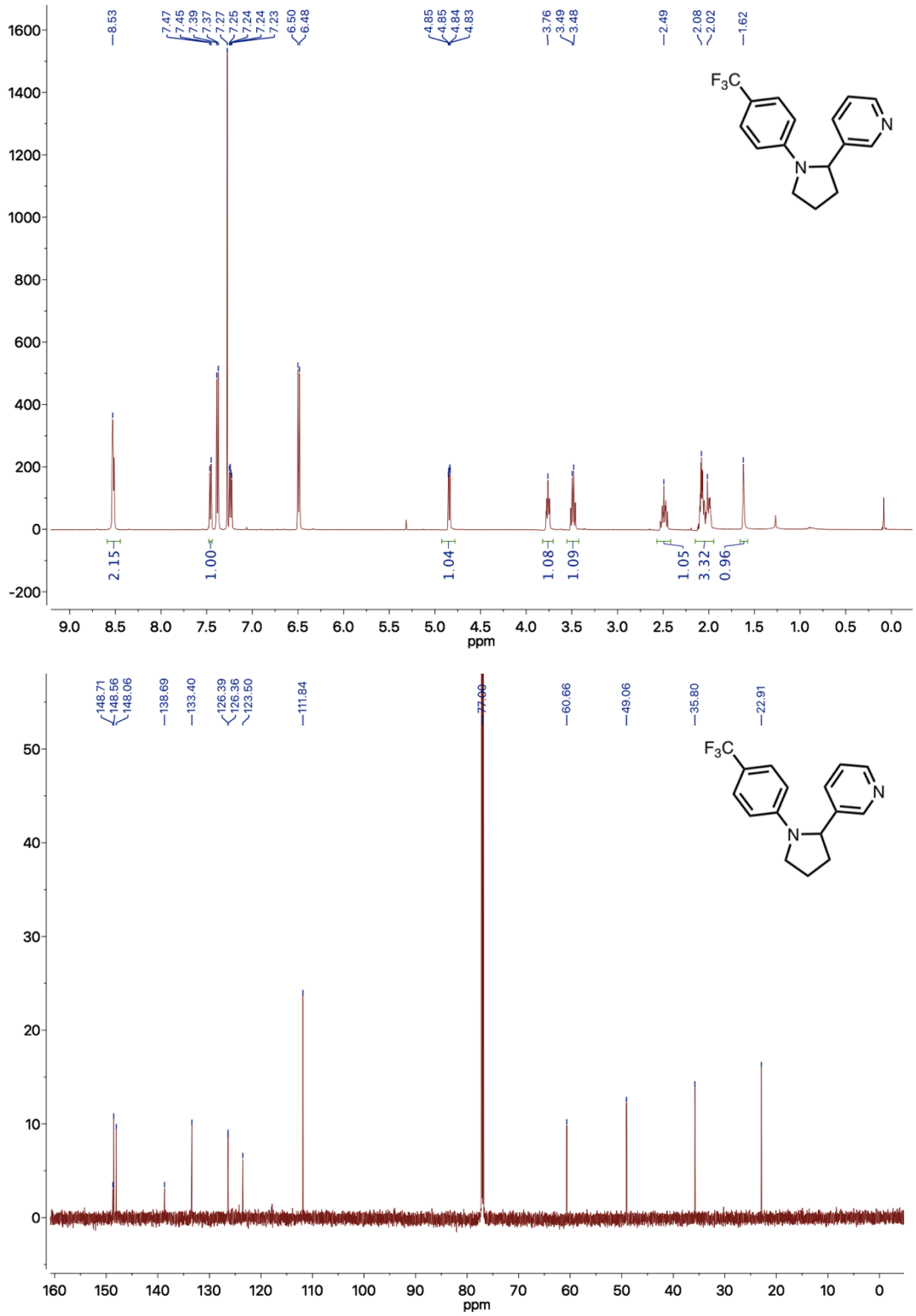


**Figure 5-82.** 3-58 - **$^{1}$H NMR (500 MHz), $^{13}$C NMR (176 MHz)**

## Bibliography


(1) Mond, L.; Langer, C; Quinke, F. *J. Chem. Soc.* **1890**, 749.

(2) Wilke, G. Contributions to Organo-Nickel Chemistry. *Angew. Chemie Int. Ed. English* **1988**, *27* (1), 185–206.

(3) Montgomery, J. *Organometallics in Synthesis: Fourth Manual*; Lipshutz, B. H., Ed.; WILEY-VCH Verlag: Hoboken, NJ, 2013.

(4) Tamao, K.; Sumitani, K.; Kumada, M. Selective Carbon-Carbon Bond Formation by Cross-Coupling of Grignard Reagents with Organic Halides. Catalysis by Nickel-Phosphine Complexes. *J. Am. Chem. Soc.* **1972**, *94* (12), 4374–4376.

(5) Hazari, N.; Melvin, P. R.; Beromi, M. M. Well-Defined Nickel and Palladium Precatalysts for Cross-Coupling. *Nat. Rev. Chem.* **2017**, *1* (3), 25.

(6) Wolfe, J. P.; Buchwald, S. L. Nickel-Catalyzed Amination of Aryl Chlorides. *J. Am. Chem. Soc.* **1997**, *119* (26), 6054–6058.

(7) Gradel, B.; Brenner, E.; Schneider, R.; Fort, Y. Nickel-Catalysed Amination of Aryl Chlorides Using a Dihydroimidazoline Carbene Ligand. *Tetrahedron Lett.* **2001**, *42* (33), 5689–5692.

(8) Desmarets, C.; Schneider, R.; Fort, Y. Nickel(0)/dihydroimidazol-2-Ylidene Complex Catalyzed Coupling of Aryl Chlorides and Amines. *J. Org. Chem.* **2002**, *67* (9), 3029–3036.

(9) Manolikakes, G.; Gavryushin, A.; Knochel, P. An Efficient Silane-Promoted Nickel-Catalyzed Amination of Aryl and Heteroaryl Chlorides. *J. Org. Chem.* **2008**, *73* (4), 1429–1434.

(10) Caddick, S.; Cloke, F. G. N.; Hitchcock, P. B.; Lewis, A. K. D. K. Unusual Reactivity of a Nickel N-Heterocyclic Carbene Complex: Tert-Butyl Group Cleavage and Silicone Grease Activation. *Angew. Chemie - Int. Ed.* **2004**, *43* (43), 5824–5827.

(11) Kelly, R. A.; Scott, N. M.; Díez-González, S.; Stevens, E. D.; Nolan, S. P. Simple Synthesis of CpNi(NHC)Cl Complexes (Cp = Cyclopentadienyl; NHC = N-Heterocyclic Carbene). *Organometallics* **2005**, *24* (14), 3442–3447.

(12) Iglesias, M. J.; Blandez, J. F.; Fructos, M. R.; Prieto, A.; Álvarez, E.; Belderrain, T. R.;

Nicasio, M. C. Synthesis, Structural Characterization, and Catalytic Activity of IPrNi(styrene) $_2$ in the Amination of Aryl Tosylates. *Organometallics* **2012**, *31* (17), 6312–6316.

(13) Martin, A. R.; Makida, Y.; Meiries, S.; Slawin, A. M. Z.; Nolan, S. P. Enhanced Activity of [Ni(NHC)CpCl] Complexes in Arylamination Catalysis. *Organometallics* **2013**, *32* (21), 6265–6270.

(14) Martin, A. R.; Nelson, D. J.; Meiries, S.; Slawin, A. M. Z.; Nolan, S. P. Efficient C–N and C–S Bond Formation Using the Highly Active [Ni(allyl)Cl(IPr*OMe)] Precatalyst. *European J. Org. Chem.* **2014**, *2014* (15), 3127–3131.

(15) Wu, J.; Faller, J. W.; Hazari, N.; Schmeier, T. J. Stoichiometric and Catalytic Reactions of Thermally Stable nickel(0) NHC Complexes. *Organometallics* **2012**, *31* (3), 806–809.

(16) Chen, C.; Yang, L. M. Ni(II)-(σ-Aryl) Complex: A Facile, Efficient Catalyst for Nickel-Catalyzed Carbon-Nitrogen Coupling Reactions. *J. Org. Chem.* **2007**, *72* (16), 6324–6327.

(17) Gao, C.-Y.; Cao, X.; Yang, L.-M. Nickel-Catalyzed Cross-Coupling of Diarylamines with Haloarenes. *Org. Biomol. Chem.* **2009**, *7* (19), 3922.

(18) Huang, J. H.; Yang, L. M. Nickel-Catalyzed Amination of Aryl Phosphates through Cleaving Aryl C-O Bonds. *Org. Lett.* **2011**, *13* (14), 3750–3753.

(19) Alkyls, S.; Derivatives, N. I.; Chatt, B. J.; Shaw, B. L. Chatt and Shaw: Alkyls and 345. Alkyls and Aryls. *Methods* No. Iv, 1718–1729.

(20) Shields, J. D.; Gray, E. E.; Doyle, A. G. A Modular, Air-Stable Nickel Precatalyst. *Org. Lett.* **2015**, *17* (9), 2166–2169.

(21) Park, N. H.; Teverovskiy, G.; Buchwald, S. L. Development of an Air-Stable Nickel Precatalyst for the Amination of Aryl Chlorides, Sulfamates, Mesylates, and Triflates. *Org. Lett.* **2014**, *16* (1), 220–223.

(22) Magano, J.; Monfette, S. Development of an Air-Stable, Broadly Applicable Nickel Source for Nickel-Catalyzed Cross-Coupling. *ACS Catal.* **2015**, *5* (5), 3120–3123.

(23) Sawatzky, R. S.; Ferguson, M. J.; Stradiotto, M. Thieme Chemistry Journals Awardees - Where Are They Now? Efficient Cross-Coupling of Secondary Amines/Azoles and Activated (Hetero)Aryl Chlorides Using an Air-Stable DPEPhos/Nickel Pre-Catalyst. *Synlett* **2017**, *28* (13), 1586–1591.

(24) Clark, J. S. K.; Lavoie, C. M.; MacQueen, P. M.; Ferguson, M. J.; Stradiotto, M. A Comparative Reactivity Survey of Some Prominent Bisphosphine nickel(II) Precatalysts in C-N Cross-Coupling. *Organometallics* **2016**, *35* (18), 3248–3254.

(25) Lavoie, C. M.; Macqueen, P. M.; Rotta-Loria, N. L.; Sawatzky, R. S.; Borzenko, A.;

Chisholm, A. J.; Hargreaves, B. K. V.; McDonald, R.; Ferguson, M. J.; Stradiotto, M. Challenging Nickel-Catalysed Amine Arylations Enabled by Tailored Ancillary Ligand Design. *Nat. Commun.* **2016**, *7*, 1–11.

(26) Corcoran, E. B.; Pirnot, M. T.; Lin, S.; Dreher, S. D.; Dirocco, D. A.; Davies, I. W.; Buchwald, S. L.; Macmillan, D. W. C. Aryl Amination Using Ligand-Free Ni (II) Salts and Photoredox Catalysis. *Science (80-. ).* **2016**, *353* (6296), 279–284.

(27) Ge, S.; Green, R. A.; Hartwig, J. F. Controlling First-Row Catalysts: Amination of Aryl and Heteroaryl Chlorides and Bromides with Primary Aliphatic Amines Catalyzed by a BINAP-Ligated Single-Component Ni(0) Complex. *J. Am. Chem. Soc.* **2014**, *136* (4), 1617–1627.

(28) Marín, M.; Rama, R. J.; Nicasio, M. C. Ni-Catalyzed Amination Reactions: An Overview. *Chem. Rec.* **2016**, 1819–1832.

(29) Eberhardt, N. A.; Guan, H. Nickel Hydride Complexes. *Chem. Rev.* **2016**, *116* (15), 8373–8426.

(30) Keim, W. Oligomerization of Ethylene to α-Olefins: Discovery and Development of the Shell Higher Olefin Process (SHOP). *Angew. Chemie - Int. Ed.* **2013**, *52* (48), 12492–12496.

(31) Joseph, J.; Rajanbabu, T. V; Jemmis, E. D. A Theoretical Investigation of the Ni ( II ) - Catalyzed Hydrovinylation of Styrene. **2009**, No. Ii, 3552–3566.

(32) Nomura, N.; Jin, J.; Park, H.; RajanBabu, T. V. The Hydrovinylation Reaction: A New Highly Selective Protocol Amenable to Asymmetric Catalysis. *J. Am. Chem. Soc.* **1998**, *120* (2), 459–460.

(33) Park, H.; RajanBabu, T. V. Tunable Ligands for Asymmetric Catalysis: Readily Available Carbohydrate-Derived Diarylphosphinites Induce High Selectivity in the Hydrovinylation of Styrene Derivatives. *J. Am. Chem. Soc.* **2002**, *124* (5), 734–735.

(34) Ho, C. Y.; Jamison, T. F. Highly Selective Coupling of Alkenes and Aldehydes Catalyzed by [Ni(NHC){P(OPh)3}]: Synergy between a Strong Donor and a Strong Acceptor. *Angew. Chemie - Int. Ed.* **2007**, *46* (5), 782–785.

(35) Ho, C. Y.; He, L. Catalytic Intermolecular Tail-to-Tail Hydroalkenylation of Styrenes with α Olefins: Regioselective Migratory Insertion Controlled by a Nickel/n-Heterocyclic Carbene. *Angew. Chemie - Int. Ed.* **2010**, *49* (48), 9182–9186.

(36) Chen, W.; Li, Y.; Chen, Y.; Ho, C. Y. (NHC)NiH-Catalyzed Regiodivergent Cross-Hydroalkenylation of Vinyl Ethers with α-Olefins: Syntheses of 1,2- and 1,3-Disubstituted Allyl Ethers. *Angew.Chem. Int.Ed.* **2018***, 57,2677 –2681*.

(37) Ritleng, V.; Henrion, M.; Chetcuti, M. J. Nickel N-Heterocyclic Carbene-Catalyzed C-Heteroatom Bond Formation, Reduction, and Oxidation: Reactions and Mechanistic Aspects. *ACS Catal.* **2016**, *6* (2), 890–906.

(38) Chaulagain, M. R.; Mahandru, G. M.; Montgomery, J. Alkyne Hydrosilylation Catalyzed by Nickel Complexes of N-Heterocyclic Carbenes. *Tetrahedron* **2006**, *62* (32), 7560–7566.

(39) Tamao, K.; Miyake, N.; Kiso, Y.; Kumada, M. A Novel Dehydrogenative Cis Double Silylation of Internal Acetylenes with Hydrosilanes. Catalysis by Diethyl(bipyridyl)nickel(II). *J. Am. Chem. Soc.* **1975**, *97* (19), 5603–5605.

(40) Pulst, S.; Baumann, W.; Baud, H.; Kortus, K.; Rosenthal, U. : I &,,. **1997**, No. 96.

(41) Bennett, E. W.; Orenski, P. J. Nickel Complexes As Hydrosilation Catalysts. *Top. Catal.* **1971**, *28* (1), 137–144.

(42) Pappas, I.; Treacy, S.; Chirik, P. J. Alkene Hydrosilylation Using Tertiary Silanes with α-Diimine Nickel Catalysts. Redox-Active Ligands Promote a Distinct Mechanistic Pathway from Platinum Catalysts. *ACS Catal.* **2016**, *6* (7), 4105–4109.

(43) Miller, Z. D.; Dorel, R.; Montgomery, J. Regiodivergent and Stereoselective Hydrosilylation of 1,3-Disubstituted Allenes. *Angew. Chemie - Int. Ed.* **2015**, *54* (31), 9088–9091.

(44) Miller, Z. D.; Li, W.; Belderrain, T. R.; Montgomery, J. Regioselective Allene Hydrosilylation Catalyzed by N-Heterocyclic Carbene Complexes of Nickel and Palladium. *J. Am. Chem. Soc.* **2013**, *135* (41), 15282–15285.

(45) Tran, B. L.; Pink, M.; Mindiola, D. J. Catalytic Hydrosilylation of the Carbonyl Functionality via a Transient Nickel Hydride Complex. *Organometallics* **2009**, *28* (7), 2234–2243.

(46) Postigo, L.; Royo, B. N-Heterocyclic Carbene Complexes of Nickel as Efficient Catalysts for Hydrosilylation of Carbonyl Derivatives. *Adv. Synth. Catal.* **2012**, *354* (14–15), 2613–2618.

(47) Bheeter, L. P.; Henrion, M.; Brelot, L.; Darcel, C.; Chetcuti, M. J.; Sortais, J. B.; Ritleng, V. Hydrosilylation of Aldehydes and Ketones Catalyzed by an N-Heterocyclic Carbene-Nickel Hydride Complex under Mild Onditions. *Adv. Synth. Catal.* **2012**, *354* (14–15), 2619–2624.

(48) Lage, M. L.; Bader, S. J.; Sa-Ei, K.; Montgomery, J. Chemoselective Hydrosilylation of Hydroxyketones. *Tetrahedron* **2013**, *69* (27–28), 5609–5613.

(49) Iluc, V. M.; Hillhouse, G. L. Snapshots of the Oxidative-Addition Process of Silanes to

nickel(0). *Tetrahedron* **2006**, *62* (32), 7577–7582.

(50) Connor, B. A.; Rittle, J.; Vandervelde, D.; Peters, J. C. A Ni0(η2-(Si-H))(η2-H2) Complex That Mediates Facile H Atom Exchange between Two σ-Ligands. *Organometallics* **2016**, *35* (5), 686–690.

(51) Xie, H.; Zhao, L.; Yang, L.; Lei, Q.; Fang, W.; Xiong, C. Mechanisms and Origins of Switchable Regioselectivity of Palladium- and Nickel-Catalyzed Allene Hydrosilylation with N-Heterocyclic Carbene Ligands: A Theoretical Study. *J. Org. Chem.* **2014**, *79* (10), 4517–4527.

(52) Zell, T.; Schaub, T.; Radacki, K.; Radius, U. Si–H Activation of Hydrosilanes Leading to Hydrido Silyl and Bis(silyl) Nickel Complexes. *Dalt. Trans.* **2011**, *40* (9), 1852.

(53) Baxter, R. D.; Montgomery, J. Mechanistic Study of Nickel-Catalyzed Ynal Reductive Cyclizations through Kinetic Analysis. *J. Am. Chem. Soc.* **2011**, *133* (15), 5728–5731.

(54) Buslov, I.; Becouse, J.; Mazza, S.; Montandon-Clerc, M.; Hu, X. Chemoselective Alkene Hydrosilylation Catalyzed by Nickel Pincer Complexes. *Angew. Chemie - Int. Ed.* **2015**, *54* (48), 14523–14526.

(55) Davies, H. M. L.; Morton, D. Recent Advances in C–H Functionalization. *J. Org. Chem.* **2016**, *81* (2), 343–350.

(56) Nakao, Y. Hydroarylation of Alkynes Catalyzed by Nickel. *Chem. Rec.* **2011**, *11* (5), 242–251.

(57) Johnson, S. A. Nickel Complexes for Catalytic C–H Bond Functionalization. *Dalt. Trans.* **2015**, *44* (24), 10905–10913.

(58) Schramm, Y.; Takeuchi, M.; Semba, K.; Nakao, Y.; Hartwig, J. F. Anti-Markovnikov Hydroheteroarylation of Unactivated Alkenes with Indoles, Pyrroles, Benzofurans, and Furans Catalyzed by a Nickel-N-Heterocyclic Carbene System. *J. Am. Chem. Soc.* **2015**, *137* (38), 12215–12218.

(59) Guihaumé, J.; Halbert, S.; Eisenstein, O.; Perutz, R. N. Hydrofluoroarylation of Alkynes with Ni Catalysts. C-H Activation via Ligand-to-Ligand Hydrogen Transfer, an Alternative to Oxidative Addition. *Organometallics* **2012**, *31* (4), 1300–1314.

(60) Nakao, Y.; Kanyiva, K. S.; Oda, S.; Hiyama, T. Hydroheteroarylation of Alkynes under Mild Nickel Catalysis. *J. Am. Chem. Soc.* **2006**, *128* (25), 8146–8147.

(61) Hatnean, J. A.; Beck, R.; Borrelli, J. D.; Johnson, S. A. Carbon-Hydrogen Bond Oxidative Addition of Partially Fluorinated Aromatics to a Ni(PiPr3)2 Synthon: The Influence of Steric Bulk on the Thermodynamics and Kinetics of C-H Bond Activation. *Organometallics* **2010**, *29* (22), 6077–6091.

(62) Bair, J. S.; Schramm, Y.; Sergeev, A. G.; Clot, E.; Eisenstein, O.; Hartwig, J. F. Linear-Selective Hydroarylation of Unactivated Terminal and Internal Olefins with Trifluoromethyl-Substituted Arenes. *J. Am. Chem. Soc.* **2014**, *136* (38), 13098–13101.

(63) Nett, A. J.; Zhao, W.; Zimmerman, P. M.; Montgomery, J. Highly Active Nickel Catalysts for C-H Functionalization Identified through Analysis of Off-Cycle Intermediates. *J. Am. Chem. Soc.* **2015**, *137* (24), 7636–7639.

(64) Laskowski, C. A.; Miller, A. J. M.; Hillhouse, G. L.; Cundari, T. R. A Two-Coordinate Nickel Imido Complex That Effects C-H Amination. *J. Am. Chem. Soc.* **2011**, *133* (4), 771–773.

(65) Kumar, P.; Thakur, A.; Hong, X.; Houk, K. N.; Louie, J. Ni(NHC)]-Catalyzed Cycloaddition of Diynes and Tropone: Apparent Enone Cycloaddition Involving an 8π Insertion. *J. Am. Chem. Soc.* **2014**, *136* (51), 17844–17851.

(66) Liu, R.-J.; Wang, P.-F.; Yuan, W.-K.; Wen, L.-R.; Li, M. Nickel Catalysis Enables Hetero [2+2+1] Cycloaddition between Yne-Isothiocyanates and Isonitriles with Low Catalyst Loading. *Adv. Synth. Catal.* **2017**, *359* (8), 1373–1378.

(67) Jackson, E. P. Advances in Regiocontrol and Bench Stability in Nickel-Catalyzed Reductive Couplings of Aldehydes and Alkynes, University of Michigan, 2015.

(68) Maity, P.; Kundu, D.; Ranu, B. C. Nickel-Copper-Catalyzed C(sp2)- N Cross-Coupling of Cyclic and Bridged Amides: An Access to Cyclic Enamides and Alkenyl Vince Lactams. *Adv. Synth. Catal.* **2015**, *357* (16–17), 3617–3626.

(69) Kundu, D.; Maity, P.; Ranu, B. C. Copper-Assisted Nickel Catalyzed Ligand-Free C(sp2)-O Cross-Coupling of Vinyl Halides and Phenols. *Org. Lett.* **2014**, *16* (4), 1040–1043.

(70) Mukherjee, N.; Kundu, D.; Ranu, B. C. A Co-Operative Ni-Cu System for Csp-Csp and Csp-Csp(2) Cross-Coupling Providing a Direct Access to Unsymmetrical 1,3-Diynes and En-Ynes. *Chem. Commun. (Camb).* **2014**, *50* (99), 15784–15787.

(71) Standley, E. A.; Jamison, T. F. Simplifying nickel(0) Catalysis: An Air-Stable Nickel Precatalyst for the Internally Selective Benzylation of Terminal Alkenes. *J. Am. Chem. Soc.* **2013**, *135* (4), 1585–1592.

(72) Hayashi, Y.; Hoshimoto, Y.; Kumar, R.; Ohashi, M.; Ogoshi, S. Nickel(0)-Catalyzed Coupling Reactions of Carbonyls and Alkenes with Reducing Reagents Giving Six- and Seven-Membered Benzocycloalkanols. *Chem. Lett.* **2017**, *46* (8), 1096–1098.

(73) Inatomi, T.; Koga, Y.; Matsubara, K. Dinuclear Nickel (I) and Palladium (I) Complexes for Highly Active Transformations of Organic Compounds. *Molecules* **2018**, *23* (1), 140.

(74) Lin, C.-Y.; Power, P. P. Complexes of Ni(I): A “rare” Oxidation State of Growing Importance. *Chem. Soc. Rev.* **2017**, *46*, 5347–5399.

(75) Morrell, D. G.; Kochi, J. K. Mechanistic Studies of Nickel Catalysis in the Cross Coupling of Aryl Halides with Alkylmetals. The Role of Arylalkylnickel(II) Species as Intermediates. *J. Am. Chem. Soc.* **1975**, *97* (25), 7262–7270.

(76) Kitiachvili, K. D.; Mindiola, D. J.; Hillhouse, G. L. Preparation of Stable Alkyl Complexes of Ni(I) and Their One-Electron Oxidation to Ni(II) Complex Cations. *J. Am. Chem. Soc.* **2004**, *126* (34), 10554–10555.

(77) Anderson, T. J.; Jones, G. D.; Vicic, D. A. Evidence for a NiIactive Species in the Catalytic Cross-Coupling of Alkyl Electrophiles. *J. Am. Chem. Soc.* **2004**, *126* (26), 8100–8101.

(78) Jones, G. D.; Martin, J. L.; McFarland, C.; Allen, O. R.; Hall, R. E.; Haley, A. D.; Brandon, R. J.; Konovalova, T.; Desrochers, P. J.; Pulay, P.; et al. Ligand Redox Effects in the Synthesis, Electronic Structure, and Reactivity of an Alkyl-Alkyl Cross-Coupling Catalyst. *J. Am. Chem. Soc.* **2006**, *128* (40), 13175–13183.

(79) Zhou, J. S.; Fu, G. C. Cross-Couplings of Unactivated Secondary Alkyl Halides : Room-Temperature Nickel-Catalyzed Negishi Reactions of Alkyl Bromides and Iodides. **2003**, 14726–14727.

(80) Arp, F. O.; Fu, G. C. Catalytic Enantioselective Negishi Reactions of Racemic Secondary Benzylic Halides. *J. Am. Chem. Soc.* **2005**, *127* (30), 10482–10483.

(81) Phapale, V. B.; Buñuel, E.; García-Iglesias, M.; Cárdenas, D. J. Ni-Catalyzed Cascade Formation of C(sp3)-C(sp3) Bonds by Cyclization and Cross-Coupling Reactions of Iodoalkanes with Alkyl Zinc Halides. *Angew. Chemie - Int. Ed.* **2007**, *46* (46), 8790–8795.

(82) Schley, N. D.; Fu, G. C. Nickel-Catalyzed Negishi Arylations of Propargylic Bromides: A Mechanistic Investigation. *J. Am. Chem. Soc.* **2014**, *136* (47), 16588–16593.

(83) Rettenmeier, C.; Wadepohl, H.; Gade, L. H. Stereoselective Hydrodehalogenation via a Radical-Based Mechanism Involving T-Shaped Chiral nickel(I) Pincer Complexes. *Chem. - A Eur. J.* **2014**, *20* (31), 9657–9665.

(84) Dible, B. R.; Sigman, M. S.; Arif, A. M. Oxygen-Induced Ligand Dehydrogenation of a Planar Bis-μ-chloronickel(I) Dimer Featuring an NHC Ligand. *Inorg. Chem.* **2005**, *44* (11), 3774–3776.

(85) Nagao, S.; Matsumoto, T.; Koga, Y.; Matsubara, K. Monovalent Nickel Complex Bearing a Bulky *N* -Heterocyclic Carbene Catalyzes Buchwald–Hartwig Amination of Aryl Halides under Mild Conditions. *Chem. Lett.* **2011**, *40* (9), 1036–1038.

(86) Matsubara, K.; Fukahori, Y.; Inatomi, T.; Tazaki, S.; Yamada, Y.; Koga, Y.; Kanegawa, S.; Nakamura, T. Monomeric Three-Coordinate N-Heterocyclic Carbene nickel(I) Complexes: Synthesis, Structures, and Catalytic Applications in Cross-Coupling Reactions. *Organometallics* **2016**, *35* (19), 3281–3287.

(87) Zhang, K.; Conda-Sheridan, M.; R. Cooke, S.; Louie, J. N-Heterocyclic Carbene Bound nickel(I) Complexes and Their Roles in Catalysis. *Organometallics* **2011**, *30* (9), 2546–2552.

(88) Cornella, J.; Gómez-Bengoa, E.; Martin, R. Combined Experimental and Theoretical Study on the Reductive Cleavage of Inert C-O Bonds with Silanes: Ruling out a Classical Ni(0)/Ni(II) Catalytic Couple and Evidence for Ni(I) Intermediates. *J. Am. Chem. Soc.* **2013**, *135* (5), 1997–2009.

(89) Nadal, M. L.; Bosch, J.; Vila, J. M.; Klein, G.; Ricart, S.; Moretó, J. M. The Ni-Mediated Cyclocarbonylation of Allyl Halides and Alkynes Made Catalytic. Evidence Supporting the Involvement of Pseudoradical NiI Species in the Mechanism. *J. Am. Chem. Soc.* **2005**, *127* (30), 10476–10477.

(90) Beromi, M. M.; Nova, A.; Balcells, D.; Brasacchio, A. M.; Brudvig, G. W.; Guard, L. M.; Hazari, N.; Vinyard, D. J. Mechanistic Study of an Improved Ni Precatalyst for Suzuki-Miyaura Reactions of Aryl Sulfamates: Understanding the Role of Ni(I) Species. *J. Am. Chem. Soc.* **2017**, *139* (2), 922–936.

(91) Mohadjer Beromi, M.; Banerjee, G.; Brudvig, G. W.; Hazari, N.; Mercado, B. Q. Nickel(I) Aryl Species: Synthesis, Properties, and Catalytic Activity. *ACS Catal.* **2018**, No. I, 2526–2533.

(92) Guard, L. M.; Mohadjer Beromi, M.; Brudvig, G. W.; Hazari, N.; Vinyard, D. J. Comparison of Dppf-Supported Nickel Precatalysts for the Suzuki-Miyaura Reaction: The Observation and Activity of Nickel(I). *Angew. Chemie - Int. Ed.* **2015**, *54* (45), 13352–13356.

(93) Castro, L. C. M.; Chatani, N. Nickel Catalysts/ *N* , *N* ′-Bidentate Directing Groups: An Excellent Partnership in Directed C–H Activation Reactions. *Chem. Lett.* **2015**, *44* (4), 410–421.

(94) Nakao, Y. Hydroarylation of Alkynes Catalyzed by Nickel. *Chem. Rec.* **2011**, *11* (5), 242–251.

(95) Kulkarni, A. A.; Daugulis, O. Direct Conversion of Carbon-Hydrogen into Carbon-Carbon Bonds by First-Row Transition-Metal Catalysis. *Synthesis (Stuttg)*. **2009**, No. 24, 4087–4109.

(96) Tsuda, T.; Kiyoi, T.; Saegusa, T. Nickel(0)-Catalyzed Hydroacylation of Alkynes with Aldehydes to A,β-Enones. *J. Org. Chem.* **1990**, *55* (8), 2554–2558.

(97) Xu, H.; Muto, K.; Yamaguchi, J.; Zhao, C.; Itami, K.; Musaev, D. G. Key Mechanistic Features of Ni-Catalyzed C-H/C-O Biaryl Coupling of Azoles and Naphthalen-2-Yl Pivalates. *J. Am. Chem. Soc.* **2014**, *136* (42), 14834–14844.

(98) Xiao, L. J.; Fu, X. N.; Zhou, M. J.; Xie, J. H.; Wang, L. X.; Xu, X. F.; Zhou, Q. L. Nickel-Catalyzed Hydroacylation of Styrenes with Simple Aldehydes: Reaction Development and Mechanistic Insights. *J. Am. Chem. Soc.* **2016**, *138* (9), 2957–2960.

(99) Staudaher, N. D.; Stolley, R. M.; Louie, J. Synthesis, Mechanism of Formation, and Catalytic Activity of Xantphos Nickel π-Complexes. *Chem. Commun.* **2014**, *50* (98), 15577–15580.

(100) Watson, M. P.; Jacobsen, E. N. Asymmetric Intramolecular Arylcyanation of Unactivated Olefins via C # CN Bond Activation Asymmetric Intramolecular Arylcyanation of Unactivated Olefins via C - CN. **2008**, 1–3.

(101) Nyce, G. W.; Csihony, S.; Waymouth, R. M.; Hedrick, J. L. A General and Versatile Approach to Thermally Generated N-Heterocyclic Carbenes. *Chem. - A Eur. J.* **2004**, *10* (16), 4073–4079.

(102) Zimmerman, P. M. Automated Discovery of Chemically Reasonable Elementary Reaction Steps. *J. Comput. Chem.* **2013**, *34* (16), 1385–1392.

(103) Zimmerman, P. Reliable Transition State Searches Integrated with the Growing String Method. *J. Chem. Theory Comput.* **2013**, *9* (7), 3043–3050.

(104) Zimmerman, P. M. Growing String Method with Interpolation and Optimization in Internal Coordinates: Method and Examples. *J. Chem. Phys.* **2013**, *138* (18).

(105) Zimmerman, P. M. Single-Ended Transition State Finding with the Growing String Method. *J. Comput. Chem.* **2015**, *36* (9), 601–611.

(106) Hilton, M. J.; Xu, L. P.; Norrby, P. O.; Wu, Y. D.; Wiest, O.; Sigman, M. S. Investigating the Nature of Palladium Chain-Walking in the Enantioselective Redox-Relay Heck Reaction of Alkenyl Alcohols. *J. Org. Chem.* **2014**, *79* (24), 11841–11850.

(107) Juliá-Hernández, F.; Moragas, T.; Cornella, J.; Martin, R. Remote Carboxylation of Halogenated Aliphatic Hydrocarbons with Carbon Dioxide. *Nature* **2017**, *545* (7652), 84–88.

(108) Hicks, F. A.; Jenkins, J. C.; Brookhart, M. Synthesis and Ethylene Polymerization Activity of a Series of 2-Anilinotropone-Based Neutral nickel(II) Catalysts. *Organometallics* **2003**, *22* (17), 3533–3545.

(109) Shultz, L. H.; Brookhart, M. Measurement of the Barrier to β-Hydride Elimination in a β-

Agostic Palladium-Ethyl Complex: A Model for the Energetics of Chain-Walking in (α-diimine)PdR+ Olefin Polymerization Catalysts. *Organometallics* **2001**, *20* (19), 3975–3982.

(110) Svejda, S. A.; Johnson, L. K.; Brookhart, M. Low-Temperature Spectroscopic Observation of Chain Growth and Migratory Insertion Barriers in (α-diimine)Ni(II) Olefin Polymerization Catalysts [5]. *J. Am. Chem. Soc.* **1999**, *121* (45), 10634–10635.

(111) Leatherman, M. D.; Svejda, S. A.; Johnson, L. K.; Brookhart, M. Mechanistic Studies of nickel(II) Alkyl Agostic Cations and Alkyl Ethylene Complexes: Investigations of Chain Propagation and Isomerization in (α-diimine)Ni(II)-Catalyzed Ethylene Polymerization. *J. Am. Chem. Soc.* **2003**, *125* (10), 3068–3081.

(112) Musaev, D. G.; Musaev, D. G.; Svensson, M.; Svensson, M.; Morokuma, K.; Morokuma, K.; Stro, S.; Stro, S.; Zetterberg, K.; Zetterberg, K.; et al. Density Functional Study of the Mechanism of the Palladium(II)-Catalyzed Ethylene Polymerization Reaction. *Organometallics* **1997**, *16* (9), 1933–1945.

(113) Deng, L.; Margl, P.; Ziegler, T. A Density Functional Study of nickel(II) Diimide Catalyzed Polymerization of Ethylene. *J. Am. Chem. Soc.* **1997**, *119* (5), 1094–1100.

(114) Dewyer, A. L.; Zimmerman, P. M. Finding Reaction Mechanisms, Intuitive or Otherwise. *Org. Biomol. Chem.* **2017**, *15* (3), 501–504.

(115) Sato, Y.; Takimoto, M.; Mori, M. Further Studies on Nickel-Promoted or -Catalyzed Cyclization of 1,3- Diene and a Tethered Carbonyl Group. *J. Am. Chem. Soc.* **2000**, *122* (8), 1624–1634.

(116) Rösch, N.; Hoffmann, R. Geometry of Transition Metal Complexes with Ethylene or Allyl Groups as the Only Ligands. *Inorg. Chem.* **1974**, *13* (11), 2656–2666.

(117) Nakao, Y.; Kashihara, N.; Kanyiva, K. S.; Hiyama, T. Nickel-Catalyzed Alkenylation and Alkylation of Fluoroarenes via Activation of C - H Bond over C - F Bond Whereas Many Late Transition Metal Complexes Undergo the. *J. Am. Chem. Soc.* **2008**, *130* (Scheme 2), 16170–16171.

(118) Blackmond, D. G. Reaction Progress Kinetic Analysis: A Powerful Methodology for Mechanistic Studies of Complex Catalytic Reactions. *Angew. Chemie - Int. Ed.* **2005**, *44* (28), 4302–4320.

(119) Baxter, R. D.; Sale, D.; Engle, K. M.; Yu, J. Q.; Blackmond, D. G. Mechanistic Rationalization of Unusual Kinetics in Pd-Catalyzed C-H Olefination. *J. Am. Chem. Soc.* **2012**, *134* (10), 4600–4606.

(120) Burés, J. A Simple Graphical Method to Determine the Order in Catalyst. *Angew. Chemie - Int. Ed.* **2016**, *55* (6), 2028–2031.

(121) Burés, J. Variable Time Normalization Analysis: General Graphical Elucidation of Reaction Orders from Concentration Profiles. *Angew. Chemie - Int. Ed.* **2016**, *55* (52), 16084–16087.

(122) Rodrigo, S. K.; Guan, H. Mechanistic Study of Nickel-Catalyzed Reductive Coupling of Ynoates and Aldehydes. *J. Org. Chem.* **2017**, *82* (10), 5230–5235.

(123) Jones, W. D.; Hessell, E. T. Photolysis of Tp'Rh(CN-neopentyl)(.eta.2-PhN:C:N-Neopentyl) in Alkanes and Arenes: Kinetic and Thermodynamic Selectivity of [Tp'Rh(CN-Neopentyl)] for Various Types of Carbon-Hydrogen Bonds. *J. Am. Chem. Soc.* **1993**, *115* (c), 554–562.

(124) Wick, D. D.; Jones, W. D. Energetics of Homogeneous Intermolecular Vinyl and Allyl Carbon−Hydrogen Bond Activation by the 16-Electron Coordinatively Unsaturated Organometallic Fragment [Tp'Rh(CNCH $_2$ CMe $_3$ )]. *Organometallics* **1999**, *18* (4), 495–505.

(125) Bryndza, H. E.; Fong, L. K.; Paciello, R. A.; Tam, W.; Bercaw, J. E. Relative Metal-Hydrogen, -Oxygen, -Nitrogen, and -Carbon Bond Strengths for Organoruthenium and Organoplatinum Compounds; Equilibrium Studies of Cp*(PMe3)2RuX and (DPPE)MePtX Systems. *J. Am. Chem. Soc.* **1987**, *109* (5), 1444–1456.

(126) Clot, E.; Me, C.; Eisenstein, O.; Perutz, R. N.; Gerhardt, I. C.; Uni, V. Exceptional Sensitivity of Metal - Aryl Bond Energies to Ortho -Fluorine Substituents : Influence of the Metal , the Coordination Sphere , and the Spectator Ligands on M - C / H - C Bond Energy Correlations. *J. Am. Chem. Soc.* **2009**, No. 131, 7817–7827.

(127) Todd, D. P.; Thompson, B. B.; Nett, A. J.; Montgomery, J. Deoxygenative C-C Bond-Forming Processes via a Net Four-Electron Reductive Coupling. *J. Am. Chem. Soc.* **2015**, *137* (40), 12788–12791.

(128) Delarmelina, M.; Marelli, E.; José, J. W.; Nolan, S. P.; Bühl, M. Mechanism of the Catalytic Carboxylation of Alkylboronates with CO2 Using Ni−NHC Complexes: A DFT Study. *Chem. - A Eur. J.* **2017**, *23* (59), 14954–14961.

(129) Abernethy, C. D.; Clyburne, J. A. C.; Cowley, A. H.; Jones, R. A. Reactions of Transition-Metal Metallocenes with Stable Carbenes [12]. *J. Am. Chem. Soc.* **1999**, *121* (10), 2329–2330.

(130) Iglesias, M. J.; Prieto, A.; Nicasioa, M. C. Well-Defined Allylnickel chloride/N-Heterocyclic Carbene [(NHC)Ni (allyl)Cl] Complexes as Highly Active Precatalysts for C-N and C-S Cross-Coupling Reactions. *Adv. Synth. Catal.* **2010**, *352* (11–12), 1949–1954.

(131) Dible, B. R.; Sigman, M. S. Unusual Reactivity of Molecular Oxygen with π-

allylnickel(N-Heterocyclic Carbene) Chloride Complexes. *J. Am. Chem. Soc.* **2003**, *125* (4), 872–873.

(132) Hoshimoto, Y.; Hayashi, Y.; Suzuki, H.; Ohashi, M.; Ogoshi, S. One-Pot, Single-Step, and Gram-Scale Synthesis of Mononuclear [(η6-arene)Ni(N-Heterocyclic Carbene)] Complexes: Useful Precursors of the Ni0-NHC Unit. *Organometallics* **2014**, *33* (5), 1276–1282.

(133) Clement, N. D.; Cavell, K. J.; Ooi, L. L. Zerovalent N-Heterocyclic Carbene Complexes of Palladium and Nickel Dimethyl Fumarate: Synthesis, Structure, and Dynamic Behavior. *Organometallics* **2006**, *25* (17), 4155–4165.

(134) Baxter, R. D.; Montgomery, J. Dehydrogenative Cyclocondensation of Aldehydes, Alkynes, and Dialkylsilanes" *J. Am. Chem. Soc.* **2008**, *130*, 9662.

(135) Malik, H. A.; Sormunen, G. J.; Montgomery, J. A General Strategy for Regiocontrol in Nickel-Catalyzed Reductive Couplings of Aldehydes and Alkynes. *J. Am. Chem. Soc.* **2010**, *132* (18), 6304–6305.

(136) Shareef, A.-R.; Sherman, D. H.; Montgomery, J. Nickel-Catalyzed Regiodivergent Approach to Macrolide Motifs. *Chem. Sci.* **2012**, *3* (3), 892–895.

(137) Baba, S.; Negishi, E. ichi. A Novel Stereospecific Alkenyl-Alkenyl Cross-Coupling by a Palladium- or Nickel-Catalyzed Reaction of Alkenylalanes with Alkenyl Halides. *J. Am. Chem. Soc.* **1976**, *98* (21), 6729–6731.

(138) Hie, L.; Ramgren, S. D.; Mesganaw, T.; Garg, N. K. Nickel-Catalyzed Amination of Aryl Sulfamates and Carbamates Using an Air-Stable Precatalyst. *Org. Lett.* **2012**, *14* (16), 4182–4185.

(139) Liu, J.; Robins, M. J. Azoles as Suzuki Cross-Coupling Leaving Groups: Syntheses of 6-Arylpurine 2???-Deoxynucleosides and Nucleosides from 6-(Lmidazol-1-Yl)- and 6-(1,2,4-Triazol-4-Yl)purine Derivatives. *Org. Lett.* **2004**, *6* (19), 3421–3423.

(140) Bantreil, X.; Nolan, S. P. Synthesis of N-Heterocyclic Carbene Ligands and Derived Ruthenium Olefin Metathesis Catalysts. *Nat. Protoc.* **2011**, *6* (1), 69–77.

(141) Meiries, S.; Speck, K.; Cordes, D. B.; Slawin, A. M. Z.; Nolan, S. P. [Pd(IPr*OMe)(acac)Cl]: Tuning the N-Heterocyclic Carbene in Catalytic C-N Bond Formation. *Organometallics* **2013**, *32* (1), 330–339.

(142) Shao, Y.; Gan, Z.; Epifanovsky, E.; Gilbert, A. T. B.; Wormit, M.; Kussmann, J.; Lange, A. W.; Behn, A.; Deng, J.; Feng, X.; et al. Advances in Molecular Quantum Chemistry Contained in the Q-Chem 4 Program Package. *Mol. Phys.* **2015**, *113* (2), 184–215.

(143) Becke, A. D. Density-Functional Thermochemistry. III. The Role of Exact Exchange. *J.*

*Chem. Phys.* **1993**, *98* (7), 5648–5652.

(144) Hay, P. J.; Wadt, W. R. *Ab Initio* Effective Core Potentials for Molecular Calculations. Potentials for K to Au Including the Outermost Core Orbitals. *J. Chem. Phys.* **1985**, *82* (1), 299–310.

(145) Hay, P. J.; Wadt, W. R. Ab Initio Effective Core Potentials for Molecular Calculations. Potentials for the Transition Metal Atoms Sc to Hg. *J. Chem. Phys.* **1985**, *82* (1), 270–283.

(146) Marenich, A. V.; Cramer, C. J.; Truhlar, D. G. Unviersal Solvation Modle Based on Solute Electron Density and a Contiuum Model of the Solvent Defind by the Bulk Dielectric Constant and Atomic Surface Tensions. *J. Phys. Chem. B.* **2009**, *113*, 6378–6396.

(147) M.W. Schmidt; K. K. Baldridge; J. A. Boatz; S. T. Elbert; M. S. Gordon; J. H. Jensen; S. Koseki; N. Matsunaga; K. A. Nguyen; S. J. Su; et al. General Atomic and Molecular Electronic Structure System. *J. Comput. Chem.* **1993**, *14* (14), 1347.

(148) Chai, J.-D.; Head-Gordon, M. Long-Range Corrected Hybrid Density Functionals with Damped Atom–atom Dispersion Corrections. *Phys. Chem. Chem. Phys.* **2008**, *10* (44), 6615.

(149) Peterson, K. A.; Figgen, D.; Dolg, M.; Stoll, H. Energy-Consistent Relativistic Pseudopotentials and Correlation Consistent Basis Sets for the 4d Elements Y-Pd. *J. Chem. Phys.* **2007**, *126* (12).

(150) Nakao, Y.; Idei, H.; Kanyiva, K. S.; Hiyama, T. Direct Alkenylation and Alkylation of Pyridone Derivatives by Ni/AlMe3catalysis. *J. Am. Chem. Soc.* **2009**, *131* (44), 15996–15997.

(151) Wang, M.; Wang, L.; Li, P.-H.; Yan, J.-C. A Novel Debromination of Vic-Dibromides to Alkenes with InCl(cat.)/Sm System in Aqueous Media. *Chinese J. Chem.* **2004**, *22* (8), 2002–2005.

(152) Valizadeh, H.; Khalili, E. Efficient Synthesis of Symmetrical Phthalate and Maleate Diesters Using Phosphinite Ionic Liquids. *J. Iran. Chem. Soc.* **2012**, *9* (4), 529–534.

(153) Geny, A.; Agenet, N.; Iannazzo, L.; Malacria, M.; Aubert, C.; Gandon, V. Air-Stable {(C5H5)Co} Catalysts for [2+2+2] Cycloadditions. *Angew. Chemie - Int. Ed.* **2009**, *48* (10), 1810–1813.